Crystal Engineering of Selected Phenolic Acids

by

Francoise Mystere Amombo Noa

Thesis submitted in fulfilment of the requirements for the degree

Master of Technology: Chemistry

in the Faculty of Applied Science

at the

CAPE PENINSULA UNIVERSITY OF TECHNOLOGY

Supervisor: Professor A. Jacobs

Cape Town

April 2014

TABLE OF CONTENTS

DECLARATION

I, Francoise Mystere Amombo Noa, declare that the contents of this thesis represent my own work, and that the thesis has not previously been submitted for academic examination towards any qualification. Furthermore, it represents my own ideas and not necessarily those of the Cape Peninsula University of Technology.

ABSTRACT

Crystal engineering based upon acid: base compounds have been studied in this thesis. Selected phenolic acids such as: vanillic acid (VA), phenylacetic acid (PAA), 4-hydroxyphenylacetic acid (HPAA), 3-chloro-4-hydroxyphenylacetic acid (CHPAA), caffeic acid (CFA), *p*-coumaric acid (*p*CA), *trans*-ferulic acid (*t*FER), 2-phenylpropionic acid (PPA) and 2-phenylbutyric acid (PBA) were the main compounds investigated. These phenolic acids have formed co-crystals/co-crystal hydrates, salts/salt hydrates and hybrid salt-co-crystals with acridine (ACRI), caffeine (CAF), cinchonidine (CIND), isonicotinamide (INM), isonicotinic acid (INA), nicotinamide (NAM), quinidine (QUID), quinine (QUIN), theobromine (THBR), theophylline (THPH) and urea (U).

The two racemic compounds 2-phenylpropionic acid (PPA) and 2-phenylbutyric acid (PBA) were used to study chiral discrimination leading to the understanding of separation enantiomers.

Compounds were prepared in different solvents (alcohols, ketone and distilled water) to investigate the relationship between solvents used and the crystalline product obtained. (If there is any effect on the crystalline compound obtained by changing the solvent).

The structures were elucidated using single crystal X-ray diffraction. Ground products of obtained compounds were characterized by powder X-ray diffraction (PXRD). Thermal analyses like thermogravimetry (TG), differential scanning calorimetry (DSC) and hot stage microscopy (HSM) were used for the determination of thermal character of the new compounds. IR was also performed to characterize the new compounds.

Non-isothermal TG was utilised to obtain kinetic parameters for the water and the methanol release in (***p*CA^{-})(QUIN^{+})•*p*CA•MeOH•H$_2$O**.

A selective experiment was done in which quinidine and quinine were used to compete between selected phenolic acids (PAA and HPAA).

The comparison of the crystal structures determined showed that, changing the phenolic acid while using the same co-crystal former has a significant effect on the type of compounds obtained. The obtained crystal structures were either co-crystal/co-crystal hydrates, salts/salt hydrates or hybrid salt-co-crystals which formed network via means of supramolecular interactions.

ACKNOWLEDGEMENTS

I wish to thank Prof. Ayesha Jacobs for her patience and understanding, and for assisting me throughout my project, Prof. Luigi R Nassimbeni and Dr. Nikoletta Báthori for the continuous guidance and encouragement throughout my study. I have been privilege to work with them, especially my supervisor Prof. Ayesha Jacobs as she taught me to resolve problems throughout my project.

I will like to acknowledge and thank my parents, my closest family and friends for their constant support throughout the years of studies.

Last but not least the Cape Peninsula University of Technology.

PUBLICATION

Parts of this thesis have been published:

- Jacobs. A & Amombo Noa. F. M. *J. Chem. Crystallogr.* 2014, 44 (2), 57 - 62.

LIST OF FIGURES

LIST OF TABLES

ABBREVIATIONS/TERMS/ACRONYMS

CSD	Cambridge Structural Database
TGA	Thermogravimetric Analysis
DSC	Differential Scanning Calorimetry
PXRD	powder X-ray diffraction
HSM	hot stage microscopy
SXRD	single x-ray diffraction
R	universal gas constant
E_a	activation energy
ΔT	temperature difference
T	temperature
FT-IR	Fourier transform infra-red
IR	infra-red
kJ mol^{-1}	kilojoules per mole
Z	number of formula units per cell
%	percentage
K	kelvin
º	degree
a,b,c	unit cell axes
α	alpha interaxial angle between b and c
β	beta interaxial angle between a and c
γ	gamma interaxial angle between a and b
min	minutes
hr	hour
ACRI	acridine
CAF	caffeine
CFA	caffeic acid
CHPAA	3-chloro-4-hydroxyphenylacetic acid
CIND	cinchonidine
HPAA	4-hydroxyphenylacetic acid
INM	isonicotinamide
NAM	nicotinamide
*p*CA	*p*-coumaric acid
PAA	phenylacetic acid
QUID	quinidine
QUIN	quinine
THBR	theobromine
THPH	theophylline
*t*FER	*trans*-ferulic acid
VA	vanillic acid
U	urea
API	active pharmaceutical ingredients
T_{on}	onset temperature
R	correlation coefficient
k	rate constant
P	vapour pressure
l	liquid
g	gas
s	solid
2-PPA	(*R, S*)-*2*-phenylpropionic acid
R-PPA	(*R*)-(-)-2-phenylpropionic acid
2-PBA	(*R, S*)-*2*-phenylbutyric acid
S-PBA	(*S*)-(+)-2-phenylbutyric acid

ATOM COLOUR SCHEME

CARBON

HYDROGEN

NITROGEN

OXYGEN

CHLORINE

CHAPTER 1

INTRODUCTION

1.1 Supramolecular Chemistry

Jean-Marie Lehn has defined supramolecular chemistry as “chemistry beyond the molecule”. The organisation of entities that results from associating two or more chemical compounds linked together by non-covalent interactions can also be defined as supramolecular chemistry.[1-7]

Supramolecular chemistry defined by Steed *et al* [8] is the study of molecular systems that are made up of groups of molecules or ions that are bonded by non-covalent interactions. This type of chemistry is involved in diverse disciplines and fields, with complete control over supramolecules, molecular assemblies and materials.[9]

Complex systems of components which interact by non-covalent forces are developed by supramolecular chemistry as shown in **Figure 1.1**.[9]

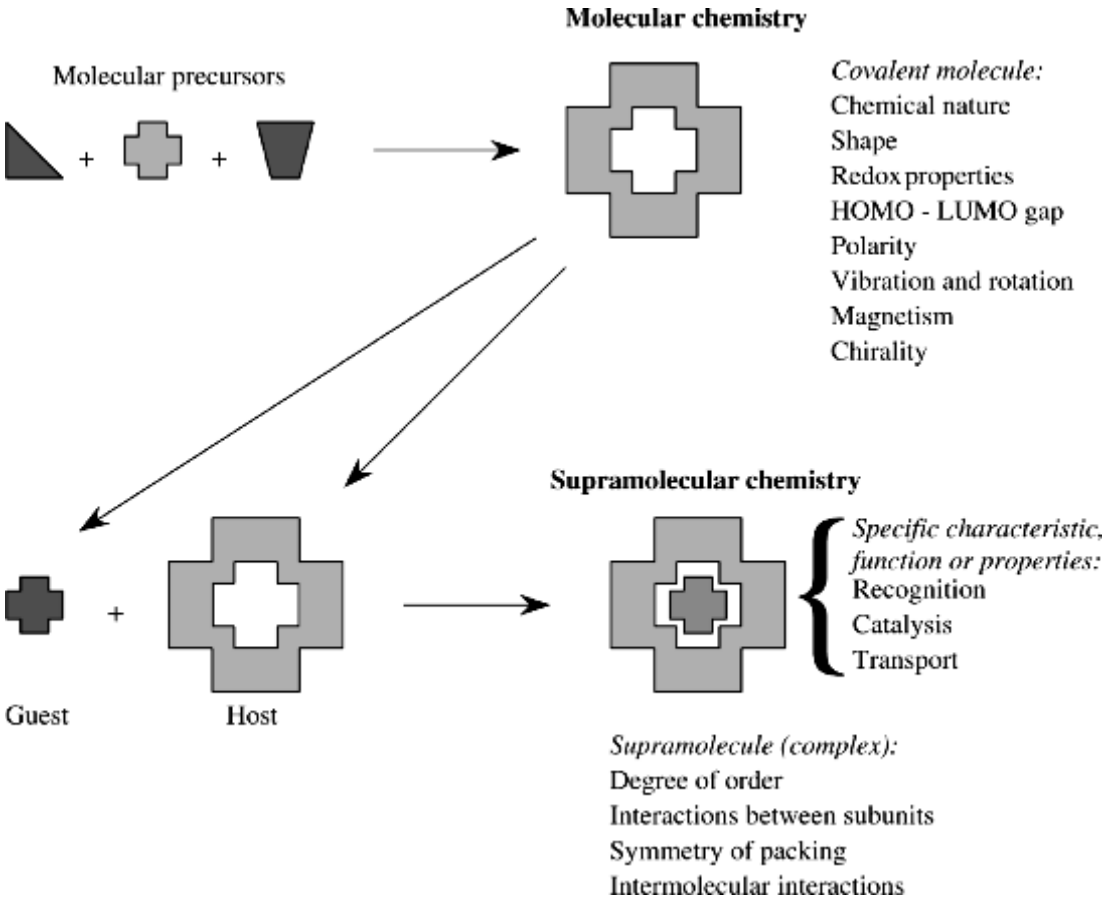

Figure 1.1: Comparison between the scope of molecular and supramolecular chemistry according to Lehn.[9]

1.2 Crystal Engineering

A sub-discipline within supramolecular chemistry is crystal engineering where interactions within crystalline solids and attempts to apply the knowledge gained in the rational design of novel materials are explored.[10]

Crystal engineering can be defined as the design and synthesis of molecular solid-state structures with desired properties, through knowledge of intermolecular interactions and supramolecular synthons.[11, 12]

It is also defined by Desiraju as "the understanding of intermolecular interactions in which the crystal packing context and the utilization of such understanding of the design of new solids having desired physical and chemical properties."[13,14]

The term crystal engineering has advanced rapidly since its initial use in 1971 by Schmidt[11,7] (**Table 1.1**) and relies upon systematic studies of known structures for the examination of recurring patterns of interactions between functional groups as a means of making general prediction about likely structural features.[8] Recurring motifs within functional groups (-COOH and amine) are named supramolecular synthons as illustrated in **Figure 1. 2. 1.**

(a) **(b)**

Figure 1.2.1: **(a)** Supramolecular homosynthon and **(b)** supramolecular heterosynthon.[15]

Table 1.1: Crystal Engineering Time Line.

Year	Event
1921	W. H. Bragg relates the crystal structures of naphthalene and anthracene.
1935	J. D. Bernal advocates the study of groups of crystal structures. The forerunner of crystallographic databases.
1948	H. M. Powell describes the β-hydroquinone structure as a network.
1951	J. M. Robertson's paper on the crystal structures of polynuclear aromatic hydrocarbons.
1954	Crystal structure of the Hofmann complex by J. H. Rayner and H. M Powell.
1955	R. Pepinsky uses the term *crystal engineering*.
1959	R. Feynman's lecture on building a structure from bottom up. There's room at the bottom.
1964 - 1985	G. M. J. Schimdt publishes a series of papers in *Journal of the Chemical Society* on the solid state chemistry of cinnamic acids and other alkenes. The topochemical principle.
1971	Schimdt formally introduces the term *crystal engineering* in his paper in *Pure and Applied Chemistry.*
1970 - 1985	Development of organic solid-state chemistry in the Weizmann Institute (M. D. Cohen, M. Lahav, L. Leiserowitz), University of Illinois (D. Y. Curtin, I. C. Paul), University of Freiburg (G. Wegner) and University of Cambridge (J. M. Thomas).
1977	Crystal structure determination of Prussian Blue by A. Ludi *et al*. published in *Inorganic Chemistry*.
1988	First analysis of an interpenetrated organic solid. O. Ermer's paper in *Journal of the American Chemical Society* on adamantane-1, 3, 5, 7-tetracarboxylic acid.
1989	Robertson revisited. Paper by G. R. Desiraju and A. Gavezzotti entitled from *molecular to crystal structure in Chemical Communications.*
1989	G. R. Desiraju's book *Crystal Engineering*. *The Design of Organic Solids* is published signifying the beginning of modern organic crystal engineering. This is still the only single authored book on the subject.
1990	R. Robson's paper in *Journal of the American Chemical Society* on interpenetrated transition metal coordination compounds. The field of coordination polymers is born.
1990	M. C. Etter identifies the hydrogen bond as an important design element in crystal construction in her review in *Accounts of Chemical Research.*

1991	J. D. Dunitz terms the crystal as a supramolecule par excellence in his paper in *Pure and Applied Chemistry.*
1991	J. D. Wuest introduces the concept of molecular tectonics. This term was originally introduced by N. N. Greenwood in 1984 in the context of polyhedral boron clusters.
1993	Trial of Glaxo's action against Novopharm, a Canada-based generic company, for infringement of one of Glaxo's patents covering the block-buster anti-ulcer drug Zantac. The importance of polymorphism in crystal engineering becomes apparent.
1995	The relationship between crystal engineering and organic synthesis is highlighted in a review by G. R. Desiraju in *Angewandte Chemie.* Supramolecular retrosynthesis is introduced with the term *supramolecular synthon*.
1995	O. M. Yaghi describes selective binding and removal of guest molecules in porous metal organic framework structures. Functional coordination polymers are launched.
1996	The first keynote lectures on crystal engineering in a Congress of the International Union of Crystallography are delivered by A. Gavezzotti and G. R. Desiraju in Seattle.
1996	The first scientific meeting devoted entirely to crystal engineering is organized by M. J. Zaworotko and K. R. Seddon in Nova Scotia.
1998	Crystal engineering becomes a microsymposium topic for the first time in a Congress of the International Union of Crystallography in Glasgow.
1999	The Royal Society launches the journal *CrystEngComm* with D. Braga as the chairman of the editorial board.
2001	The American Chemical Society launches the journal *Crystal Growth & Design* with R. D. Rogers as the editor-in-chief.
2004	M. J. Zaworotko and Ö. Almarsson describe the importance of pharmaceutical co-crystals in a review in *Chemical Communications.*
2004	S. Kitagawa describes third generation coordination polymers in which the cavities in the metal-organic framework structure are responsive to guest shape.
2010	The first Gordon Research Conference in Crystal Engineering is held in New Hampshire.
2011	The first textbook devoted exclusively to crystal engineering is published and is co-authored by G. R. Desiraju, J. J. Vittal and A. Ramanan.

Source: Desiraju. G. R, Vittal. J. J and Ramanan. A. Crystal Engineering: A Textbook. World Scientific Publishing Co. Pte. Ltd. 2011.

1.3 Supramolecular Interactions

In supramolecular chemistry, non-covalent interactions are the energies that hold together supramolecular components. These interactions are considerably weaker than covalent interactions which range between 150 kJ mol^{-1} to 450 kJ mol^{-1} for single bonds.[7, 8]

By contrast, the range at which non-covalent bonds vary is from 2 kJ mol^{-1} for dispersion interactions to 300 $kJmol^{-1}$ for ion-ion interactions. The existence of a stable supramolecular species exists when non-covalent interactions are present. **Table 1.2** describes in detail the term “non-covalent” comprising a wide range of attractions and repulsions.

Table 1.2: Summary of Supramolecular Interactions.[8]

Interaction	**Strength ($kJmol^{-1}$)**	**Example**
Ion-ion	200-300	Tetrabutylammonium chloride
Ion-dipole	50-200	Sodium [15]crown-5
Dipole-dipole	5-50	Acetone
Hydrogen bonding	4-120	Guanine and Cytosine
Cation-π	5-80	K^+ in benzene
π-π	0-50	Benzene and graphite
Van der Waals	< 5 kJ mol^{-1} depending on surface area	Argon; packing in molecular crystals
Hydrophobic	Related to solvent-solvent interaction energy	Inclusion compounds of cyclodextrin

1.3.1 Ion-Ion interactions

Ion-ion interactions are the strongest of these supramolecular interactions.[16] They are non-directional as shown in **Figure 1.3.1**.

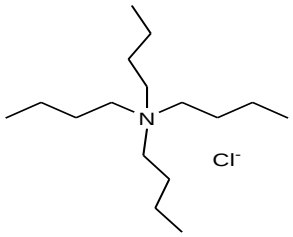

Figure 1.3.1: Illustration of ion-ion interaction in tetrabutylammonium chloride.[8]

1.3.2 Ion-dipole interactions

This type of interaction is seen both in the solid-state and in solution. For example the bonding of ions with polar molecules such as water. The term 'crown ether' is derived from complexes of alkali metal cations with macrocyclic ether. In the crown ether, ether oxygen has lone pairs of electrons that are attracted to positively charged ions.

Ion-dipole interactions are directional and the orientation aspects depend on the two entities which must be aligned such that the interactions occur in the most favourable direction.[7, 8]

1.3.3 Dipole-dipole

Dipole-dipole interactions are the weakest directional interaction and occur when one dipole aligns with a neighbour. The interaction depends on a specific orientation of both components [7, 8] as illustrated in **Figure 1.3.2**.

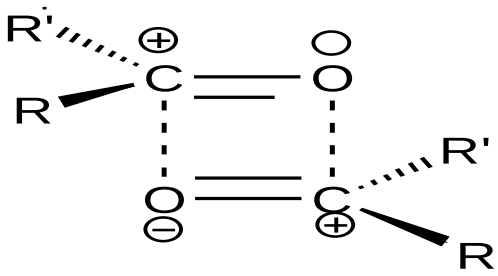

Figure 1.3.2: Dipole-dipole interaction between carbonyl groups.[7]

1.3.4 Hydrogen Bonding

In supramolecular architectures, the most important non-covalent interaction is hydrogen bonding. This kind of non-covalent interaction has good strength and a high degree of directionality.[17] Laurence and Berthelot[18] have described a hydrogen bond as an attractive interaction between a hydrogen bond donor (DH) and the hydrogen bond acceptor in the same molecule or between different molecules.

The hydrogen atom and the attached electronegative atom (oxygen or nitrogen) form a hydrogen bond donor group. This interaction will form a dipole which includes the positively charged hydrogen (the hydrogen carrying a small positive charge is the atom which is chosen to form dipole interaction). Dipoles having electron withdrawing species where the interaction of positively charged hydrogen atoms occurs form hydrogen bond acceptors. There are different types of hydrogen bonding geometries as shown in **Figure 1.3.3**.

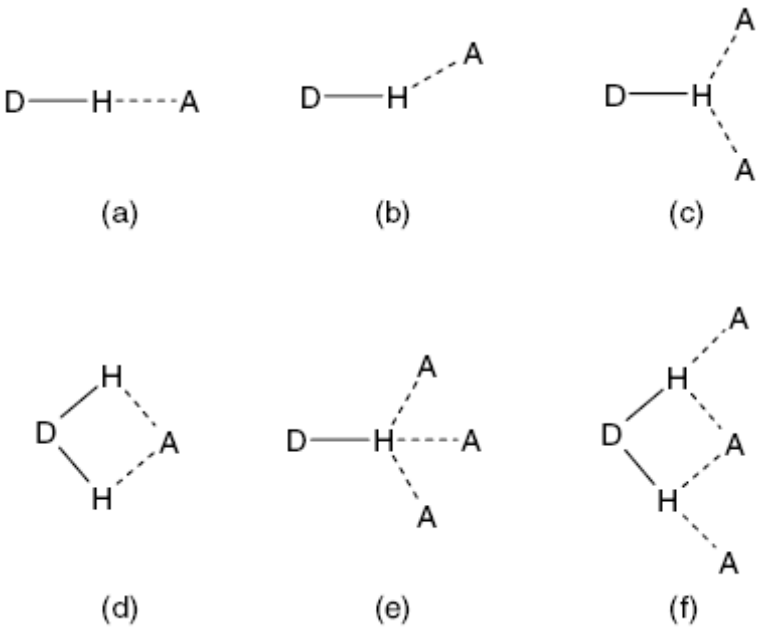

Figure 1.3.3: Illustration of the different types of geometries found in hydrogen bonding: (a) linear (b) bent (c) donating bifurcated (d) accepting bifurcated (e) trifurcated (f) three centre bifurcated.[16, 19]

The hydrogen bond may also be described geometrically by the parameters d, D, θ and r (**Figure 1.3.4**).

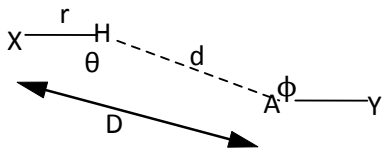

Figure 1.3.4: Hydrogen bond geometry description.[20]

The properties of the donor and acceptor in hydrogen bonding determine the hydrogen bond length, D.[21] Depending on the number of acceptors involved in the hydrogen bond, the distance D will vary. The bigger the number of acceptors, the shorter the D distance.

The influence of charged species on bond lengths illustrated by Taylor *et al* [21] concluded that charged species are formed by shorter bonds. Longer bonds form uncharged groups.

The strength of the hydrogen bond is classified into three important categories.

- **Very strong hydrogen bonds** range from 62.8 to 167.5 kJ mol^{-1}. This interaction is between a conjugate base and its acid or involves a base and its conjugate acid. These bonds affect the crystal packing but their use in crystal engineering is not fully understood.[22]
- **Strong hydrogen bonds**, which are electrostatic interactions, have bond energies ranging from 16.7 – 62.8 kJ mol^{-1}. This interaction has recognisable effects on the crystal packing, control and modulates supramolecular structures and is useful in crystal engineering.
- **Weak hydrogen bonds** have bond energies less than 16.7 kJ mol^{-1}. The electrostatic nature is according to the character of the donor and acceptor groups, which influence dispersive and covalence components. The uses to crystal engineering are not much. This type of interaction has various effects on the crystal packing.[20]

1.3.5 Cation- π interactions

Cation- π interactions occur between a cation and the face of a simple π-system. These interactions deal with positively charged metal ions and are regarded as

electrostatic. There is attraction of the charged metal ion to the negative electrostatic face of the π-system. There is preferred binding of the smaller ions than bigger ions. Ionic radius and binding energy have an association with the effect of ions on the binding strength. The electrostatic effect is the result of the sp^2 carbon. This sp^2 carbon is more electronegative than the hydrogen in the $C^{\delta-}$-$H^{\delta+}$ bond dipoles. **Figure 1.3.5** illustrates a cation binding to benzene, thus giving it a negative charge.

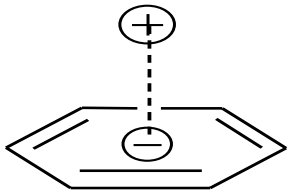

Figure 1.3.5: Illustration of cation-π interactions diagram.[23, 24]

1.3.6 π-π stacking

Interactions such as π -π stacking are weak electrostatic interactions. These interactions occur between aromatic rings with one ring having a poor electron density and the other ring rich in electrons.[7]

Delocalisation of π-electrons is found in these interactions. The aromatic rings involved in the π -π stacking interactions are flat. There are two types of π-π interactions illustrates in **Figure 1.3.6** and **Figure 1.3.7** are face-to-face and edge-to-face.[7, 8]

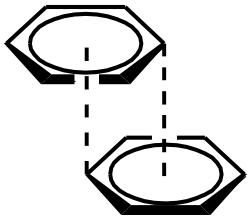

Figure 1.3.6: The off-set face-to-face π-π stacking representation.[7, 8]

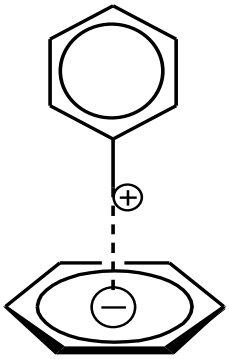

Figure 1.3.7: Representation of the edge-to-face stacking.[7, 8]

Face-to-face interaction having parallel ring systems are often separated by approximately distance of 3.5 Å and slightly offset so that oppositely charged areas of the compound are closest.[25-27]

Edge-to-face interactions have a positively charged hydrogen atom from one ring which interacts in perpendicular orientation with the negative centre of π-electron density of the other ring [25-27] (**Figure 1.3.7**).

1.3.7 van der Waals

van der Waals interactions are dispersive intermolecular forces. [25] They are also named *London interactions*, the *exchange and repulsion interaction*. They arise from fluctuations of the electron clouds of the interacting molecules.

These forces have a limited impact on supramolecular design and are non-directional. Van der Waals strength depends on the polarisability of the molecule and their interactions are important in the formation of inclusion compounds where small organic guests are incorporated in crystal lattices or molecular cavities.[28]

1.4 Co-crystals

There is a debate about the definition of a co-crystal,[29-31] broadly defined as a mixed crystal or crystal that contains two different molecules.[30, 32] It seems that the community at large cannot agree on whether it is “cocrystal” or “co-crystal”, but most agree with the general statement “a co-crystal is a crystalline solid containing multiple components”. Supramolecular chemistry and crystal engineering define a

co-crystal as a consequence of a molecular recognition event between different molecular species.

According to Aakeröy, co-crystals are prepared from reactants that are solids at ambient temperature. He also states that "all hydrates and other solvates are excluded which, in principle, eliminates compounds that are typically classified as clathrates or inclusion compounds (where the guest molecule is a solvent or a gas molecule)".[33]

In 1844, the first entry of a co-crystal was reported by Wöhler, the co-crystal of benzoquinone and hydroquinone. (Ref code: QUIDON, **Figure 1.4.1**).[34]

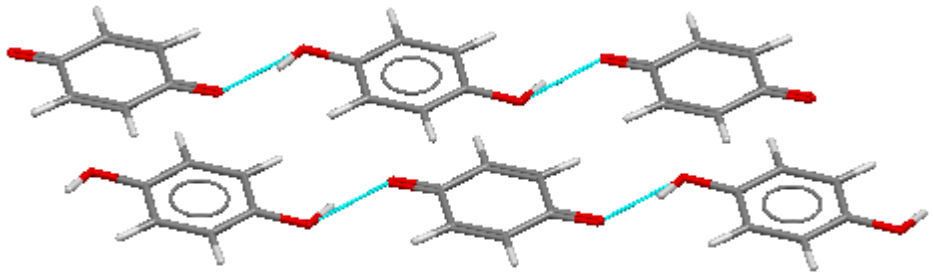

Figure 1.4.1: Crystal structure of the triclinic form of quinhydrone.

These two components were studied as organic molecular compounds [35] and until the 1960's the structural information on co-crystals was absent and the term complexes arose. Different nucleic base complexes [36-39] were reported in the 1960's and the term co-crystal was first used.[40]

A new base pair known as a "Hoogsteen base pair" (**Figure 1.4.2**) which is considered as the first prototypal co-crystal was reported in 1963 by K. Hoogsteen.[36] The term "Hoogsteen base pair" refers to a co-crystal formed between 9-methyladenine and 1-methylthymine obtained by evaporation of an aqueous solution at room temperature (reported during the elucidation of DNA structures).

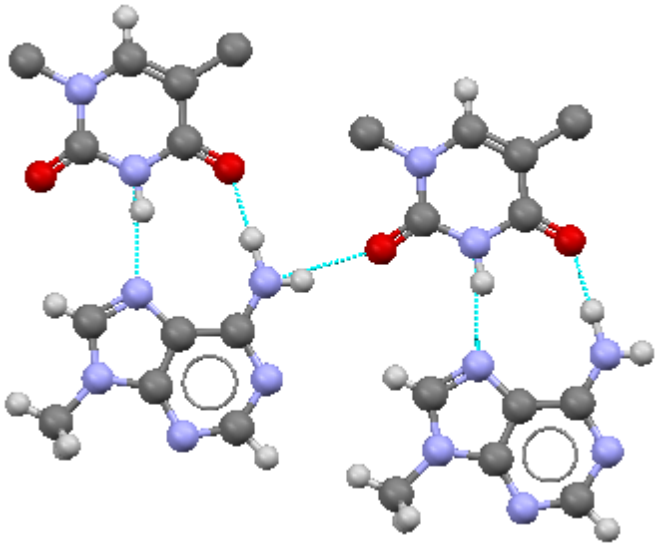

Figure 1.4.2: The Hoogsteen base-pair.

Co–crystals have applications in the pharmaceutical industry.[15] Co–crystallization of pharmaceutically active molecules can enhance the physical properties of the active pharmaceutical ingredient (API) (the substance in a pharmaceutical drug or a pesticide that is biologically active) such as solubity, physical and chemical stability, dissolution rates and hygroscopicity. Co-crystals of poorly soluble drugs are sometimes used to improve the performance of the crystalline drugs solubility and bioavailability.[41] Co–crystals also offer multiple opportunities to modify the chemical and the physical properties of an API without making or breaking covalent bonds.

1.5 Co-crystals and Salts

Pharmaceutical co-crystals (**Figure 1.5.1**) are generally formed between an acid and a base because many drugs are basic in nature.[14] Co-crystals and salts are multicomponent crystals that can be recognised by the position of the proton between an acid and a base. The hydrogen bond (O–H•••N) is the operative interaction in co-crystal formation.

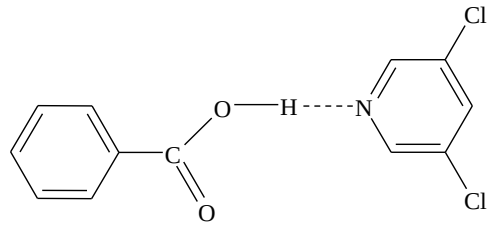

Figure 1.5.1: Co-crystal representation.

When the acidity and the basicity of two compounds are sufficiently different, proton transfer occurs across the hydrogen bond and a charge assisted hydrogen bond of the type O^{-}•••H–N^{+} results.

The difference between a salt and a co-crystal is based on whether proton transfer occurs from an acid (A) to a base (B).[42] A transfer of a proton from an acid to a base results in the formation of a salt (**Figure 1.5.2**): A–H + B → (A^{-}) (B^{+}–H).[41]

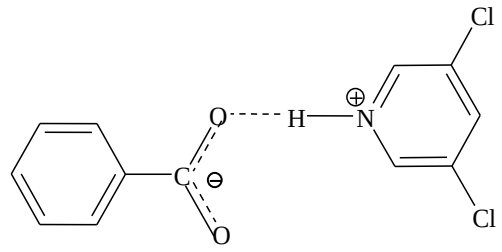

Figure 1.5.2: Representation of a Salt.

Salt formation is dependent on the difference in pK_a values of the two molecules. If the ΔpK_a ($\Delta pK_a = pK_a(base) - pK_a(acid)$) is greater than 2 or 3 a salt is expected.[43,44]

Nangia[45] noted, a smaller Δpk_a (less than 0) will almost exclusively result in co-crystal formation, and when ΔpK_a is between 0 and 3, it is a poor prediction of salt/co-crystal formation.

Co-crystals have two inherent advantages over salts, firstly co-crystal formation may potentially be employed with all active pharmaceutical ingredients (APIs), including acidic, basic and non-ionisable molecules. Secondly there is a large number of potential 'counter molecules' that may be considered to be non-toxic and there may be a possible increase in the scope of the pharmaceutical co-crystallisation over salt forms.[46]

Solution chemistry suggests that a pK_a difference between an acid and a base is needed to form a salt that is stable in water.[47]

Another interesting observation about co-crystals is that they provide a powerful means to tailor the desired solubility and dissolution of APIs, even when the API is a non-ionisable compound.[48]

Co-crystals and salts can also be distinguished by the proton location,[49-51] bond lengths of atoms involved, *eg*. C–O distances of carboxyl groups or phenolic alcohol groups[52,53] and bond angles[54] obtained *via* single crystal X-ray diffraction analysis.

Spectroscopic analysis using infrared (IR) allows detecting the positions of O–H, N–H and COOH signals[43,53,55-64] and allows identifying shifts due to hydrogen bonding.[43,55,62-64]

NMR spectroscopy observes carbon, nitrogen and phosphorus chemical shifts.[60,61,65]

1.6 Nutraceuticals

A nutraceutical can be described as being a medical or nutritional component which is present in food, plant or a naturally occurring material and can be used to improve health by prevention and treatment of diseases.[66]

For many years, food has been used for more than its nutritional value. This term (nutraceutical) was coined in 1976 by Dr. Stephen De Felice,[67] founder and chairman of Foundation of Innovation in Medicine, to describe food or parts of food that can provide medical or health benefits which include prevention and treatment of diseases.[66]

Nutraceuticals have a role in preventing and treating many diseases,[68] such as the common cold, weight problems and even cardiovascular diseases and cancer.[69] Nutraceuticals include a wide range of products such as polyphenols (epigallocatechingallate (EGCG) from tea or resveratrol from red grapes), vitamins, oils from fish and flax, calcium fortified juices, theobromine from the cacao tree, caffeine from coffee leaves.[66]

1.7 Compounds under study

A diet rich in fresh fruit and vegetables is beneficial to our health. Fresh products are rich in various nutrients such as fibre, vitamins, minerals, organic substances and also phenolic compounds. Phenolic compounds are a class of naturally occurring compounds generally synthesized via many pathways.[70-84]

1.7.1 Caffeic acid

Caffeic acid (**Figure 1.7.1**) is key in the biosynthesis of lignin, which is one of the principal source of biomass. This compound has antioxidant effects *in vitro* and might contribute to the prevention of cardiovascular diseases.[85] Caffeic acid is a hydroxycinnamic acid derivative, that is distributed in plant derived food products.[86] Caffeic acid inhibits the production of carcinogenic and mutagenic N-nitrosation compound. [87] The phenolic acid also protects from DNA damages *in vitro*.[88,89]

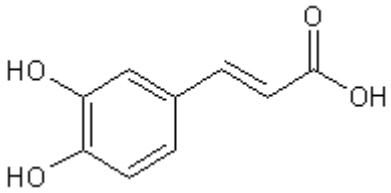

Figure 1.7.1: 3-(3,4-dihydroxyphenyl)-2-propenoic acid.

1.7.2 *p*-coumaric acid

The molecule (**Figure 1.7.2**) is a hydroxy derivative of cinnamic acid,[90] has antioxidant properties and is used in peroxidising lipid systems mediated by metamyoglobin.[91] The demonstration of the antioxidant effects of LDL cholesterol has been shown and it also prevents atherosclerosis.[92] *p*-coumaric acid reduces the risk of having stomach cancer by the reduction of the formation of carcinogenic nitrosamines.[91]

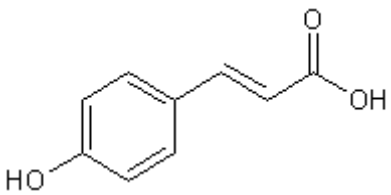

Figure 1.7.2: 3-(4-hydroxyphenyl)-2-propenoic acid.

1.7.3 *trans*-ferulic acid

Ferulic acid (**Figure 1.7.3**) has concentration-dependent antioxidant effects in terms of inhibition of lipid peroxidation and reactive oxygen species.[87] The above compound has shown photoprotective properties of human keratinocytes and helps to prevent damage by ultra-violet (UV) radiation and skin carcinogenisis.[93,94] Ferulic acid effects on the proliferation of neutral stem/progenitor cells (NCS/NPCs) *in vitro* and *in vivo* was studied.[95]

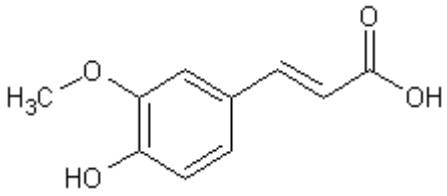

Figure 1.7.3: (*E*)-3-(4-hydroxy-3-methoxyphenyl)prop-2-enoic acid.

1.7.4 Phenylacetic acid

Phenylacetic acid (**Figure 1.7.4**) has been found to be an active auxin (a type of plant hormone),[96] found predominantly in fruits. This compound is an oxidation product of phenethylamine when acted on by the enzyme monoamine oxidase found in humans and many organisms. It is used in some perfumes with a honey-like odour in low concentration, in the production of penicillin G and in the treatment of hyperammonemia.[97]

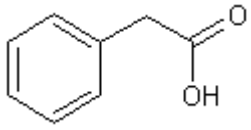

Figure 1.7.4: Phenylacetic acid.

1.7.5 4-Hydroxyphenylacetic acid

The compound shown in **Figure 1.7.5** is found in olive oil [98] and also found in beer in bound form.[99] It has anti-inflammatory activity for the treatment of arthritis, asthma,

Raynaud's disease, inflammatory bowel disorders, trigeminal or herpetic neuralgia, inflammatory eye disorders, psoriasis and have analgesic activity.[100]

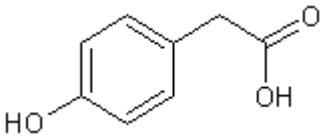

Figure 1.7.5: 4-Hydroxyphenylacetic acid.

1.7.6 3-Chloro-4-Hydroxyphenylacetic acid

3-chloro-4-hydroxyphenylacetic acid (**Figure 1.7.6**) is a synthetic compound used to disrupt auxin influx.[101]

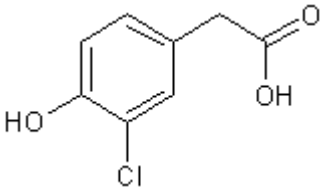

Figure 1.7.6: 3-chloro-4-hydroxyphenylacetic acid.

1.7.7 Vanillic acid

The chemical structure of vanillic acid is shown in **Figure 1.7.7**, which is a benzoic acid derivative used as a flavouring agent. This molecule is oxidized from vanillin produced during the conversion of vanillin to ferulic acid.[102, 103]

Vanillic acid is found in high quantity in roots of *Angelica sinensis* which is a plant used in traditional Chinese medecine.[104] It is one of the natural phenols in argan oil [105] and one of the rich ingredients of açai palm fruit.[106]

This phenolic compound is also found in wine and vinegar[107] and studies have reported that vanillic acid has a hepatoprotective effect,[108] and that mice with dextran sodium sulphate (DSS) induced colitis (inflammatory of the inner lining of the colon) exhibit phenotypical characteristics similar to human acute and chronic UC.[109]

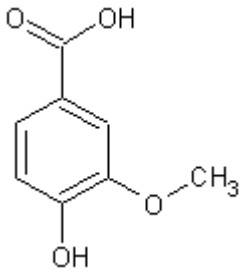

Figure 1.7.7: 4-hydroxy-3-methoxybenzoic acid.

1.7.8 2-Phenylpropionic acid

The compound 2-phenylpropionic acid (**Figure 1.7.8**) is an important group of non-steroidal anti-inflammatory agents.

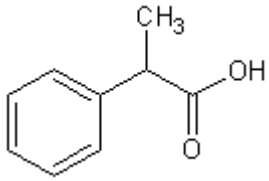

Figure 1.7.8: 2-phenylpropionic acid.

It exhibits optical activity originating from the chiral (asymmetric) centre to which functional group such as –C=O is attached. 2-phenylpropionic acid exists as pairs of stereoisomers. When their optical activity is known these pairs are referred as (+) and (-), but when their absolute configuration is established, they are referred to as *R* and *S* according to the sequence rule (**Figure 1.7.9**).[110]

S- (+) **R- (-)**

Figure 1.7.9: Stereochemical representations of the *R*-(-) and *S*-(+) enantiomers of 2-phenylpropionic acid.

1.7.9 2-Phenylbutyric acid

The molecule shown in **Figure 1.7.10** is a chiral compound with two configurations known as *R* and *S* (**Figure 1.7.11**). It is used as an anticholesteremic. The *S* enantiomer is a chiral building block and a resolving agent.[111,112]

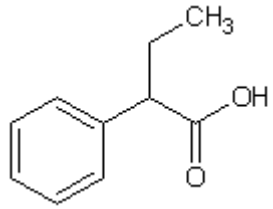

Figure 1.7.10: 2-Phenylbutyric acid

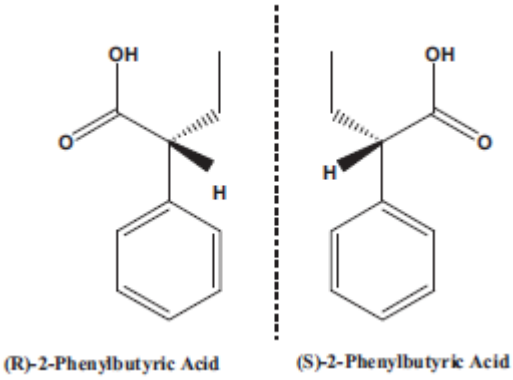

Figure 1.7.11: Stereochemical representations of the *R*-(-) and S-(+) enantiomers of 2-phenylbutyric acid.

1.8 Research Aims

The main objective of this research was to form co-crystals or salts of the selected acids with organic amines or amides and comparisons of the obtained structures were made.

When the acid was chiral, its racemic modification employed and combined with a chiral base with a view to form diastereomeric salts. This would lead to an understanding of the mechanism of enantiomeric resolution.

The study will therefore use small amounts of the chosen compounds and a salt or co-crystal will be obtained depending on their pK_a differences.

To achieve the objectives, minor objectives of this study were to:

- Study the method of preparation of the compounds eg neat grinding, solvent assisted grinding, etc.
- Study the choice of solvent on the resultant product.
- Characterise the compounds and determine their thermal stability.
- Grow suitable crystals for single crystal X-ray diffraction.

The study was performed systematically and the same crystallisation method was used for most of the acid base combinations, and all under the same conditions. Alcohols, ketones and distilled water were chosen as solvents.

REFERENCES

1. Lehn. J. M. *Struct. Bonding*. 1973, 16, 1.
2. Lehn. J. M. *Pure. Appl. Chem*. 1978, 50, 871.
3. Lehn. J. M. *Science*. 1985, 227, 849.
4. Lehn. J. M, Atwood. J. L, Davies. J. E, MacNicol. D. D & Vögtle. F. *Comprehensive Supramolecular Chemistry*. Pergamon: Oxford. 1996.
5. Vögtle. F. *Supramolecular Chemistry*. Wiley & Sons, New York. 1991.
6. Lehn. J. M. *Supramolecular Chemistry: Concepts and Perspectives*. VCH: Weinheim. 1995.
7. Steed. J. W & Atwood. J. L. *Supramolecular Chemistry*. John Wiley & Sons. Chichester. 2000.
8. Steed. J. W, Turner. D. R & Wallace. K. J. *Core Concepts in Supramolecular Chemistry & Nanochemistry*. Singapore: John Wiley & Sons. 2007.
9. Lehn. J. M. *Angew. Chem. Int.* Ed. Engl. (Nobel lecture). 1988, 27, 89-112.
10. Tiekink. E. R. T & Vittal. J. J. *Frontiers in Crystal Engineering*. John Wiley & Sons, Ltd, Chichester, UK. 2006.
11. Schmidt. G. M. *J. Pure. Appl. Chem*. 1971, 27, 647.
12. Brammer. L. *Chem. Soc. Rev*. 2004, 33, 476-489.
13. Desiraju. G. R. *Amsterdam and New York: Elsevier Scientific Publishers*. 1989.
14. Desiraju. G. R, Vittal. J. J & Ramanan. A. *Crystal Engineering: A Textbook*. World Scientific Publishing Co. 2011.
15. Vishweshwer. P, Mc Mahon. J. A, Bis. J & Zaworotko. M. J. *J. Pharm. Sci*. 2006, 95(3), 499-516.
16. Anslyn. E. V & Dougherty. D. A. *Modern Physical Organic Chemistry*, University Sciences Book, Sausalito, CA, USA. 2006, 162-168.
17. Jeffrey. G. A. *Introduction to Hydrogen Bonding*. Oxford University Press, Oxford, UK. 1997.
18. Laurence. C & Berthelot. M. *Perspectives in Drug Discovery & Design*. 2000, 18(1), 36-60.

19. Desiraju. G. R. Hydrogen Bonding. Encyclopaedia of Supramolecular Chemistry (Eds). Atwood. J. L & Steed. J. W, New York, Taylor & Francis. 2004, 1, 658-664.
20. Clyburne. J. A. C, Hamilton. T & Jenkins. H. A. *Cryst. Eng*. 2001, 4, 1-9.
21. Taylor. R & Kennard. O. *Acc. Chem. Res*. 2002, 17, 320-326.
22. Desiraju. G. R. *Chem. Commun*. 1997, 1475 – 1482.
23. Ma. J. C & Dougherty. *Chem. Rev*. 1997, 97, 1303-1324.
24. Dougherty. D. A. Cation-π Interaction. Encyclopaedia of Supramolecular Chemistry (Eds). Atwood. J. l & Steed. J. W. 2004, 1, 214-218.
25. Hunter. C. A, Lawson. K. R, Perkins. J & Urch. C. J. *J. Chem. Soc*, *Perkin Trans*. 2001, 2, 651-669.
26. Dance. I. π-π Interactions: Theory and Scope. Encyclopaedia of Supramolecular Chemistry (Eds). Atwood. J. L & Steed. J. W, New York, Taylor & Francis. 2004, 2, 1076-1092.
27. Hunter. C. A & Sanders. J. K. M. *J. Am. Chem. Soc*. 1990, 112, 5525-5534.
28. Schneider. H. J. Van der Waals Forces. Encyclopaedia of Supramolecular Chemistry (Eds). Steed. J. W & Atwood. J. L, Marcel Dekker, New York, NY, USA. 2004, 2, 1550-1556.
29. Desiraju. G. R. *CrystEngComm*. 2003, 5, 466.
30. Dunitz. J. D. *CrystEngComm*. 2003, 5, 506.
31. Child. S. L, Stahly. G. P & Park. A. *Mol. Pharm*. 2007, 4, 323.
32. Kitaigorodskii. A. I. *Mixed Crystals*. New York, *Springer-Verlag*. 1984.
33. Aakeröy. C. B. *CrystEngComm*. 2003, 5, 439-448.
34. Wöhler. F. *Justus Liebigs Am. Chem*. 1844, 51, 153.
35. Anderson. J. S. *Nature*. 1937, 140, 583-584.

36. Hoogsteen. K. *Acta. Crystallogr*. 1963, 16, 907.

37. Kim. S. H & Rich. A. *J. Mol. Biol*. 1969, 42, 87.

38. Hoogsteen. K. *Acta. Crystallogr*. 1959, 12, 822.

39. O'Brien. E. J. *Acta. Crystallogr*. 1967, 23, 92.

40. Schmidt. J & Snipes. W. *Int. J .Radiat. Biol*. 1967, 13, 101-109.

41. Serajuddin. A. T. M. *Adv. Drug. Del. Rev*. 2007, 59, 603-616.

42. Lide. D. R. CRC *Handbook of Chemistry and Physics*. 81st, CRC Press: Boca Raton. 2000, 2-55.

43. Huang. K. S, Britton. D, Etter. M. C & Byrn. S. R. *J. Mater. Chem*. 1997, 7, 713-720.

44. Stahl. P. H & Wermuth. C. G. *Handbook of Pharmaceutical Salts: Properties, Selection and Use. International Union of Pure and Applied Chemistry*, VHCA: Wiley-VCH: Weinheim, New York. 2002.

45. Bhogala. B. R, Basavoju. S & Nangia. A. *CrystEngComm*. 2005, 7, 551-562.

46. Yadav. A. V, Sthete. A. S, Dake. A. P, Kulkanri. P. V & Sakhare. S. S. *India J .Pharm. Sci*. 2009, 71(4), 359-370.

47. Serajuddin. A. T, Pudipeddi. M, Stahl. P. H & Wermuth. C. G. *Handbook of Pharmaceutical Salts.* Weinheim: Wiley-VCH. 2002, 138.

48. Koji. S, Noriyuki. T, Ryusuke. T, Yoshiki. H & Katsuhide. T. *Pharm. Res.* 2006, 23, 1144-1156.

49. Ratajczak. H & Orville-Thomas. W. J. *Molecular Interactions*. John Wiley, Chichester [Engl], New York. 1980.

50. Lehtonen. O, Hartikainen. J, Rissanen. K, Ikkala. O & Piehla. L. O. *J. Chem. Phys*. 2002, 116, 2417-2424.

51. Steiner. T. *Angew. Chem. Int*. 2002, 41, 49-76.

52. Majerz. I, Malarski. Z & Sobczyk. L. *Chem. Phys. Lett*. 1997, 274, 361-364.

53. Aakeröy. C. B, Hussain. I & Desper. J. *Cryst .Growth. Des*. 2006, 6, 474-480.

54. Bœnigk. D & Mootz. D. *J. Am. Chem. Soc*. 1988, 110, 2135-2139.

55. Hamilton. W. C. *Hydrogen Bonding in Solids: Methods of Molecular Structure Determination*. Benjamin. W. A: New York. 1968.

56. Bellamy. L. J. *The Infra-red Spectra of Complex Molecules*, 2nd ed; Methuen, Wiley: London, New York. 1958.

57. Bellamy. L. J. *The Infra-red Spectra of Complex Molecules,* 2nd ed; Chapman & Hall: London, New York. 1980, 1.

58. Williams. D, H & Fleming. I. *Spectroscopic Methods in Organic Chemistry*, 2nd Ed; McGraw-Hill: London, New York. 1973.

59. Gunnar. A & Zundel. G. *J. Chem. Soc, Faraday Trans. 1.* 1984, 80, 553-561.

60. Etter. M. C & Reutzel. S. M. *J. Am. Chem. Soc*. 1991, 113, 2586-2598.

61. Wojciechowski. G, Ratajczak-Sitarz. M, Katrusiak. A, Schilf. W, Przybylski. P & Brzezinski. B. *J .Mol. Struct*. 2003, 650, 191-199.

62. Johnson. S. L & Rumon. K. A. *J. Phys. Chem*. 1965, 69, 74-86.

63. Aakeröy. C. B, Desper. J & Fasulo. M. E. *CrystEngComm*. 2006, 8, 586-588.

64. Pimentel. G. C & McClellan. A. L. *The Hydrogen Bond*. Freeman. W. H, Reinhold Corp; New York, San Francisco. 1960.

65. Li. Z. J, Abramov. Y, Bordner. J, Leonard. J, Medek. A & Trask. A. V. *J. Am. Chem. Soc*. 2006, 128, 199-210.

66. Lockwood. B. *Nutraceuticals*. Pharmaceutical Press: London, UK. 2007.

67. Mannion. M. *Am. J. Nat. Med*. 1998, 5, 30-33.

68. Espin. J. C, Garcia-Conesa. M. T & Tomās-Barberān. F. A. *Phytochemistry*. 2007, 68, 2986-3008.

69. Jang. M, Cai. L, Udeani. G. O, Slowing. K. V, Thomas. C. F, Beecher. C. W. W, Fong. H. H. S, Farnsworth. N. R, Kinghorn. A. D, Mehta. R. G, Moon. R. C & Pezzuto. J. M. *Sci*. 1997, 275, 218-220.

70. Bruneton. J. *Pharmacognosy, Phytochemistry, Medicinal Plants*, 2nd ed.; Lavoisier: Paris, France. 1999.

71. Cartea. M. E, Francisco. M, Soengas. P & Velasco. P. *Molecules*. 2010**,** *16*, 251-280.

72. Ferretti. G, Bacchetti. T, Belleggia. A & Neri. D. *Molecules*. 2010, *15*, 6993-7005.

73. Sochor. J, Zitka. O, Skutkova. H, Pavlik. D, Babula. P, Krska. B, Horna. A, Adam. V, Provaznik. I & Kizek. R. *Molecules*. 2010, *15*, 6285-6305.

74. Sisa. M, Bonnet. S. L & Ferreira. D. Van der Westhuizen, J. H. *Molecules*. 2010, *15*, 5196-5245.

75. Ghasemzadeh. A, Jaafar. H. Z. E & Rahmat. A. *Molecules*. 2010, *15*, 7907-7922.

76. Kelsey. N. A, Wilkins. H. M & Linseman. D. A. *Molecules*. 2010, *15*, 7792-7814.

77. Rechner. A. R, Wagner. E, Van Buren. L, Van de Put. F, Wiseman. S & Rice-Evans. C. A. *Free Radic. Res.* 2002, *36*, 1127-1135.

78. Gonzalez-Gallego. J, Garcia-Mediavilla. M. V, Sanchez-Campos. S & Tunon. M. J. *Br. J. Nutr.* 2010, *104*, S15-S27.

79. Galleano. M, Pechanova. O & Fraga. C. G. *Curr. Pharm. Biotechnol.* 2010, 11, 837-848.

80. Fang. Z. X & Bhandari. B. *Trends. Food. Sci. Technol .*2010, *21*, 510-523.

81. Michalowicz. J, Duda. W. & Pol. J. Environ. Stud. *Pol. J. Environ. Stud.* 2007, *16*, 347-362.
82. Chen. H. L, Yao. J, Wang. F, Zhou. Y, Chen. K, Zhuang. R. S, Choi. M. M. F. & Zaray. G. *Sci. Total. Environ.* 2010, *408*, 1043-1049.
83. Shadnia. H & Wright. J. S. *Chem. Res. Toxicol.* 2008, *21*, 1197-1204.
84. Lepoittevin. J. P & Benezra. C. *Pharm. Weekblad-Sci. Ed.* 1991, *13*, 119-122.
85. Zhao. Z. H & Moghadasian. M. H. *Phytochem. Rev.* 2010, *9*, 133-145.
86. Clifford. M.N. *J. Sci. Food Agric.* 1999, *79*, 362-372.
87. Kono. Y, Shibata. H, Kodama. Y & Sawa. Y. *Biochem. J.* 1995, *312*, 947-953.
88. Kasai. H, Fukada. S, Yamaizumi. Z, Sugie. S & Mori. H. *Food. Chem. Toxicol.* 2000, 38, 467-471.
89. Shibata. H, Sakamoto. Y, Oka. M & Kono. Y. *Biosci. Biotechnol. Biochem.* 1999, 63, 1295-1297.
90. Utsumi. H, Fujii. K, Irie. H, Furusaki. A & Nitta. I. *Bull. Chem. Soc. Jpn.* 1967, 40, 426-426.
91. Castelluccio. C, Paganga. G, Melikian. N, Bolwell. G. P, Pridham. J, Sampson. J & Riceevans. C. *FEBS. Lett.* 1995, 368, 188-192.
92. Sharma. R. D. *Lipids*. 1979, *14*, 535-540.
93. Bingjiang. L, Wei. M & Dan. L. *J. Invest. Dermatol.* 2010, 130, 796.
94. Zhang. L. W, Al-Suwayeh. S. A, Hsieh. P.W & Fang. J.Y. *Int. J. Pharm.* 2010, 399, 44-51.
95. Yabe. T, Hirahara. H, Harada. N, Ito. N, Nagai. T, Sanagi. T & Yamada. H. *Neuroscience*. 2010, *165*, 515-524.
96. Wightman. F & Lighty. D. L. *Physiologia Plantarum*. 1982, 55(1), 17-24.

97. Adams. R & Tha. A. F. Phenylacetic acid. *Org. Synth*. 2: 59: Coll. 1992, 1, 436.
98. Papadopoulos. G & Boskou. D. *J. Am. Oil. Chem. Soc*. 1991, 68 (9), 669.
99. Nardini. M & Ghiselli. A. *Food. Chem*. 2004, 84, 137-143.
100. Johnson. G, Arbor. A, Mich, Michael F. R & Branford. N. C. Substituted 4-Hydroxyphenylacetic acid Derivatives Having Antiflammatory and Analgesic Activity. United States Patent, Patent number: 5,220,064. Jun. 15, 1993.
101. Laňkovă. M, Smith. R. S, Peŝek. B, Kubeŝ. M, Zazimalovă. E, Petrăsek. J & Hoyerovā. K. *J. Exp. Bot*. 2010, 61(13), 3589-3598.
102. Lesage-Meessen. L, Delattre. M, Haon. M, Thibault. J. F, Ceccaldi. B. C, Brunerie. P & Asther. M. *J. Biotechnol*. 1996, 50, 107-113.
103. Civolani. C, Barghini. P, Roncetti. A. R, Ruzzi. M & Schiesser. A. *Appl. Environ. Microbiol*. 2000, 66, 2311-2317.
104. Duke. J. A. *Handbook of Phytochemical Constituents of GRAS Herbs and other Economic Plants.* 999thed, CRC Press: Boca Raton, FL, USA. 1992.
105. Charrouf. Z & Guillaume. D. *Am.J. Food. Technol*. 2007, 2, 679-683.
106. Pacheco-Palencia. L. A, Mertens-Talcott. S & Talcott. S. T. *J. Argri. Food. Chem*. 2008, 58(12), 4631-4636.
107. Gālvez. M. C, Barroso. C. G & Pérez-Bustamante. J. A. *Zeitschrift für Lebensmitteluntersuhung und-Forshung*. 1994, 199, 1, 29-31.
108. Itoh. A, Isoda. K, Kondoh. M, Kawase. M, Kobayashi. M, Tamesada. M &Yadi. K. *Biol. Pharm. Bull*. 2009, 32, 1215-1219.
109. Okayasu. I, Hatakeyama. S, Yamada. M, Ohkusa. T, Inagaki. Y & Nakaya. R. *Gastroenterology*. 1990, 98, 694-702.
110. Hutt. A. J. & Caldwell, J. *J. Pharm. Pharmacol. 1983, 35,693-704*

111. SIGMA-ALDRICH life science: Where BIO Begins, Products for life science research. 2011-2012, 1419.

112. Yishan. L, Ping. H, Xiao-yan. L, Kaimin. S & Ji-Dong. G. *J. Hazard. Mater*. 2011, 192, 1633-1640.

CHAPTER 2

EXPERIMENTAL METHODS AND MATERIALS

2.1 Materials

2.1.1 Compounds studied

Phenylacetic acid (PAA), 4-hydroxyphenylacetic acid (HPAA), 3-chloro-4-hydroxyphenylacetic acid (CHPAA), vanillic acid (VA), 2-phenylpropionic acid (2-PPA), 2-phenylbutyric acid (2-PBA), *p*-coumaric acid (*p*CA), *t*rans-ferulic acid (*t*FER) and caffeic acid (CFA) are molecules as shown in **Figure 2.1.1** that have functional groups that can hydrogen bond to donor or acceptor compounds. The chosen phenolic acids have functional groups (-COOH) acting as both hydrogen donor and acceptor moieties. Vanillic acid (VA) and *t*rans-ferulic acid (*t*FER) both have ether oxygens which are potential hydrogen bond acceptors. The proton in the selected acids (-COOH) can be transferred to a base to form a salt which result in a charge assisted hydrogen bond.

The physical properties of the chosen compounds and their pK_a values are illustrated in **Table 2.1**.

These phenolic acid molecules were purchased from Sigma Aldrich and have a purity of at least 99%. The compounds were used with no further purification.

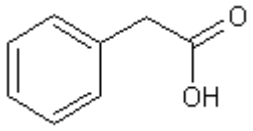

Phenylacetic acid (PAA)

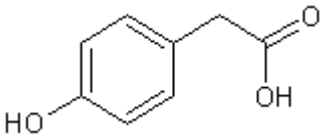

4-Hydroxyphenylacetic acid (HPAA)

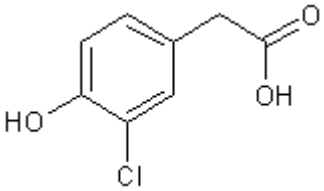

3-Chloro-4-Hydroxyphenylacetic acid (CHPAA)

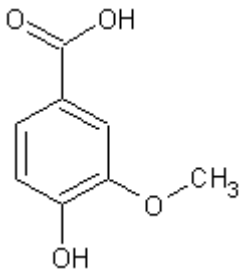

Vanillic acid (VA)

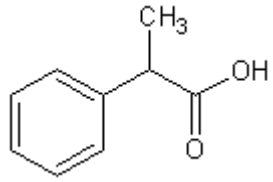

2-Phenylpropionic acid (2-PPA)

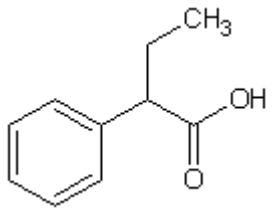

2-Phenylbutyric acid (2-PBA)

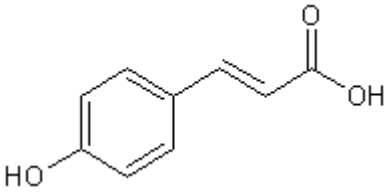

p-Coumaric acid (*p*CA)

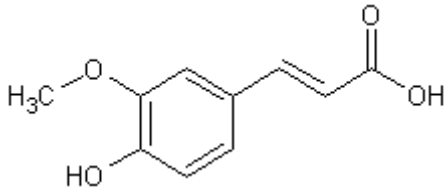

trans-Ferulic acid (*t*FER)

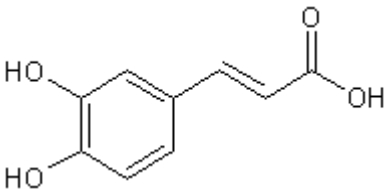

Caffeic acid (CFA)

Figure 2.1.1: Chemical structures of investigated compounds.

Table 2.1: Physical properties of the investigated compounds[1] and their pK_a values.

Compounds	Formula	Mr ($g.mol^{-1}$)	Bp (°C)	Mp (°C)	pK_a
Caffeic acid	$C_9H_8O_4$	180.16		211-213	4.40[2]
p-coumaric acid	$C_9H_8O_3$	164.16		214	4.40
					9.35[2]
trans-Ferulic acid	$C_{10}H_{10}O_4$	194.18		168-172	4.80
					9.40[2]
Phenylacetic acid	$C_8H_8O_2$	136.15		76-77	4.31[3]
4-Hydroxyphenylacetic acid	$C_8H_8O_3$	152.15		148-151	4.50[4]
					10.20[5]
3-Chloro-4-Hydroxyphenylacetic acid	$C_8H_7ClO_3$	186.59		108-110	8.50[5,6]
Vanillic acid	$C_8H_8O_4$	168.14	-	210-213	4.50[7]
Racemic 2-phenylpropionic acid	$C_9H_{10}O_2$	150.17	260-262		4.50[8]
Racemic 2-phenylbutyric acid		164.20	270-272	39-42	4.66[9]

2.1.2 Co-crystal Formers

Acridine (ACRI), caffeine (CAF), cinchonidine (CIND), isonicotinamide (INM), isonicotinic acid (INA), nicotinamide (NAM), quinidine (QUID), quinine (QUIN), theobromine (THBR), theophylline (THPH) and urea (U) were supplied by Sigma Aldrich.

The experimental aim was to use small and large molecules that have the potential to form hydrogen bonds with the phenolic acids listed in **Table 2.1**. Physical properties of the co-crystal formers and their pK_a values are given in **Table 2.2**. The chemical structures of the co-crystal formers are represented in **Figure 2.1.2**. All of the co-crystal formers were used as is without further purification.

Table 2.2: Physical properties of the co-crystal formers studied[1] and their pK_a values.

Compounds	Formula	Mr ($g.mol^{-1}$)	Bp (°C)	Mp (°C)	pK_a
Acridine	$C_{13}H_9N$	179.20	346	107	5.60[10]
Caffeine	$C_8H_{10}N_4O_2$	194.20	178	238	14
					0.6 (amine)[11]
Cinchonidine	$C_{19}H_{22}N_2O$	294.43	464.50	205	4.2(1^{st})
					8.4(2^{nd})[12]
Isonicotinamide	$C_6H_6N_2O$	122.13	334	155-157	14.96
					3.67[13]
Nicotinamide	$C_6H_6N_2O$	122.13	150-160	128-131	0.50[14]
					3.40
Quinidine	$C_{20}H_{24}N_2O_2$	324.42	-	168-172	4.2 (1^{st})
					8.3 (2^{nd})[12]
Quinine	$C_{20}H_{24}N_2O_2$	324.42	-	176	4.2 (1^{st})
					8.8 (2^{nd})[12]
Theobromine	$C_7H_8N_4O_2$	180.16	-	290-295	0.7 (amine)[15]
					8.8
					10.1
					0.1
Theophylline	$C_7H_8N_4O_2$	180.16	454.09 at 760 mmHg	270-274	8.8[15]
					0.7 (amine)
					3.5[16]
Urea	CH_4N_2O	60.06	-	133	0.2[17]

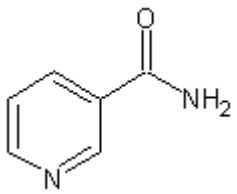

Nicotinamide (NAM)

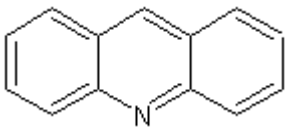

Acridine (ACRI)

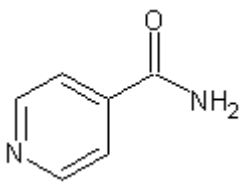

Isonicotinamide (INM)

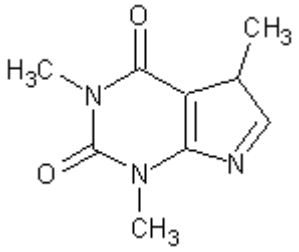

Caffeine (CAF)

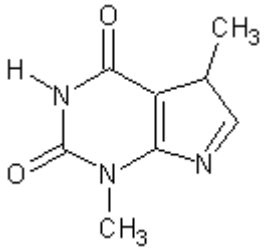

Theobromine (THBR)

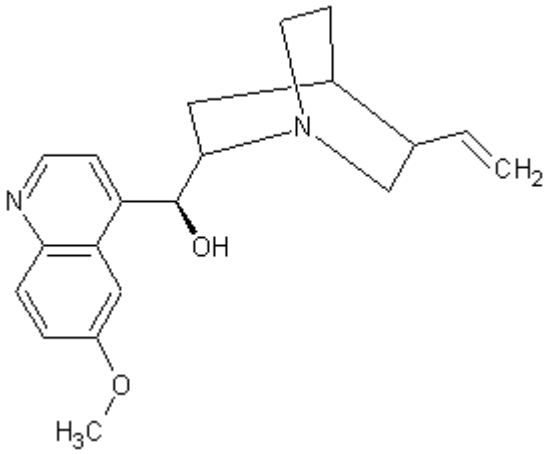

Quinidine (QUID)

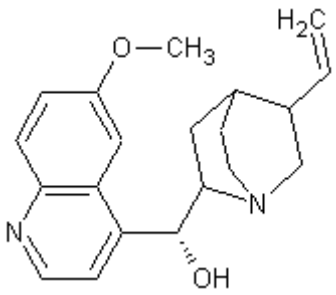

Cinchonidine (CIND)

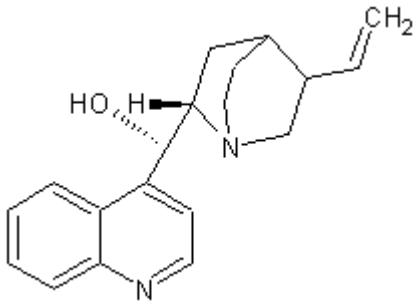

Quinine (QUIN)

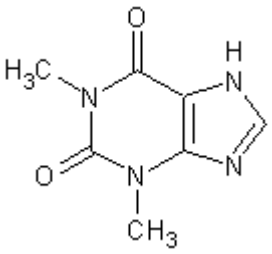

Theophylline (THPH)

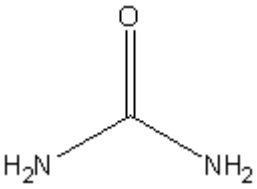

Urea (U)

Figure 2.1.2: Chemical structures of the co-crystal formers.

2.2 Methods

2.2.1 Crystal Growth

The required molar ratios of the solid acid and solid base were dissolved in a suitable solvent, followed by gentle heating on a hot plate. The solvents were allowed to evaporate slowly at ambient temperature. For the liquid bases and acids, both components were mixed in calculated molar ratios with a common solvent. The diluted solutions were left to slowly evaporate at ambient temperature.

2.2.2 Slurry Conversion

Slurry conversion experiments were conducted using different solvents. 5 – 10 ml of solvent was added to the known mixture of acid and base and the resulting suspensions stirred at room temperature overnight. The solid material was filtered and then characterized using PXRD.

2.2.3 Grinding

Molar ratios of the known mixture of acid and base were ground together manually with or without solvent using a mortar and pestle. The resultant product was analysed using PXRD.

2.2.4 Thermal Analysis

Thermal analysis was used to determine the thermal decomposition profiles of the resultant compounds.

- **Differential Scanning Calorimetry (DSC)**

The exposure of the sample and the reference material to a temperature programme and the heat flow was recorded as a function of time or temperature.

Samples (2-5 mg) were removed from their mother liquor, dried with the filter paper then crushed and analysed by heating at a constant rate of 10 K/min with a nitrogen gas flow rate of 20 mL/min. The DSC curves indicated thermal events such as desolvation, phase transformations and melting.

The resultant thermal events were either endothermic (positive peaks) or exothermic (negative peaks). This method uses two identical 50 μl crimped and vented aluminium pans, one containing a sample and the other is empty and used as a reference. DSC runs were performed using a Perkin-Elmer DSC6 instrument.

- **Thermogravimetry (TGA)**

Thermogravimetric analysis is used to study the chemical change in the co-crystal/salt; this is done via measurement of the sample weight as a function of temperature or time. A curve resulting from the TGA analysis is referred to as a mass loss curve, exception is made in the case where the sample reacts with the atmosphere, eg: oxidation. A number of events such as decomposition stages and fractional weight loss can be evaluated by TGA curves.[18]

In TGA (using a Perkin-Elmer PC6-series) analysis, samples were scooped out of the mother liquor, dried, crushed, weighed and analysed. These samples were heated at a constant rate typically 10 K/min resulting in a mass loss as a function of temperature measurement as the compound degrades. Nitrogen is used as an inert gas with a flow rate of 20 mL/min. Measurements were taken from 303-573 K.

2.2.5 Hot Stage Microscopy (HSM)

A transmitted light microscope, MEIJI TECHNO EMZ-8TR, was used to observe the crystals; the images were recorded with a CANON DS126191 camera. A platinum hot stage (T_{MAX}: 400°C) was provided with the microscope and a temperature controller LINKAM TMS 94 allowing the analysis of the morphology of the samples as function of temperature, using a controlled heating rate.

Most of the co-crystals/salts/hydrates obtained were analysed. The temperature program used was the same as that used for the DSC. Silicone oil was used to cover the crystals during the experiment and allow for the observation of bubbling.

However, since the temperature measuring device was not as close to the sample as in the DSC, the temperature associated with the thermal event (e.g. the melting of the crystals) was typically 10-20°C higher than the temperature registered in the DSC. Also for the HSPOM experiments whole crystals were placed on the heating

stage whereas for the TG/DSC measurements crushed crystals were used. This also affected the onset temperatures observed for the thermal events. The experiments were performed at ambient conditions because no nitrogen purge was available.

2.2.6 Single Crystal X-ray Diffraction

X-ray diffraction is a non-destructive analytical technique that determines the crystal and molecular structure of molecules. Information such as unit cell dimensions, details of site-ordering, bond-lengths and bond-angles in the molecule are obtained from this technique. In order to solve the crystal structure, data obtained from X-ray analysis have to be refined and interpreted.[19]

Single crystals of good quality and suitable size were selected for single crystal X – ray diffraction for the determination of the crystal structure. This part of the experiment was completed at the University of Cape Town. The structure solution was completed at the Cape Peninsula University of Technology.

SHELXS-97[20] was the computer programme used to solve structures. These were run on a graphical user interface, X-SEED.[21] SHELXL-97[22] was utilised for the refinement of the structures and uses full-matrix least-squares for the minimisation of the function $\sum w\left(F_0^2 - kF_c^2\right)^2$. The residual R is the link agreement between the observed F_0 and the calculated F_c structure factors. The indirect measurement of the accuracy of the structure is the residual R and must be in lower value if the model is satisfactory. R_1 (residual index) is the agreement between the observed and the calculated structure factors based on F (Eq. 1) and wR_2 (residual index) is the agreement based on F^2, (Eq. 2).

Equation 1: $$R_1 = \frac{\sum \left| |F_0| - |F_c| \right|}{\sum |F_0|} \qquad \text{Eq. 1}$$

$$wR = \sqrt{\frac{\sum w\left(F_0^2 - F_c^2\right)^2}{\sum w\left(F_0^2\right)^2}} \qquad \text{Eq. 2}$$

Where w is the weight allocated to the structure factor during the refinement.

$$w = \frac{1}{\sigma^2 F_0^2 + (aP)^2 + bP} \qquad \text{Eq. 3}$$

$$\text{Where } P = \frac{\max(0, F_0^2) + 2F_c^2}{3} \qquad \text{Eq. 4}$$

While a and b were also refined for each structure.

S (goodness of fit) was obtained for all the structures and is dependent on F^2, see Eq. 5.

$$S = \left(\frac{\sum w (F_0^2 - F_c^2)^2}{n - P} \right)^{\frac{1}{2}} \qquad \text{Eq.5}$$

Where n can be defined as the number of reflections and p as the total number of parameters refined.

Unit cell parameters were determined from intensity data measured on a Bruker DUO APEX II[23, 24] or Nonius Kappa CCD[25] diffractometer using graphite-monochromated Mo-Kα radiation of a wavelength of 0.7107 Å. The data was scaled and reduced using the DENZO-SMN[26] program for Nonius Kappa CCD. For the Bruker APEX 2, the cell refinement and data reduction was achieved by using program SAINT.[27] Hydrogen atoms (not hydroxyl or amine) in the crystal structures were placed and refined isotropically.

2.2.7 Powder X-ray Diffraction

The PXRD method was used for the identification of new phases and compounds as each compound shows a unique PXRD pattern due to its structural features. Unit cell dimensions[28] can also be obtained from PXRD.

Samples were powdered manually and the sample was placed in a sample holder in the path of the X-ray beam. A D2 PHASER Bruker diffractometer with Cu-Kα radiation (1.54184 Å) was the instrument which measured the PXRD patterns of the

obtained products. The voltage tube and current were at 30 kV and 10 mA max, respectively with a scintillation counter, 1-dim LYNXEYE, Xflash detector. The samples were each scanned between 4-50° 2θ.

The experimental powder patterns were compared to both the PXRDs of the physical mixtures of the components and to the calculated patterns (generated from known structures using LAZYPULVERIX.[29]

2.2.8 Non-Isothermal Kinetics

Activation energies (E_a) were obtained while kinetic studies were performed during the releasing of the solvent from the new compounds.

$$H{\cdot}G_{(s)} \rightarrow H_{(s)} + nG\uparrow$$

Kinetics of desolvation were investigated non-isothermally using a thermogravimetric technique.[30]

Crushed crystals were used for the kinetic studies.

The TGA rate can be obtained by the equation $dC/dT = A / \beta\, f(C)\, e^{-Ea/RT}$ Eq.6

Where: C is the mass loss of the sample

β is the heating rate

Equation 6 can be reduced to $d \log \beta/d (1/T) = (0.457/ R) E_a$ Eq.7

The curves obtained were analysed by plotting $-\log \beta$ vs T^{-1}

Where T is the absolute temperature. A straight line with a slope: $-(0.457E_a)/R$ was obtained.

2.2.9 Infrared (IR) Spectroscopy

Fourier transform (FT) infrared spectra were gathered using a Perkin Elmer, FT-IR spectrum 1000 spectrometer in a dispersive mode with potassium bromide discs. The disc consists of 1mg of the sample with 250 mg of potassium bromide.

One of the important advantages of this technique is that samples can be analysed in any state.[31] The vibrations of the atoms in the molecule are the main interaction in which the infrared depends on, and their frequencies are characteristic of the functional groups.

The spectra obtained were recorded in the range of 440 – 4400 cm^{-1} at 2 cm^{-1} spectral resolution. The IR instrument version used was SPECTRUM V.5.3.1.

2.2.10 Selectivity Experiments

Two component competition experiments classified as competition between two base compounds were carried out on selected acid/base systems. These experiments were done using quinine and quinidine as base compounds and phenylacetic acid (PAA) and 4-hydroxyphenylacetic acid (HPAA) as the selected phenolic acids. Two experiments were performed, one where the QUIN: QUID: phenolic acid ratio = 1: 1 :1 and another with the QUIN: QUID: phenolic acid ratio = 1: 1: 2.

2.2 11 Computing Components

- Layer[32]: the intensity data of the crystal can be displayed as the simulated precession photographs of the reciprocal lattice levels and the investigation of the systematic absences which occur is allowed.
- Lazy Pulverix[29]: This software calculates the theoretical powder X-ray diffraction pattern from single crystal X-ray diffraction data.
- Section[33]: gives a graphical interpretation of the packing in the crystal structure by effectively cutting slices through the unit cell. Here, the guest molecules can be removed and the host shown with its van der Waals radii so that channels or cavities can be studied.
- PovRay[34]: renders graphics for structures.
- POVLabel[35]: a component of X-SEED used to edit the atomic labels of POV-Ray images.

- Xprep[36]: processing of Bruker diffraction data. SHELX input files can be set up and the space group determined.
- PLATON[37]: the structure molecular parameters are calculated by this software.
- MsRoll[38]: the program is utilised for the calculation of the void spaces in the structure and can calculate the solvent volume.
- ConQuest [39]: exploration of the Cambridge Structural Database for compound information.

REFERENCES

1. Windholz. M. Ed. The Merck Index: An Encyclopaedia for chemicals and drugs, Merck & Co. Inc., New Jersey. 1976.
2. Conners. K. A & Lipari. J. M. *J. Pharm. Sci*. 1976, 65, 380.
3. Dippy. J. F. J, Hughes. S. R.C, Rozanski. A. *J. Chem. Soc*. 1959, 2492-2498.
4. Qian Tao, Jia-Mei, Lei Ma & Tong-Bulu. *Cryst. Growth Des*. 2012, 12, 3144-3152.
5. Kemp. L. R, Dunstan. M. S, Fisher. K, Warwicker. J & Leys. D. *Phil. Trans. R Soc B 368*. 2012O323. 2013.
6. Mazon. H, Gábor. K, Ley. D, Heck. A. J. R, Van der Oost. J & Van der Heuvel. R. H. H. *J. Biol. Chem*. 2007, 282(15), 11281-11290.
7. Washburn. E. W (Ed in Chief). *International Critical Tables*. New York, McGraw-Hill. 1929, 57, 335.
8. Dahab. A. A, Smith. N. W. *J. Encapsulation Adsorpt Sci*. 2012, 2, 48-59.
9. Yuichiro. A & Motoo. H. *Preparation of 2-phenylbutyric acids*. Jpn. Kokai Tokyo Koho. 1998, 4.
10. Brown. H. C, Baude. E. A & Nachod. F. C. *Determination of Organic Structures by Physical Methods.* Academic Press, New York. 1955.
11. Martin. A. N, *et al*. Physical Pharmacy ed. 2 p. 194, Philadelphia, Lea & Febiger. 1969.
12. Perrin. D. D. *Dissociation Constants of Organic Bases*. London, Butterworths. 1965.
13. Sikorski. A & Trzybiński. D. *Tetrahedron Letters.* 2013, 54, 1463-1466.
14. Gressel. P. D & Galleli. S. F. *J. Pharm*. Sci. 1968, 57, 335.
15. Ballard. B. B & Nelson. E. *J. Pharmacol. Exp. Ther.* 1962, 135, 120.
16. Wiseman. E. H, Schreiber. E. C & Pinson. R. *Biochem. Pharmacol*. 1964, 13, 1421-1435.
17. McLean. W.M, Poland. D.M, Cohen. M.S, Penzotti. S. C & Mattocks. A. M. *J. Pharm. Sci*. 1967, 56, 1614-1621.
18. Haines. P. J. *Thermal Methods of Analysis*. Blackie Academic & Professional, London. 1995.
19. Brown. P. J. & Forsyth. J. B. *The crystal structure of solids*. Edward Arnold Limited, London.1973.

20. Sheldrick. G. M. A short history of SHELX, *Acta. Crystallogr.* Sect *A*: 112-122. 2008.
21. Barbour. L. J. X-Seed, graphical interface for SHELX program, *J. Supramol. Chem*. 2003, 1, 189.
22. Sheldrick. G. M. *Program for Crystal Structure Determination*. University of Göttingen, Germany. 1997.
23. APEX 2 v1.0-27, Bruker AXS Inc. Madison, Wisconsin, USA. 2005.
24. SAINT-Plus Version 7.12, Bruker AXS Inc. Madison, Wisconsin, USA. 2004.
25. COLLECT data collection software. Nonius, Delft, The Netherlands. 1998.
26. Otwinowski. Z & Minor. W, Inc: Carter. W. Jr., sweet RM (eds). Methods in enzymology macromolecular crystallography, part A, vol 276. Academic Press, New York. 1997, 307.
27. Program SAINT, (2006), Version 7,60a, Bruker AXS Inc., Madison, WI, USA.
28. Karki. S, Fábián. L, Friščić. T & Jones. W. Powder X-ray Diffraction as an Emerging Method to Structurally Characterize Organic Solids, *Organic* Letters. 2007, 9, 3133-3136
29. Yvon. K.: Jeitschko. W. Parthe, E. *Appl. Crystallogr.* 1977, Vol.10. 73-74.
30. Flynn. J. H.: Wall. L. *A.* J. *Polym. Sci; Part B: Polym. Lett.* 1966,4323.
31. Stuart. B, George. B & McIntyre. P. Modern Infrared Spectroscopy, John Wiley & Sons, NewYork, USA. 1996.
32. Barbour. L. J. LAYER: A computer program for the graphic display of intensity data as simulated precession photographs: *Appl. Crystallogr.* 1999, 32, 351.
33. Barbour. L. J. SECTION: A computer program for the graphic display of cross sections through a unit cell: *J. Appl. Crystallogr.* 1999, 32, 353.
34. PoV-Ray for Windows: Version 3.le.watcom.win32: The persistence of Vision Development Team: © 1991-1999.
35. Barbour. L. J. X-Seed - A Software Tool for Supramolecular Crystallography, *J. Supramol. Chem*. 2001, 1, 189-191.
36. XPREP: Data Preparation & Reciprocal Space Group Exploration: Version 5. IINT: © 1997: Bruker Analytical X-ray Systems.
37. Spek. A. L. PLATON: A multipurpose crystallographic tool: Version 10500: e 1980-2000.
38. Connolly. M. L. The molecular surface package. *J. Mol. Graphics*. 1993, 11, 139 –141.

39. Allen. F.H. *Acta. Crystallogr*. 2002, B58, 380 - 388.

CHAPTER 3

VANILLIC ACID CO-CRYSTALS AND CO-CRYSTAL HYDRATES

According to the Cambridge Structural Database (CSD, version 5.34, November 2012),[1] the compound vanillic acid (VA) was found to form a co-crystal with pyrazine-2-carboxamide[2] and ethenzamide.[3] In this research, vanillic acid has been numbered as shown in **Figure 3.1**. In cases where there are two vanillic acid molecules in the asymmetric unit a suffix A was used for the parent C and O atoms as shown in **Figure 3.2**.

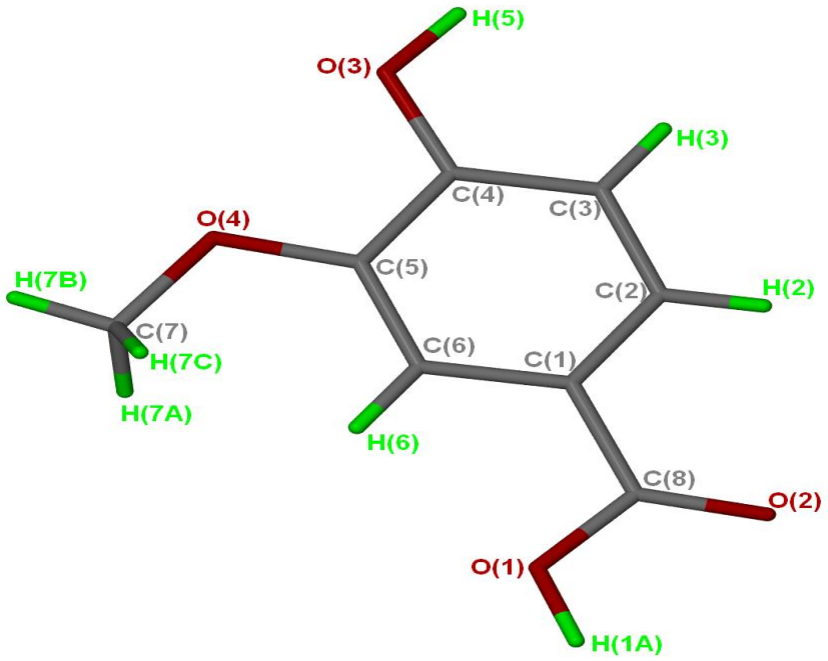

Figure 3.1: Numbering scheme of vanillic acid molecule.

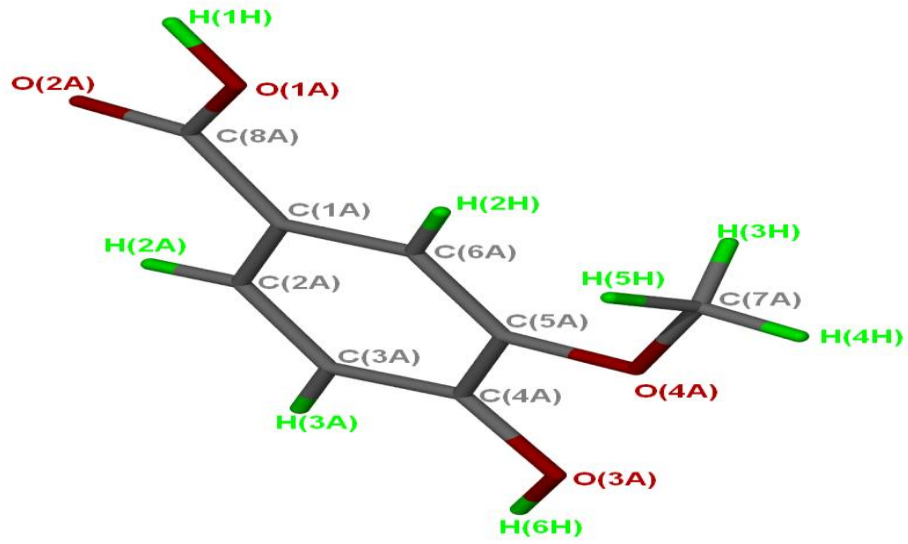

Figure 3.2: Numbering of the second vanillic acid molecule when forming a 2: 1 (vanillic acid: co-crystal former) ratio.

Vanillic acid has various functional groups (-COOH, -OH and $–OCH_3$) capable of forming hydrogen bonds. In this study vanillic acid formed co-crystals and co-crystal hydrates with acridine (ACRI), caffeine (CAF), isonicotinamide (INM), nicotinamide (NAM), theobromine (THBR), theophylline (THPH) and urea (U).

3.1 Vanillic acid and acridine (VA•ACRI)

Acridine, $C_{13}H_9N$ is a heterocyclic molecule derived from anthracene by replacement of one meso-CH group by nitrogen.[4]

The vanillic acid acridine co-crystal shown in **Figure 3.1.1** was obtained by dissolving a 1:1 ratio of both components in diethyl ether. The concentrated solution was left to crystallize by slow evaporation at ambient temperature. This acid-base combination resulted in a co-crystal not a salt due to the ΔpK_a (pK_a (base) – pK_a (acid)) = (5.60[5] – 4.50[6]) = 1.1. It is generally accepted that reaction of an acid with a base will be expected to form a salt if the ΔpK_a (ΔpK_a = pK_a (base) - pK_a (acid)) is greater than 2 or 3.[7 - 10]

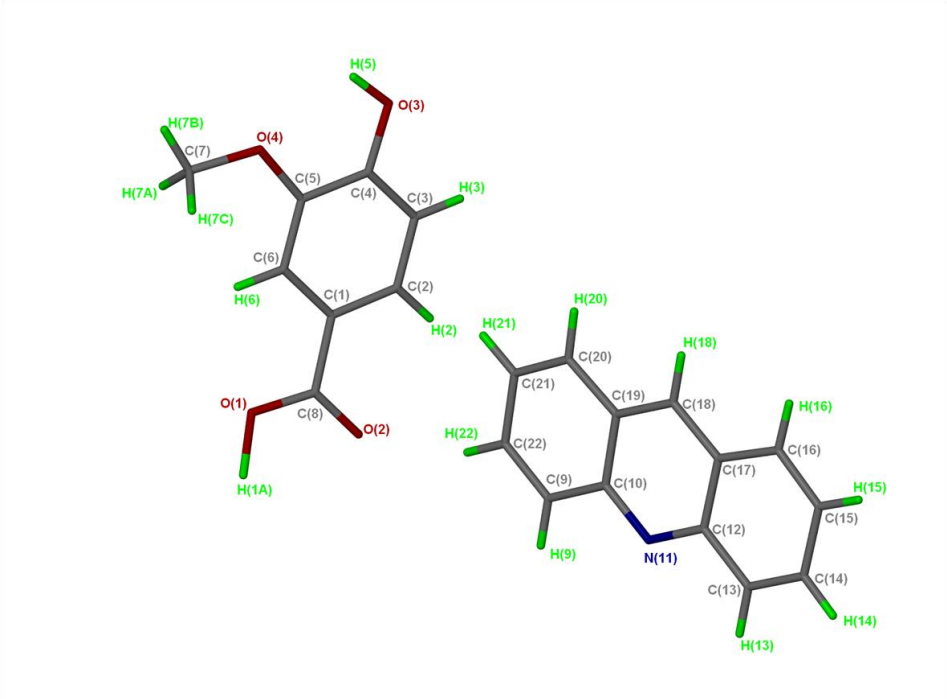

Figure 3.1.1: Asymmetric unit for the **VA•ACRI** structure with all the hydrogen atoms shown for numbering clarity.

3.1.1 Thermal Analysis

Thermal analysis data for the **VA•ACRI** co-crystal are given in **Table 3.1** and the DSC results are shown in **Figure 3.1.2**. The melting point of the **VA•ACRI** co-crystal was found to be higher than the melting point of acridine and lower than the melting point of vanillic acid.

Table 3.1: Thermal analysis data for **VA•ACRI**.

Compounds	**DSC Endo$_1$(T_{onset},K)**	**DSC Endo$_2$(T_{onset},K)**
Acridine	363.5	375.8
Vanillic acid	-	482.3
VA•ACRI	-	438.7

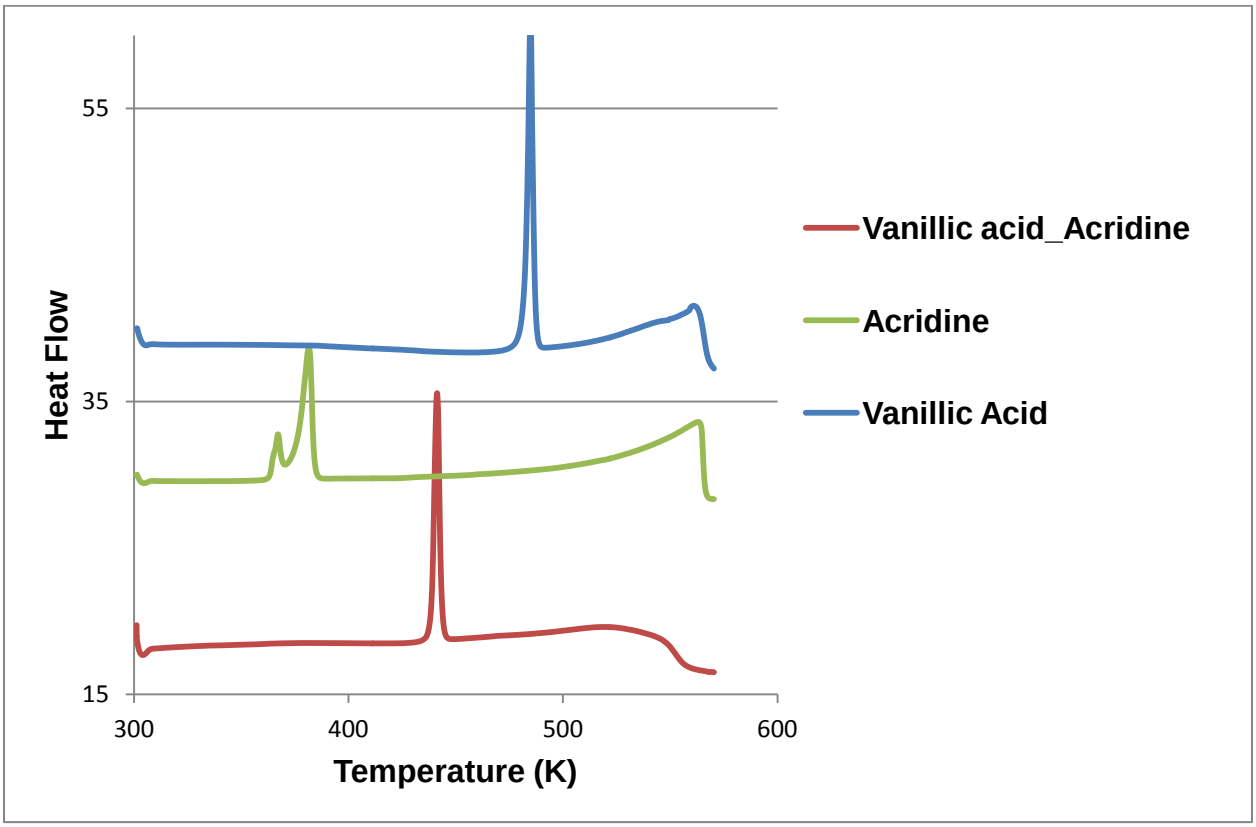

Figure 3.1.2: DSC curves of vanillic acid (blue), acridine (green) and **VA•ACRI** (red).

3.1.2 Hot Stage Microscopy

The crystal was immersed in silicone oil and the crystal was monitored over a temperature range starting at 303 K. At 435 K crystal opacity is observed. However, the crystal started melting at 440 K and the entire crystal had melted at 460 K. The melting process of the crystal is shown in **Figure 3.1.3**.

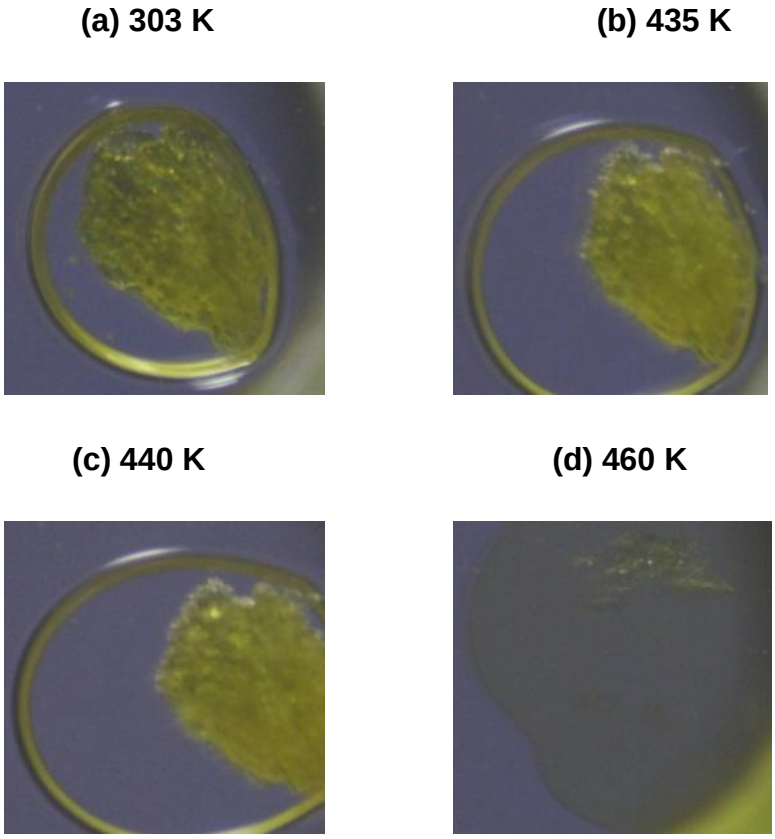

Figure 3.1.3: HSM photography of **VA•ACRI (a)** crystal immersed in silicone oil, **(b)** opacity of the crystal, **(c)** melting of the crystal and **(d)** crystal completely melts.

3.1.3 IR Spectroscopy

The co-crystal **VA•ACRI** was characterized using FT-infrared spectroscopy. IR positions and assignments are given in **Table 3.2**; the spectra of vanillic acid, acridine and the co-crystal are shown in **Figure 3.1.4**.

The spectra of the **VA•ACRI** confirmed that there is no new band within the range 1550-1650 cm^{-1} (νC-O of COO^-) which indicates that no proton has been transferred.[2] There is a shift of the COOH wavenumber of the **VA•ACRI** (1733 cm^{-1}) which is 30 cm^{-1} less than the corresponding band of the vanillic acid (1763 cm^{-1}) indicating the participation of the hydrogen bonding in the co-crystal. A formation of a hydrogen bond, D-H···A will cause the COOH peak to shift to a lower wavenumber.[11] The free OH stretch (sharp

peak) in vanillic acid is observed at 3480 cm^{-1}, whereby the hydrogen bonded OH in the **VA•ACRI** co-crystal is obtained at 3190 cm^{-1} which is broader than the free OH stretch.

Table 3.2: IR positions and assignments for the peaks in VA, **VA•ACRI** and ACRI.

VA	**VA•ACRI**	ACRI	Proposed assignment
3480	-	-	Free OH stretch
3099, 2988	3190, 2970	-	Combination: OH and C-H stretch
-	3056	3051	Aromatic ring stretch
1866	-	2285, 1815	Overtone or combination bands
1763, 1667	1733, 1647	-	C=O
1599, 1524, 1478, 1454	1593,1512, 1462	1617,1461, 1437	C=C stretch
1275, 1202	1230, 1186	-	C-O stretch

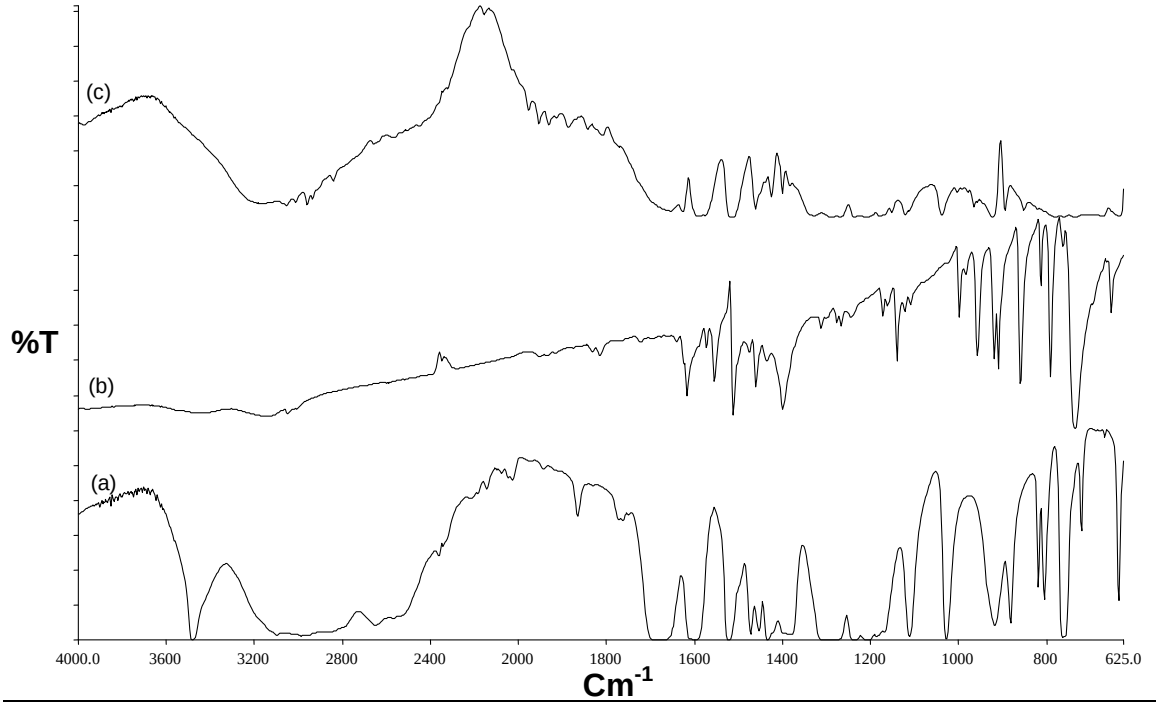

Figure 3.1.4: IR spectrums (a) vanillic acid, (b) acridine and (c) **VA•ACRI**.

3.1.4 Powder X-ray Diffraction

Vanillic acid and acridine were ground in a 1:1 ratio for 30 min and the powder X-ray diffraction (PXRD) spectrum was compared to that of the physical mixture and the calculated PXRD of the **VA•ACRI** obtained from LAZYPULVERIX.[12] The PXRD pattern from the grinding experiment did not match the calculated and the physical mixture patterns. The calculated and the physical mixture PXRD patterns each had a peak at 2θ (approximately 7.83) for the calculated and at 2θ (approximately 7.27) for the physical mixture) at the beginning of their spectrum. These peaks are missing in the ground product PXRD pattern.

However, a slurry conversion experiment of a 1:1 ratio of both components in diethyl ether was in good agreement with the PXRD pattern of the calculated crystal structure (**VA•ACRI**). However, the height of the peak around 2θ (approximately 7.15) in the slurry conversion is very small compare to the one in the calculated pattern (2θ approximately 7.83).

The PXRD patterns of all the experiments utilized to characterize the co-crystal are shown in **Figure 3.1.5**.

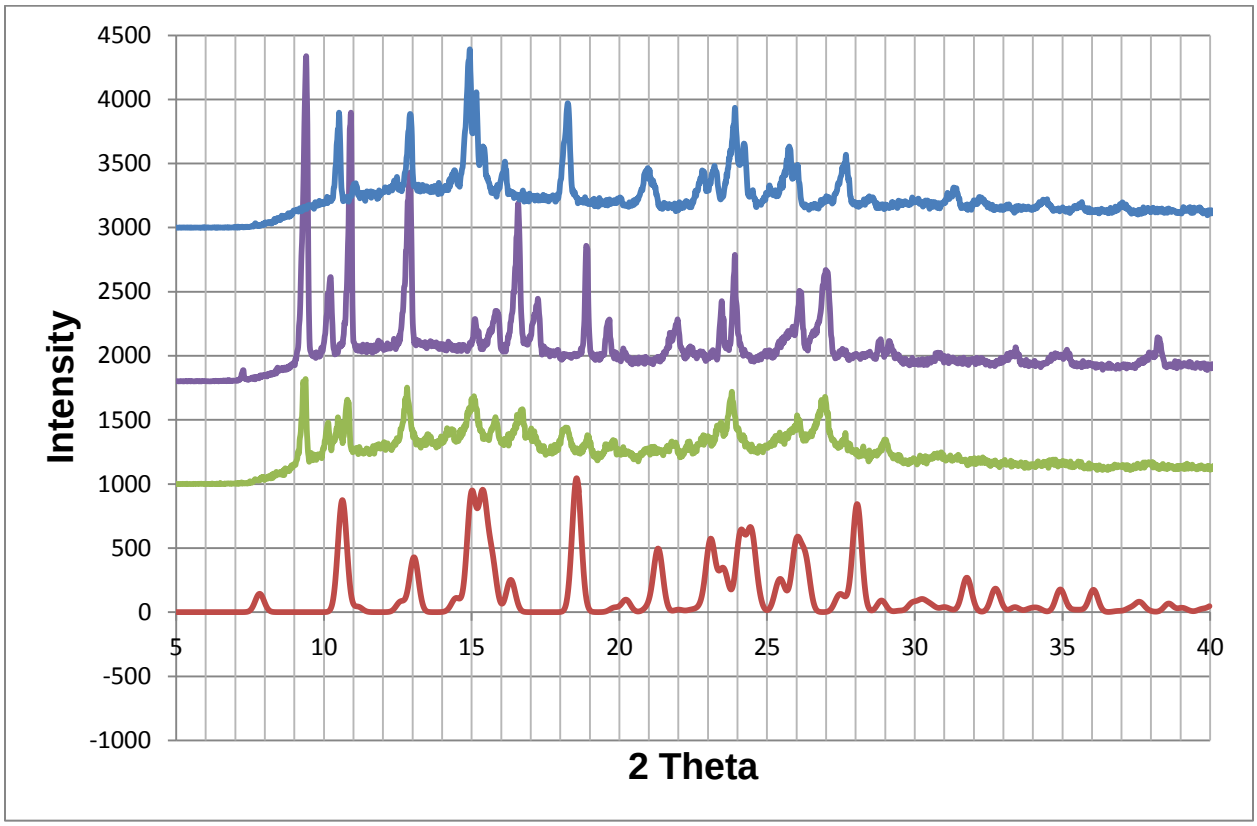

Figure 3.1.5: PXRD patterns of **VA•ACRI** (red), ground product (green), physical mixture (purple) and slurry (blue).

3.1.5 Structure Determination

All the non-hydrogen atoms were found by direct methods and refined anisotropically. The hydrogen atoms involved in hydrogen bonding were located in the difference electron density map. The crystal data of **VA•ACRI** is reported in **Table 3.3**. The vanillic acid: acridine ratio found in the crystal structure was 1:1. The crystal selected for the single crystal data collection had size dimensions of 0.03 mm x 0.08 mm x 0.12 mm. The structure solved successfully in the monoclinic space group $P2_1/n$, with Z = 4. The asymmetric unit contains one vanillic acid and one acridine molecule, all in general positions. The structure refined successfully to R_1 = 0.0511 with wR_2 = 0.1045 (R indices ([I>2sigma (I)]).

Table 3.3: VA•ACRI crystal data.

Compound	**VA•ACRI**
Structural Formula	$C_8H_8O_4$•$C_{13}H_9N$
VA:ACRI ratio	1: 1
Molecular Mass (g mol^{-1})	347.36
Data collection temperature (K)	173(2)
Crystal system	Monoclinic
Space group	*$P2_1/n$*
a (Å)	8.4690 (17)
b (Å)	22.621 (5)
c (Å)	8.9534 (18)
α (°)	90.00
β (°)	90.68 (3)
γ (°)	90.00
Volume ($Å^3$)	1715.2 (6)
Z	4
D_c, Calculated density (g cm^{-3})	1.345
Final R indices [I>2sigma(I)]	R_1= 0.0511
	wR_2 = 0.1056
R indices (all data)	R_1 = 0.1090
	wR_2 = 0.1270
Largest diff. peak and hole ($eÅ^{-3}$)	0.235; -0.234

The packing diagram of the **VA•ACRI** structure down [001] is shown in **Figure 3.1.6.** The acridine molecules stabilize the structure via π-π stacking interactions between their adjacent aromatic rings having a Cg-Cg (distance between ring centroids) with a minimum distance of 3.656 Å. Layers of VA molecules [001] are sandwiched between layers of acridine molecules.

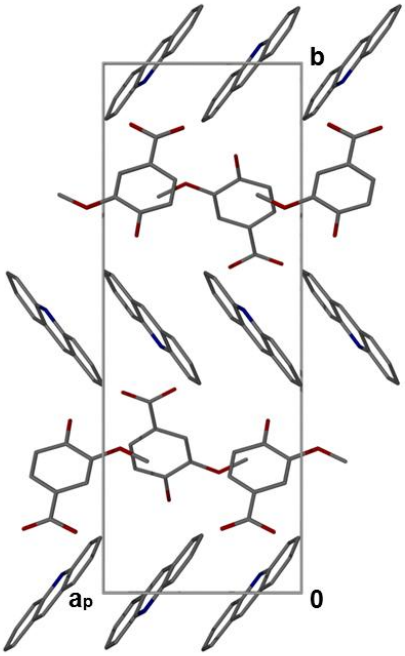

Figure 3.1.6: Packing diagram of **VA•ACRI** down [001] with the hydrogen atoms removed.

One vanillic acid molecule is hydrogen bonded to two vanillic acid molecules and one acridine molecule. The structure is stabilized by (VA) O-H•••O (VA) with an O•••O distance of 2.647(2) Å and (VA) O-H•••N (ACRI) with an O•••N distance of 2.560(2) Å, as shown in **Figure 3.1.7**. There are different types of motifs in this crystal structure. The first order graph set[13] indicates a noncyclic chain C motif through OH•••O hydrogen bonds. The second order graph set shows a noncyclic dimer D motif via OH•••N, OH•••O and OH•••N hydrogen bonds. The graph sets descriptors of the **VA•ACRI** co-crystal are:

- $N_1 = C_1^1(8)$
- $N_2 = D_3^3(15)$

The hydrogen bond parameters of **VA•ACRI** are given in **Table 3.4**.

Table 3.4: Hydrogen Bond parameters of **VA•ACRI**.

COMPOUND	D-H···A	D···A (Å)	D-H (Å)	H···A (Å)	D-H···A (º)
VA•ACRI	O3-H5···O2[a]	2.647 (2)	0.925 (3)	1.769 (3)	157 (3)
	O1-H1A···N11[b]	2.562 (2)	0.960 (1)	1.605 (3)	174 (3)

a = x-1/2, -y+1/2, z + 1/2; *b* = -x +1,-y,-z +2

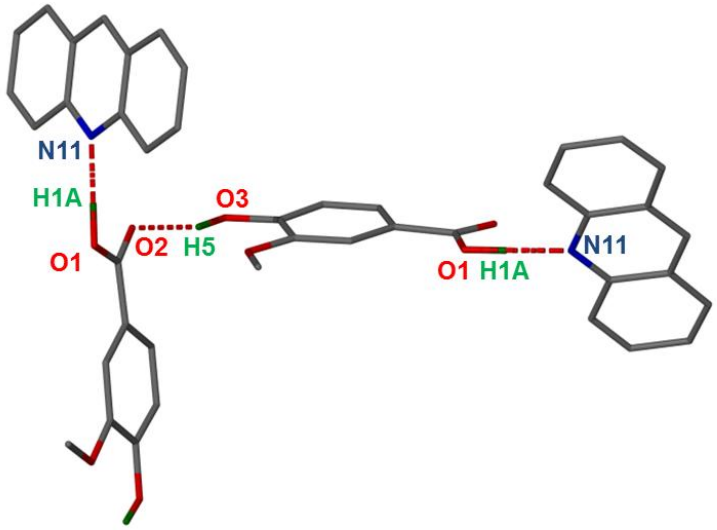

Figure 3.1.7: Hydrogen bonding in **VA•ACRI**.

3.2 Vanillic acid and Caffeine (VA•2CAF)

Caffeine (1, 3, 7- trimethyl purine-2, 6-dione), $C_8H_{10}N_4O_2$ is a xanthine derivative molecule which serves as a stimulant of the central nervous system and smooth muscle relaxant. It can also be employed as a formulation additive to analgesic remedies.[14]

The co-crystal was obtained by dissolving a 1: 1 ratio of both components in ethyl methyl ketone (EMK) and the solution was allowed to evaporate at room temperature. The resultant vanillic acid: caffeine ratio in the co-crystal was 1: 2. The same co-crystal was also obtained when dissolving the acid: base (1: 1) combination in a 50/50 (*v/v*)

chloroform/methanol mixture. The asymmetric unit of **VA•2CAF** with all the hydrogen atoms of the crystal structure shown is illustrated in **Figure 3.2.1**.

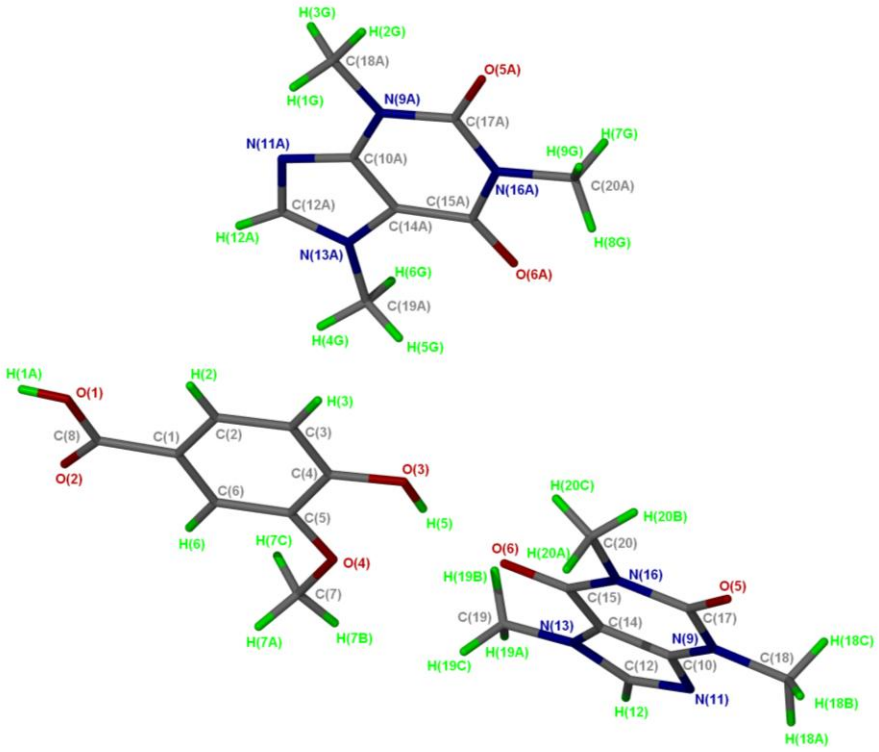

Figure 3.2.1: Asymmetric unit of the **VA•2CAF** structure with all the hydrogen atoms shown for numbering clarity.

3.2.1 Thermal Analysis

The melting point of **VA•2CAF** is lower than both individual components. Thermal analysis data are given in **Table 3.5** and **Figure 3.2.2** shows the DSC curves of the individual components and the co-crystal **VA•2CAF**.

Table 3.5: Thermal analysis data of **VA•2CAF**.

Compounds	**DSC Endo$_1$(T_{onset},K)**	**DSC Endo$_2$(T_{onset},K)**
Caffeine	419.6	508.4
Vanillic acid	-	482.3
VA•2CAF	-	437.7

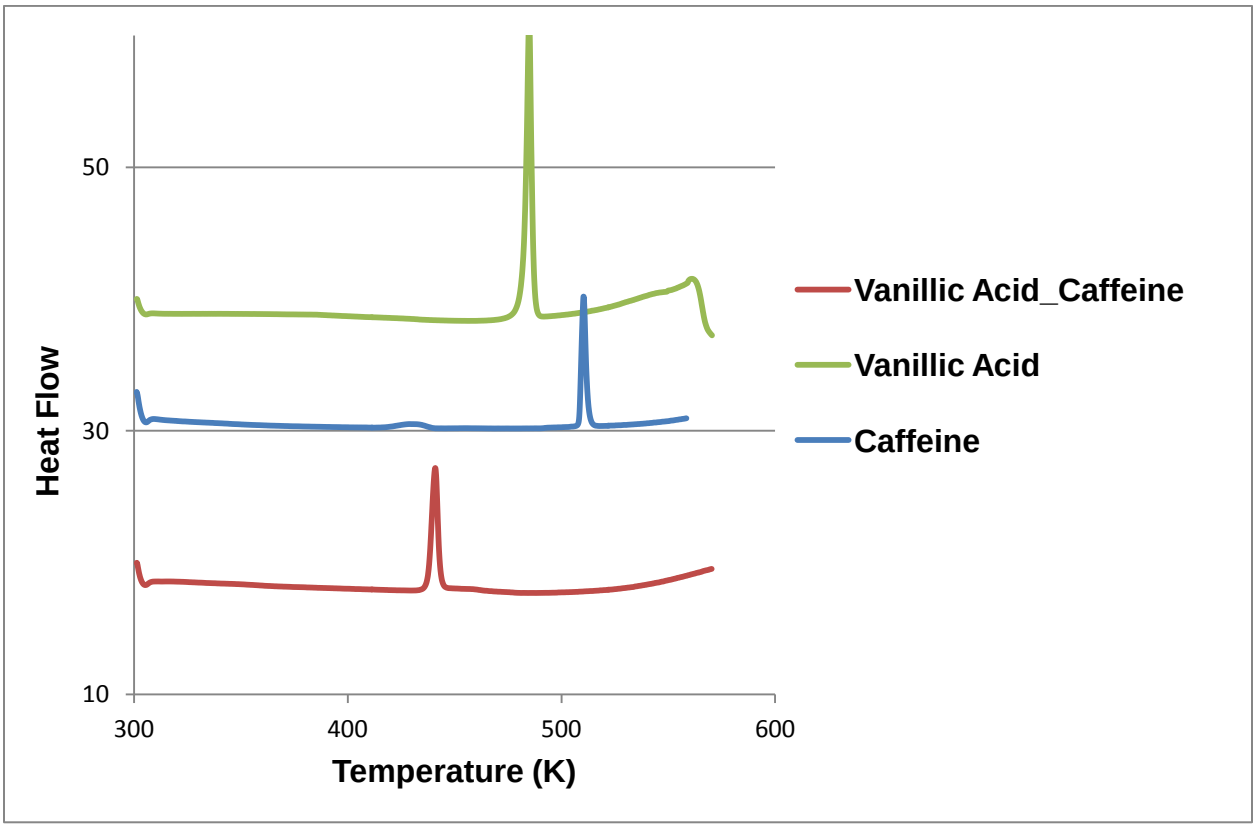

Figure 3.2.2: DSC curves of vanillic acid (green), caffeine (blue) and **VA•2CAF** (red).

3.2.2 Hot Stage Microscopy

A crystal was placed between two cover slips on a hot stage microscope at room temperature and one drop of silicone oil was added onto the crystal. The crystal

becomes opaque at a temperature of 428.2 K and starts to melt at 445.3 K. (**Figure 3.2.3).**

(a) 295 K **(b) 428.2 K**

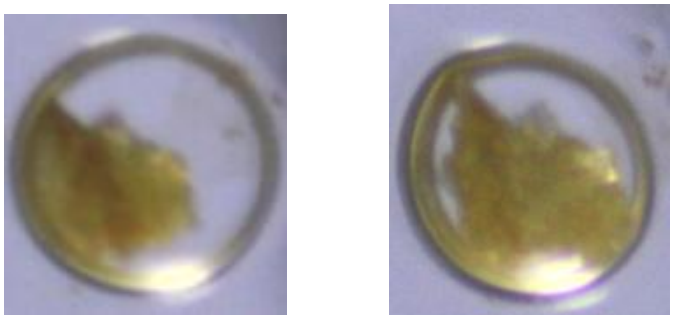

(c) 445.3 K **(d) 449.1 K**

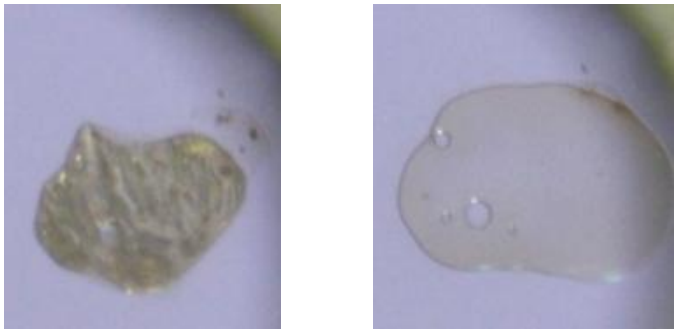

Figure 3.2.3: HSM photography of **VA•2CAF**. **a)** crystal immersed in silicone oil, **(b)** crystal starts melting, **(c)** melting of the crystal and **(d)** crystal completely melts.

3.2.3 IR Spectroscopy

The spectra of the **VA•2CAF** co-crystal contains both components as shown in **Figure 3.2.4**, no new band was depicted between the range 1550 - 1650 cm^{-1} confirming no salt formation.[2] There is confirmation of a co-crystal formation showing a lower shift of peaks of the C=O wavenumber in **VA•2CAF** due to the hydrogen bond formation as reported in **Table 3.6**. The C=O wavenumbers of vanillic acid and caffeine are higher than that of the co-crystal. The hydrogen bonded OH stretch (broad) in **VA•2CAF** was

observed at 3400 cm^{-1} which is less than the free OH stretch (3480 cm^{-1}) found in vanillic acid.

Table 3.6: IR positions and assignments of peaks in VA, **VA•2CAF** and CAF.

VA	**VA•2CAF**	CAF	Proposed assignment
3480, 3099	3400	-	OH stretch
2988	3110, 2954	3112, 2954	C-C ring modes
1763, 1667	1702, 1654	1708, 1658	C=O stretch
1599, 1524, 1478, 1454	1594, 1552, 1494, 1478	1599, 1549, 1486, 1455	C=C stretch
1275, 1202	1290, 1264	1286, 1239	C-O stretch

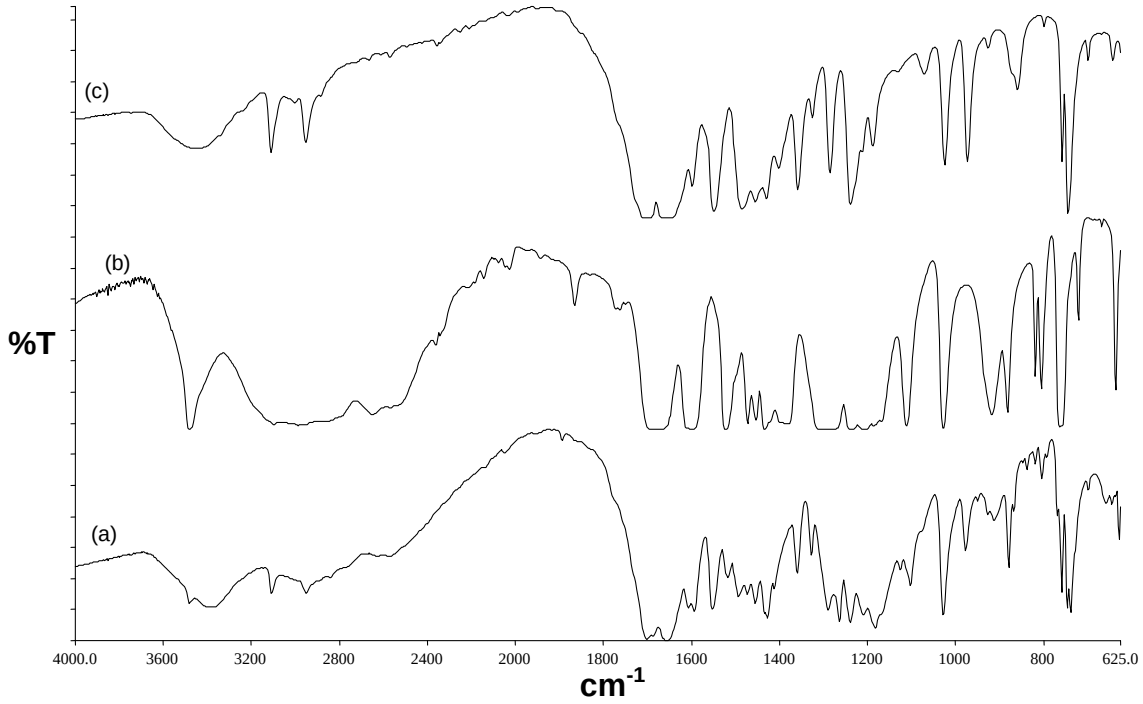

Figure 3.2.4: IR spectrums of (a) **VA•2CAF**, (b) vanillic acid and (c) caffeine.

3.2.4 Powder X-ray Diffraction

The grinding experiment whereby a 1: 2 ratio of vanillic acid and caffeine was ground for 30 min gave a PXRD pattern (**Figure 3.2.5**) which contained peaks found in the PXRD patterns of the co-crystal (calculated) and in the physical mixture, indicating that the reaction did not go to completion.

The mixture was ground for a further 15 min (total grinding time of 45 min) and again a further 15 min (total grinding time of 1 hr). These two PXRD patterns matched that of the co-crystal (calculated) indicating a successful experiment.

In the same context, the slurry experiment performed in ethyl methyl ketone was also successful and gave a PXRD pattern which was the same as the calculated PXRD obtained from LAZYPULVERIX.[12]

The PXRD patterns of the different type of experiments are shown in **Figure 3.2.5**.

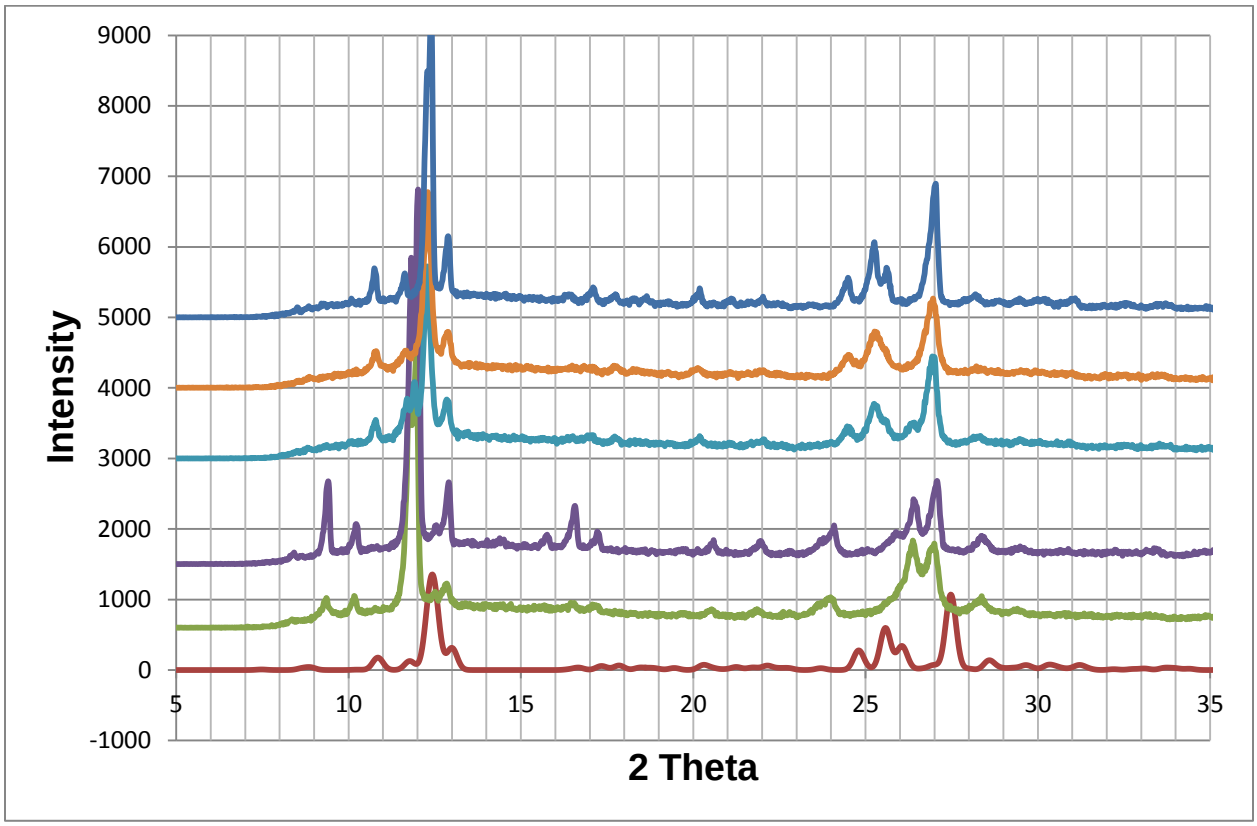

Figure 3.2.5: PXRD patterns of **VA•2CAF** (red), ground product after 30 min (green), physical mixture (purple), ground product after 45 min (sky blue), ground product after 1 hr (orange) and slurry (blue).

3.2.5 Structure Determination

The crystal data is reported in **Table 3.7**. Direct methods yielded all vanillic acid and caffeine non-hydrogen atoms and these were refined anisotropically. The hydrogen atoms involved in the hydrogen bonding were located in the difference electron density map. The structure refined successfully to R_1 = 0.0540 with wR_2 = 0.1450 ([I>2sigma (I)]).

Table 3.7: VA•2CAF crystal data.

Compound	**VA•2CAF**
Structural Formula	$C_8H_8O_4$•$2C_8H_{10}N_4O_2$
VA:CAF ratio	1: 2
Molecular Mass (g mol^{-1})	556.54
Data collection temperature (K)	173(2)
Crystal system	Triclinic
Space group	*P-1*
a (Å)	10.110 (2)
b (Å)	10.525 (2)
c (Å)	12.221 (2)
α (°)	77.69 (3)
β (°)	81.26 (3)
γ (°)	82.69 (3)
Volume ($Å^3$)	1249.7 (6)
Z	2
D_c, Calculated density (g cm^{-3})	1.479
Final R indices [I>2sigma(I)]	R_1= 0.0540
	wR_2 = 0.1450
R indices (all data)	R_1 = 0.0780
	wR_2 = 0.1607
Largest diff. peak and hole ($eÅ^{-3}$)	0.600; -0.265

The two components crystallize in a 1: 2 ratio in the triclinic space group *P-1*, with Z = 2. A crystal with dimensions of 0.10 mm x 0.18 mm x 0.51 mm was analyzed using single crystal X-ray diffraction. The asymmetric unit as shown in **Figure 3.2.1** contains one vanillic acid and two caffeine molecules.

The structure is stabilized via π-π stacking interactions between the five membered ring and the six membered ring of caffeine molecules with a shortest distance of 3.420 Å as shown in **Figure 3.2.6** representing a packing diagram of **VA•2CAF** viewed down [100].

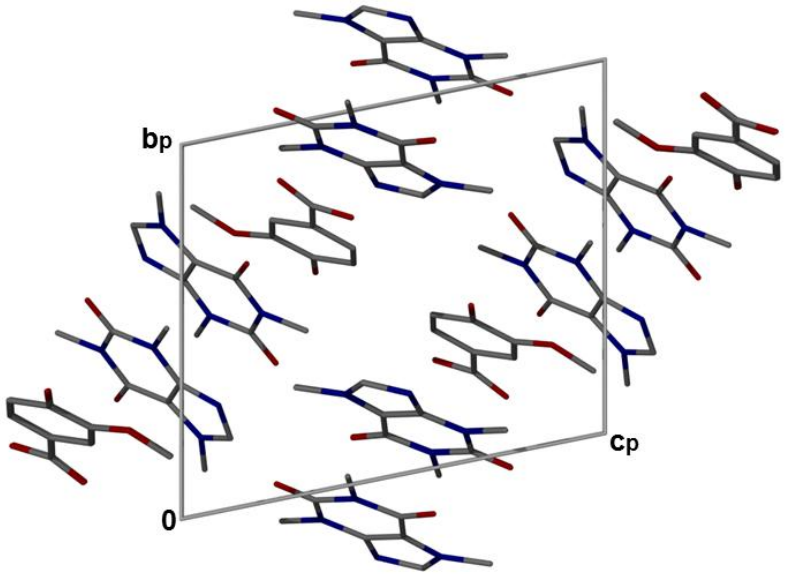

Figure 3.2.6: Packing diagram of **VA•2CAF** down [100] with the hydrogen atoms removed**.**

The hydrogen bonding of **VA•2CAF** (**Figure 3.2.7**) structure has one vanillic acid molecule bonded to two caffeine molecules as reported in **Table 3.8**. The hydrogen bond (VA) O-H•••N (CAF) has an O•••N distance of 2.685 (2) Å and an O-H•••N angle of 157 (3) º. This hydrogen bonding pattern can be described using Etter notation as D_2^2 (11) motifs. The 1:2 acid: base ratio is further stabilized via (VA) O-H•••O (CAF) hydrogen bonds with an O•••O distance of 2.802 (2) Å and an O-H•••O angle of 157 (3) º.

Table 3.8: VA•2CAF hydrogen bonding parameters.

COMPOUND	D-H···A	D···A (Å)	D-H (Å)	H···A (Å)	D-H···A (º)
VA•2CAF	O1-H1A···N11A[a]	2.685 (2)	0.852 (3)	1.882 (3)	157 (3)
	O3-H5···O6	2.802 (2)	0.825 (3)	2.023 (3)	157 (3)

a = 1-x, -y+2, -z + 1

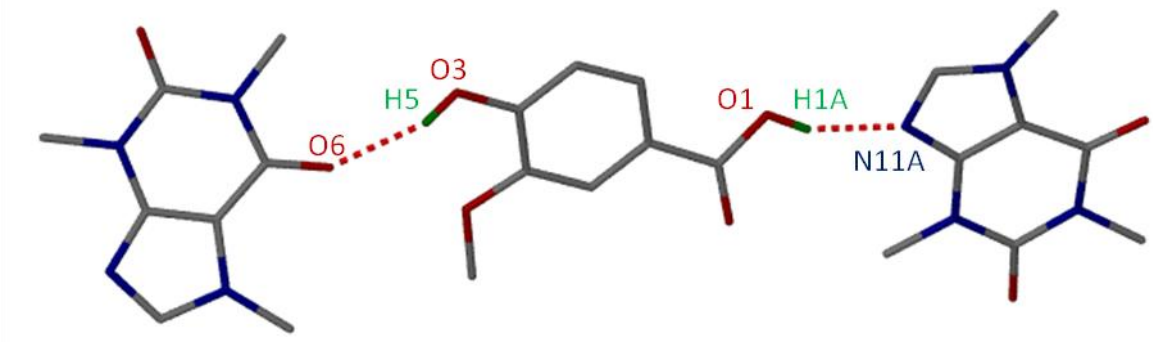

Figure 3.2.7: Hydrogen bonding in **VA•2CAF**.

3.3 Vanillic acid and Isonicotinamide (2VA•2INM•2H_2O)

Isonicotinamide (INM), $C_6H_6N_2O$ (pyridine-4-carboxamide) is a molecule based on the nicotinamide structure and has been investigated in relation to anti-inflammatory activity and Huntington's disease.[15, 16]

A 1:1 ratio of both compounds was dissolved in methanol by slight heating on a hot plate. The solution was allowed to evaporate at ambient temperature. The obtained crystals contained a VA: INM: H_2O ratio of 2: 2: 2 (**2VA•2INM•2H_2O**). The same crystal was obtained when tetrahydrofuran was used as a solvent.

The co-crystal hydrate is shown in **Figure 3.3.1**, where all the hydrogen atoms are illustrated for numbering clarity.

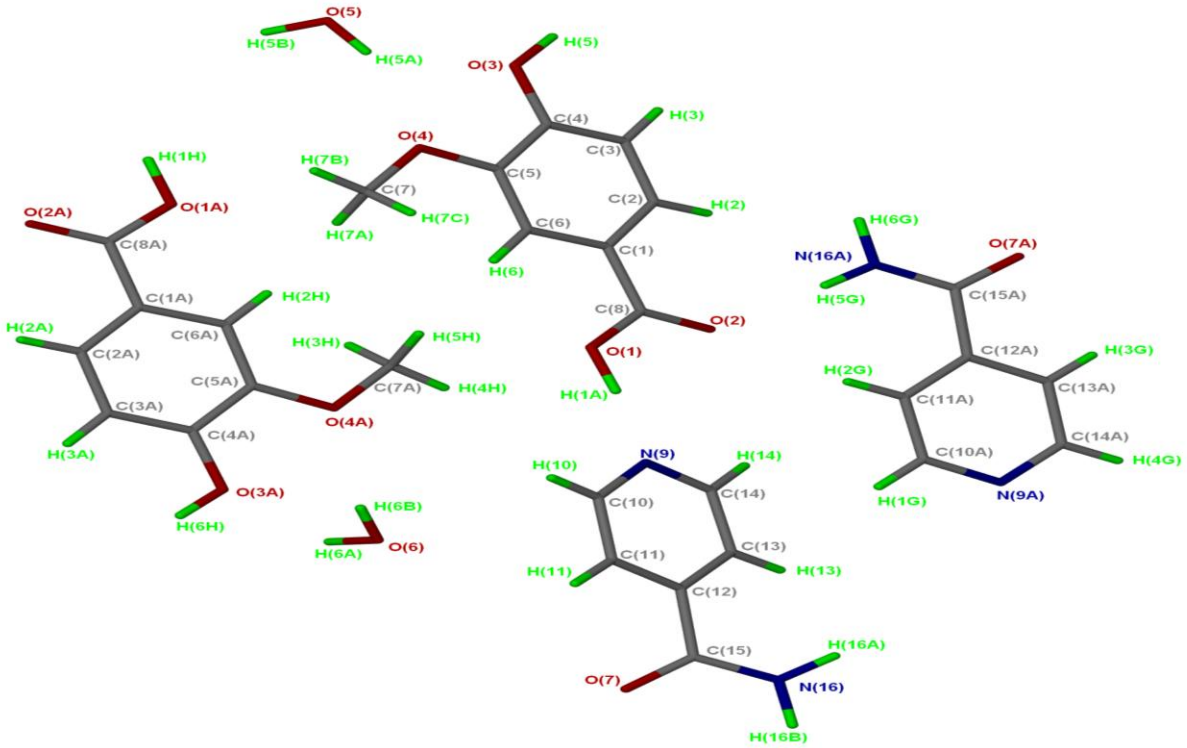

Figure 3.3.1: Asymmetric unit of the **2VA•2INM•2H_2O** structure with all the hydrogen atoms shown for numbering clarity.

3.3.1 Thermal Analysis

The **2VA•2INM•2H_2O** co-crystal hydrate has a melting point that is lower than both components as given in **Table 3.9**. This is an indication of a decrease in thermal stability of the co-crystal hydrate as compared to the starting material. The TG curve shows multiple mass loss steps. The first step of 5.0 % corresponds to the loss of one water molecule (calc 5.9 %). The second step is the melt of the crystal.

Thermal analysis curves of **2VA•2INM•2H_2O**, vanillic acid and isonicotinamide are illustrated in **Figure 3.3.2**.

Table 3.9: Thermal analysis data of **2VA•2INM•2H$_2$O**.

Compounds	Vanillic acid	**2VA•2INM•2H$_2$O**	Isonicotinamide
DSC Endo$_1$ (T$_{onset,}$K)	-	356.3	382.1
DSC Endo$_2$ (T$_{onset,}$K)	482.3	410.2	428.4
TG calculated % mass loss		5.9	
TG experimental % mass loss	-	5.0	-
VA: INM: H$_2$O ratio		2: 2: 2	

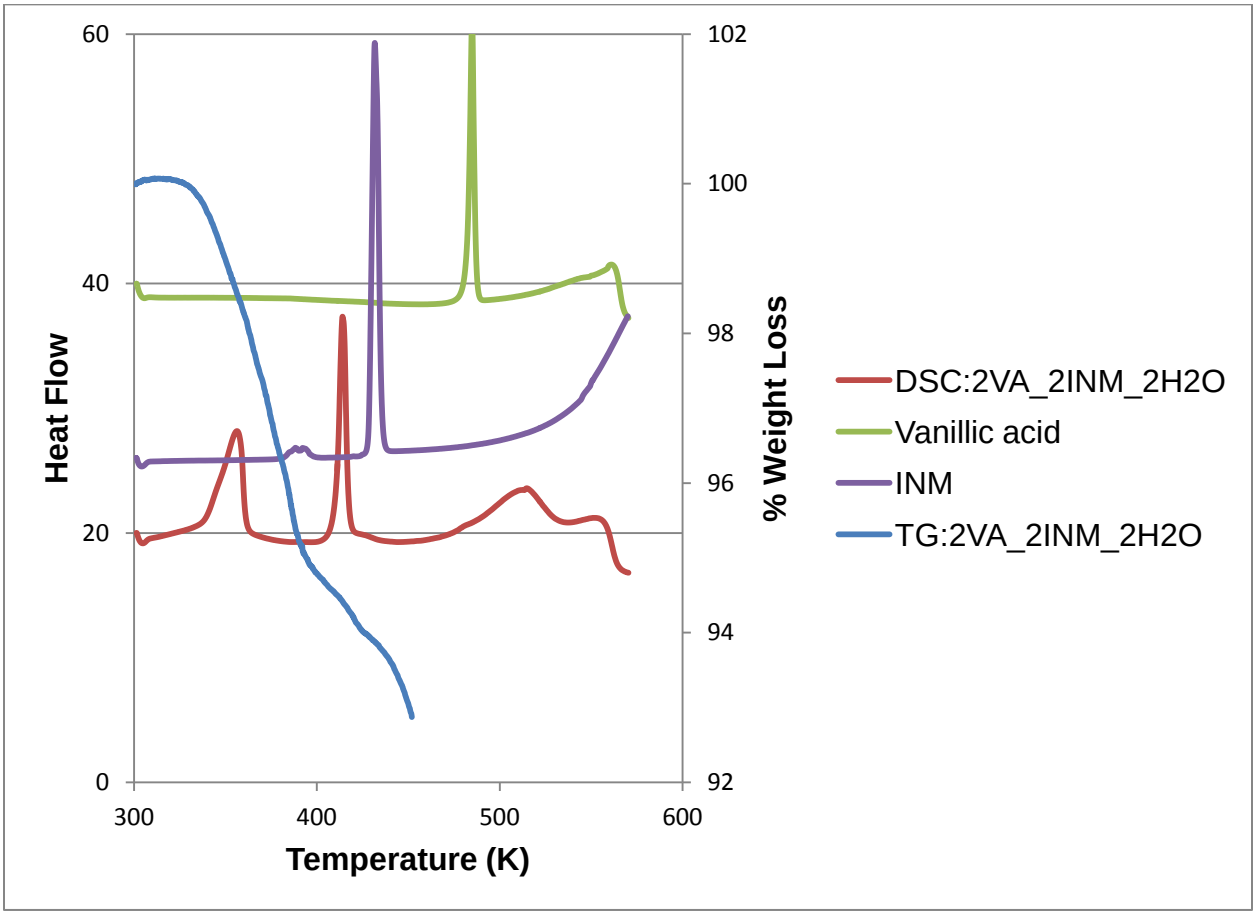

Figure 3.3.2: Thermal analysis of **2VA•2INM•2H$_2$O** DSC (red), **2VA•2INM•2H$_2$O** TG (blue), isonicotinamide (purple) and vanillic acid (green).

3.3.2 Hot Stage Microscopy

The first step in the thermal decomposition of **2VA•2INM•2H_2O** is the release of water included in the crystal structure which was observed at 360 K. The crystal starts melting at 414 K and the melt is complete at 431 K as indicated in **Figure 3.3.3**.

(a) 295 K **(b) 360 K**

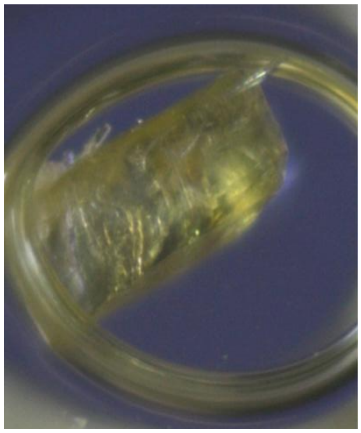

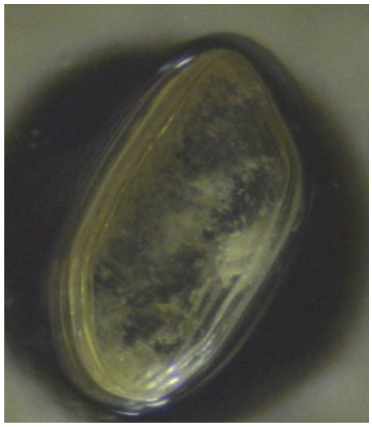

(c) 414 K **(d) 431 K**

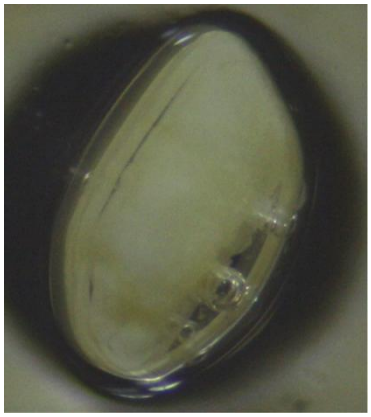

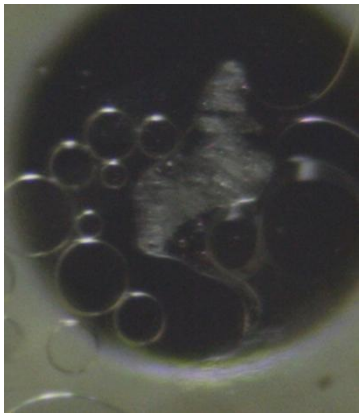

Figure 3.3.3: HSM photography of **2VA•2INM•2H_2O**: **(a)** The crystal is immersed in silicone oil, **(b)** Release of water, **(c)** The crystal begins to melt and **(d)** vanillic acid melt is completed.

3.3.3 IR Spectroscopy

The spectrum of the co-crystal hydrate **2VA•2INM•2H_2O** shown in **Figure 3.3.4** demonstrates the formation of a co-crystal by the presence of new bands observed at 3506 and 3166 cm^{-1}.[17] The band at 3166 cm^{-1} is assigned to the H-bonded NH_2 stretching modes. The peak at 3506 cm^{-1} is assigned to the solvated water molecules in the crystal structure.

There is a shift in the C=O vibration bands for the co-crystal hydrate **2VA•2INM•2H_2O**. These vibration bands are lower than vanillic acid and isonicotinamide C=O bands.

Table 3.10: IR positions and assignments of peaks in VA, **2VA•2INM•2H_2O** and INM.

VA	**2VA•2INM•2H_2O**	INM	Proposed assignment
3480, 3099	3506, 3404	-	OH stretch
-	3404, 3166	3370, 3186	H-bonded NH_2 stretching mode
2988	2832, 2432	2783	C-C ring modes
1763, 1667	1674	1680	C=O
-	1631, 1608	1624	Amide II band (NH_2 scissor), C-N, C=O stretching mode combination
1599, 1524, 1478, 1454	1556, 1530, 1450,1324	1595, 1551,	C=C stretch
-	1402	1399	Amide III band (C-N stretch, N-H bend)
1275, 1202	1271, 1242, 1207	1218	C-O stretch

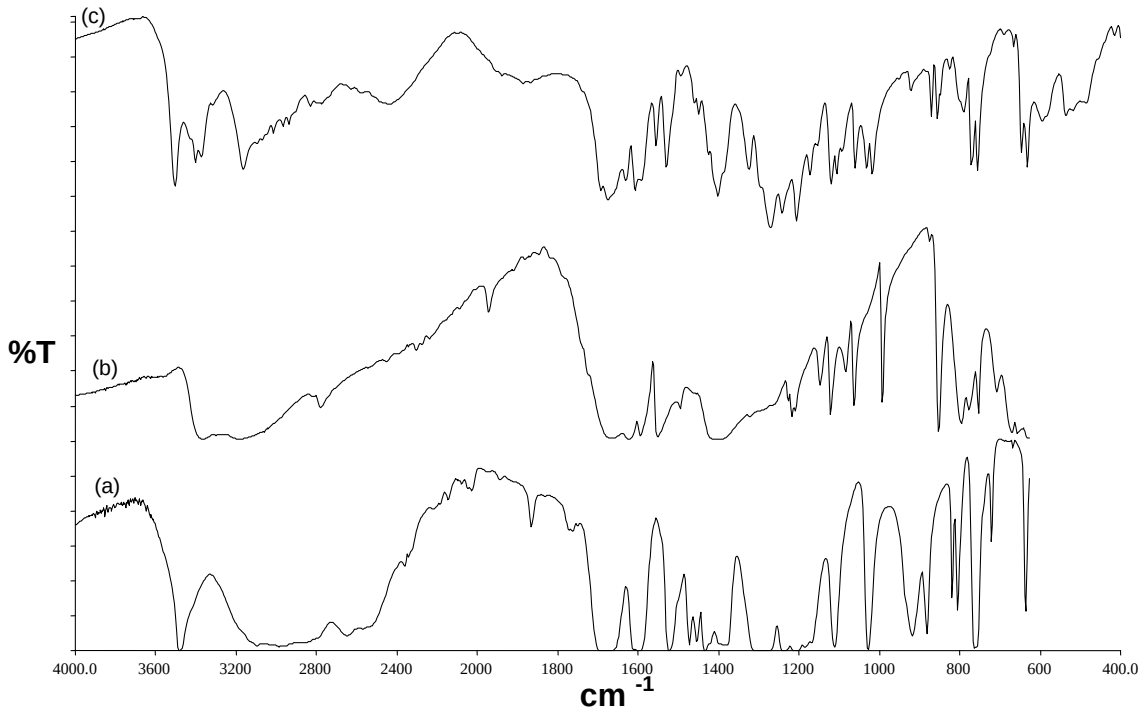

Figure 3.3.4: IR spectrum (a) VA, (b) INM and (c) **2VA•2INM•2H_2O**.

3.3.4 Powder X-ray Diffraction

A 1: 1 mixture of VA and INM was ground for 30 min. The PXRD spectrum of the ground product matched that of the physical mixture (**Figure 3.3.5**).

A few drops of water were added to this mixture and the powder was ground for another 15 min. The water drop grind experiment showed good agreement to the calculated PXRD pattern obtained from LAZYPULVERIX.[12]

A slurry experiment was performed in methanol and the PXRD pattern recorded. A different PXRD pattern than the calculated spectrum was obtained. However, the PXRD of the slurry experiment still contained peaks found in the PXRD of the physical mixture but the overall pattern differs. Thus it can be concluded that the powder contained unreacted starting material and perhaps another form of the co-crystal or a different unknown compound.

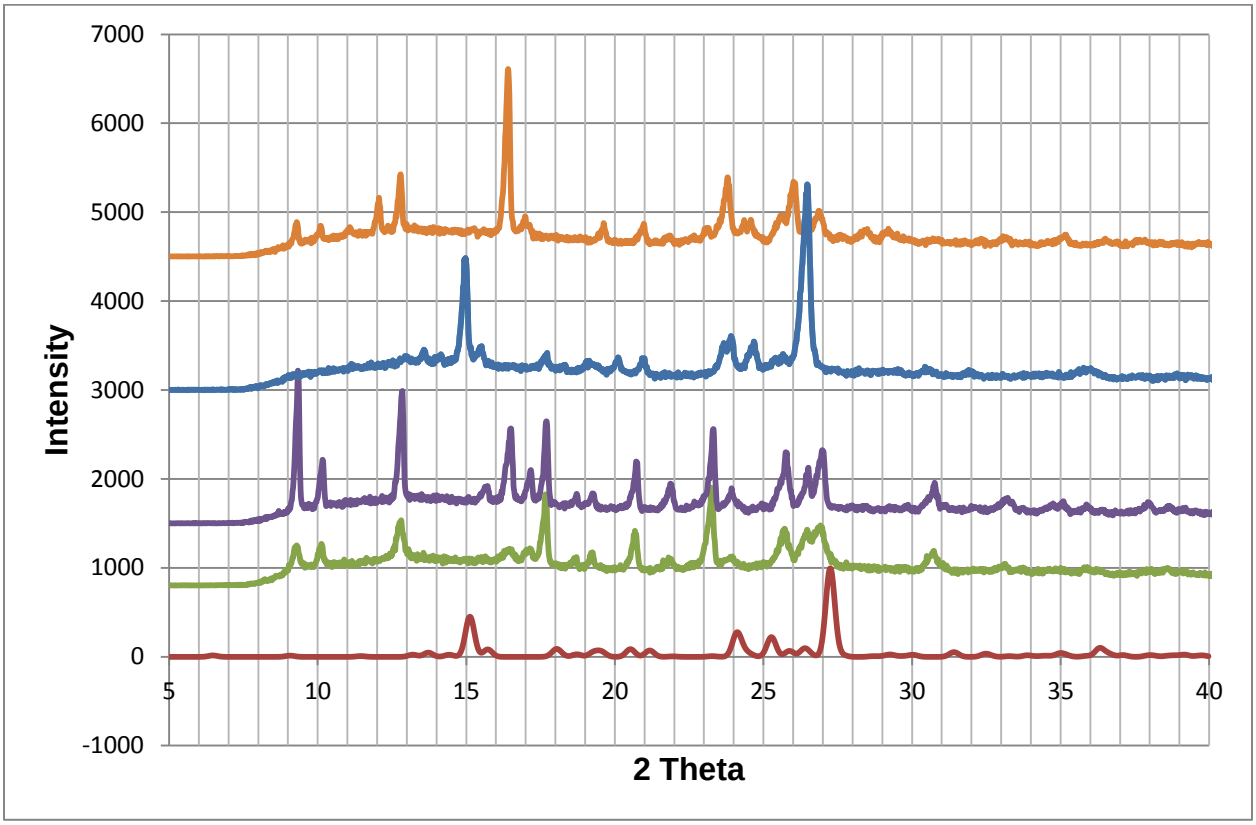

Figure 3.3.5: PXRD patterns of **2VA•2INM•2H$_2$O** (red), ground product (green), physical mixture (purple), slurry in methanol (orange) and liquid assisted ground product (blue).

3.3.5 Structure Determination

The **2VA•2INM•2H$_2$O** (**Figure 3.3.1**) structure crystallized in *P-1* with two vanillic acid molecules, two isonicotinamide molecules and two water molecules in the asymmetric unit. The structure was solved using direct methods and refined by full matrix least squares with SHELX-97[18] refining on F^2. All non-hydrogen atoms were found in the difference electron density map and were refined anisotropically. The hydroxyl hydrogens of the VA and the hydrogens attached to nitrogen were located in the electron density map and allowed to refine isotropically. The graphical interface used was X-seed.[19] The crystal data is given in **Table 3.11**.

Table 3.11: 2VA•2INM•2H_2O crystal data.

Compound	**2VA•2INM•2H_2O**
Structural Formula	$2C_8H_8O_4$•$2C_6H_6N_2O$•$2H_2O$
VA:INM:H_2O ratio	2: 2: 2
Molecular Mass (g mol^{-1})	616.58
Data collection temperature (K)	173(2)
Crystal system	Triclinic
Space group	*P-1*
a (Å)	7.9000 (16)
b (Å)	13.196 (3)
c (Å)	13.735 (3)
α (°)	85.02 (3)
β (°)	85.32 (3)
γ (°)	78.68 (3)
Volume ($Å^3$)	1395.6 (5)
Z	2
D_c, Calculated density (g cm^{-3})	1.467
Final R indices [I>2sigma(I)]	R_1= 0.0503
	wR_2 = 0.1142
R indices (all data)	R_1 = 0.0958
	wR_2 = 0.1366
Largest diff. peak and hole ($eÅ^{-3}$)	0.212; -0.259

The face to face π-π stacking interaction between the vanillic acid aromatic ring (C1 - C6) and the six membered ring of the isonicotinamide (N9 - C14) has a Cg-Cg (distance between ring centroids) distance of 3.668 Å. The packing diagram of the co-crystal hydrate is shown in **Figure 3.3.6 (a)**. VA and INM molecules packing in layers in the general direction [101] down [010] (**Figure 3.3.6 (b)**). The cavities occupied by the water molecules are shown in **Figure 3.3.6 (c)** with a void volume of 20.20 $Å^3$ (1.4 % of

the unit cell). A probe radius of 1.0 Å and a grid spacing of 0.70 Å (contact surface) were used using Mercury[20] software. The **2VA•2INM•2H$_2$O** structure is also stabilized by a weaker C-H•••π interaction between VA molecules shown in **Figure 3.3.7** with a distance of 2.645 Å and a C-H•••π angle of 148 °.

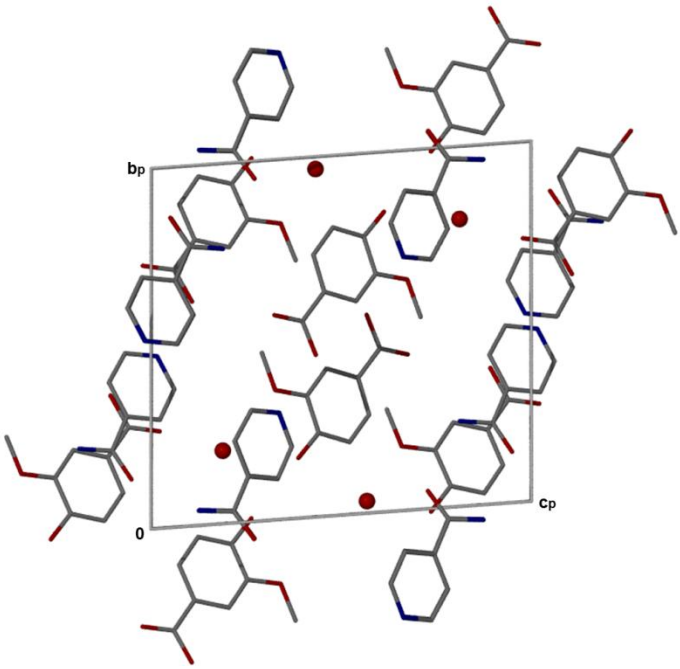

(a)

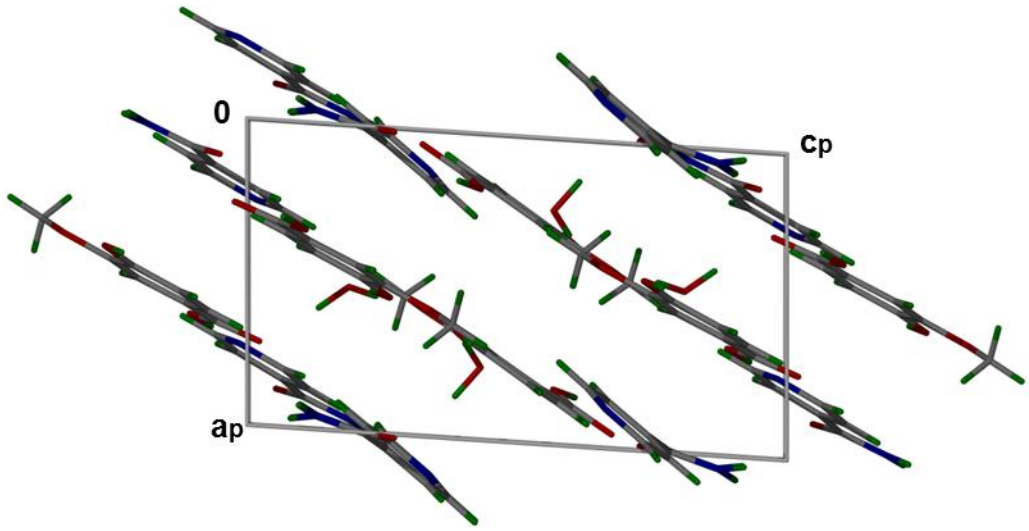

(b)

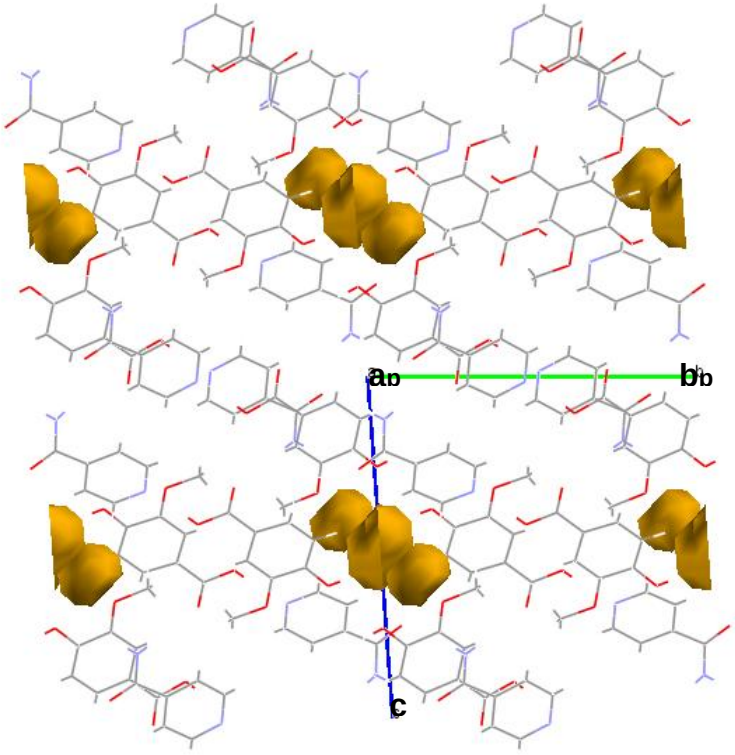

(c)

Figure 3.3.6: (a) Packing diagram of **2VA•2INM•2H$_2$O** down [100] with the hydrogen atoms removed, **(b)** packing diagram of 2VA•2INM•2H$_2$O showing VA and INM molecules in layers down [010] in general direction [101] and **(c)** cavities in which water molecules are located down [100].

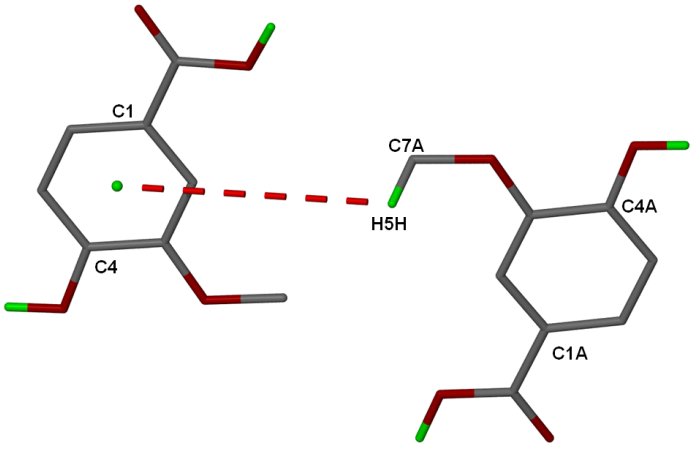

Figure 3.3.7: C-H•••π interaction in **2VA•2INM•2H$_2$O**.

The hydrogen bonding in **2VA•2INM•2H_2O** is very complex. All four hydrogen bond donor/acceptor sites of vanillic acid and isonicotinamide are utilized in the hydrogen bond network (**Figure 3.3.8**). The water molecule with oxygen labelled O6 plays a bridging role connecting two vanillic acid molecules and one isonicotinamide molecule. However, the water with the oxygen labeled O5 links two vanillic acid molecules, only through these water molecules are three VA linked. This kind of hydrogen bonding where the water plays a bridging role has been reported by Jacobs *et al.*[21]

One of the vanillic acid molecules is hydrogen bonded to two isonicotinamide molecules via the COOH group (O1-H1A•••N9 and N16A-H5G•••O2). The hydroxyl and the methoxy groups of the same VA molecule is involved in hydrogen bonding with water molecules. The carboxylic acid of the other vanillic acid is connected to one isonicotinamide molecule and one molecule of water. Both the OH and OCH_3 groups are hydrogen bonded to two separate molecules of water.

The oxygen (O7A) in the second isonicotinamide molecule is a bifurcated acceptor because it is hydrogen bonded to two NH_2 hydrogen atoms (H16A and H16B) belonging to two different INM molecules.

In the same context, the oxygen (O7) in the first isonicotinamide molecule is also a bifurcated acceptor. This oxygen (O7) is hydrogen bonded to one of the hydrogen atoms in the second isonicotinamide molecule (H6G) and one of the hydrogen atoms in the second water molecule (H6A).

There is a ring formation of hydrogen bonding between the two isonicotinamide molecules. The crystal structure has a $R_4^4(20)$ ring motif involving two VA and two water molecules; $R_4^4(16)$ and $R_4^2(8)$ ring motifs are between four INM molecules via N-H•••O; $R_2^2(8)$ ring is between two INM molecules and a $D_2^2(11)$ involving one water, one VA and one INM molecule. The hydrogen bond parameters of **2VA•2INM•2H_2O** are given in **Table 3.12**.

Table 3.12: Hydrogen bond parameters in **2VA•2INM•2H_2O**.

COMPOUND	D-H···A	D···A (Å)	D-H (Å)	H···A (Å)	D-H···A (º)
2VA•2INM•2H$_2$O	N16-H16B···O7A[a]	2.899 (2)	0.998 (1)	1.906 (1)	172 (1)
	N16A-H6G···O7[b]	2.930 (2)	0.978 (1)	1.965 (1)	168 (1)
	O3-H5···O6[b]	2.657 (2)	1.002 (1)	1.668 (1)	168 (1)
	O1-H1A···N9	2.629 (2)	0.999 (2)	1.634 (2)	174 (2)
	O5-H5A···O4	3.051 (2)	0.855 (3)	2.243 (3)	158 (2)
	O5-H5A···O3	2.945 (2)	0.855 (3)	2.296 (2)	133 (2)
	O6-H6A···O7[c]	2.823 (2)	0.977 (3)	1.868 (3)	165 (2)
	N16-H16A···O7A[d]	3.002 (2)	0.948 (2)	2.190 (2)	143 (2)
	O5-H5B···O2[e]	2.831 (2)	0.965 (3)	1.872 (3)	172 (3)
	O6-H6B···O4A	2.983 (2)	0.844 (3)	2.210 (3)	152 (2)
	O6-H6B···O3A	2.911 (2)	0.844 (3)	2.291 (3)	131 (2)
	N16A-H5G···O2	3.044 (2)	0.932 (2)	2.112 (2)	178 (2)
	O1A-HIH···N9A[f]	2.604 (2)	1.003 (3)	1.605 (3)	173 (2)
	O3A-H6H···O5[a]	2.648 (2)	0.912 (3)	1.748 (3)	169 (2)

a = 1-x, y-1, z; b = x, y+1, z; c = -x, -y, -z+1; d = -x, -y+1, -z; e = -x+1, -y+1, -z+2; f=x+1,y,z +1

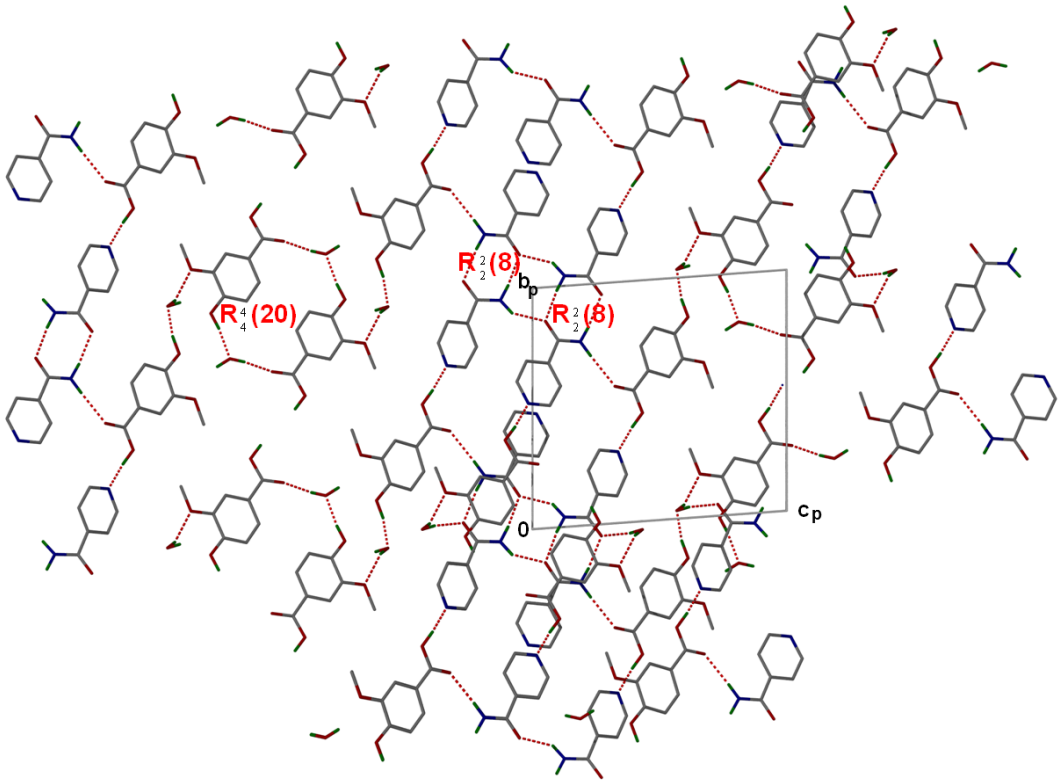

Figure 3.3.8: Hydrogen bonding in **2VA•2INM•2H$_2$O** down [100].

3.4 Vanillic acid and Nicotinamide (VA•NAM)

Nicotinamide ($C_6H_6N_2O$) (also known as niacinamide and nicotinic acid amide, which is vitamin B_3) has demonstrated both anti-inflammatory actions beneficial to patients with inflammatory skin conditions.[22]

A 1:1 molar ratio of vanillic acid and nicotinamide was dissolved in ethyl methyl ketone by gently heating on a hot plate. The solution was allowed to evaporate at room temperature and platy crystals were obtained. The same crystal structure was obtained in acetone and methanol. The two ∆pkas (ΔpK_{a1}= pK_a(base) - pK_aacid = 0.50[23] - 4.50 [6] = - 4.00 and ΔpK_{a2} = 3.40 [23] - 4.50 = - 1.10) of this acid:base combination indicates the formation of a co-crystal.

The asymmetric unit of the co-crystal **VA•NAM** is shown in **Figure 3.4.1**.

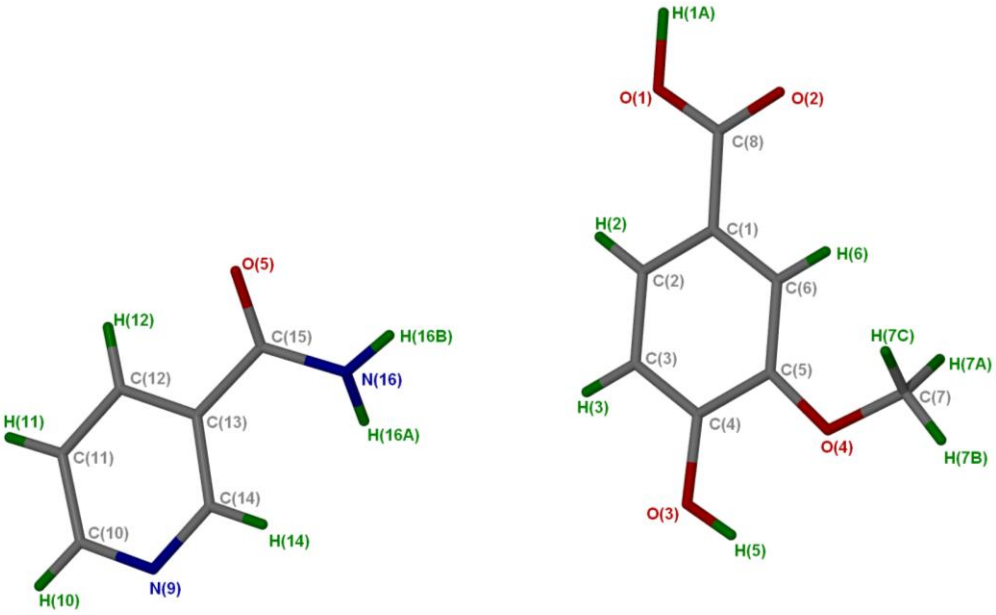

Figure 3.4.1: Asymmetric unit of **VA•NAM** with all the hydrogen atoms shown for numbering clarity.

3.4.1 Thermal Analysis

The DSC results for the compounds are given in **Table 3.13** and the DSC curves are illustrated in **Figure 3.4.2**. The **VA•NAM** co-crystal has a melting point which lies in-between that of the two starting components.[24, 25]

Table 3.13: Thermal analysis data of **VA•NAM**.

Compounds	**DSC Endo$_1$(T_{onset},K)**	**DSC Endo$_2$(T_{onset},K)**
Nicotinamide	-	401.6
Vanillic acid	-	482.3
VA•NAM	407.6	417.1

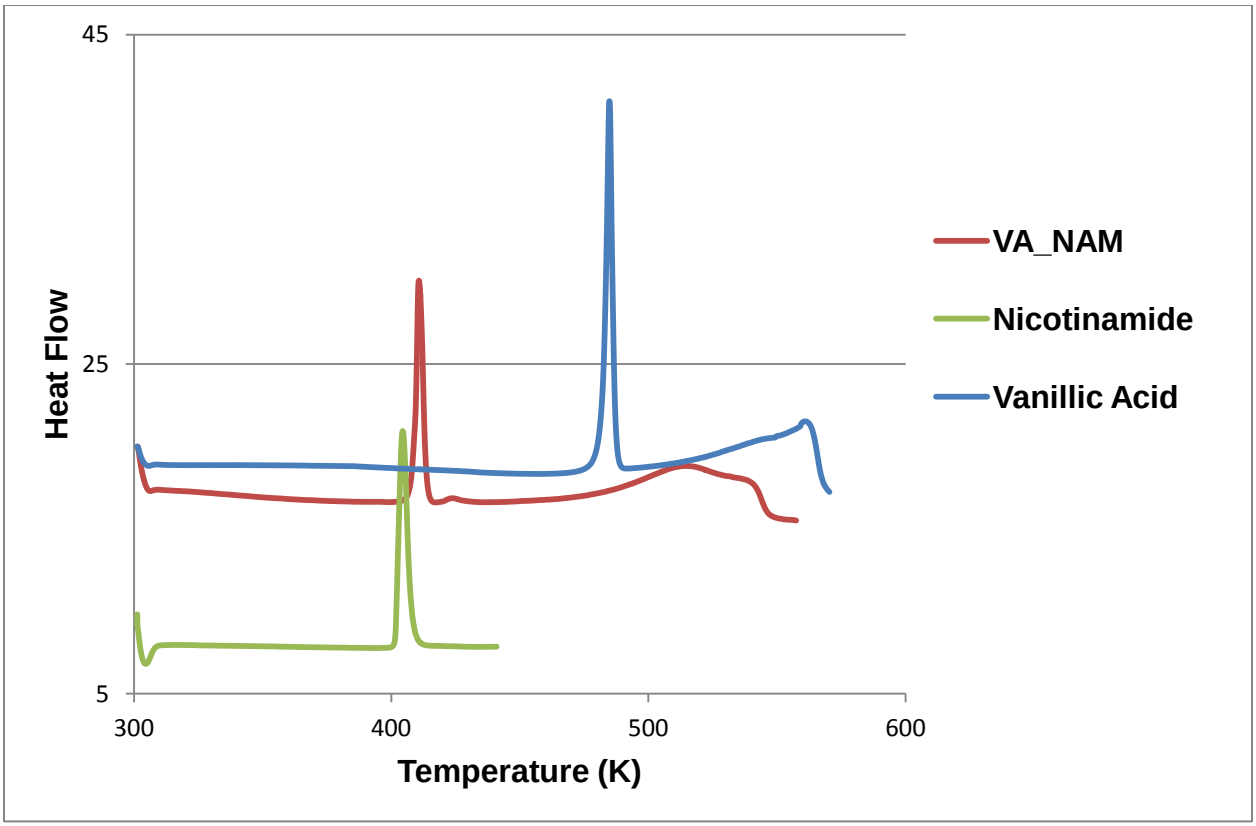

Figure 3.4.2: DSC curves of **VA•NAM** (red), nicotinamide (green) and vanillic acid (blue).

3.4.2 Hot Stage Microscopy

A single crystal was placed on a hot stage microscope at room temperature and immersed in silicone oil. Loss of transparency in the crystal is observed at a temperature of 405.6 K and the melt at 410.1 K. The melting process was not completed at a temperature of 421.4 K as shown in **Figure 3.4.3**.

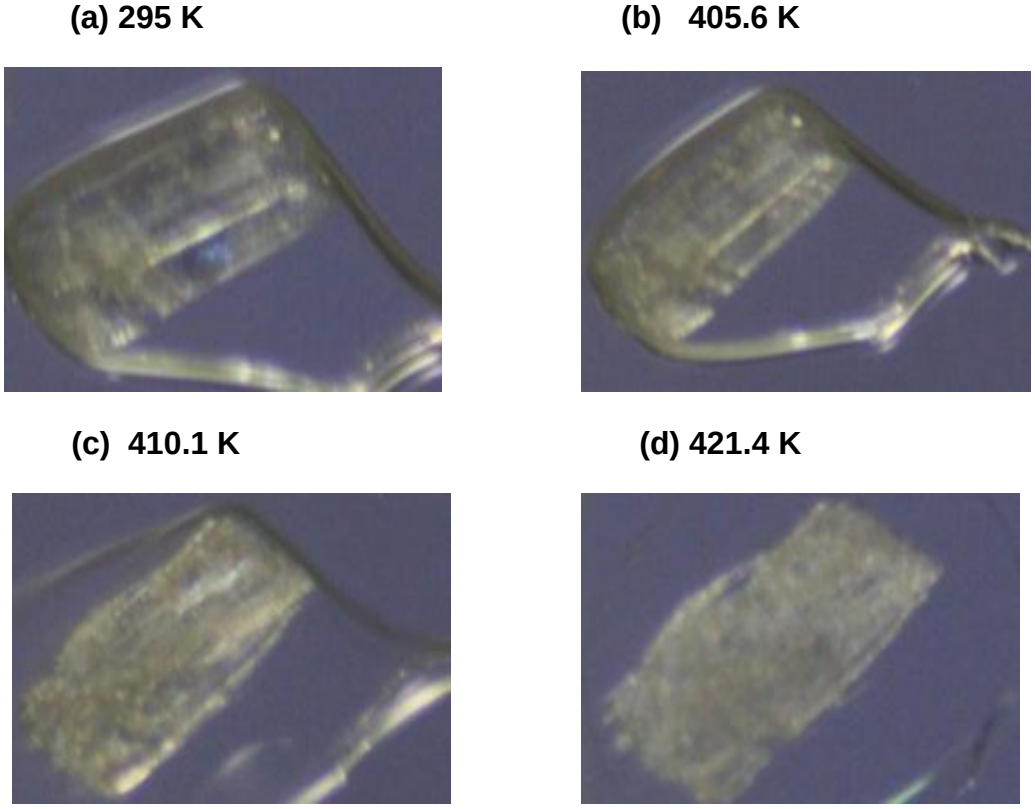

Figure 3.4.3: HSM photography of **VA•NAM**: **(a)** Crystal immersed in silicone oil, **(b)** Crystal loses transparency, **(c)** Crystal starts melting, **(d)** Crystal continuous to melt.

3.4.3 IR Spectroscopy

The spectra of **VA•NAM** in **Figure 3.4.4** shows the formation of two new peaks at 3385 cm^{-1} and 3206 cm^{-1}. These bands are assigned to the H-bonded NH_2 stretching mode.

There is a shift in the OH stretch (3206, 3004 cm^{-1}) and C=O (1673 cm^{-1}) of the **VA•NAM** co-crystal.

The lack of shift in the vibrational frequencies for the C-N stretch and N-H bend in the co-crystal (1399 cm^{-1}) indicates that the patterns of molecular structure of the supramolecular synthon are not significantly different relative to those of the initial reactants. This indicates that the force constants of the homosupramolecular synthons (i.e., nicotinamide and vanillic acid) are not strongly changed upon formation of the heterosupramolecular synthon of the co-crystal).[17]

The infrared spectrum of vanillic acid is dominated by bands associated with oxygen-hydrogen and carbon-hydrogen vibrational modes.

However, nicotinamide infrared spectrum has dominance in two stretching modes of the hydrogen-bonded NH_2 group, one C-N stretch and one strong C-H stretching mode.

Table 3.14: IR positions and assignments of peaks in VA, **VA•NAM** and NAM.

VA	**VA•NAM**	NAM	Proposed assignment
3480, 3099	3206, 3004	-	OH stretch
-	3385, 3206	3366, 3163	H-bonded NH_2 stretching mode
2988	3004, 2960	3060, 2360	C-C ring modes
1763, 1667	1673	1683	C=O
-	1625	1619	Amide II band (NH_2 scissor), C-N, C=O stretching mode combination
1599, 1524, 1478, 1454	1553, 1522, 1457,1428	1593, 1574, 1485, 1426	C=C stretch
-	1399	1399	Amide III band (C-N stretch, N-H bend)
1275, 1202	1232, 1226	1230, 1202	C-O stretch

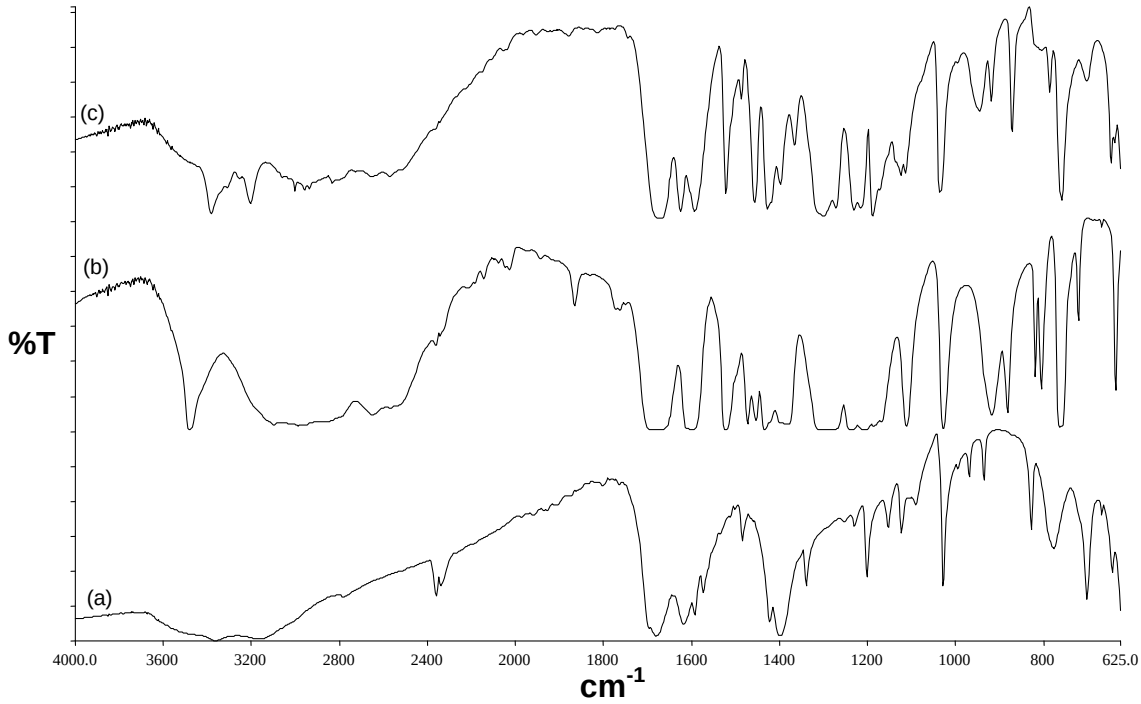

Figure 3.4.4: IR spectrum (a) NAM, (b) VA and (c) **VA•NAM**.

3.4.4 Powder X-ray Diffraction

A 1:1 ratio of the acid: base combination was ground for 30 min and the resultant PXRD pattern was the same as that of the physical mixture. This result proved that the grinding experiment was not successful.

In the contrary, the slurry performed in ethyl methyl ketone was a success due to agreement with the calculated pattern from LAZYPULVERIX.[12]

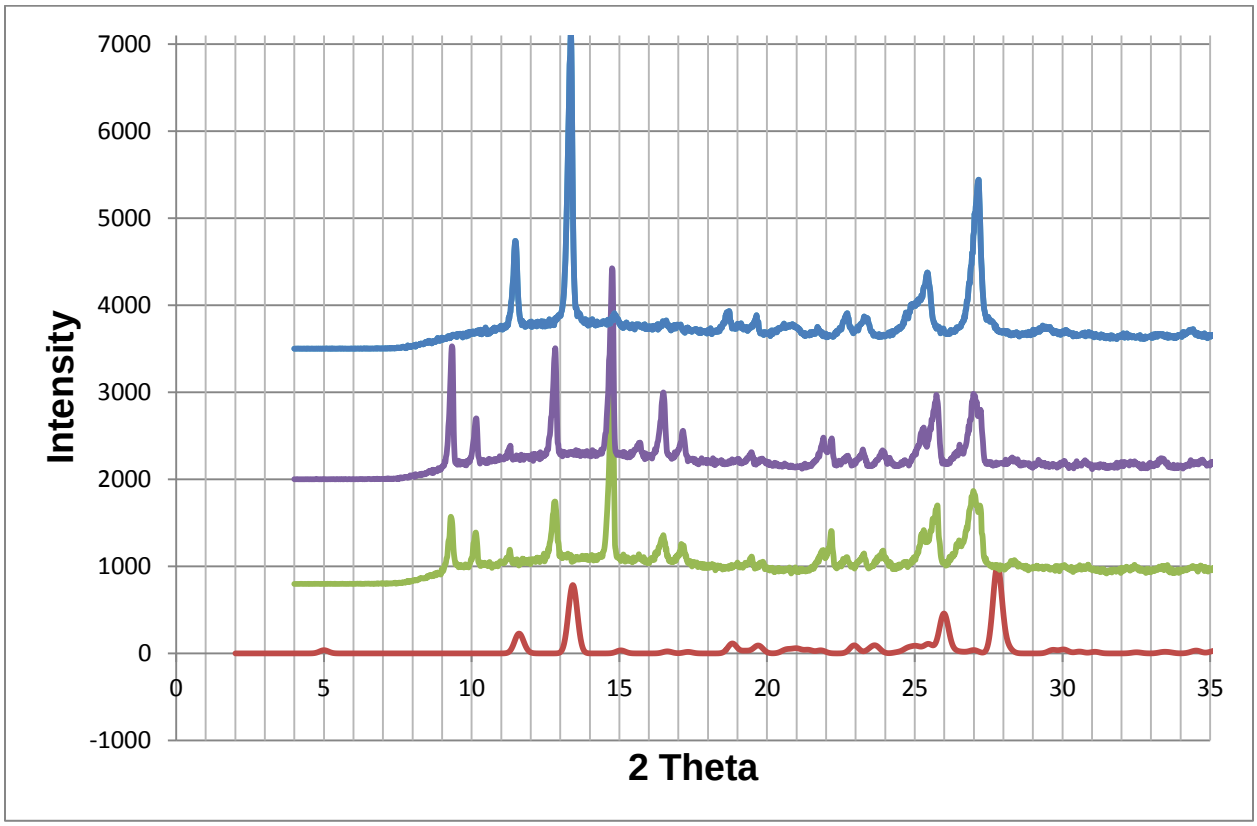

Figure 3.4.5: PXRD patterns of **VA•NAM** (red), ground product (green), physical mixture (purple) and slurry (blue).

3.4.5 Structure Determination

Non-hydrogen atoms were found in the difference electron density map. The hydroxyl hydrogens of the VA and the hydrogens attached to nitrogen were located in the difference electron density map and allowed to refine isotropically. The crystal data is given in **Table 3.15**.

Table 3.15: VA•NAM crystal data.

Compound	**VA•NAM**
Structural Formula	$C_8H_8O_4$•$C_6H_6N_2O$
VA:NAM ratio	1: 1
Molecular Mass (g mol^{-1})	290.28
Data collection temperature (K)	173(2)
Crystal system	Triclinic
Space group	*P-1*
a (Å)	4.8723 (10)
b (Å)	8.0058 (16)
c (Å)	18.018 (4)
α (°)	78.85 (3)
β (°)	84.50 (3)
γ (°)	75.62 (3)
Volume ($Å^3$)	667.1 (2)
Z	2
D_c, Calculated density (g cm^{-3})	1.445
Final R indices [I>2sigma(I)]	R_1= 0.0434
	wR_2 = 0.1010
R indices (all data)	R_1 = 0.0670
	wR_2 = 0.1131
Largest diff. peak and hole ($eÅ^{-3}$)	0.269; -0.286

The acid: base 1:1 ratio crystallizes in the triclinic space group *P-1* and Z = 2. The asymmetric unit contains one vanillic acid molecule and one nicotinamide molecule. The crystal size dimensions were 0.06 x 0.15 x 0.48 mm. The crystal structure is stabilized by π-π stacking interactions between the vanillic acid aromatic ring (C1 – C6) and the nicotinamide molecule (N9 – C14) with a minimum distance of 4.470 Å. The structure

refined with R1= 0.0434 [I>2sigma(I)]. The packing diagram down [100] is shown in **Figure 3.4.6**.

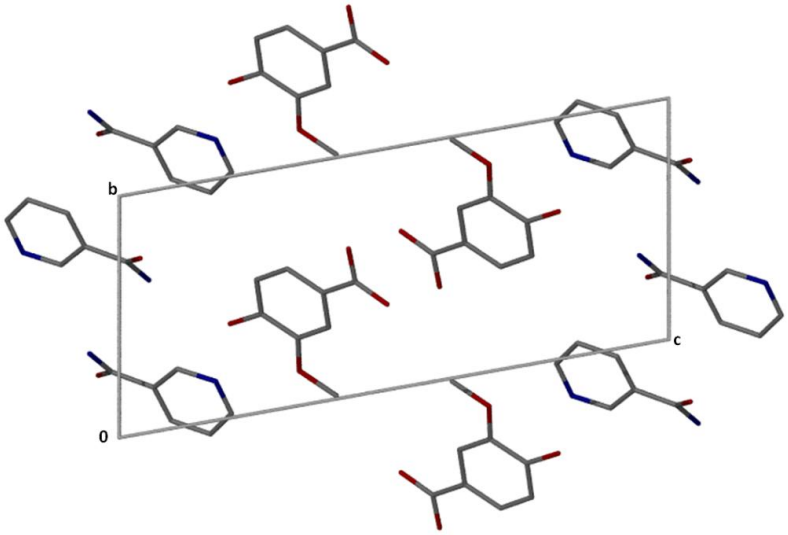

Figure 3.4.6: Packing diagram of **VA•NAM** down [100] with the hydrogen atoms removed.

The structure is mostly stabilized via (NAM) N-H•••O (VA) hydrogen bonds (**Figure 3.4.7**). One nicotinamide nitrogen atom labelled N16 is connected to the oxygen (O5) of a second nicotinamide molecule via the hydrogen H16A. The second hydrogen (H16B) of the nicotinamide molecule is connected to the oxygen (O3) of the vanillic acid. The hydrogen (H5) of the vanillic acid is hydrogen bonded to the nitrogen (N9) of the nicotinamide to give the O3-H5•••N9 connection.

There is a ring formation of hydrogen bonding between two vanillic acid molecules. This hydrogen bonding can be characterized as $R_2^2(8)$. A chain $C_1^1(4)$ motif is found between two NAM molecules. The list of dimers noncyclic motifs in the structure is: D_3^3 (9), D_3^3 (13), D_3^3(17) and D_3^3 (19) which are observed between two VA and two NAM molecules. Another ring $R_4^4(16)$ motif found in the structure involved two VA and two NAM molecules. Only the ring motifs are represented in **Figure 3.4.7**. The hydrogen bond parameters are given in **Table 3.16**.

Table 3.16: VA•NAM hydrogen bonding parameters.

COMPOUND	D-H···A	D···A (Å)	D-H (Å)	H···A (Å)	D-H···A (º)
VA•NAM	N16-H16A···O5[a]	2.847 (2)	0.881 (1)	1.996 (1)	162 (1)
	N16-H16B···O3[b]	2.973 (2)	0.921 (1)	2.061 (1)	170 (1)
	O3-H5···N9[c]	2.674 (2)	0.912 (1)	1.859 (1)	148 (1)
	O1-H1A···O2[d]	2.604 (2)	0.960 (2)	1.648 (5)	173 (3)

a = x+1, y, z ; b = x-1, y, z; c = -x+3, -y+1, -z; d = -x+1, -y+1, -z+1

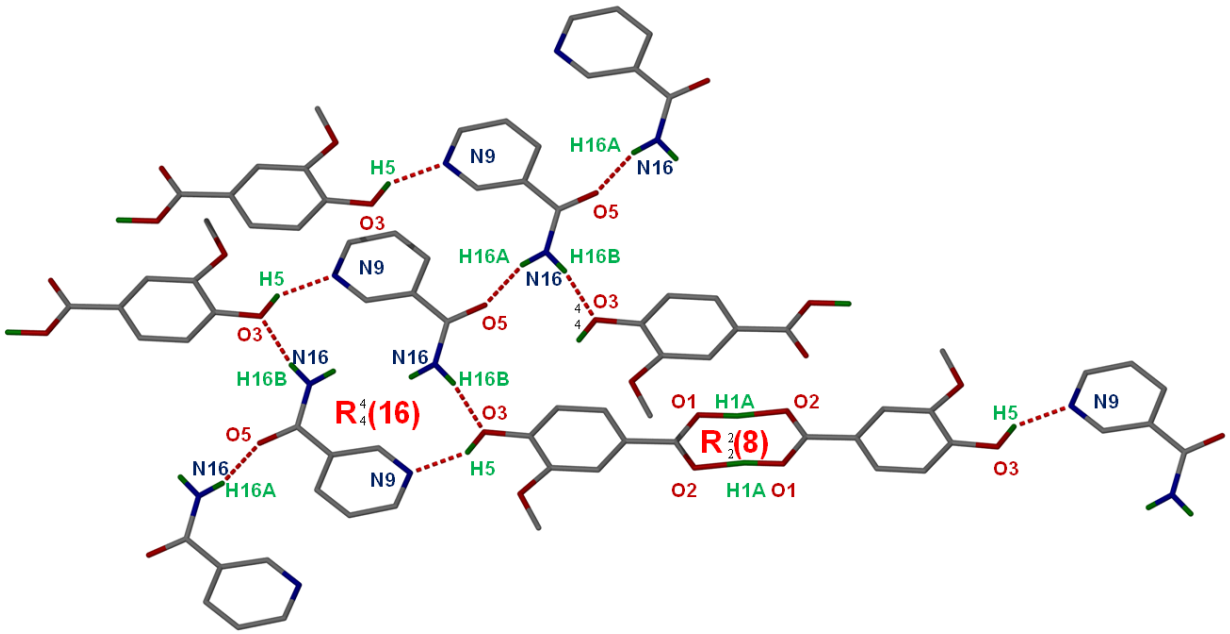

Figure 3.4.7: Hydrogen bonding in **VA•NAM**.

3.5 Vanillic acid and Theobromine (VA•THBR•2H_2O)

Theobromine formerly known as xantheose[26] is a bitter alkaloid of the cacao plant, found in chocolate as well as in many other foods such as leaves of the tea plant. It is a methylxanthine.[27]This compound is used as a vasodilator (blood vessel widener) and heart simulant.[26]

A 1:1 ratio of vanillic acid and theobromine was dissolved in distilled water via slightly heating the solution on a hot plate. The above solution was allowed to evaporate at room temperature and small needle-like crystals were obtained after two days. These crystals included the water from the solvent.

The co-crystal hydrate **VA•THBR•2H_2O** asymmetric unit is illustrated in **Figure 3.5.1**.

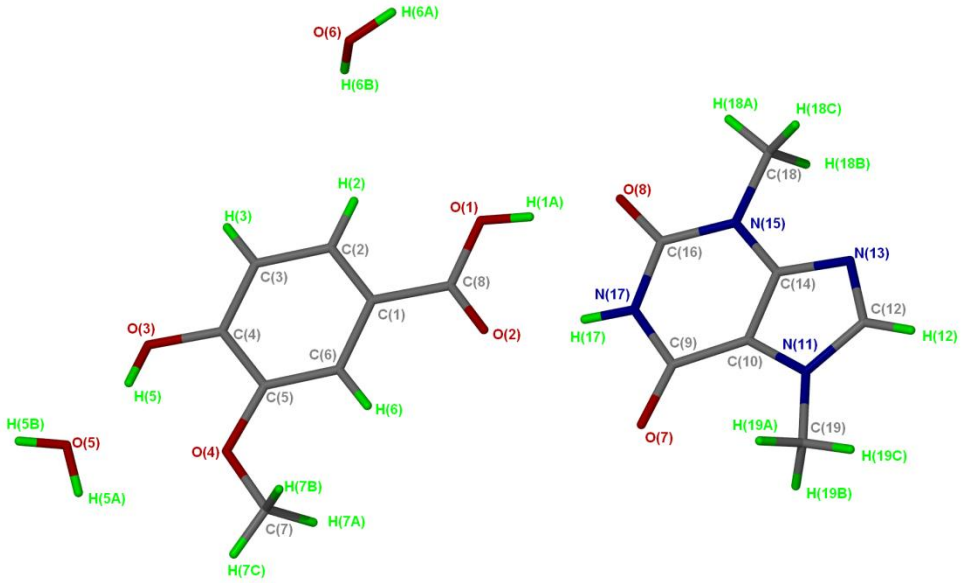

Figure 3.5.1: Asymmetric unit of **VA•THBR•2H_2O** with all the hydrogen atoms shown for numbering clarity.

3.5.1 Thermal Analysis

The thermal analysis results are listed in **Table 3.17** and shown in **Figure 3.5.2**. The TG indicates a single mass loss step. The total mass loss of 9.3 % corresponds to the release of 2 moles of water which is 1.0 % less than the calculated mass loss (10.3%), this falls within experimental error. The DSC curve shows three endotherms, the first one is due to the release of water; the second one is due to the melt of the co-crystal followed by decomposition.

Table 3.17: Thermal analysis data of **VA•THBR•2H_2O**.

Compounds	Vanillic acid	**VA•THBR•2H_2O**	Theobromine
DSC Endo$_1$ ($T_{onset,}$K)	-	362.9	-
DSC Endo$_2$ ($T_{onset,}$K)	482.3	467	623.7
DSC Endo$_3$ ($T_{onset,}$K	-	617.6	-
TG calculated % mass loss		10.3	
TG experimental % mass loss	-	9.3	-
VA:THBR:H_2O ratio		1: 1: 2	

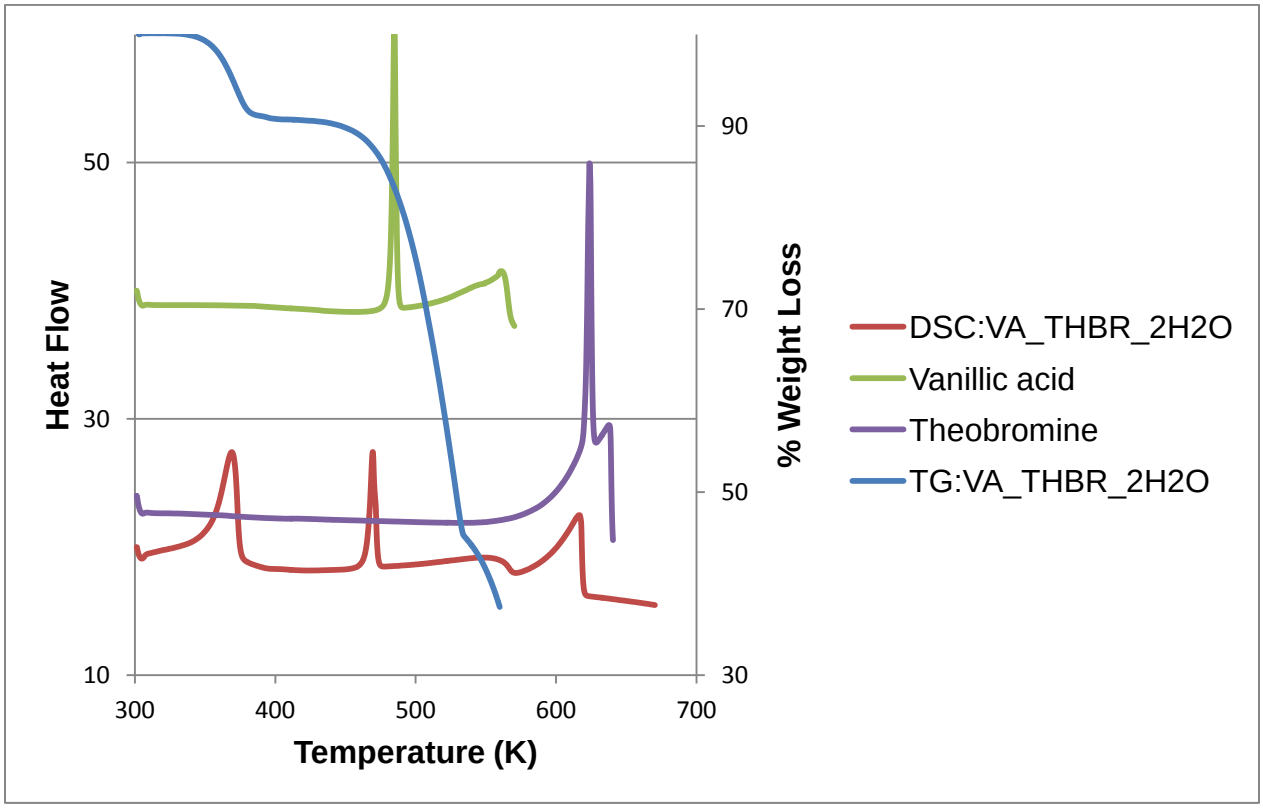

Figure 3.5.2: Thermal analysis of **VA•THBR•2H_2O** DSC (red), **VA•THBR•2H_2O** TG (blue), theobromine (purple), and vanillic acid (green).

3.5.2 IR Spectroscopy

In the IR spectra (KBr disk) of **VA•THBR•2H_2O** some bands were shifted relative to that of the starting components (**Table 3.18**). Shifts in both carbonyl and amine IR stretching frequencies indicated the formation of a new co-crystal phase. The OH stretching frequency at 3424 cm^{-1} is characteristic of **VA•THBR•2H_2O**. The spectra of all components are shown in **Figure 3.5.3**.

Table 3.18: IR positions and assignments of peaks in VA, **VA•THBR•2H_2O** and THBR.

VA	**VA•THBR•2H_2O**	THBR	Proposed assignment
3480, 3099	3424	-	OH stretch
-	3100, 3017	3114, 3027	H-bonded NH_2 stretching mode
2988	2788, 2361	2827, 2367	C-C ring modes
1763, 1667	1690	1711	C=O
-	1556	1547	N-H bend
1599, 1524, 1478, 1454	1598	1593	C=C stretch
1275, 1202	1226	1224	C-O stretch

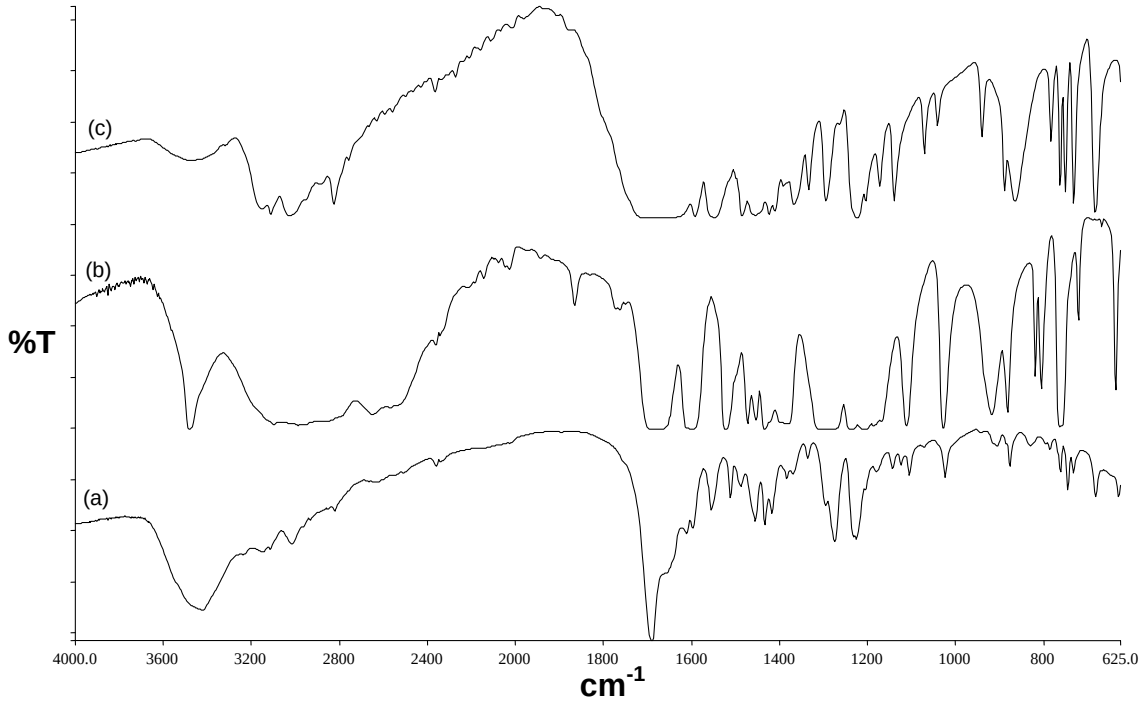

Figure 3.5.3: IR spectrum (a) **VA•THBR•2H_2O**, (b) VA and (c) THBR.

3.5.3 Powder X-ray Diffraction

The PXRD results of all the experiments are given in **Figure 3.5.4**. The grinding experiment did not work because the PXRD gave the same pattern as that of the physical mixture.

However, addition of a few drops of water with grinding gave **VA•THBR•2H_2O**. The PXRD pattern of the liquid assisted ground product was in overall good agreement with that of the calculated PXRD pattern obtained from LAZYPULVERIX.[12] The intensity of the first peak in the assistance liquid ground product is very small than the calculated pattern.

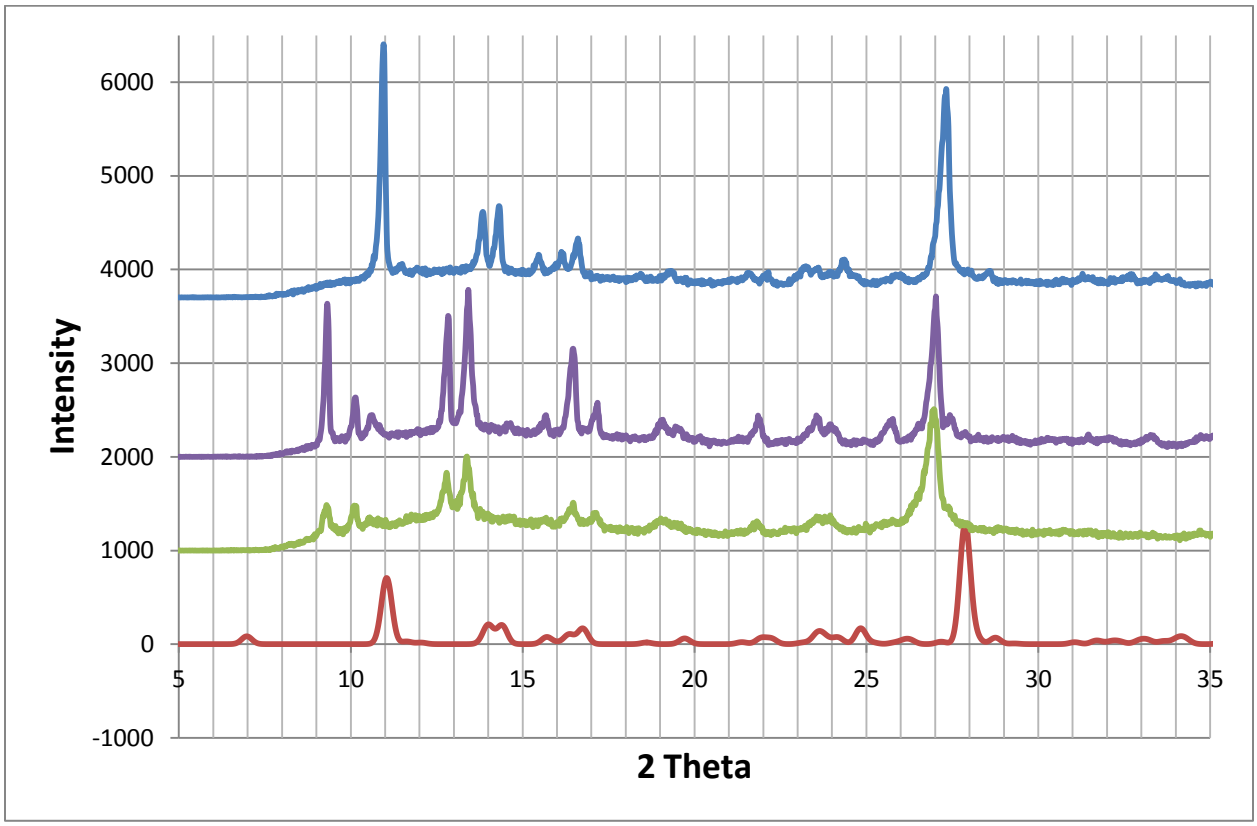

Figure 3.5.4: PXRD patterns of **VA•THBR•2H$_2$O** (red), ground product (green), physical mixture (purple) and assistance liquid ground product (blue).

3.5.4 Structure Determination

Intensity data were collected by the standard phi scan and omega scan techniques scaled and reduced using SAINT-Plus.[28] Direct methods were used to solve the structures, refinement was completed by full matrix least squares with SHELX-97,[18] refining on F^2. X-Seed[19] was used as a graphical interface. The hydroxyl hydrogens of the vanillic acid and the hydrogens attached to nitrogen atoms were located in the difference electron density map and refined isotropically. All the non-hydrogen atoms were found in the difference electron density map. The crystal data of **VA•THBR•2H$_2$O** is given in **Table 3.19**.

Table 3.19: VA•THBR•2H_2O crystal data.

Compound	**VA•THBR•2H_2O**
Structural Formula	$C_8H_8O_4$•$C_7H_8N_4O_2$•2H_2O
VA:THBR:H_2O ratio	1: 1: 2
Molecular Mass (g mol^{-1})	384.35
Data collection temperature (K)	173(2)
Crystal system	Triclinic
Space group	*P-1*
a (Å)	8.2148 (16)
b (Å)	8.2504 (17)
c (Å)	13.132 (3)
α (°)	102.82 (3)
β (°)	97.46 (3)
γ (°)	93.98 (3)
Volume ($Å^3$)	856.1 (3)
Z	2
D_c, Calculated density (g cm^{-3})	1.491
Final R indices [I>2sigma(I)]	R_1= 0.0415
	wR_2 = 0.1045
R indices (all data)	R_1 = 0.0609
	wR_2 = 0.1156
Largest diff. peak and hole ($eÅ^{-3}$)	0.260; -0.236

VA•THBR•2H_2O (**Figure 3.5.1**) crystallized in the triclinic space group *P-1* with one vanillic acid molecule, one theobromine molecule and two water molecules in the asymmetric unit. The crystal size dimensions were 0.05 x 0.11 x 0.53 mm. The structure was successfully refined to R_1 = 0.0415 with wR_2 = 0.1045 ([I>2sigma (I)]). The co-crystal hydrate is stabilised via π-π stacking interactions between theobromine five-membered ring (N11 – C12) and vanillic acid six-membered ring (C1 – C6) with a shortest distance of 3.532 Å.

There is a very weak C-H•••π interaction between the five membered ring of the theobromine molecule and the hydrogen atom (H12) of another theobromine five membered ring with a minimum distance of 3.214 Å and a C-H•••π angle of 103 °.

The packing diagrams and the cavities occupied by the water molecules obtained from Mercury[20] software (contact surface, probe radius: 1.4 Å and grid spacing 0.7 Å) are shown in **Figure 3.5.5 (a), (b) and (c)**.

The void volume was found to be 52.57 $Å^3$ with a unit cell percentage volume of 6.10 %.

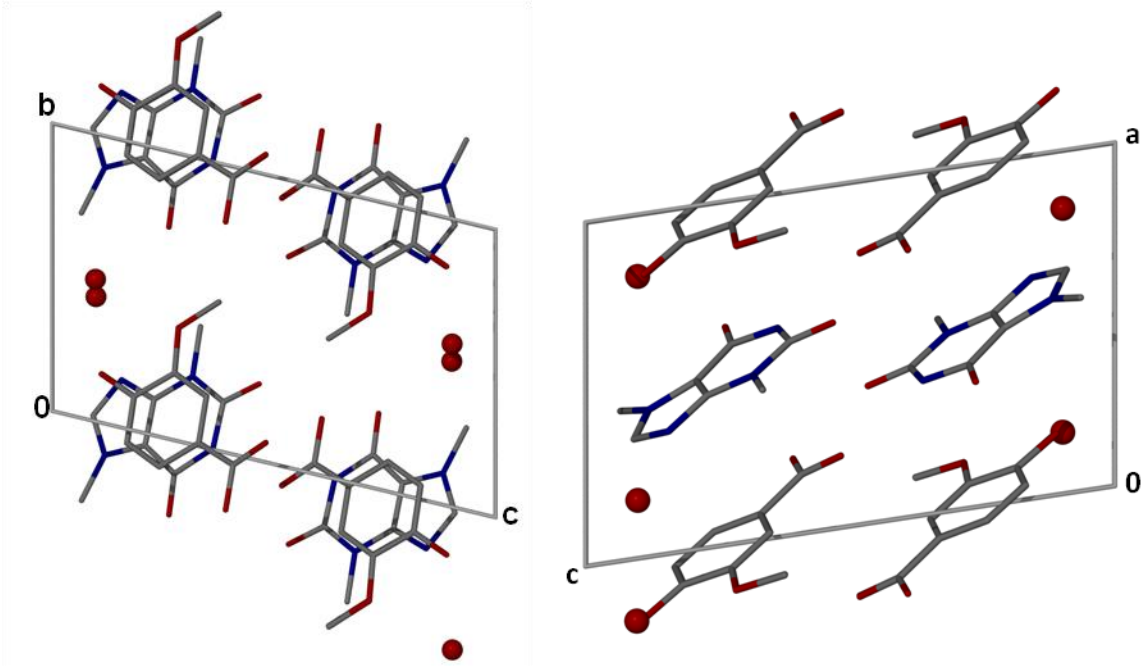

(a) **(b)**

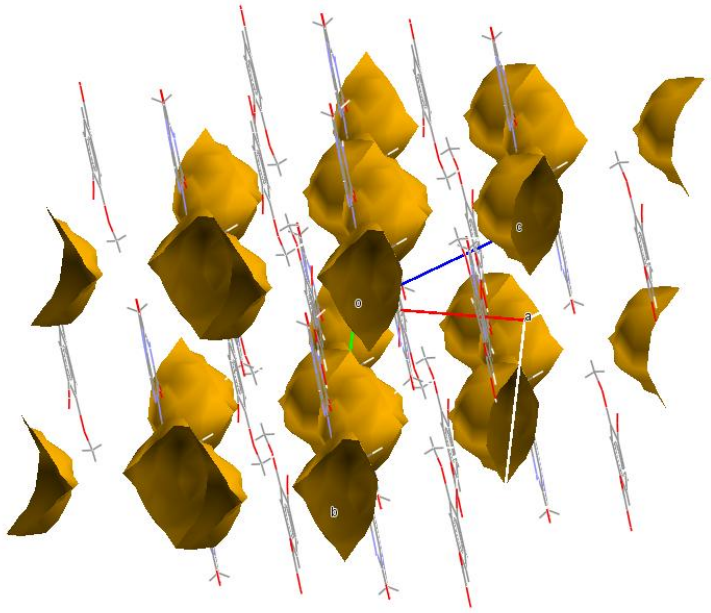

(c)

Figure 3.5.5: (a) Packing diagram of **VA•THBR•2H$_2$O** down [100] with the hydrogen atoms removed **(b)** Packing diagram of **VA•THBR•2H$_2$O** down [010] with the hydrogen atoms removed, **(c)** cavities in which water molecules are located.

The structure is further stabilized via (VA) O1-H1A•••O8 (THBR) and (THBR) N17-H17•••O2 (VA) hydrogen bonds (**Figure 3.5.6**). This hydrogen bonding can be represented as $R_2^2(8)$ ring motifs. The water molecule with the oxygen atom labelled O5 is a bifurcated acceptor where it connects to one hydrogen (H6B) atom of the second water molecule and the hydrogen (H5) of the VA. O5 is a also a bifurcated donor where it links a water molecule and a THBR molecule.

In addition, the hydrogen (H5A) of the water molecule is hydrogen bonded to the oxygen (O7) of the theobromine molecule. The other hydrogen (H5B) of the same molecule of water is connected to the oxygen (O6) of the second water molecule in the structure. Hydrogen bonds between four molecules of water result in an $R_4^4(8)$ ring

motifs. There is also the presence of a dimer $D_2^1(3)$ noncyclic motif which is between two water molecules and one VA. The other dimer noncyclic motifs ($D_2^2(4)$, $D_2^2(5)$, $D_2^2(6)$, $D_2^2(7)$, $D_2^2(8)$, $D_2^2(10)$ and $D_2^2(11)$) in the crystal structure involve one VA molecule, one THBR molecule and one water molecule. The ring motifs are illustrated in **Figure 3.5.6**.

Thus all the hydrogen bond donor/acceptor sites of the theobromine molecule are utilized in the structure. **Table 3.20** is listing the hydrogen bonding parameters.

Table 3.20: VA•THBR•2H_2O hydrogen bonding parameters.

COMPOUND	D-H···A	D···A (Å)	D-H (Å)	H···A (Å)	D-H···A (º)
VA•THBR•2H_2O	O1-H1A···O8	2.652 (2)	0.939 (3)	1.719 (3)	172 (2)
	O3-H5···O5	2.719 (2)	0.881 (3)	1.859 (3)	165 (2)
	O6-H6B···O5[a]	2.868 (2)	0.853 (3)	2.064 (3)	157 (3)
	O6-H6A···N13[b]	2.901 (2)	0.899 (3)	2.013 (3)	169 (2)
	O5-H5A···O7[c]	2.802 (2)	0.861 (3)	1.941 (3)	179 (3)
	O5-H5B···O6[d]	2.763 (2)	0.840 (2)	1.929 (3)	172 (2)
	N17-H17···O2	2.825 (2)	0.916 (2)	1.915 (2)	172 (2)

a = x, y+1, z ; b = -x+1, -y+1, -z+1; c = -x, -y-1, -z+1; d = -x, -y, -z+2

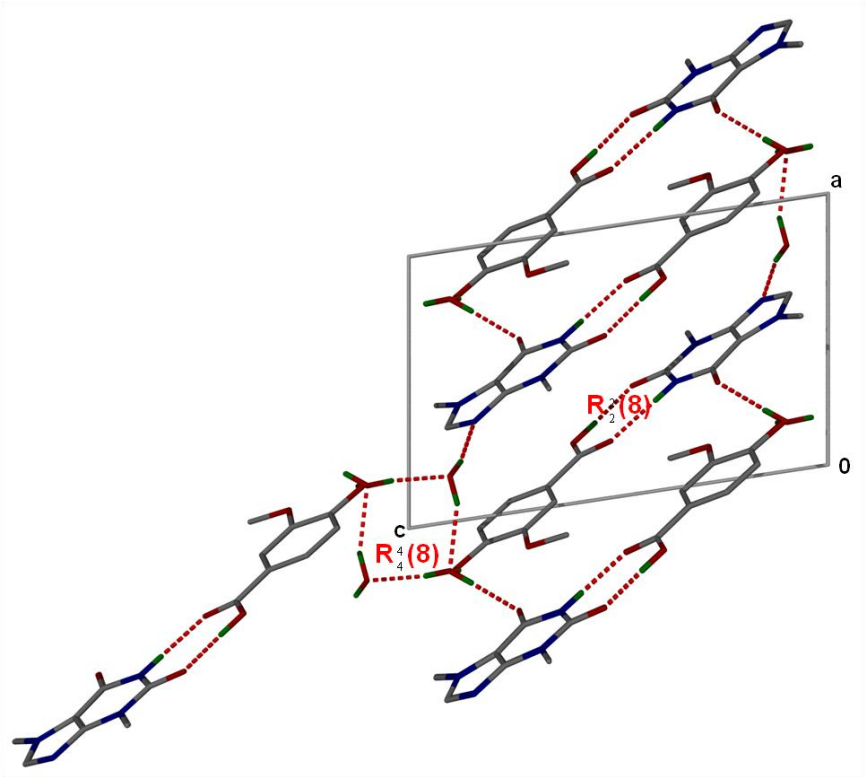

Figure 3.5.6: Hydrogen bonding in **VA•THBR•2H$_2$O** down [010].

3.6 Vanillic acid and Theophylline (2VA•THPH)

Theophylline (1, 3-dimethylxanthine) is used in the treatment of respiratory diseases and asthma. It is found in the cocoa bean.[14]

The two solid components, vanillic acid (VA) and theophylline (THPH) were dissolved in distilled water via slight heating on a hot plate in a 1: 1 ratio. The solution was allowed to evaporate at ambient temperature and needle-like crystals with an acid: base ratio of 2: 1 was obtained. The asymmetric unit of **2VA•THPH** is shown in **Figure 3.6.1**.

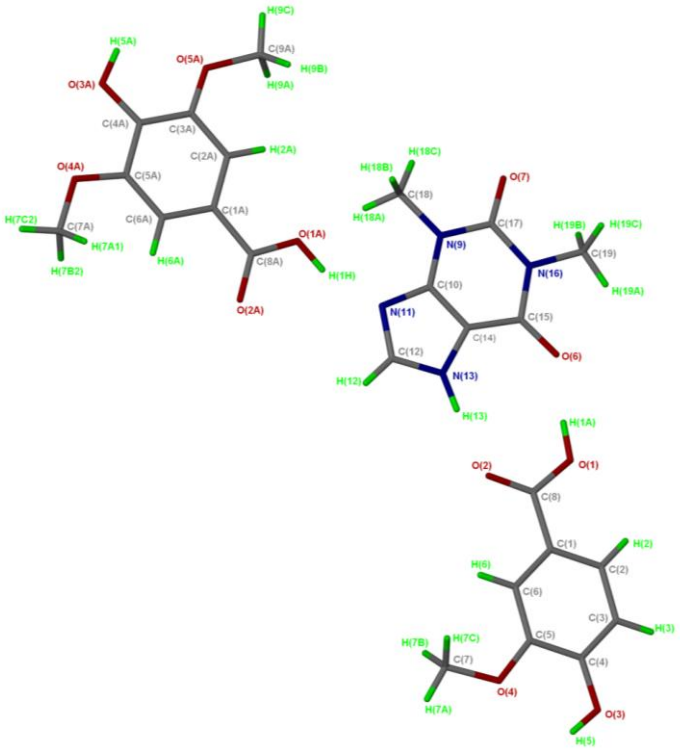

Figure 3.6.1: Asymmetric unit of **2VA•THPH** structure with all the hydrogen atoms shown for numbering clarity.

3.6.1 Thermal Analysis

The thermal stability of the **2VA•THPH** co-crystal is reduced due to it lower melting point than the two starting materials. Thermal analysis data are given in **Table 3.21** and the DSC curves are shown in **Figure 3.6.2**.

Table 3.21: Thermal analysis data of **2VA•THPH**.

Compounds	**DSC Endo$_2$(T_{onset},K)**
Theophylline	547.7
Vanillic acid	482.3
2VA•THPH	459.7

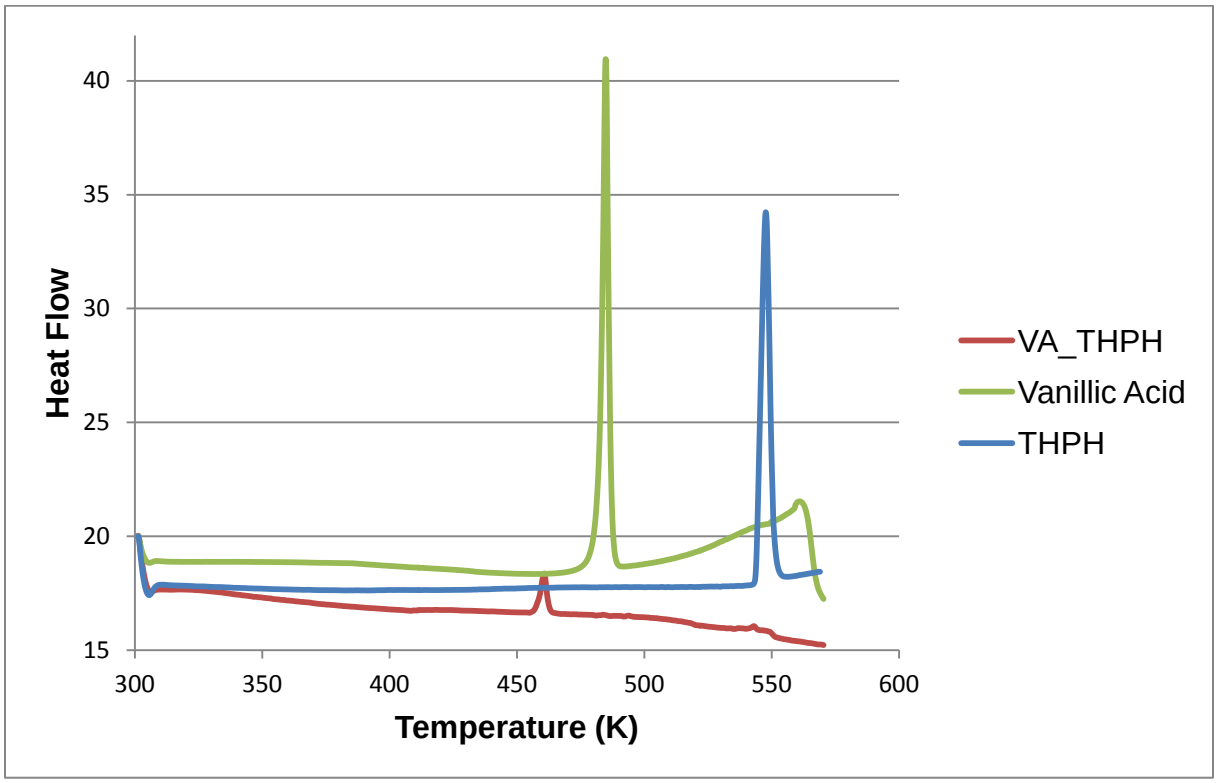

Figure 3.6.2: DSC curves of **2VA•THPH** (red), vanillic acid (green) and theophylline (blue).

3.6.2 Hot Stage Microscopy

Needle-like crystals were placed on a hot stage and immersed in silicone oil at ambient temperature. The crystals became opaque at a temperature of 452 K and started bubbling at 456 K. The crystals were completely melted at a temperature of 461 K. **Figure 3.6.3** shows the HSM photography of the crystals.

(a) 295 K **(b) 452 K**

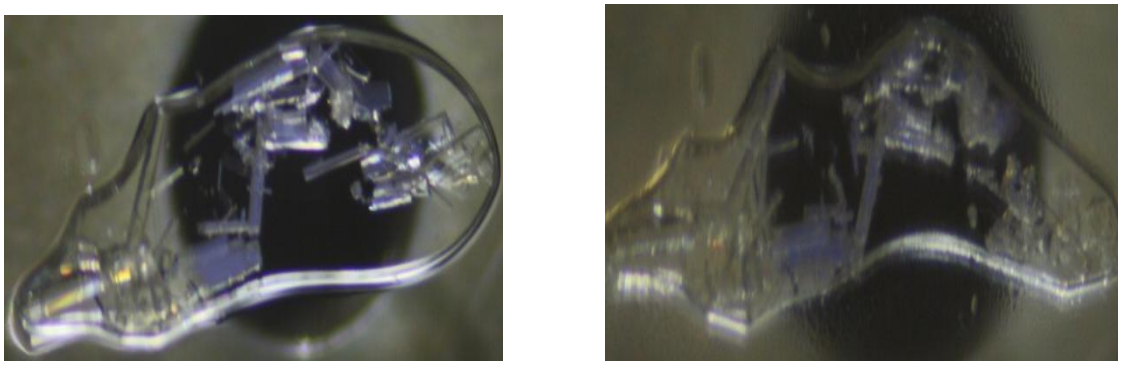

(c) 456 K **(d) 461 K**

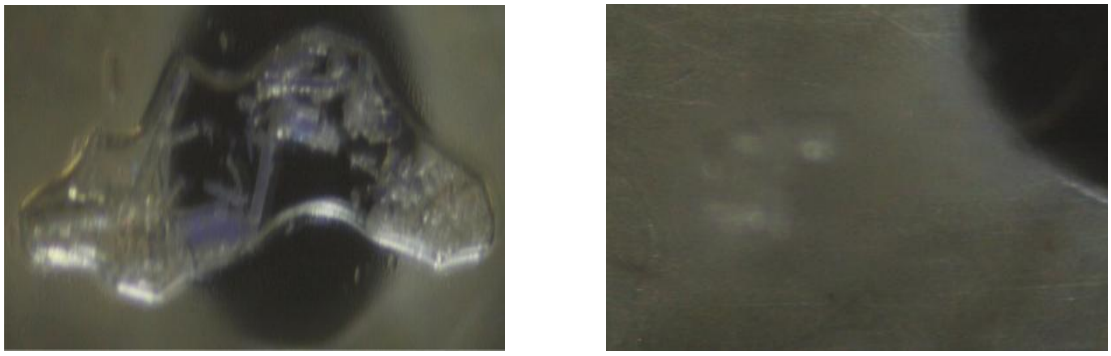

Figure 3.6.3: HSM photography of **2VA•THPH**: **(a)** Crystals immersed in silicone oil, **(b)** Crystals become opaque, **(c)** Crystals begin to melt, **(d)** Crystals completely melt.

3.6.3 IR Spectroscopy

There is a shift in the OH stretch frequency (3420 cm^{-1}) and the H-bonded NH_2 stretching mode (3124 and 3010 cm^{-1}) of the **2VA•THPH**. This is an indication of co-crystal formation. The IR results are tabulated in **Table 3.22**.

Figure 3.6.4 shows the IR spectra of the starting material and the resultant co-crystal.

There is a shift in the OH stretch frequency (3420 cm^{-1}) and the H-bonded NH_2 stretching mode (3124 and 3010 cm^{-1}) of the **2VA•THPH**. This is an indication of a co-crystal formation.

Table 3.22: IR positions and assignments of peaks in VA, **2VA•THPH** and THPH.

VA	**2VA•THPH**	THPH	Proposed assignment
3480, 3099	3420	-	OH stretch
-	3124, 3010	3347, 3121	H-bonded NH_2 stretching mode
2988	2810	2787, 2598	C-C ring modes
1763, 1667	1701, 1672	1688	C=O
-	1558	1484	N-H bend
1599, 1524, 1478, 1454	1591	1570	C=C stretch
1275, 1202	1227	1240	C-O stretch

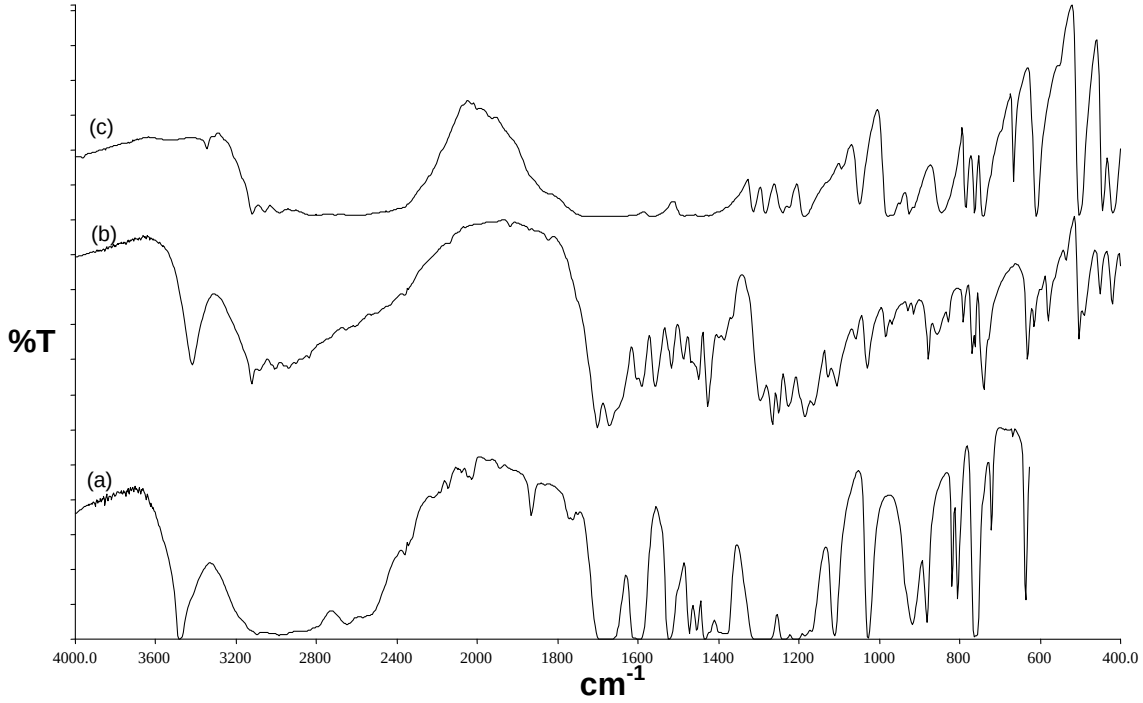

Figure 3.6.4: IR spectrum (a) VA, (b) **2VA•THPH** and (c) THPH.

3.6.4 Powder X-ray Diffraction

For both the slurry and the grinding experiments 2: 1 mixtures of VA: THPH were used. The slurry experiment performed in water and the ground products both after 20 and 30 min are similar and contain some of the peaks found in the PXRD of the physical mixture as illustrated in **Figure 3.6.5**. The PXRD spectra of the slurry and the ground mixtures do not match that of the co-crystal.

Thermal analysis was performed on the powdered sample obtained from the slurry and both the TG and DSC curves showed that the co-crystal hydrate had been prepared. The experiment mass loss of water in the slurry conversion powder was found to be 6.6 % (Calc 5.8 %) which corresponds to 2 moles of water (**2VA•THPH•2H_2O**). The onset of both the release of water and the co-crystal are 336.3 K and 457.6 K respectively. The TG and DSC curves of the co-crystal hydrate are shown in **Figure 3.6.6**. Attempts at obtaining single crystals of the hydrate were unsuccessful. The assumption of the co-crystal hydrate **2VA•THPH•2H_2O** was only confirmed via thermal analysis.

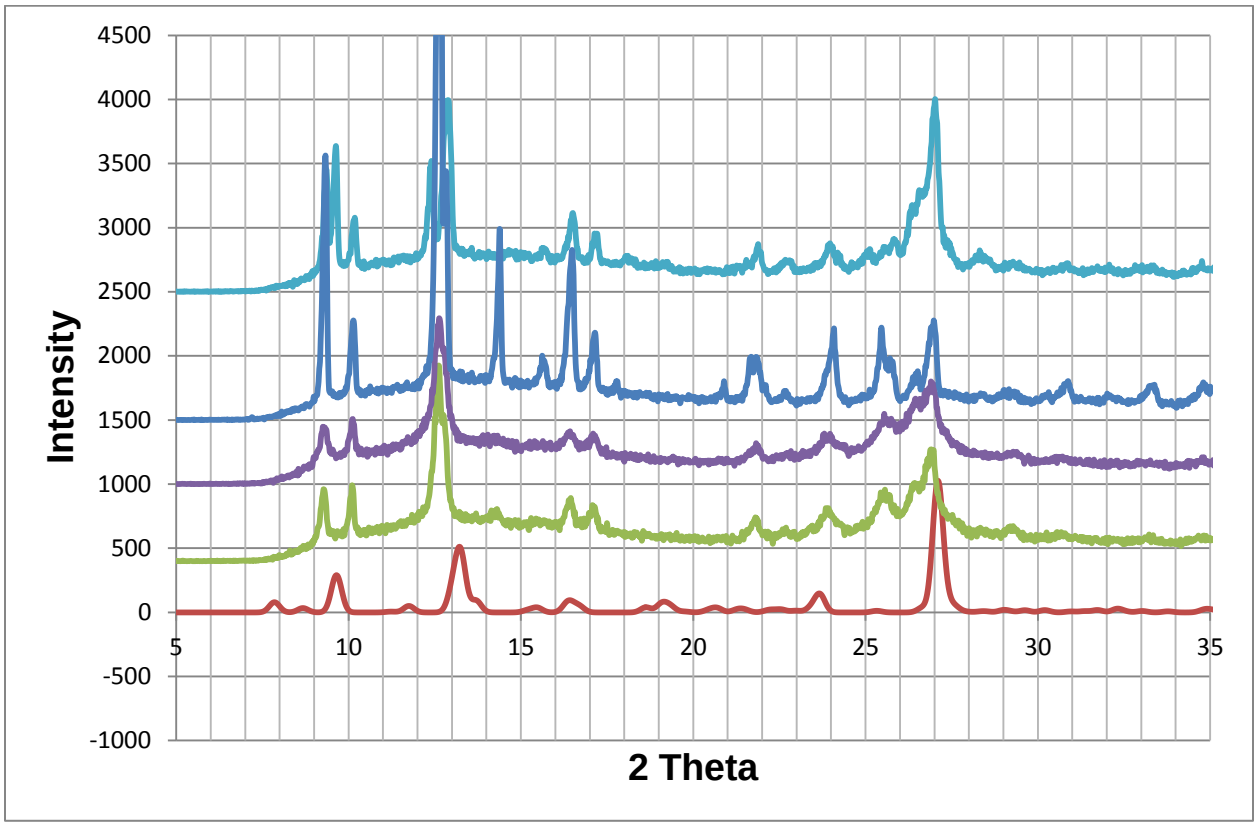

Figure 3.6.5: PXRD patterns of **2VA•THPH** (red), ground product after 20 min (green), ground product after 30 min (purple), slurry (sky blue) and physical mixture (blue).

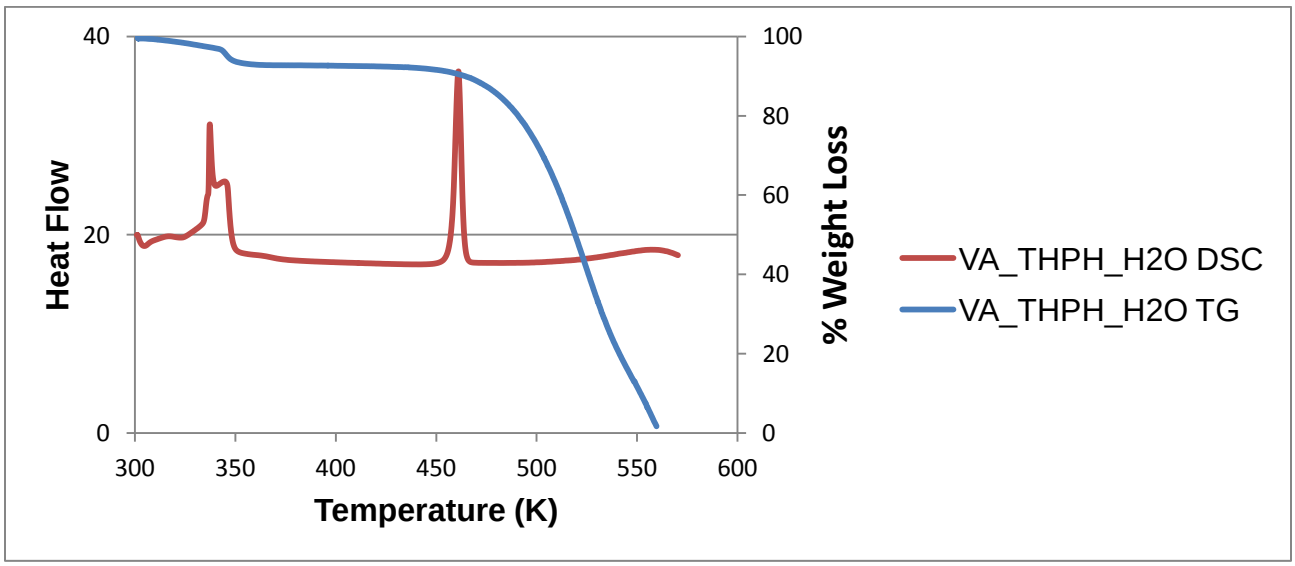

Figure 3.6.6: Thermal analysis curves: **2VA•THPH** Hydrate DSC (red) and **2VA•THPH** Hydrate (**2VA•THPH•2H_2O**) TG (blue).

3.6.5 Structure Determination

The positions of all the non-hydrogen atoms in the asymmetric unit including two vanillic acid molecules and one theophylline molecule were found by direct methods. The vanillic acid and theophylline molecules were located in general positions. The amine hydrogen was located in the difference electron density map. In the subsequent refinement all vanillic acid and theophylline non-hydrogen atoms were refined anisotropically.

Table 3.23: Crystal data of **2VA•THPH**.

Compound	**2VA•THPH**
Structural Formula	$2C_8H_8O_4 \bullet C_7H_8N_4O_2$
VA:THPH ratio	2: 1
Molecular Mass (g mol^{-1})	515.45
Data collection temperature (K)	173(2)
Crystal system	Monoclinic
Space group	$P2_1/c$
a (Å)	11.2741 (6)
b (Å)	15.7712 (10)
c (Å)	13.3746 (8)
α (°)	90.00 (0)
β (°)	90.572 (2)
γ (°)	90.00 (0)
Volume ($Å^3$)	2378.0 (2)
Z	4
D_c, Calculated density (g cm^{-3})	1.440
Final R indices [I>2sigma(I)]	R_1= 0.0472
	wR_2 = 0.1201
R indices (all data)	R_1 = 0.0655
	wR_2 = 0.1305
Largest diff. peak and hole ($eÅ^{-3}$)	0.316; -0.242

2VA•THPH crystallizes in the monoclinic crystal system. A crystal with dimensions of 0.16 x 0.22 x 0.50 mm was used. The structure was solved in the space group $P2_1/c$. The structural formula of this co-crystal is $2C_8H_8O_4•C_7H_8N_4O_2$. The structure refined successfully to R_1 = 0.0472 with wR_2 = 0.1201 [I>2sigma (I)]. The methoxy group of the second vanillic acid molecule is disordered. The site occupancy factors for the two VA molecules in the final refinement were 0.812 and 0.188 respectively. The structure is stabilised via π-π stacking interactions between neighbouring vanillic acid molecules and between vanillic acid and theophylline molecules. The shortest distance of 3.401 Å was observed between the aromatic ring (C1 - C6) of a vanillic acid molecule and the six membered ring of a theophylline molecule (N9 - C17). The crystal structure also contains a C-H•••π interaction between the vanillic acid ring (C1 – C6) and hydrogen atom (H9A) found in a second vanillic acid molecule with a distance of 2.877 Å and a C-H•••π angle of 162 ° (**Figure 3.6.7**). The packing diagram of **2VA•THPH** is shown in **Figure 3.6.8** with Z= 4.

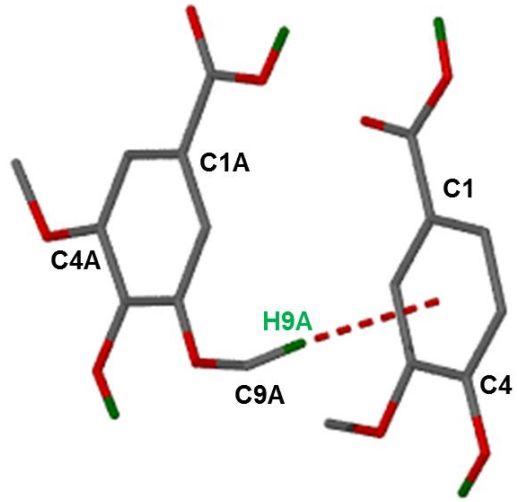

Figure 3.6.7: C-H•••π interaction in **2VA•THPH**.

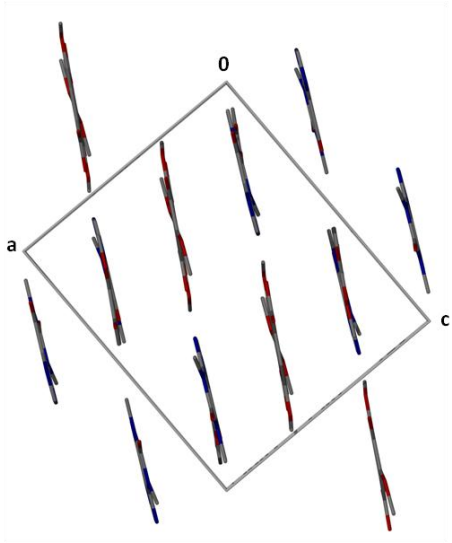

Figure 3.6.8: Packing diagram of **2VA•THPH** down [010] with the hydrogen atoms removed.

Each theophylline molecule is hydrogen bonded to four vanillic acid molecules as shown in Figure **3.6.9**. Thus all of the hydrogen bond donor/acceptor sites of the theophylline molecule are utilized. The hydrogen bonding details are given in **Table 3.24.** There are $R_2^2(9)$ and $R_3^3(9)$ ring motifs between the (VA) O1-H1A•••O6 (THPH) and (THPH) N13-H13•••O2 (VA) connection. There is a weak C-H•••O (C12-H12•••O3A) hydrogen bond with a C•••O and H•••O distances of 3.031 Å and 2.182 Å.[29, 30]

Table 3.24: 2VA•THPH hydrogen bonding parameters.

COMPOUND	D-H···A	D···A (Å)	D-H (Å)	H···A (Å)	D-H···A (º)
2VA•THPH	O3-H5···O7[a]	2.679(2)	0.876 (3)	1.937 (3)	142 (3)
	N13-H13···O2	2.770 (2)	0.955 (2)	1.820 (2)	173 (2)
	O1-H1A···O6	2.645 (2)	0.942 (3)	1.704 (3)	175 (2)
	O3A-H5A···O2[b]	2.616 (2)	0.914 (3)	1.712 (3)	170 (2)
	O1A-H1H···N11	2.679 (2)	0.937 (3)	1.772 (3)	162 (2)
	C12-H12···O3A	3.031 (1)	0.950 (1)	2.182 (1)	148 (1)

a = x, y-1, z ; b = -x+1, y+1/2, -z-1/2

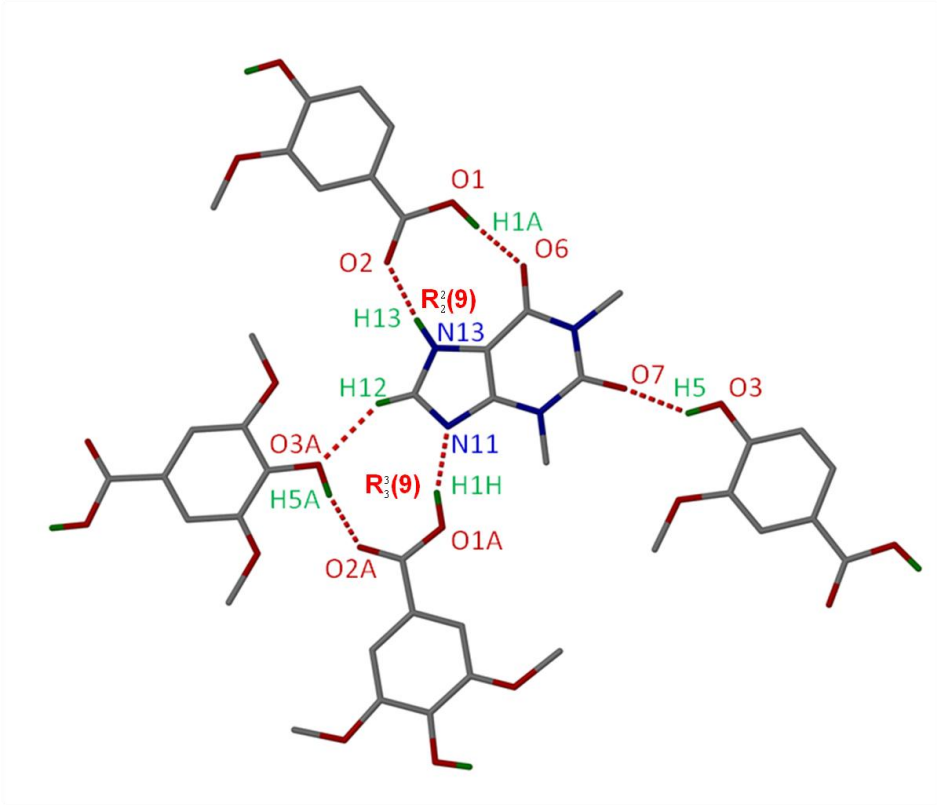

Figure 3.6.9: Hydrogen bonding in **2VA•THPH**.

3.7 Vanillic acid and Urea

Urea, CH_4N_2O is used for the denaturation of proteins and as a mild solubilization agent for insoluble or denatured proteins.[31, 32]

Both compounds (1:1 ratio of vanillic acid: urea) were dissolved in ethanol by gently heating on a hot plate. The solution was allowed to evaporate at room temperature and after 3 days crystals were obtained. Similar crystals were obtained when dissolving a 1:1 ratio of vanillic acid and urea in acetone.

The asymmetric unit of **2VA•2U** is shown in **Figure 3.7.1.**

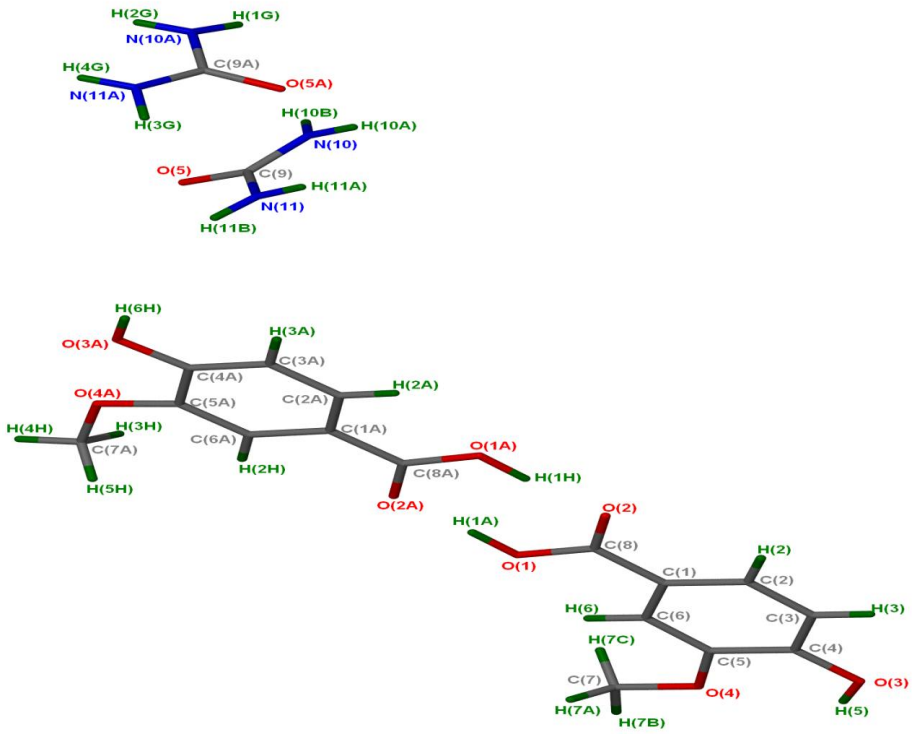

Figure 3.7.1: Asymmetric unit of **2VA•2U** structure with all the hydrogen atoms shown for numbering clarity.

3.7.1 Thermal Analysis

The thermal analysis results are listed in **Table 3.25**. The DSC of the co-crystal (**Figure 3.7.2**) shows a single endotherm which is in between the two starter materials. The **2VA•2U** co-crystal has a higher thermal stability than urea but, a lower thermal stability than vanillic acid.

Table 3.25: Thermal analysis data of **2VA•2U**.

Compounds	**DSC Endo$_2$(T_{onset},K)**
Urea	409.99
Vanillic acid	482.3
2VA•2U	435.56

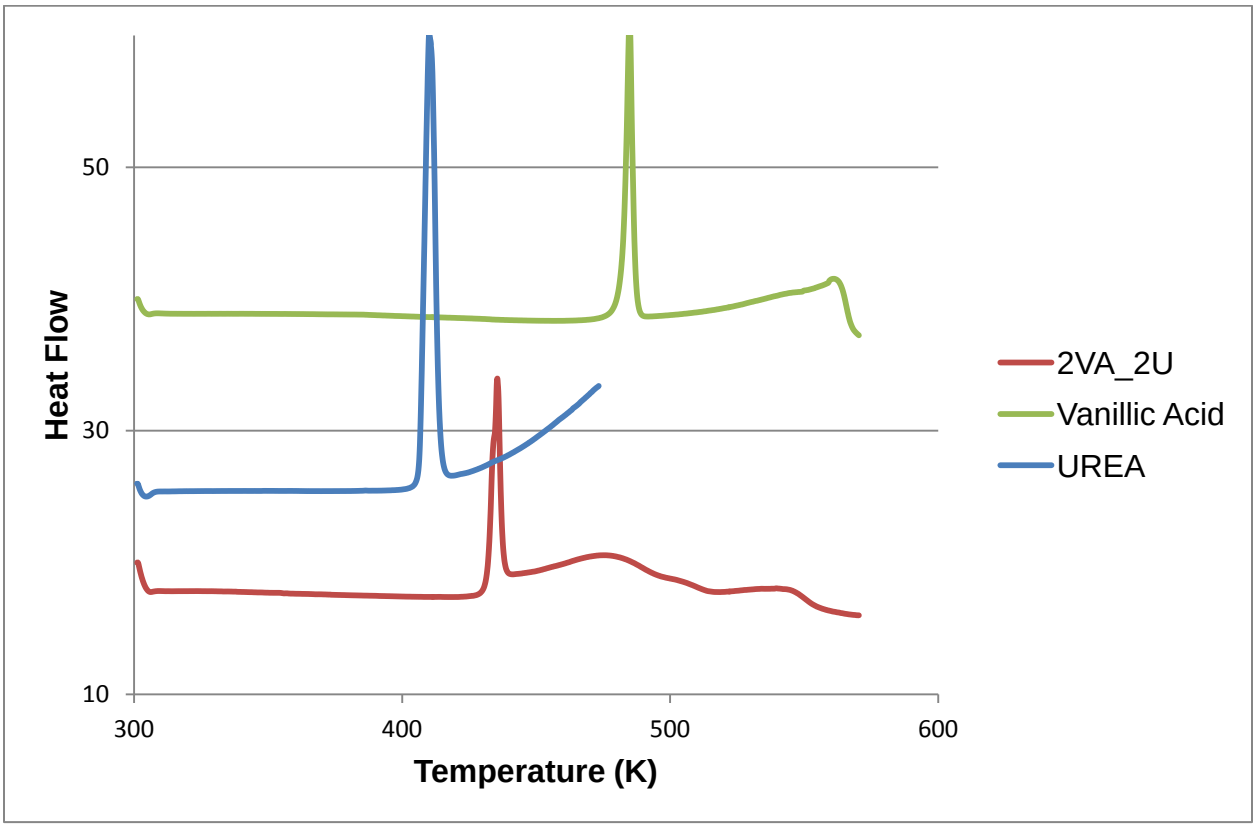

Figure 3.7.2: DSC curves of **2VA•2U** (red), vanillic acid (green) and urea (blue).

3.7.2 Powder X-ray Diffraction

A 1: 1 mixture of vanillic acid and urea was ground for 30 min. The PXRD pattern of the ground product resembled that of the physical mixture. A peak at 2θ (approximately 11.5) found in the PXRD of the co-crystal is also present in the PXRD of the ground product. A few drops of ethanol were added to the ground product and the PXRD pattern is similar to the one obtained from the slurry conversion experiment performed in ethanol. These two PXRD patterns (solvent drop ground product and slurry conversion) match that of the calculated pattern obtained from LAZYPULVERIX[12] as illustrated in **Figure 3.7.3**.

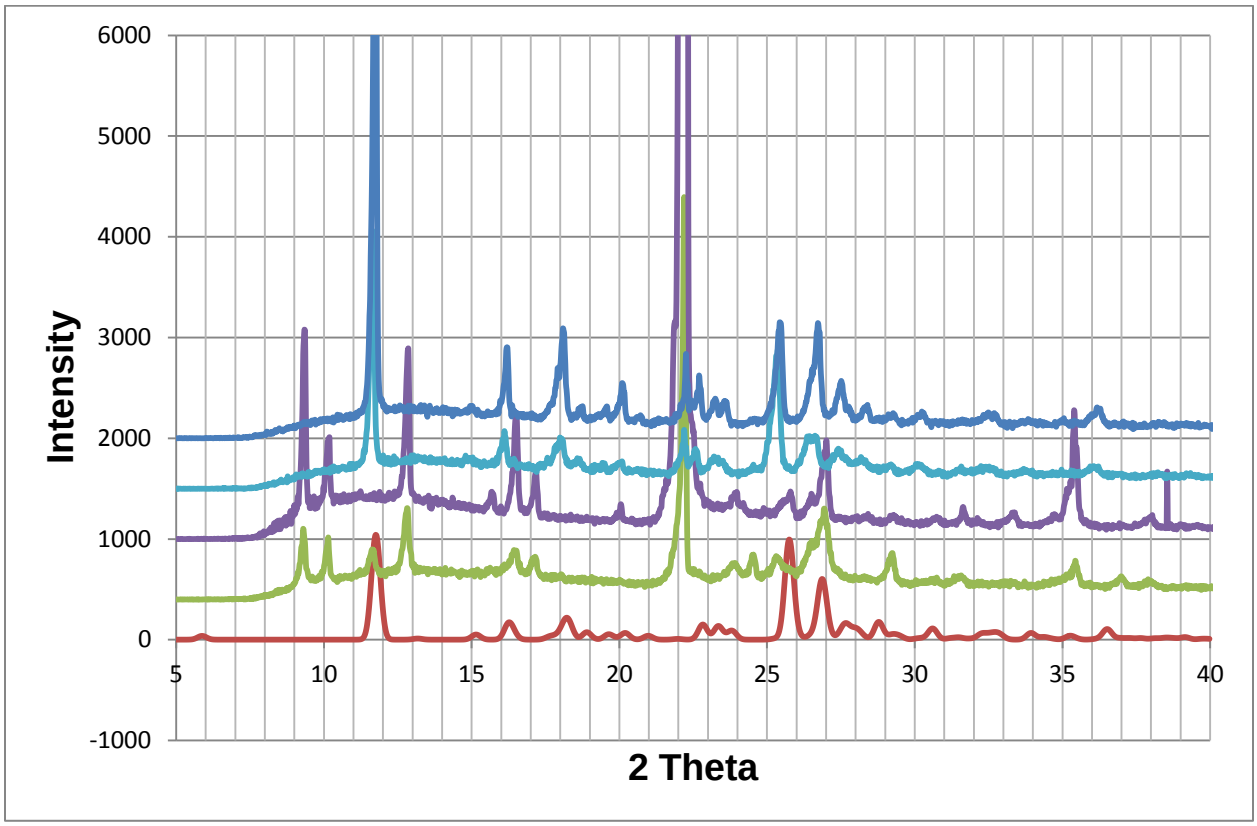

Figure 3.7.3: PXRD patterns of **2VA•2U** (red), ground product (green), physical mixture (purple), assistance liquid ground product (sky blue) and slurry (blue).

3.7.3 Structure Determination

Direct methods were used to solve the structures, refinement was completed by full matrix least squares with SHELX-97,[18] refining on F^2. X-Seed[19] was used as a graphical interface. All non-hydrogen atoms were found in the difference electron density map. The hydroxyl hydrogens of the VA and the hydrogens attached to nitrogen were located in the difference electron density map and were allowed to refine isotropically. The remaining hydrogens were placed with geometric constraints and refined isotropically. The crystal data is given in **Table 3.26**.

Table 3.26: Crystal data of **2VA•2U**.

Compound	**2VA•2U**
Structural Formula	$2C_8H_8O_4 \bullet 2CH_4N_2O$
VA:U ratio	2: 2
Molecular Mass (g mol^{-1})	456.41
Data collection temperature (K)	173(2)
Crystal system	Triclinic
Space group	*P-1*
a (Å)	6.9821 (14)
b (Å)	10.232 (2)
c (Å)	15.388 (3)
α (°)	99.68 (3)
β (°)	95.37 (3)
γ (°)	103.46 (3)
Volume ($Å^3$)	1043.8 (4)
Z	2
D_c, Calculated density (g cm^{-3})	1.452
Final R indices [I>2sigma(I)]	R_1= 0.0473
	wR_2 = 0.1015
R indices (all data)	R_1 = 0.0844
	wR_2 = 0.1181
Largest diff. peak and hole ($eÅ^{-3}$)	0.215; -0.267

The acid: base combination crystallized in a 2: 2 ratio, triclinic space group *P-1* and Z=2. The crystal use for the data collection had dimensions of 0.03 mm x 0.14 mm x 0.34 mm where the vanillic acid and the urea molecules were located in general positions. The crystal structure was successfully refined to R_1 = 0.0473 with wR_2 = 0.1015 [I>2sigma (I)]. The co-crystal is stabilised via face to face π-π stacking interactions between two vanillic acid molecules (C1 – C6 and C1A – C6A) with a minimum distance

of 3.601 Å. The packing diagram view down [010] of the **2VA•2U** co-crystal is shown in **Figure 3.7.4**.

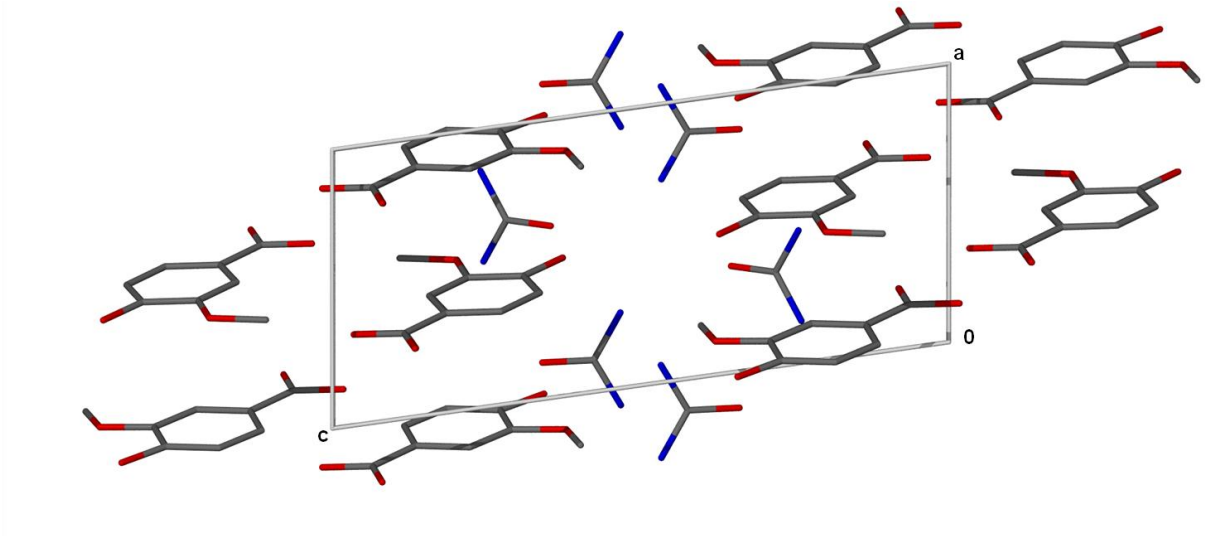

Figure 3.7.4: Packing diagram of **2VA•2U** down [010] with the hydrogen atoms removed.

The hydrogen bonding in **2VA•2U** is very complex. This is due to the fact that all of the urea hydrogen atoms are involved in hydrogen bonding. The oxygen O5 in the first urea molecule is connected to two of the hydrogen atoms (H1G and H3G) in the second urea molecule and to the hydroxyl group in the first vanillic acid compound. The same connectivity is observed with the oxygen atom O5A in the second urea molecule with an exception that O5A is hydrogen bonded to H10B, H11B and the hydroxy group of the second vanillic acid molecule. The two urea molecules form an amide-amide homodimer synthon through an $R_2^2(8)$ ring motif. This ring formation between the two urea molecules repeats itself in a chain and can also be characterized as $C_2^2(8)$.

There is a homodimer synthon interaction between the two vanillic acid molecules through an $R_2^2(8)$ ring motif. The motifs observed are robust within the **2VA•2U** co-crystal. These interactions are between the acid and the amide molecules resulting in chains and rings which form networks that can be described with the graph sets of D_2^1

(3), $D_2^2(7)$, $C_2^1(6)$, $D_2^2(10)$, $D_2^2(11)$ and $R_4^4(12)$. Hydrogen bonding details are given in **Table 3.27** and **Figure 3.7.5** illustrates the connectivity in **2VA•2U** down [010].

Table 3.27: 2VA•2U hydrogen bonding parameters.

COMPOUND	D-H···A	D···A (Å)	D-H (Å)	H···A (Å)	D-H···A (º)
2VA•2U	N11-H11B···O5A[a]	2.870 (3)	0.884 (2)	1.995 (2)	170 (2)
	N10-H10A···O2A [b]	3.193 (3)	0.886 (2)	2.374 (2)	154 (2)
	N10-H10A···O2 [c]	3.091 (2)	0.886 (2)	2.631 (2)	113 (1)
	N11-H11A···O2A [b]	3.274 (3)	0.861 (2)	2.483 (2)	153 (2)
	N11-H11A···O2 [d]	2.981 (2)	0.861 (2)	2.556 (2)	112 (2)
	N10-H10B···O5A	2.864 (3)	0.843 (2)	2.027 (2)	172 (2)
	N10A-H1G···O5 [e]	2.961 (3)	0.924 (3)	2.048 (3)	170 (2)
	N10A-H2G···O3A [f]	3.036 (3)	0.881 (2)	2.248 (2)	149 (2)
	N10A-H2G···O4A [f]	3.196 (3)	0.881 (2)	2.580 (2)	128 (2)
	N11A-H3G···O5	2.976 (2)	0.904 (2)	2.079 (2)	172 (2)
	O3A-H6H···O5A [a]	2.618 (2)	0.814 (3)	1.834 (3)	162 (3)
	O3-H5···O5 [g]	2.747 (2)	0.838 (3)	1.957 (3)	157 (3)
	O3-H5···O4	2.702 (2)	0.838 (3)	2.290 (3)	111 (2)
	N11A-H4G···O4A [f]	3.167 (3)	0.875 (2)	2.548 (2)	129 (2)
	N11A-H4G···O3 [h]	3.168 (3)	0.875 (2)	2.555 (2)	128 (2)
	N11A-H4G···O3A [f]	3.274 (3)	0.875 (2)	2.592 (2)	136 (2)
	O1A-H1H···O2	2.663 (2)	0.988 (3)	1.676 (3)	178 (3)
	O1-H1A···O2A	2.615 (2)	0.975 (3)	1.640 (3)	177 (3)

a = x-1, y, z ; b= x, y-1, z ; c= -x+1, -y+1, -z ; d= -x, -y+1, -z ; e= x+1, y, z ; f= -x+1, -y+1, -z+1
g= -x+1, -y+2, -z ; h= x, y-1, z+1

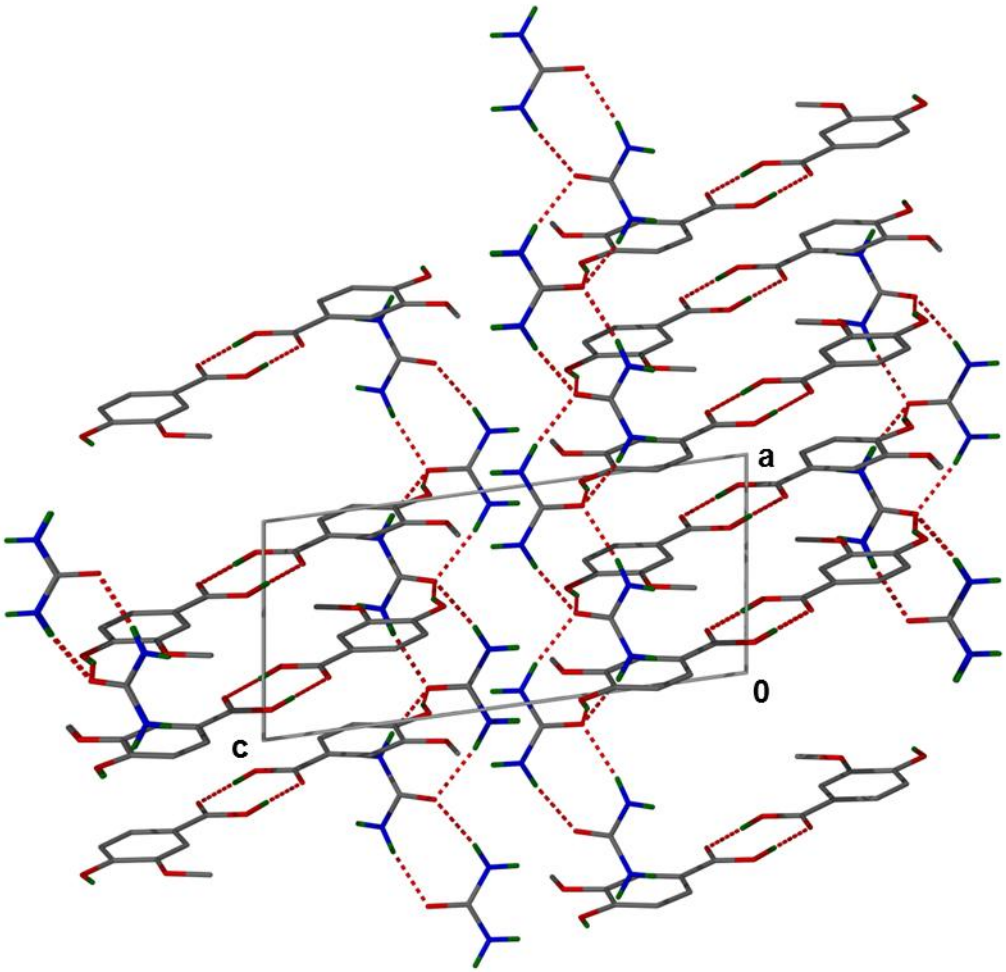

Figure 3.7.5: Hydrogen bonding in **2VA•2U** down [010].

REFERENCES

1. Allen. F.H. *Acta. Crystallogr*. 2002, B58, 380-388.
2. Adalder. T. K, Sankali. R & Dastidar. P. *Cryst. Growth Des*. 2012, 12, 2533.
3. Aitipamula. S, Wang. A, B, H, Chow. P. S & Tan. R. B. H. *CrystEngComm*. 2012, 14, 8515 – 8524.
4. Phillips. D. C, Ahmed. F. R & Barnes. W. H. *Acta. Crystallogr*. 1960, 13, 365 - 377.
5. Brown. H. C, Baude. E. A & Nacho*d.* F. C. *Determination of Organic Structures by Physical Methods.* Academic Press, New York. 1955.
6. Washburn. E. W (ed in Chief). *International Critical Tables*. New York, McGraw-Hill. 1929, 57, 335.
7. Huang. K. S, Britton. D, Etter. M. C & Byrn. S. R. *J. Mater. Chem*. 1997, 7, 713 - 720.
8. Stahl. P. H & Wermuth. C. G. *Handbook of Pharmaceutical Salts: Properties, Selection and Use. International Union of Pure and Applied Chemistry*, VHCA: Wiley-VCH: Weinheim, New York. 2002.
9. Smith. M, March. J & March. J. *March's advanced organic chemistry: reactions, mechanisms, and structure*, 5th ed.; J.Wiley: New York. 2001.
10. Bhogala. B. R, Basavoju. S & Nangia. A. *CrystEngComm*. 2005, 7, 551- 562.
11. Lin-Vien. D, Colthup. N. B, Fateley. W. G & Grasselli. J. G. *The handbook of Infrared and Raman characteristic frequencies of organic molecules.* Academic Press, San Diego. 1991.
12. Yvon. K, Jeitschko. W & Parthe. E. *Appl. Crystallogr.* 1977, 10, 73 - 74.
13. Etter. M. C, MacDonald. J. C & Bernstein. J. *Acta. Crystallogr*. 1990, B46, 256 – 262.
14. Gene. A Spiller. *Caffeine*. Taylor & Francis. CRC. Press. 2010, 171.

15. Godin. A. M, Ferreira. W. C, Rocha. L. T. S, Seniuk. J. G. T, Paiva. A. L. L, Merlo. L. A, Nascimento. Jr. E. B, Bastos. L. F.S & Coelho. M. M. *Pharmacol. Biochem. Behav*. 2011, 99, 782 - 788.
16. Sorolla. M. A, Nierga. C, Rodriguez-Colman. M. J, Reverter-Branchat. G, Arenas. A, Tamarit. J, Ros. J & Cabiscol. E. *Arch. Biochem. Biophys*. 2011, 510, 27- 34.
17. Brittain. H. G. *Cryst. Growth Des.* 2009, 9 (5), 2492 - 2499.
18. Sheldrick G. M. SHELX-97, program for crystal structure refinement; University of Go¨ttingen, Germany. 1997.
19. Barbour L. J. X-Seed, a software tool for supramolecular crystallography. *J Supramol. Chem*. 2001, 1,189 – 191.
20. Macrae. C. F, Eddington. P. R, McCabe. P, Pidcock. E, Shields. G. P, Taylor. R, Towler. M. & van de Streek. J. Mercury: visualization and analysis of crystal structures. *J. Appl .Crystallogr*. 2006, 39, 453 - 457.
21. Jacobs. A, Amombo Noa. F. M & Taljaard. J. H. *J. Chem. Crystallogr*. 2013, 43, 554 - 560.
22. Niren. N. M. Cutis. 2006, 77 (Suppl), 11- 6.
23. Gressel. P. D & Galleli. S. F. *J. Pharm*. Sci. 1968, 57, 335.
24. Frišcˇic´. T & Jones. W. *Faraday. Discuss*. 2007, 136, 167 – 178.
25. Berry. D. J, Seaton. C. C, Clegg. W, Harrington. R. W, Coles. S. J, Horton. P. N, Hurst-House. M. B, Storey. R, Jones. W, Frišcˇic´. T & Blagden. N. *Cryst. Growth Des*. 2008, 8, 1697 – 1712.
26. Malisoff. W. M. *Dictionary of Bio-Chemistry and Related Subjects.* Philosophical Library. 1943, 311, 530, 573.
27. Donald Merle. B & Elsie Merle. P. *Environment and Behavior.* West view Press. 1997, 200.
28. SAINT v7.68A © Bruker Analytical X-ray systems. Madison, W I. 1997 – 2009.
29. Desiraju. G. R. *Acc. Chem. Res*. 1996, 29, 441 – 449.
30. Desiraju. G. R, Vittal. J. J & Ramanan. A. *Crystal Engineering: A Textbook*. World Scientific Publiching Co, Pte, Ltd. 2011.
31. Smith. B. J. *Methods. Mol. Biol*. 1984, 1, 63.

32. SIGMA-ALDRICH life science: Where BIO Begins, Products for life science research. 2011- 2012, 1867.

CHAPTER 4

PHENYLACETIC ACID CO-CRYSTALS AND SALTS

The compound phenyl acetic acid (PAA) has reportedly formed inclusion compounds with organic molecules such as benzamide,[1] 2-pyridone,[2] 3,3-(hydrazine-1,2-diylidenedimethylylidene) pyridine,[3] 4,4-(hydrazine-1,2-diylidenedimethylylidene) pyridine,[4] adenine phenylacetate,[5] 1-(carboxymethyl) pyridinium,[6] and hexamethylenetetramine[7] according to the data obtained from the Cambridge Structural Database (CSD, version 5.34, November 2012).[8]

In this chapter, the co-crystals of phenyl acetic acid (PAA) with acridine (ACRI), caffeine (CAF), isonicotinamide (INM) and nicotinamide (NAM) are described. PAA also formed salt hydrates with cinchonidine (CIND), quinidine (QUID) and quinine (QUIN).

The numbering system of phenyl acetic acid is represented in **Figure 4.1**.

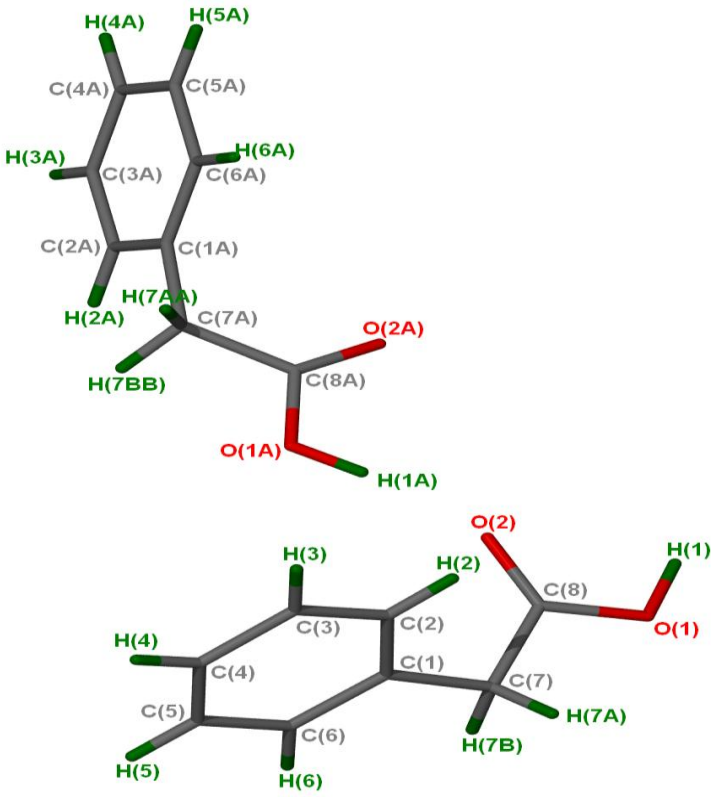

Figure 4.1: Numbering scheme of phenyl acetic acid molecules.

4.1 Phenyl acetic acid and acridine (PAA•ACRI)

Phenyl acetic acid (PAA) formed a co-crystal with acridine in a 1: 1 ratio. The two components were dissolved in diethyl ether with gently heating on a hot plate. The solution was allowed to evaporate and crystals in the form of a block were obtained after a few days. The acid: base combination results in a co-crystal rather than a salt due to the ΔpK_a value (pK_a (base) – pK_a (acid) = 5.60[9] – 4.31[10] = 1.29). It is generally accepted that reaction of an acid with a base will be expected to form a salt if the ΔpK_a (ΔpK_a = pK_a (base) - pK_a (acid)) is greater than 3.[11-14]

The co-crystal structure is illustrated in **Figure 4.1.1**.

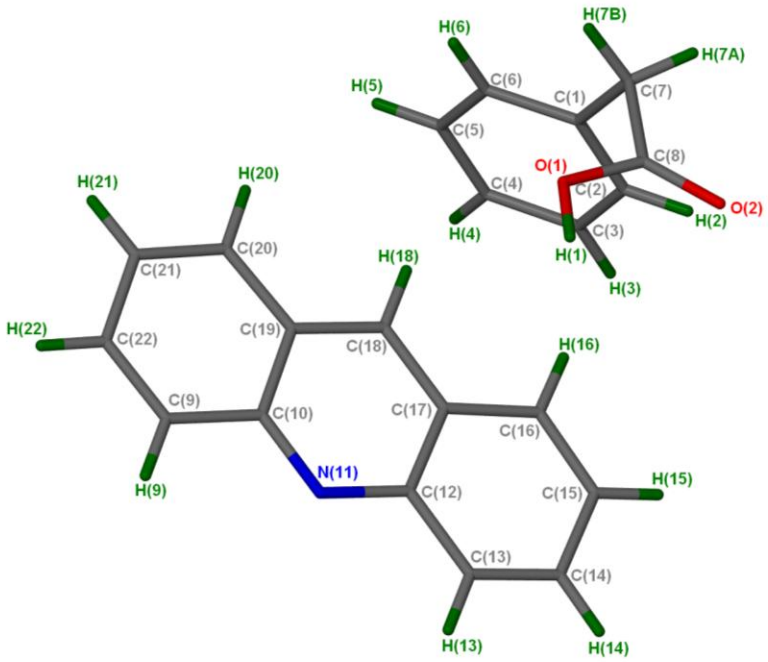

Figure 4.1.1: Asymmetric unit of the **PAA•ACRI** structure with all the hydrogen atoms shown for numbering clarity.

4.1.1 Thermal Analysis

The result obtained from the DSC curves (**Figure 4.1.2**) shows a decrease in thermal stability of the co-crystal which is due to its low melting point compared to the starting components. Thermal analysis data are given in **Table 4.1**.

Table 4.1: Thermal analysis data for **PAA•ACRI**

Compounds	**DSC Endo$_1$(T_{onset},K)**	**DSC Endo$_2$(T_{onset},K)**
Acridine	363.5	375.8
Phenyl acetic acid	-	351.8
PAA•ACRI	331.7	452.7

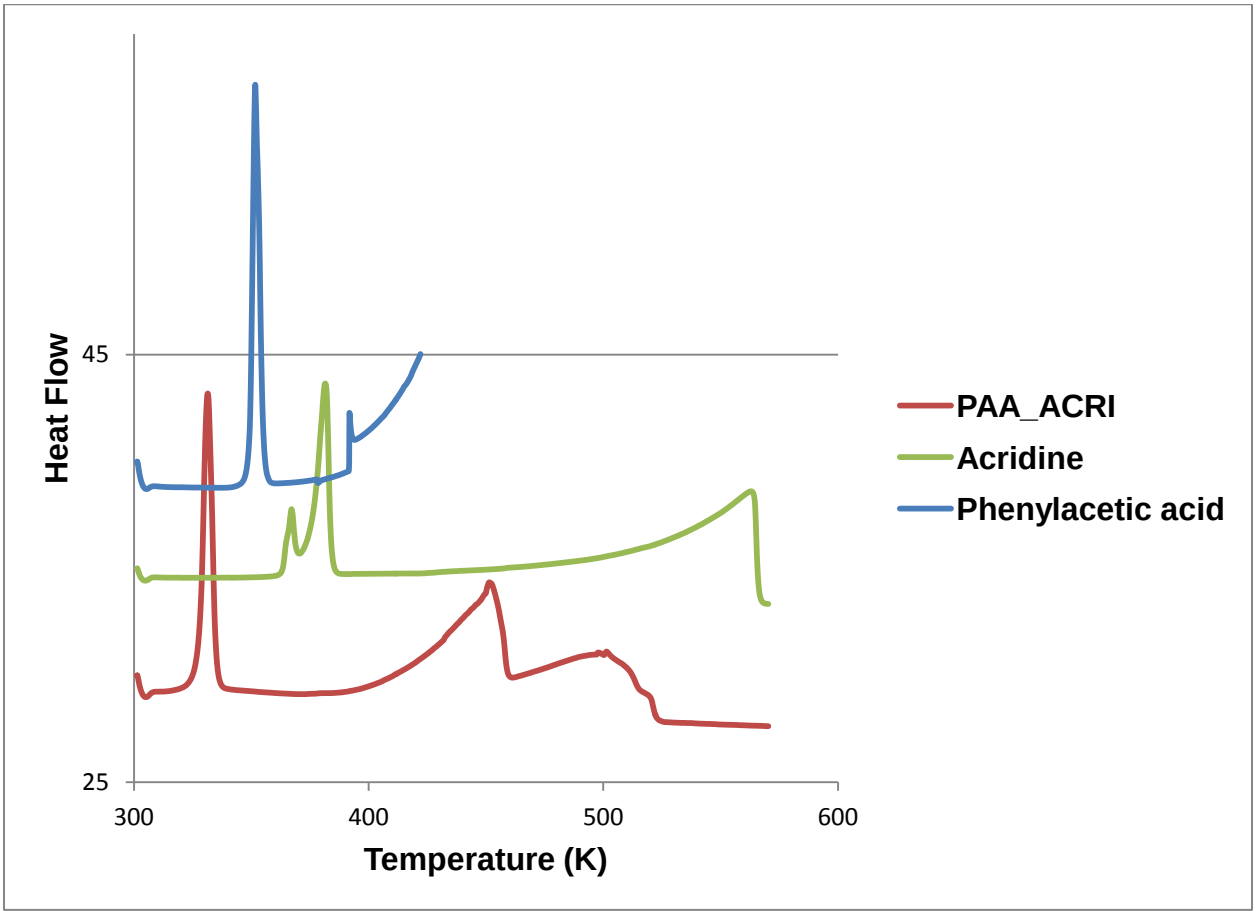

Figure 4.1.2: DSC curves of phenyl acetic acid (blue), acridine (green) and **PAA•ACRI** (red).

4.1.2 Hot Stage Microscopy

A block crystal of **PAA•ACRI** was placed onto a hot stage microscope with silicone oil at room temperature. The crystal started melting at a temperature of 314 K, melting continued at 333 K and the process was completed at 455 K. The wide melting range is not unusual due to the large crystal size. **Figure 4.1.3** shows the HSM photographs of **PAA•ACRI**.

(a) 295 K **(b) 314 K**

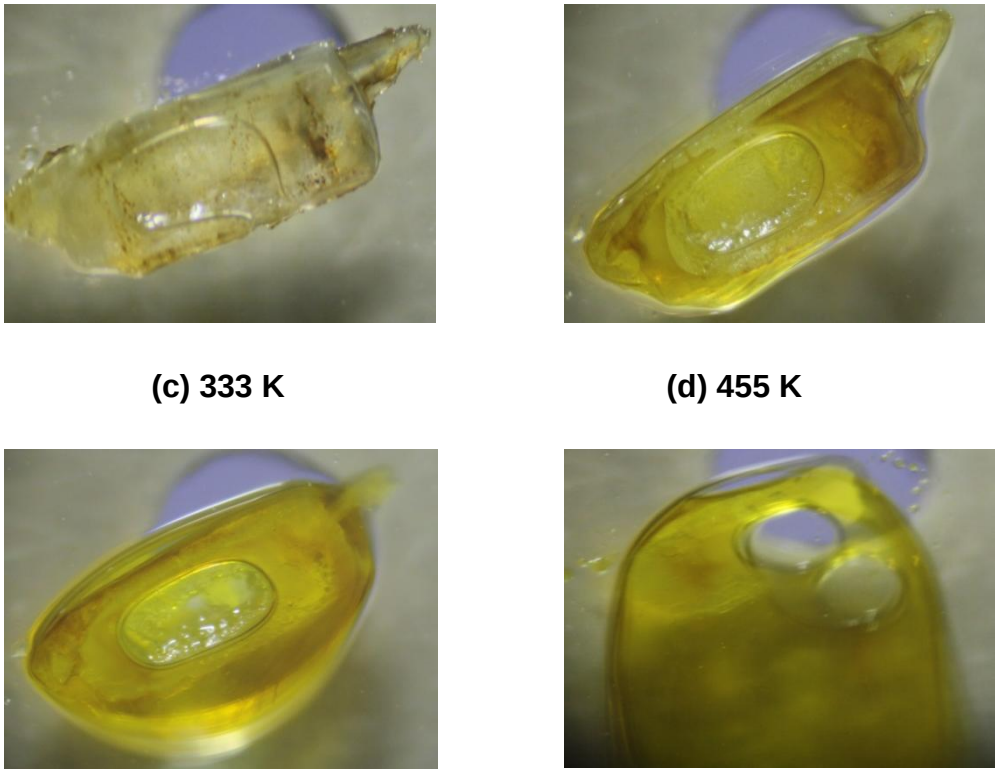

(c) 333 K **(d) 455 K**

Figure 4.1.3: HSM photography of **PAA•ACRI**: **(a)** crystal immersed in silicone oil, **(b)** crystal starts melting, **(c)** melting of the crystal and **(d)** crystal completely melts.

4.1.3 IR Spectroscopy

The IR spectrum of the co-crystal (**Figure 4.1.4**) shows IR absorption peaks of both components. There is a shift of the **PAA•ACRI** COOH wavenumber (1698 cm^{-1}) which is 1 cm^{-1} less PAA (1699 cm^{-1}). This shift indicates that the patterns of molecular

motion of the supramolecular synthon are not really significantly different to those of the initial reactants. This is an indication that the force constants of the homosupramolecular synthons (i.e., acridine and phenyl acetic acid) are not strongly changed upon formation of the heterosupramolecular synthon of the co-crystal.[15]

The PAA infrared spectrum is dominated by bands associated with OH and CH vibrational modes. The acridine infrared spectrum is dominated by C=C and C-H stretching modes.

IR positions and assignments are given in **Table 4.2** and the spectra of each component are shown in **Figure 4.1.4**.

Table 4.2: IR positions and assignments for the peaks in PAA, **PAA•ACRI** and ACRI.

PAA	**PAA•ACRI**	ACRI	Proposed assignment
3123	3125	-	OH stretch
2750, 2620	3056, 2990, 2400	3051	Aromatic ring stretch
1951	2058	2285, 1815	Overtone or combination bands
1699	1698	-	C=O
1498, 1454, 1407	1519,1496, 1466	1617,1461, 1437	C=C stretch
1290, 1243	1276, 1198	-	C-O stretch

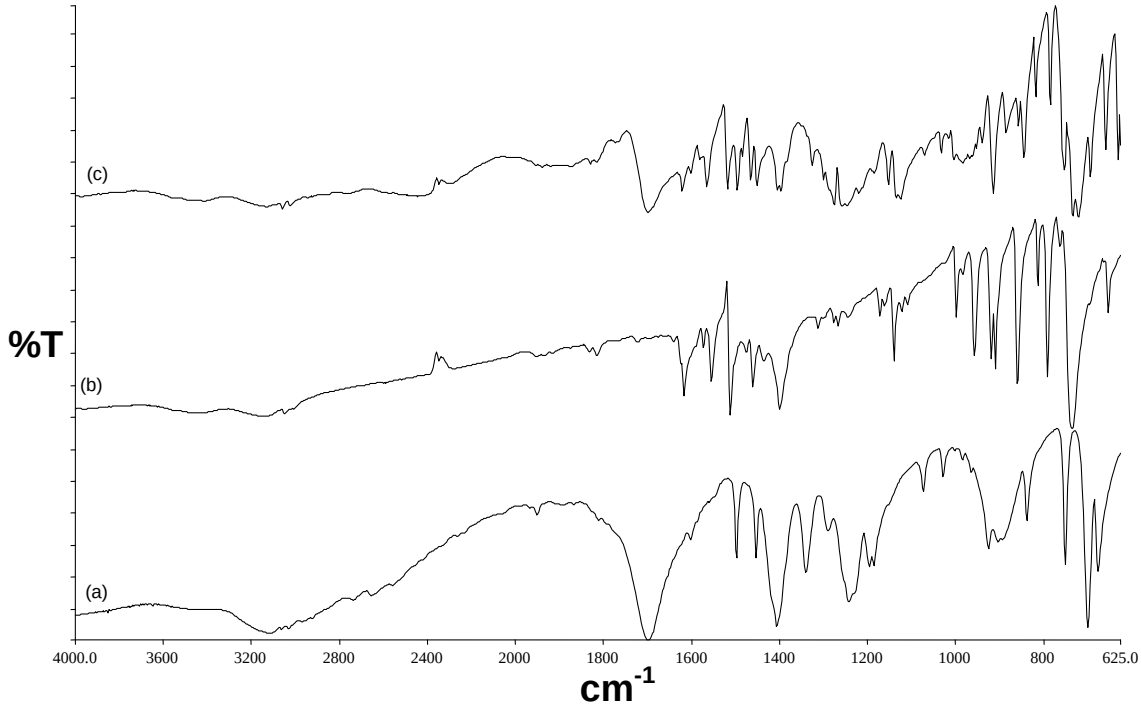

Figure 4.1.4: IR spectrums of (a) PAA, (b) acridine and (c) **PAA•ACRI**.

4.1.4 Powder X-ray Diffraction

The ground product (at 30 min) and the slurry conversion PXRD patterns (in diethyl ether) did not match the physical mixture PXRD pattern. Both ground and slurry PXRD patterns were a match with the calculated PXRD pattern obtained from LAZYPULVERIX.[16]

The PXRD patterns for the different types of experiments are illustrated in **Figure 4.1.5**.

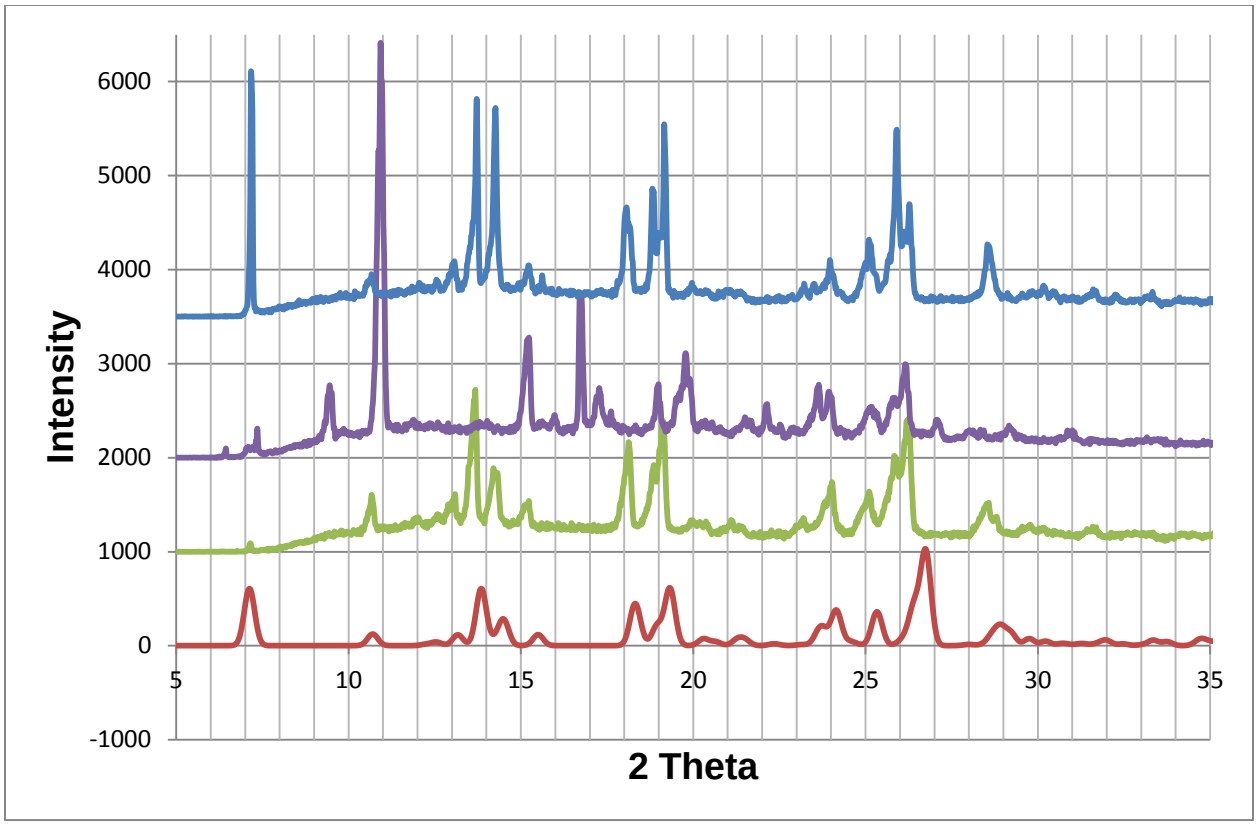

Figure 4.1.5: PXRD patterns of **PAA•ACRI** (red), ground product (green), physical mixture (purple) and slurry (blue).

4.1.5 Structure Determination

All non-hydrogen atoms were found by direct methods and refined anisotropically. The PAA carboxylic acid hydrogen was located in the difference electron density map and allowed to refine isotropically. The structure refined to R_1= 0.0418 with wR_2= 0.1050 ([I>2sigma (I)]). The crystal data of **PAA•ACRI** is reported in **Table 4.3**.

Table 4.3: PAA•ACRI crystal data.

Compound	**PAA•ACRI**
Structural Formula	$C_8H_8O_2$•$C_{13}H_9N$
PAA:ACRI ratio	1: 1
Molecular Mass (g mol^{-1})	315.37
Data collection temperature (K)	173(2)
Crystal system	Triclinic
Space group	*P-1*
a (Å)	7.7375 (15)
b (Å)	8.8544 (18)
c (Å)	12.457 (3)
α (°)	85.72 (3)
β (°)	85.73 (3)
γ (°)	69.11 (3)
Volume ($Å^3$)	794.1 (3)
Z	2
D_c, Calculated density (g cm^{-3})	1.319
Final R indices [I>2sigma(I)]	R_1= 0.0418
	wR_2 = 0.1050
R indices (all data)	R_1 = 0.0568
	wR_2 = 0.1145
Largest diff. peak and hole ($eÅ^{-3}$)	0.257; -0.205

The structure **PAA•ACRI** crystallizes in *P-1* with Z = 2. The asymmetric unit contains one PAA and one acridine molecule. The co-crystal has a structural formula of $C_8H_8O_2$•$C_{13}H_9N$ with PAA and acridine molecules located in general positions. There are π-π stacking interactions between adjacent acridine aromatic rings with a minimum distance of 3.736 Å. PAA aromatic rings are involved in π-π stacking interactions with a shortest distance of 3.835 Å as shown in **Figure 4.1.6** representing packing diagram of **PAA•ACRI** down [100]. The structure is stabilized by C-H•••π interactions between PAA

and acridine molecules with a C•••π (centroid) distance of 3.210 Å and a C-H•••π angle of 154 ° as illustrated in **Figure 4.1.7**.

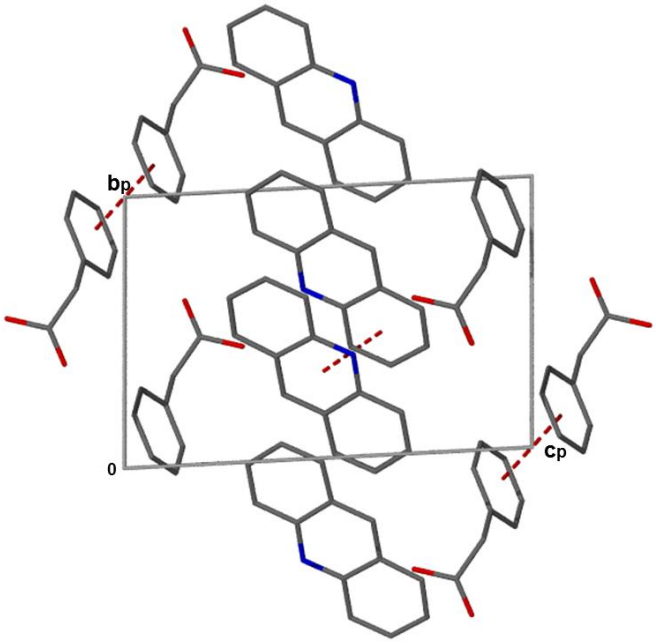

Figure 4.1.6: Packing diagram of **PAA•ACRI** down [100] with the hydrogen atoms removed.

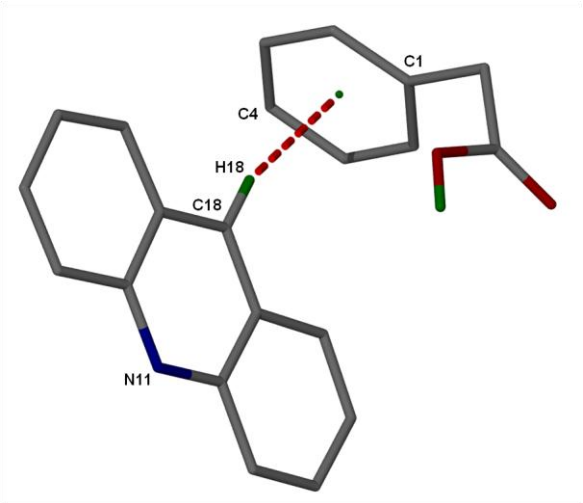

Figure 4.1.7: C-H•••π interaction between PAA and acridine molecules.

The main hydrogen bond connection found in **PAA•ACRI** is (PAA) O-H•••N (ACRI) with an O•••N distance of 2.688 (2) Å, H•••N distance of 1.751(1) Å and an O-H•••N angle of

164 (1) º. This connection can be characterized as $D\ ^{1}_{1}(2)$ and is shown in **Figure 4.1.8** with the hydrogen bond parameters given in **Table 4.4**.

Table 4.4: PAA•ACRI hydrogen bonding parameters.

COMPOUND	D-H···A	D···A (Å)	D-H (Å)	H···A (Å)	D-H···A (º)
PAA•ACRI	O1-H1···N11A[a]	2.688 (2)	0.963 (1)	1.751 (1)	164 (1)

a = -x, -y+1, -z + 1

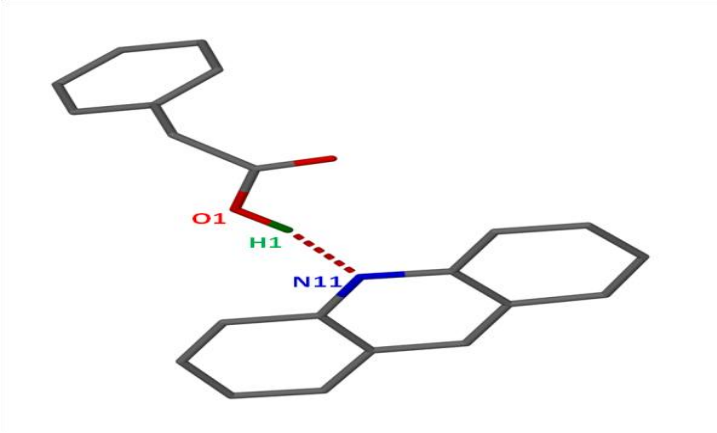

Figure 4.1.8: Hydrogen bonding in **PAA•ACRI**.

4.2 Phenyl acetic acid and caffeine (2PAA•CAF)

A co-crystal was obtained by dissolving a 1: 1 ratio of both components in 50/50 (*v/v*) chloroform/methanol with slight heating on a hot plate. The solution was allowed to evaporate at room temperature and after a few days, needle-like crystals with a 2: 1 ratio were obtained (**2PAA•CAF**). Similar crystals were also obtained when using distilled water as a solvent.

The asymmetry unit of **2PAA•CAF** co-crystal is illustrated in **Figure 4.2.1**.

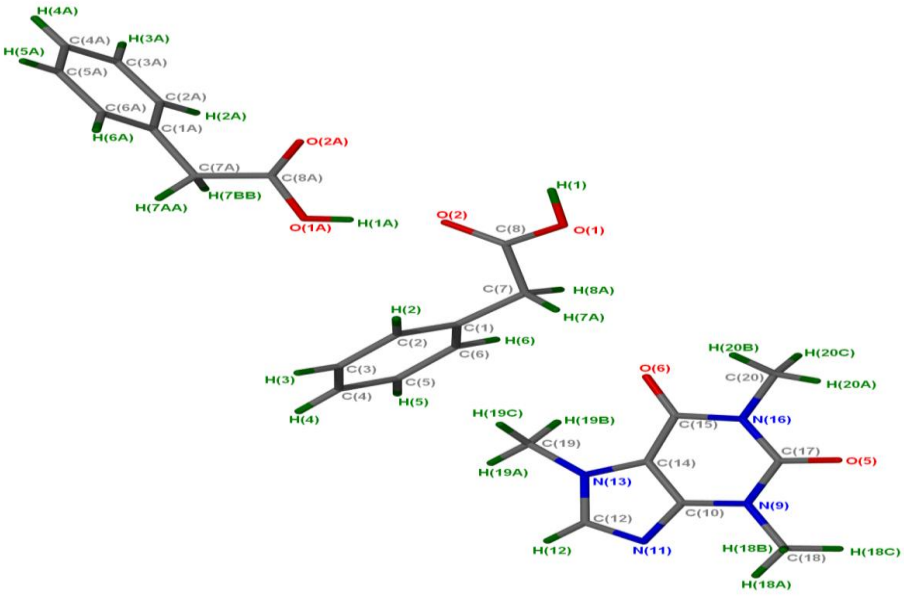

Figure 4.2.1: Asymmetric unit of **2PAA•CAF** structure with all the hydrogen atoms shown for numbering clarity.

4.2.1 Thermal Analysis

The melting point of **2PAA•CAF** was found to be in between the two starting materials melting points.[17, 18] This implies that the above co-crystal has a higher thermal stability than the PAA compound and a lower thermal stability than caffeine. Thermal analysis data of **2PAA•CAF** are given in **Table 4.5** and the DSC results are illustrated in **Figure 4.2.2**.

Table 4.5: Thermal analysis data of **2PAA•CAF**.

Compounds	**DSC Endo$_1$(T_{onset},K)**	**DSC Endo$_2$(T_{onset},K)**
Caffeine	419.6	508.4
Phenyl acetic acid	-	351.8
2PAA•CAF	-	359.9

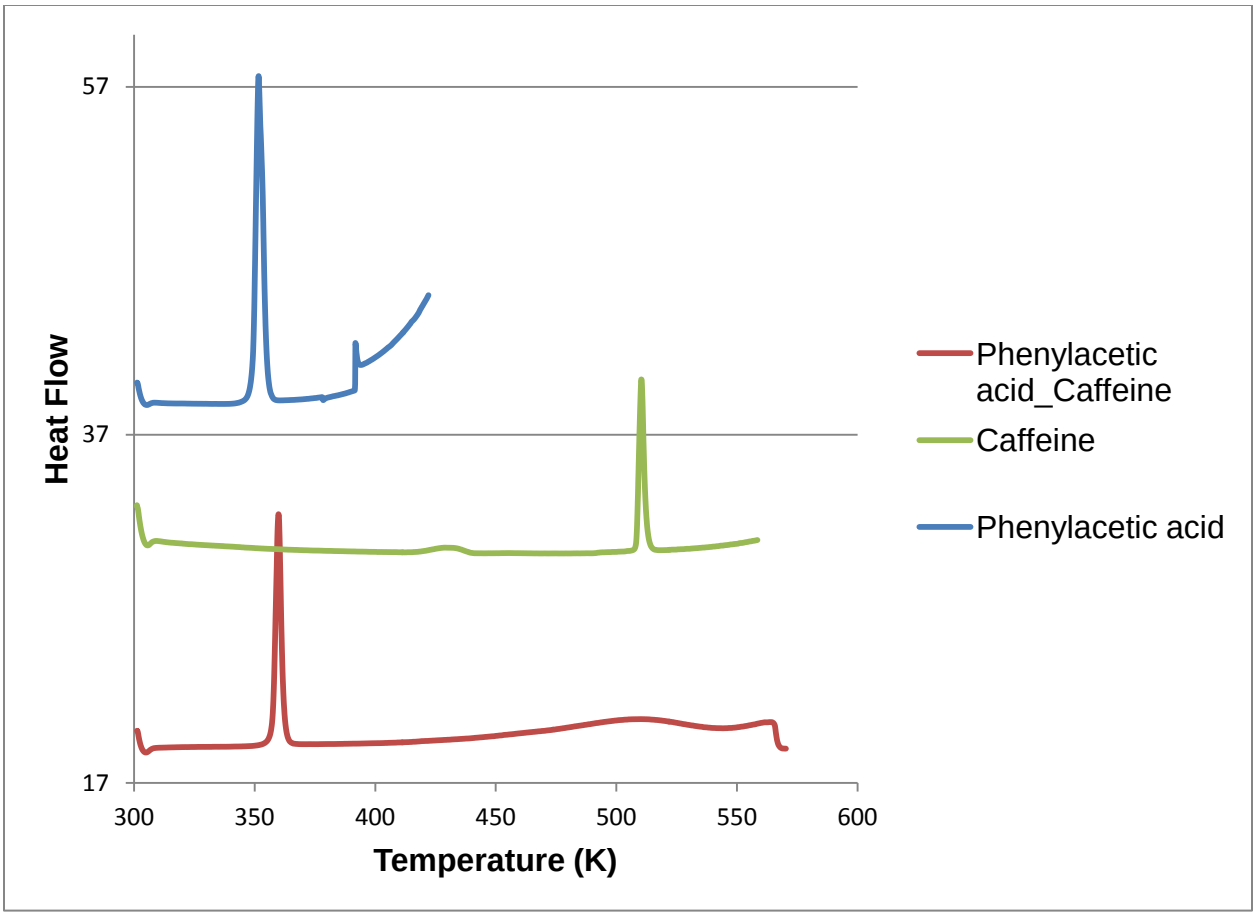

Figure 4.2.2: DSC curves of **2PAA•CAF** (red), caffeine (green) and phenyl acetic acid (blue).

4.2.2 IR Spectroscopy

A 2: 1 molar ratio of PAA and caffeine (CAF) was dissolved in 50/50 (*v/v*) of chloroform/methanol and stirred at room temperature. The powder resulting from the experiment was analyzed using infrared spectroscopy (**Figure 4.2.3**). A broad band at 3430 cm^{-1} in the IR spectrum of the stirred product was assigned to the hydrogen bonding of the OH groups and the bands at 3221 and 3104 cm^{-1} were attributed to the N-H stretching vibration.

In the physical mixture IR spectrum the C=O bands at 1710, 1698 and 1662 cm^{-1} are shifted to lower frequencies (1700, 1678 and 1644 cm^{-1}) in the slurry product.

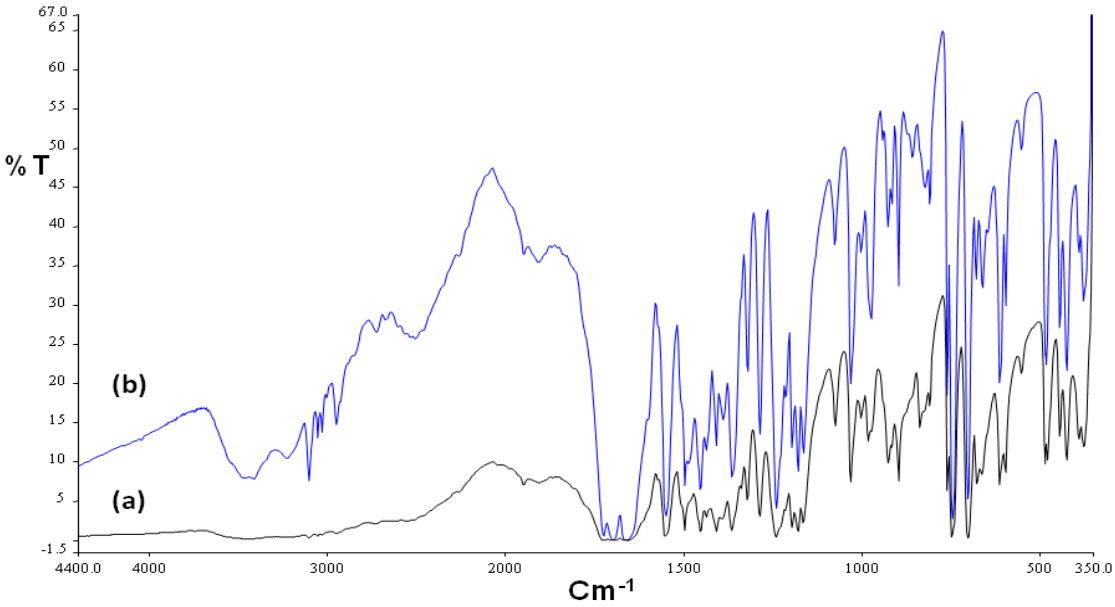

Figure 4.2.3: IR spectra; **(a)**: physical mixture of **2PAA•CAF**, **(b)** slurry product of **2PAA•CAF**.

4.2.3 Powder X-ray Diffraction

The PXRD patterns of the ground product at 20 and 30 min (**Figure 4.2.4)** did not match both the physical mixture and the calculated pattern obtained from LAZYPULVERIX.[16] The grinding experiment was incomplete because the peak at 2θ (approximately 6.05) which is in the calculated pattern is missing and the peak at 2θ (approximately 7.68) is present in both patterns (ground product and calculated). The ground product pattern also has peaks that are found in the physical mixture which are 2θ (approximately 10.65 and 11.62).

The slurry conversion performed in 50/50 (*v/v*) chloroform/methanol unlike the ground products showed good agreement to that of the calculated PXRD pattern obtained from LAZYPULVERIX.[16] The PXRD patterns is represented in **Figure 4.2.4**.

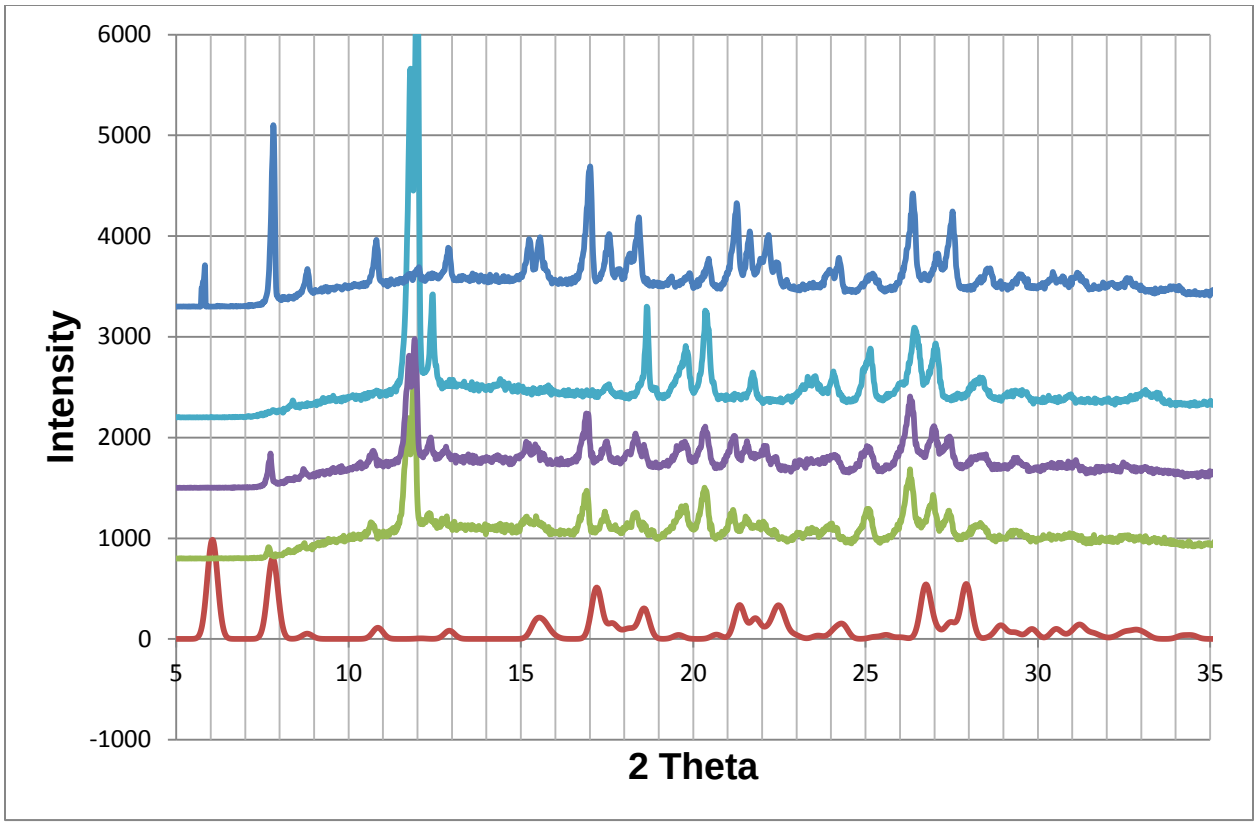

Figure 4.2.4: PXRD patterns of **2PAA•CAF** (red), ground product after 20 min (green), ground product after 30 min (purple), physical mixture (sky blue) and slurry (blue).

4.2.4 Structure Determination

2PAA•CAF successfully refined to R_1= 0.0492 with wR_2= 0.1116 ([I>2sigma (I)]). All the non-hydrogen atoms were located by direct methods in the difference electron density map and refined anisotropically. The carboxylic acid hydrogen was located in the difference electron density map and the nitrogen atoms of the caffeine molecule were identified by the highest peak magnitude in the aromatic ring. The **2PAA•CAF** crystal data are given in **Table 4.6**.

Table 4.6: 2PAA•CAF crystal data.

Compound	**2PAA•CAF**
Structural Formula	$2C_8H_8O_2•C_8H_{10}N_4O_2$
PAA:CAF ratio	2: 1
Molecular Mass (g mol^{-1})	466.49
Data collection temperature (K)	173(2)
Crystal system	Monoclinic
Space group	$P2_1/c$
a (Å)	14.9707 (12)
b (Å)	6.6629 (6)
c (Å)	23.183 (2)
α (°)	90.00
β (°)	102.338 (2)
γ (°)	90.00
Volume ($Å^3$)	2259.1 (3)
Z	4
D_c, Calculated density (g cm^{-3})	1.371
Final R indices [I>2sigma(I)]	R_1= 0.0500
	wR_2 = 0.1141
R indices (all data)	R_1 = 0.0916
	wR_2 = 0.1330
Largest diff. peak and hole ($eÅ^{-3}$)	0.277; -0.302

The 2:1 acid: base combination crystallized in the monoclinic space group $P2_1/c$, with Z= 4. PAA and CAF molecules are located in general positions with an asymmetric unit containing two PAA and one CAF molecules. The packing diagram of the co-crystal is shown in **Figure 4.2.5**.

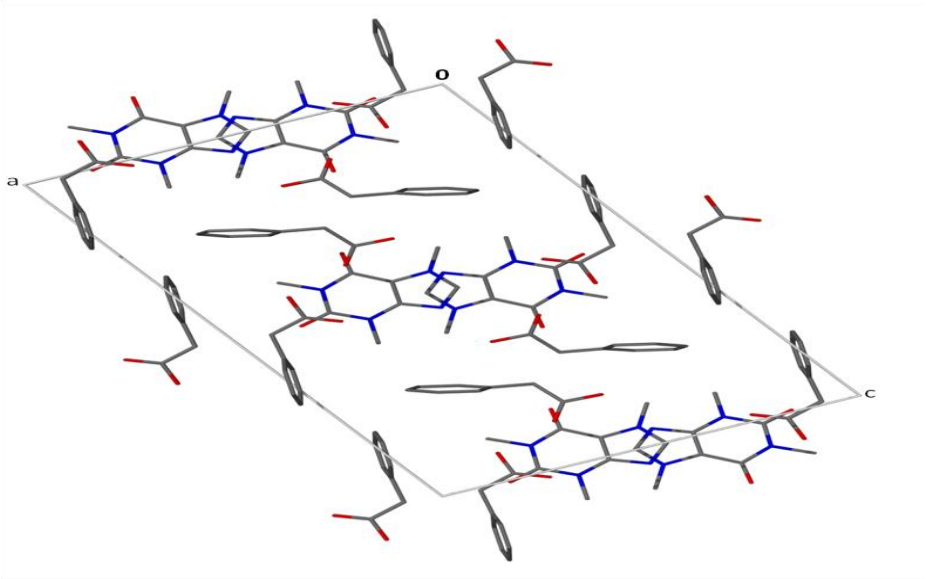

Figure 4.2.5: Packing diagram of **2PAA•CAF** down [010] with the hydrogen atoms removed.

The **2PAA•CAF** co-crystal (**Figure 4.2.6**) is stabilized via (PAA) O-H•••O (PAA) with an O•••O distance of 2.690 (2) Å and an O-H•••O angle of 170 (1) º. The other hydrogen bond connection in the structure is via (PAA) O-H•••N (CAF) with an O•••N distance of 2.669 (2) Å and an O-H•••N angle of 179 (1) º. The hydrogen bonding has graph sets of $D_1^1(2)$ and $D_2^2(6)$. The hydrogen bond parameters are given in **Table 4.7**.

Table 4.7: 2PAA•CAF hydrogen bonding parameters.

COMPOUND	D-H···A	D···A (Å)	D-H (Å)	H···A (Å)	D-H···A (º)
2PAA•CAF	O1A-H1A···O2	2.690 (2)	0.920 (1)	1.780 (1)	170 (1)
	O1-H1···N11[a]	2.669 (2)	1.015 (1)	1.654 (1)	179 (1)

a = x, -y+1/2, z -1/2

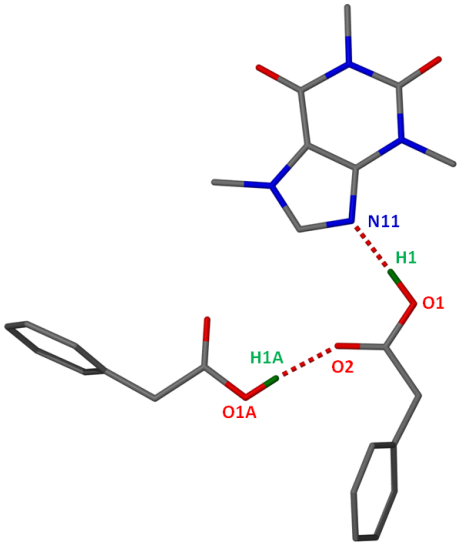

Figure 4.2.6: Hydrogen bonding in **2PAA•CAF**.

4.3 Phenyl acetic acid and cinchonidine (PAA^-)($CIND^+$)•H_2O

Cinchonidine, $C_{19}H_{22}N_2O$ is a cinchona alkaloid which is established as powerful chiral auxiliaries and favoured catalysts, effective in numerous asymmetric transformations.[19-25] This compound is a stereoisomer and pseudo-enantiomer of cinchonine.

PAA formed a salt hydrate with cinchonidine (CIND) by dissolving a 1: 1 molar ratio of both components in isopropanol. The solution was allowed to evaporate at ambient temperature and needle-like crystals were obtained after a few days. Water was included in the structure (**(PAA^-)($CIND^+$)•H_2O**).

The asymmetric unit of **(PAA^-)($CIND^+$)•H_2O** is illustrated in **Figure 4.3.1**.

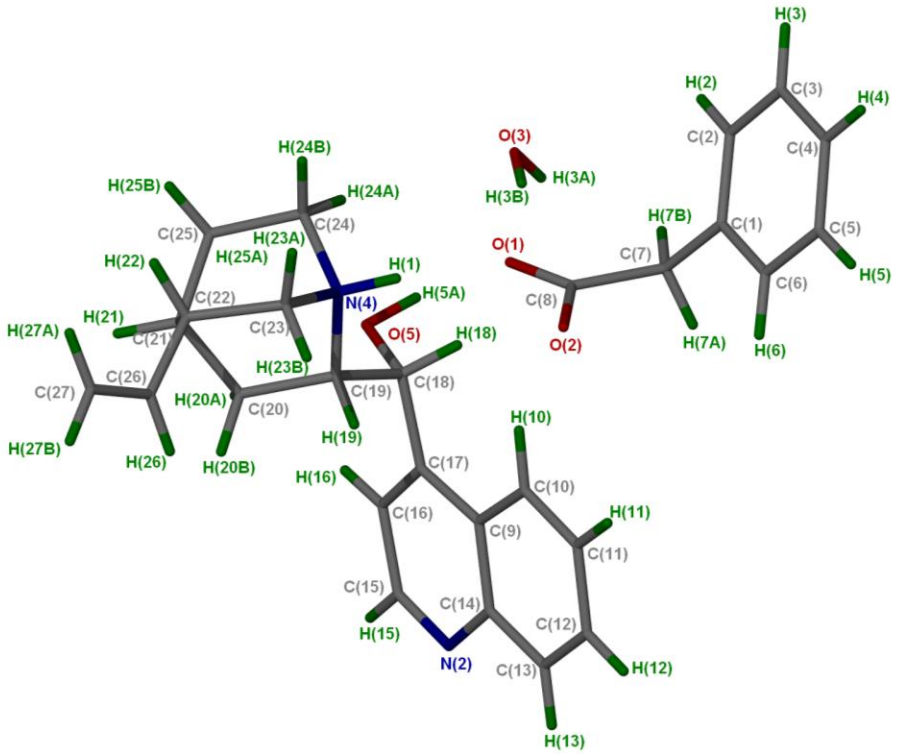

Figure 4.3.1: Asymmetric unit of **$(PAA^{-})(CIND^{+})\bullet H_2O$** structure with all the hydrogen atoms shown for numbering clarity.

4.3.1 Thermal Analysis

Thermal analysis results of **$(PAA^{-})(CIND^{+})\bullet H_2O$** are shown in **Figure 4.3.2**. The TG curve shows a single mass loss step of 3.2 % (calc. 4.0%) corresponding to the loss of water. In the DSC curve of **$(PAA^{-})(CIND^{+})\bullet H_2O$**, the first peak corresponds to the desolvation which is followed by the melt of the salt. Thermal analysis data is listed in **Table 4.8**.

Table 4.8: Thermal analysis data of **PAA•CIND•H_2O**.

Compounds	PAA	**PAA•CIND•H_2O**	Cinchonidine
DSC Endo$_1$ (T_{onset},K)	-	354.8	-
DSC Endo$_2$ (T_{onset},K)	351.8	419.6	478.6
TG calculated % mass loss	-	4.0	-
TG experimental % mass loss	-	3.2	-
PAA^-:$CIND^+$:H_2O		1: 1: 1	

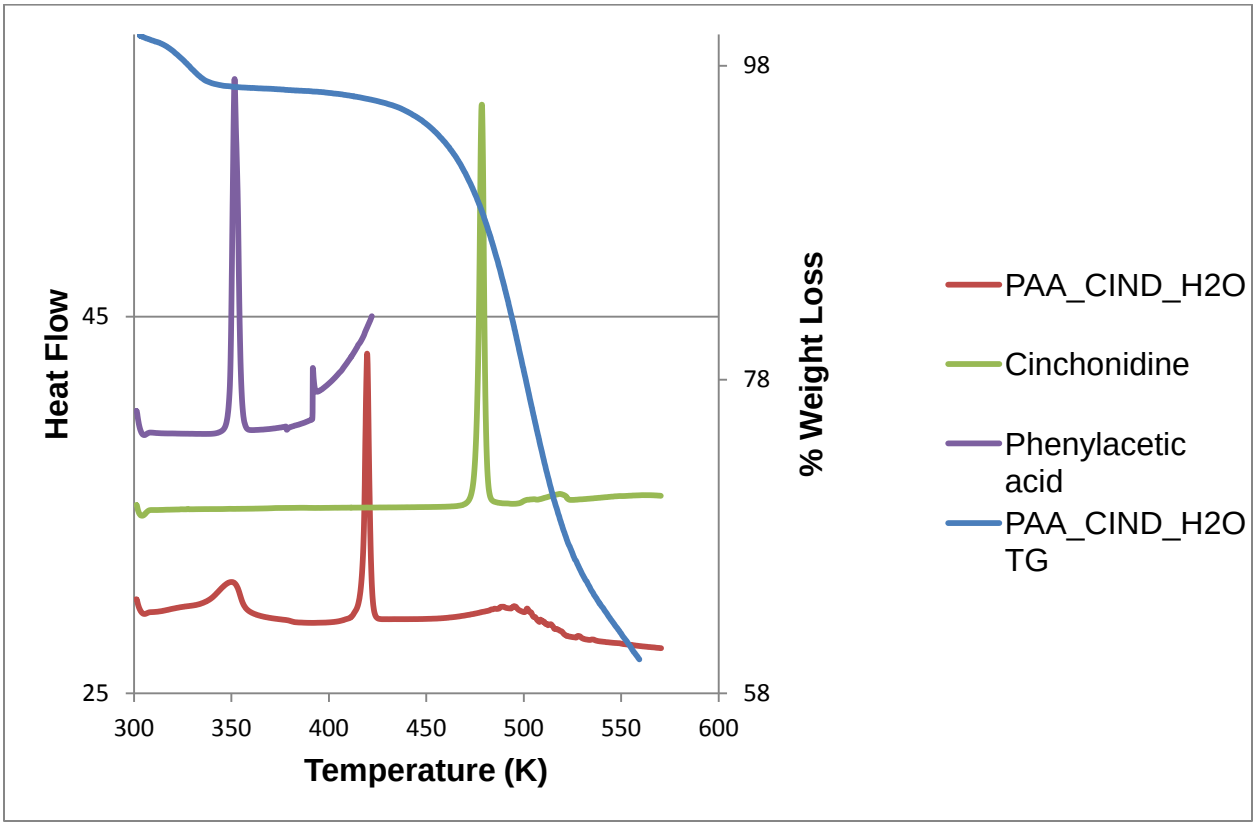

Figure 4.3.2: Thermal analysis curves of **(PAA^-)($CIND^+$)•H_2O:** DSC (red), TG (blue), cinchonidine (green) and PAA (purple).

4.3.2 Hot Stage Microscopy

HSM photographs of **$(PAA^-)(CIND^+)\bullet H_2O$** are shown in **Figure 4.3.3**. Crystals were immersed in silicone oil at a temperature of 295 K and water was released at 356 K. At 425 K the salt started melting. The melt was completed at a temperature of 430 K.

(a) 295 K

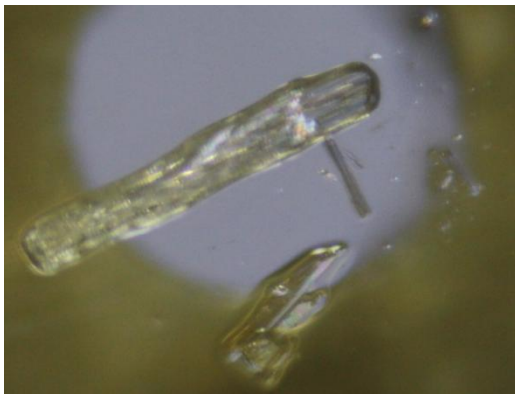

(b) 356 K

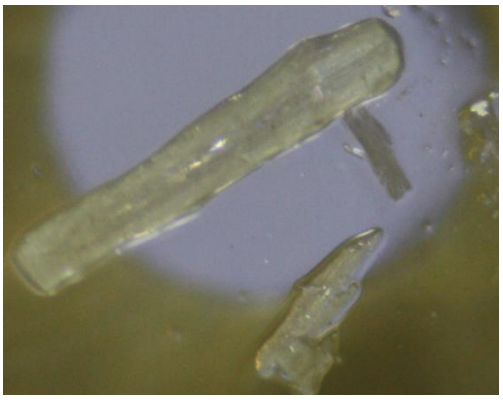

(c) 425 K

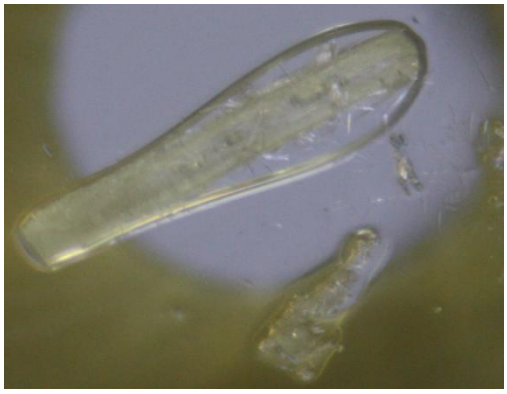

(d) 430 K

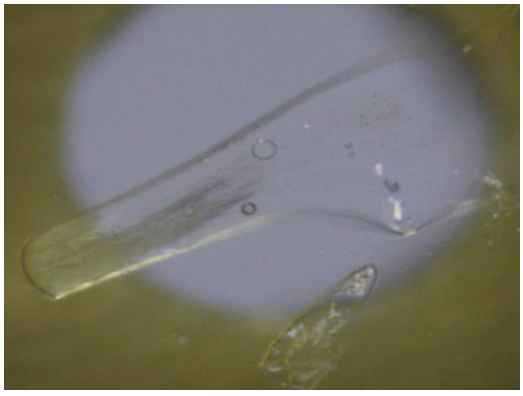

Figure 4.3.3: HSM photography of **$PAA\bullet CIND\bullet H_2O$**: **(a)** crystal immersed in silicone oil, **(b)** release of the water, **(c)** melt of the crystal and **(d)** complete melt of the crystal.

4.3.3 IR Spectroscopy

IR spectrum of **$(PAA^-)(CIND^+)\bullet H_2O$** is shown in **Figure 4.3.4**. The salt hydrate has IR absorption peaks of both components. The IR data are given in **Table 4.9**. The peak at

1570 cm^{-1} is broadened, which is within the range 1550-1650 cm^{-1} (νC-O of COO^-) indicating a transfer of a proton.[26]

The frequency at 3509 cm^{-1} can be attributed to the solvated water in the salt. The bands at 3396 and 3126 cm^{-1} can be assigned to the hydrogen bonding of the OH stretch. There is a broad band at 1384 cm^{-1} which is assigned to the C-O stretching mode.

Table 4.9: IR positions and assignments for the peaks in PAA, **$(PAA^-)(CIND^+)\bullet H_2O$** and CIND.

PAA	**$(PAA^-)(CIND^+)\bullet H_2O$**	CIND	Proposed assignment
3123	3509, 3396, 3126	3396	OH stretch
2750, 2620	2590	3072, 3003, 2939, 2866, 2720	C=C and C-H Stretching mode
1951	-	1941	Overtone or combination bands
1698	1570	-	C=O
1498, 1454, 1407	1508,1495, 1454	1636, 1618,1590, 1567, 1508	C=C stretch
1290, 1243	1384, 1281	-	C-O stretch

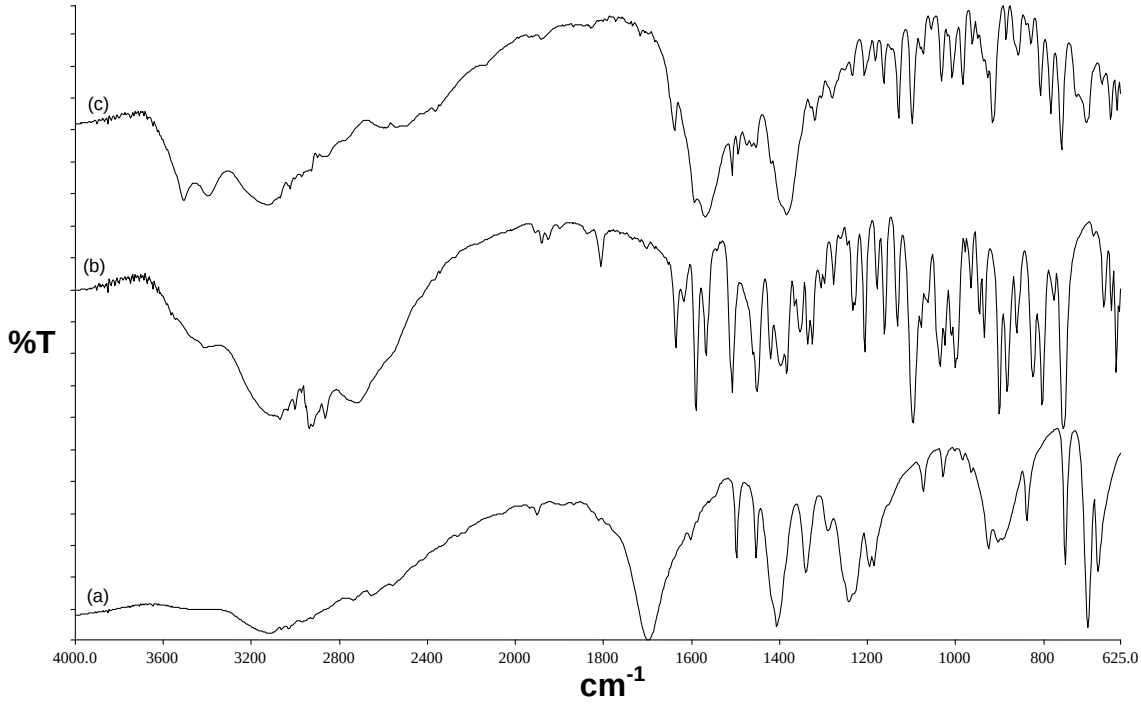

Figure 4.3.4: IR spectrums (a) PAA, (b) CIND and (c) **$(PAA^{-})(CIND^{+})\bullet H_2O$**.

4.3.4 Powder X-ray Diffraction

Grinding and liquid assisted grinding experiments were not possible. This was due to the paste-like product obtained when PAA and CIND were ground together. The slurry conversion PXRD pattern (performed in distilled water) did not match that of the calculated pattern obtained from LAZYPULVERIX.[16] Thus the slurry conversion resulted in a different compound compared to crystallization.

The physical mixture of PAA and CIND was not done in this case because while mixing the two components, a paste like product sticking on the mortar is obtained.

PXRD patterns of both the slurry and the calculated are shown in **Figure 4.3.5**.

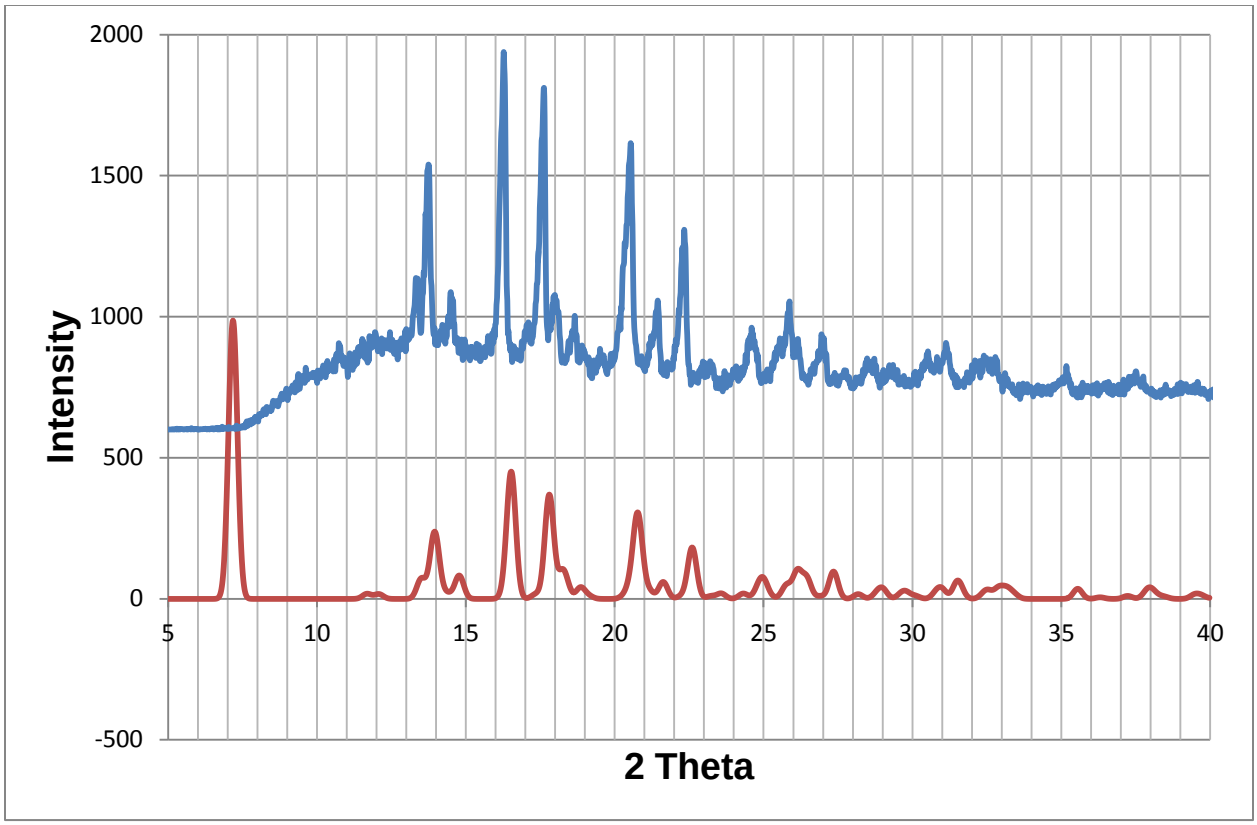

Figure 4.3.5: PXRD patterns of **$(PAA^{-})(CIND^{+})\bullet H_2O$** (red) and slurry (blue).

4.3.5 Structure Determination

The PAA non- hydrogen atoms were refined anisotropically. The aromatic and methyl hydrogen atoms were fixed in position. The hydrogen atoms involved in the hydrogen bonds were found in the difference electron density map.

The PAA^{-} ring C-C distances was fixed due to the disorder of the aromatic ring. The crystal data of **$(PAA^{-})(CIND^{+})\bullet H_2O$** structure is summarized in **Table 4.10**.

Table 4.10: $(PAA^{-})(CIND^{+})\bullet H_2O$ crystal data.

Compound	**$(PAA^{-})(CIND^{+})\bullet H_2O$**
Structural Formula	$(C_8H_7O_2^{-})(C_{19}H_{23}N_2O^{+})\bullet H_2O$
PAA^{-}:$CIND^{+}$:H_2O ratio	1: 1: 1
Molecular Mass (g mol^{-1})	448.55
Data collection temperature (K)	173(2)
Crystal system	Monoclinic
Space group	*C2*
a (Å)	28.525 (6)
b (Å)	6.5303 (13)
c (Å)	15.172 (3)
α (°)	90.00
β (°)	120.24 (3)
γ (°)	90.00
Volume ($Å^3$)	2441.6 (11)
Z	4
D_c, Calculated density (g cm^{-3})	1.220
Final R indices [I>2sigma(I)]	R_1= 0.0627
	wR_2 = 0.1572
R indices (all data)	R_1 = 0.0900
	wR_2 = 0.1752
Largest diff. peak and hole ($eÅ^{-3}$)	0.507; -0.515

The acid: base combination has a 1:1:1 ratio including one water molecule. The structure was solved in the monoclinic space group *C2.* Both PAA and CIND ions were found in a general positions, thus Z = 4.

There is transfer of a proton from the PAA anion to the nitrogen (N4) of CIND confirming a salt formation due to carboxylate C-O distances (C8-O1= 1.245 Å and C8-O2 = 1.245 Å). The packing down [010] is shown in **Figure 4.3.6 (a)**. The structure shows weak X-H•••π interactions between PAA and the hydrogen atom (H3A) in the water molecule.

This X-H•••π interaction has a distance of 3.358 Å and an angle of 118 °. C-H•••π interaction is also observed between PAA and H12 in the CIND cation having a distance of 2.761 Å and an angle of 137 °. The shortest C-H•••π interaction in the structure is between CIND aromatic ring (N2 – C15) and H15 with a distance of 2.678 Å and an angle of 144 °. **Table 4.11** lists the X-H•••π/ C-H•••π interactions.

The cavities in which water molecules are located down [010] (**Figure 4.3.6 (a)**)have a void volume (contact surface) of 31.40 $Å^3$ and a unit cell volume percentage of 1.3 % obtained while using Mercury [27] software with a probe radius of 1.4 Å and a grid spacing of 0.70 Å .

Table 4.11: X-H•••π/ C-H•••π parameters of **$(PAA^-)(CIND^+)•H_2O$**.

X-H•••π/ C-H•••π	C•••π (Å)	H•••π (Å)	C-H-π (°)	Symmetry Operator
O3-H3A•••π	3.763	3.358	118	X, -1+Y, Z
C12-H12•••π	3.516	2.761	137	-X, Y, -Z
C15-H15•••π	3.489	2.678	144	1\2-X, -1\2+Y,-Z

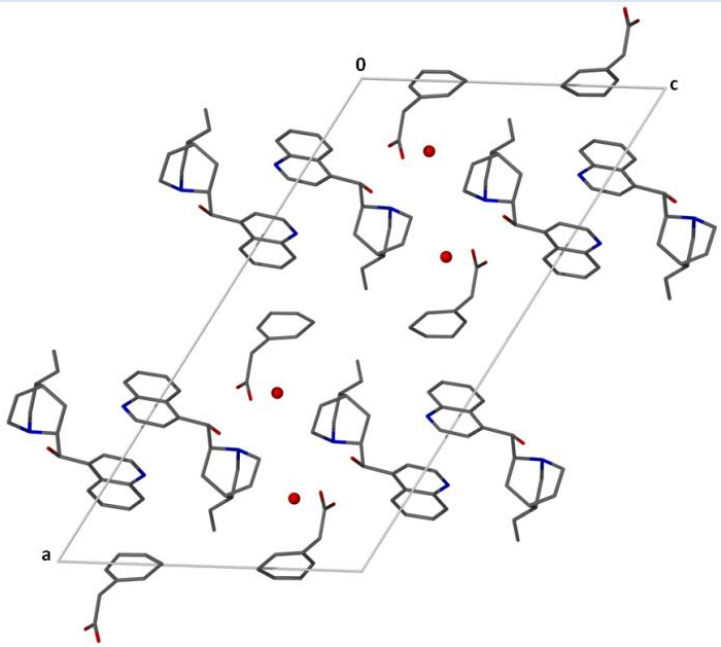

(a)

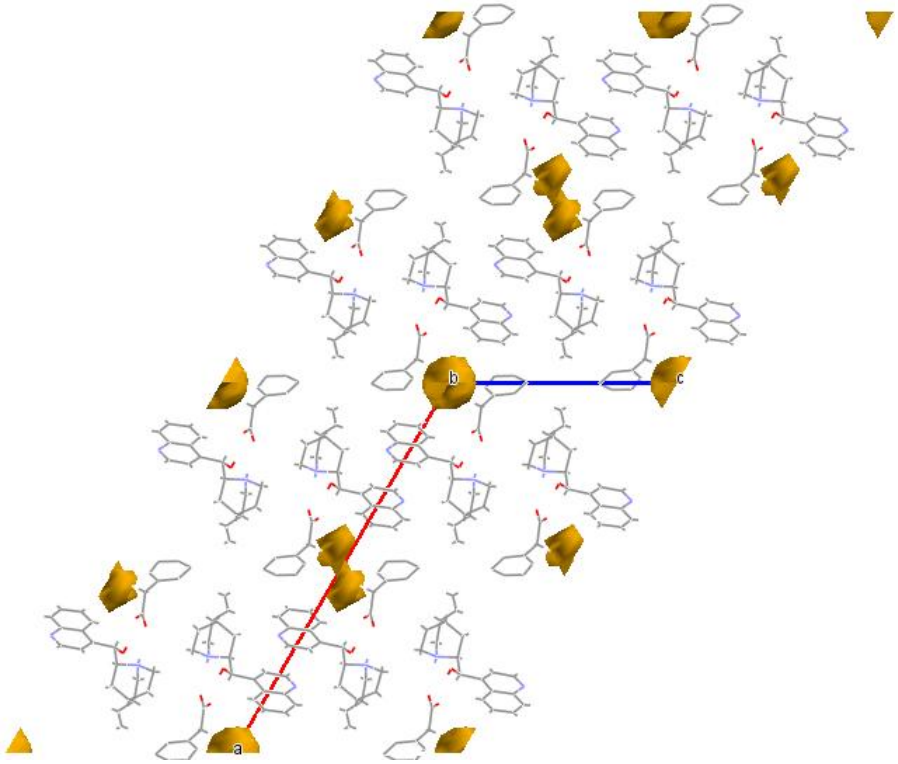

(b)

Figure 4.3.6: (a) Packing diagram of **(PAA^-)($CIND^+$)•H_2O** down [010]**, (b)** cavities in which water molecules are located down [010].

The structure interacts via hydrogen bonding (**Figure 4.3.7**) between (CIND) O5-H5A•••O2 (PAA) with a O•••O distance of 2.646 (4) Å and an O-H•••O angle of 160 (4) º. The other interaction in the structure is between O3-H3A•••O2 with a O•••O distance of 2.890 (6) Å and an O-H•••O angle of 148 (6) º. The oxygen atom labeled O2 forms a bifurcated acceptor due to the fact that it is connected to one hydrogen atom in the CIND cation and one hydrogen atom of the water molecules (H5A and H3A respectively).

The structure is further stabilized by the O3-H3B•••O1connection with a O•••O distance of 2.774 (6) Å and an O-H•••O angle of 171 (5) º, follow by the (CIND) N4-H1•••O1 (PAA) with an N•••O distance of 2.694 (4) Å and an N-H•••O angle of 167 (4) º. The oxygen atom labeled O1 also plays a bifurcated acceptor role because bonded to the protonated hydrogen (H1) and the second hydrogen (H3B) in the water molecule. The

graph sets involved in the structure are defined as $D_1^1(2)$, $D_2^1(3)$, $D_2^2(5)$, $C_2^2(6)$ and $C_2^2(9)$. Hydrogen data are given in **Table 4.12**.

Table 4.12: $(PAA^-)(CIND^+)\bullet H_2O$ hydrogen bonding parameters.

COMPOUND	D-H···A	D···A (Å)	D-H (Å)	H···A (Å)	D-H···A (º)
$(PAA^-)(CIND^+)\bullet H_2O$	N4-H1···O1	2.694 (4)	0.922 (4)	1.789 (4)	167 (4)
	O5-H5A···O2 [a]	2.646 (4)	1.070 (5)	1.616 (5)	160 (4)
	O3-H3B···O1	2.774 (4)	0.953 (7)	1.830 (7)	171 (5)
	O3-H3A···O2 [a]	2.890 (6)	0.747 (6)	2.227 (6)	148 (6)

a = x, y-1, z

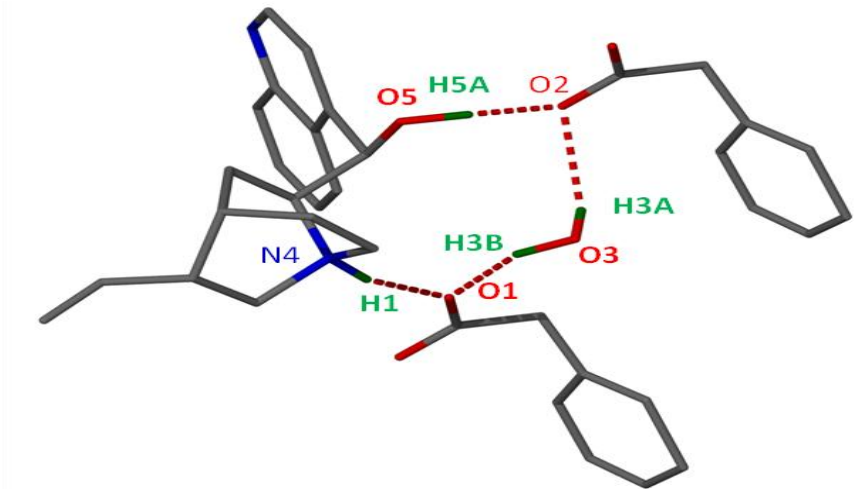

Figure 4.3.7: Hydrogen bonding in **$(PAA^-)(CIND^+)\bullet H_2O$**.

4.4 Phenyl acetic acid and isonicotinamide (PAA•INM)

A 1:1 ratio of both PAA and isonicotinamide (INM) was dissolved in ethyl methyl ketone with slight heating on a hot plate. The solution was allowed to evaporate at ambient temperature and plate-like crystals were obtained after a few days.

This acid: base combination formed a co-crystal due to the ΔpK_a (pK_a (base) – pK_a (acid) = 3.67[28] – 4.31[10] = -0.64). The asymmetric unit of **PAA•INM** is shown in **Figure 4.4.1**.

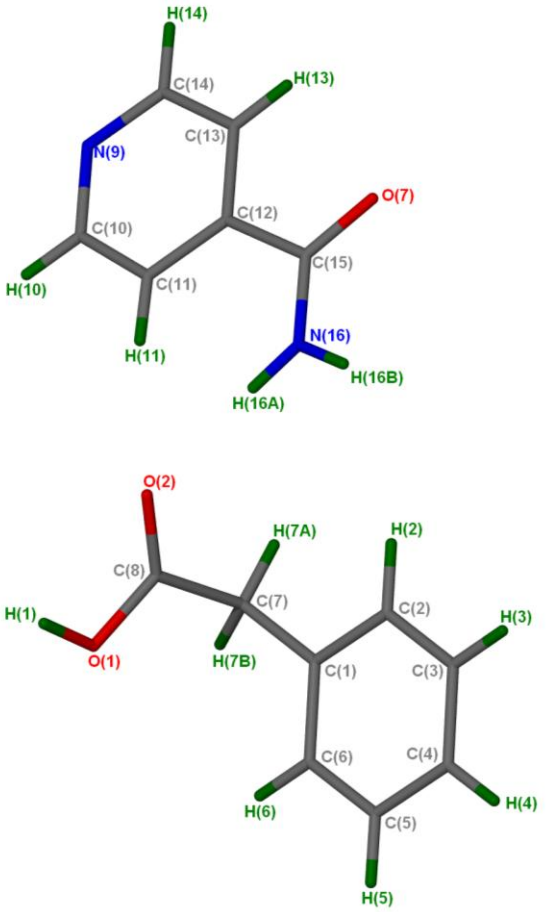

Figure 4.4.1: Asymmetric unit of the **PAA•INM** structure with all the hydrogen atoms shown for numbering clarity.

4.4.1 Thermal Analysis

The melting point of the co-crystal was found to be in-between the two components. Thermal analysis data and curves are shown in **Table 4.13** and **Figure 4.4.2** respectively.

Table 4.13: Thermal analysis data of **PAA•INM**.

Compounds	**DSC Endo$_1$(T_{onset},K)**	**DSC Endo$_2$(T_{onset},K)**
Isonicotinamide	382.1	428.4
Phenyl acetic acid	-	351.8
PAA•INM	-	363.1

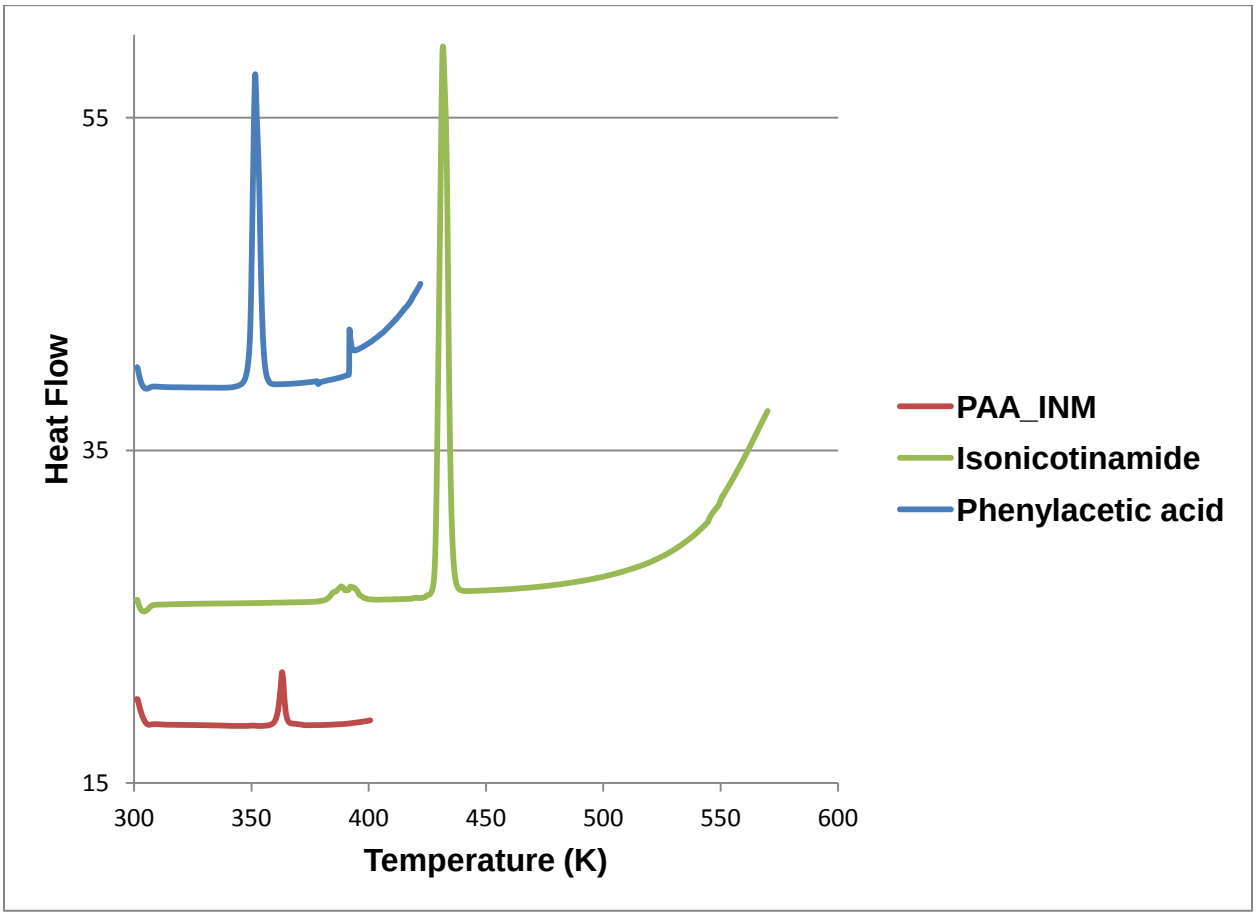

Figure 4.4.2: DSC curves of phenyl acetic acid (blue), isonicotinamide (green) and **PAA•INM** (red).

4.4.2 IR Spectroscopy

The IR spectrum of **PAA•INM** has IR absorption peaks of both starting components. As illustrated in **Figure 4.4.3**. The formation of a co-crystal is particularly demonstrated by the presence of new bands observed at 3369 and 3158 cm^{-1} which can be assigned to the H-bonded NH_2 stretching modes (**Table 4.14**).

There is a lack of shift in the vibrational frequencies for the C-N stretch and N-H bends in the co-crystal (1399 cm^{-1}). This indicates that the patterns of molecular motion of the supramolecular synthon are not significantly different to those of the initial reactants, which implies that the force constants of the homosupramolecular synthons (i.e., INM and PAA) are not strongly changed upon formation of the heterosupramolecular synthon of the co-crystal.[15]

Table 4.14: IR positions and assignments of peaks in PAA, **PAA•INM** and INM.

PAA	**PAA•INM**	INM	Proposed assignment
3123	3158	-	OH stretch
-	3369	3370, 3186	H-bonded NH_2 stretching mode
2750, 2620	2808, 2474	2783	C-C ring modes
1699	1713, 1638	1680	C=O
-	1638, 1609	1624	Amide II band (NH_2 scissor), C-N, C=O stretching mode combination
1498, 1454, 1407	1556, 1530, 1450,1324	1595, 1551	C=C stretch
-	1399	1399	Amide III band (C-N stretch, N-H bend)
1290, 1243	1231, 1214	1218	C-O stretch

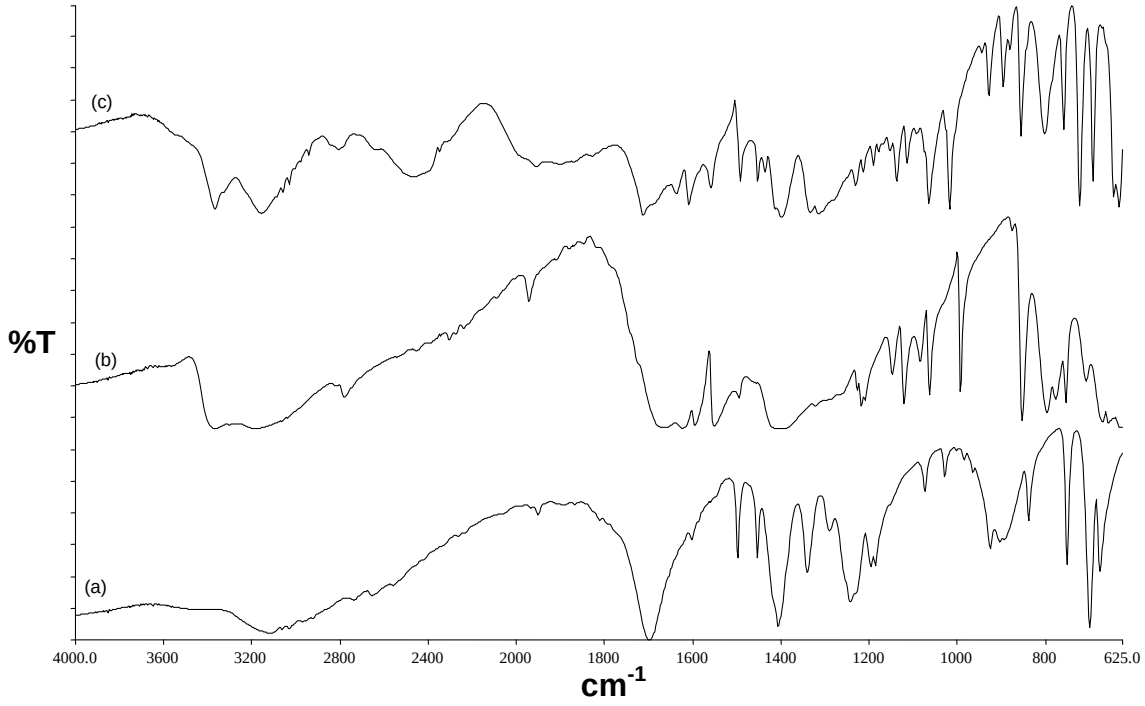

Figure 4.4.3: IR spectrum (a) PAA, (b) INM and (c) **PAA•INM**.

4.4.3 Powder X-ray Diffraction

There is good agreement between the PXRD patterns of the ground products obtained at 30 and 40 min. Both of these PXRD patterns matched that of the slurry experiment. However, PXRD pattern both ground products and slurry conversion did not match either the physical mixture PXRD pattern or the calculated pattern obtained from LAZYPULVERIX.[16] A conclusion was drawn that the slurry and grinding experiments resulted in another form of the **PAA•INM** co-crystal. **Figure 4.4.4** illustrates the PXRD patterns for the various types of experiments.

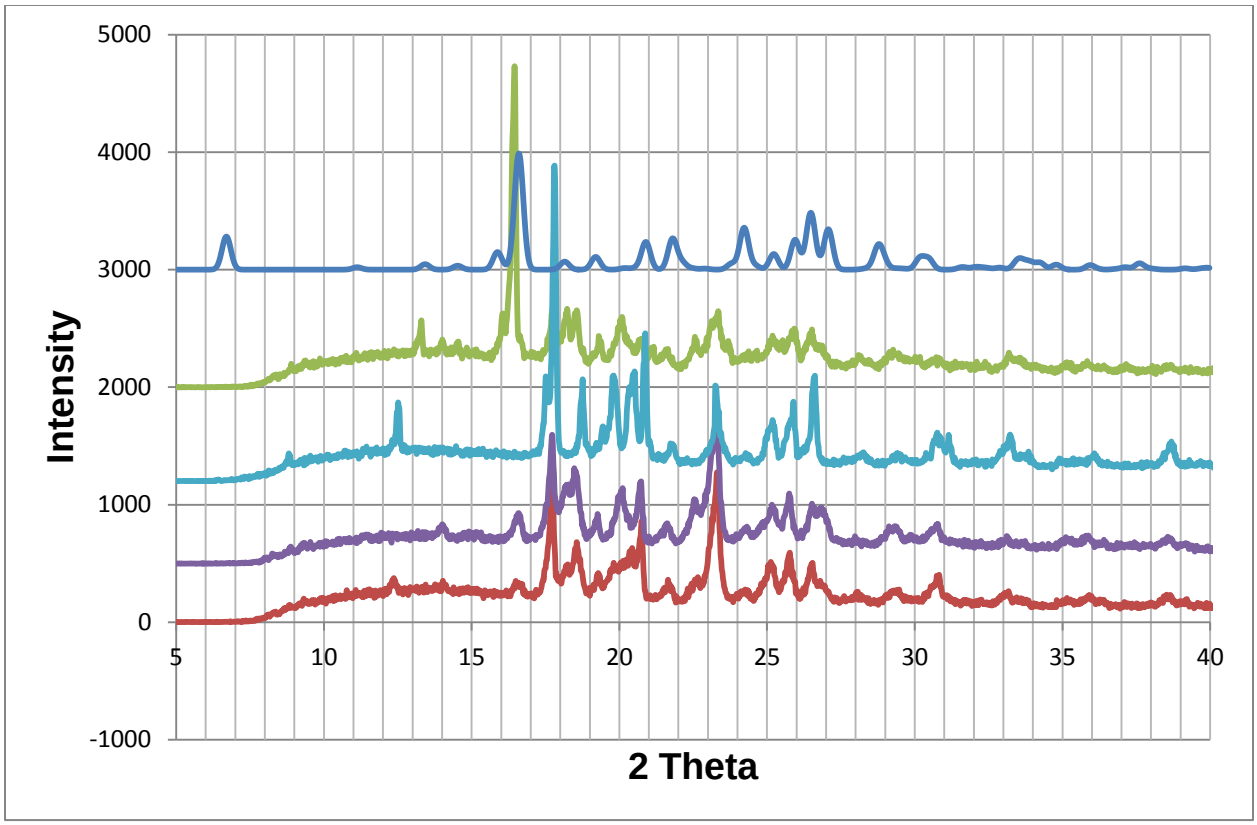

Figure 4.4.4: PXRD patterns of **PAA•INM** (blue), ground product after 30 min (red), ground product after 40 min (purple), slurry (green) and physical mixture (sky blue).

4.4.4 Structure Determination

All the non-hydrogen atoms of PAA and INM were found in the difference electron density maps and refined via direct methods. The non-hydrogen atoms of PAA were refined anisotropically and both PAA and INM molecules were found in general positions. The asymmetric unit (**Figure 4.4.1**) consists of one PAA and one INM molecule. Crystal data details of **PAA•INM** are given in **Table 4.15**.

Table 4.15: PAA•INM crystal data.

Compound	**PAA•INM**
Structural Formula	$C_8H_8O_2$•$C_6H_6N_2O$
PAA:INM ratio	1: 1
Molecular Mass (g mol^{-1})	258.28
Data collection temperature (K)	173(2)
Crystal system	Monoclinic
Space group	*C2/c*
a (Å)	32.264 (7)
b (Å)	4.3278 (9)
c (Å)	22.602 (5)
α (°)	90.00
β (°)	125.10 (3)
γ (°)	90.00
Volume ($Å^3$)	2582.0 (9)
Z	8
D_c, Calculated density (g cm^{-3})	1.329
Final R indices [I>2sigma(I)]	R_1= 0.0361
	wR_2 = 0.0975
R indices (all data)	R_1 = 0.0457
	wR_2 = 0.1049
Largest diff. peak and hole (E $Å^{-3}$)	0.225; -0.167

PAA•INM crystallized in the monocline space group *C2/c* with Z = 8. The co-crystal has a structural formula of $C_8H_8O_2$•$C_6H_6N_2O$ and a molecular mass of 258.27 g.mol^{-1}. The structure displays a very weak C-H•••π interaction between a PAA aromatic ring and H7B in another PAA molecule having a C-π distance of 3.269 Å with a C-H•••π angle of 110° as shown in **Figure 4.4.5**. The packing diagram of **PAA•INM** is represented in **Figure 4.4.6**.

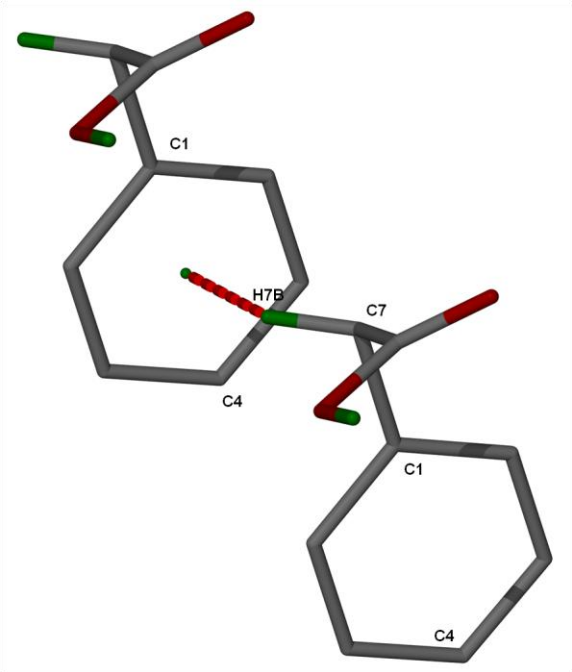

Figure 4.4.5: C-H•••π interaction between PAA molecules.

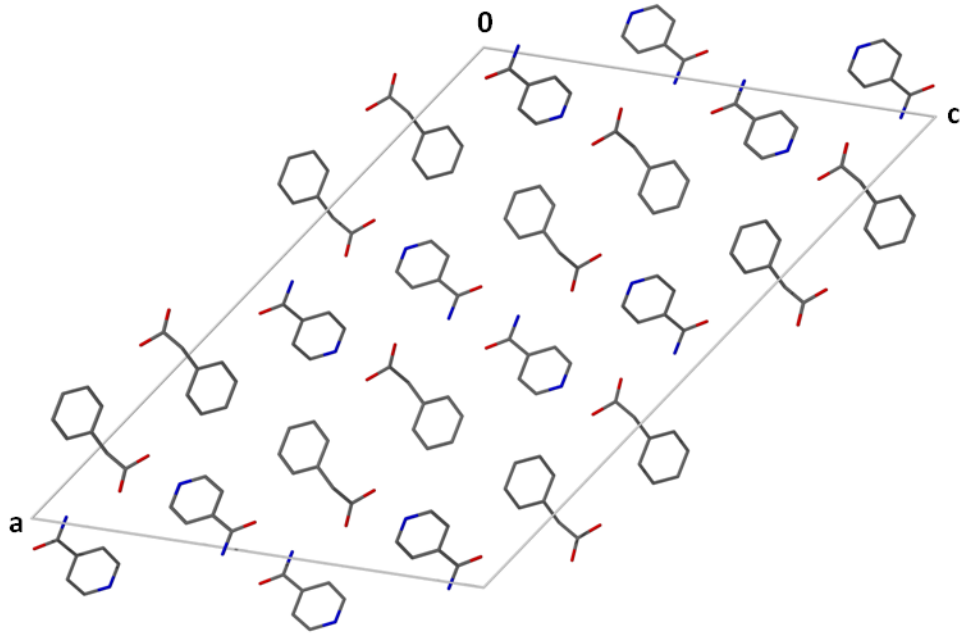

Figure 4.4.6: Packing diagram of **PAA•INM** down [010] with the hydrogen atoms removed.

The carboxylic acid hydrogen of PAA forms a hydrogen bond with nitrogen (N9) of the isonicotinamide. Two INM molecules form a dimer which can be described as

$R_2^2(8)$, **Figure 4.4.7**.

The graph sets of the structure can be characterized as $D_1^1(2)$, $C_2^2(11)$, $D_3^3(9)$ and $D_3^3(15)$. The hydrogen bond parameters of **PAA•INM** are given in **Table 4.16**.

Table 4.16: PAA•INM hydrogen bonding parameters.

COMPOUND	D-H···A	D···A (Å)	D-H (Å)	H···A (Å)	D-H···A (º)
PAA•INM	N16-H16A···O2	2.960 (1)	0.890 (1)	2.081 (1)	169 (1)
	N16-H16B···O7[a]	2.898 (2)	0.867 (1)	2.032 (1)	178 (1)
	O1-H1···N9 [b]	2.630 (2)	0.939 (1)	1.696 (1)	173 (1)

a = -x, -y+1, -z +1; b = -x, y-1, -z +1/2

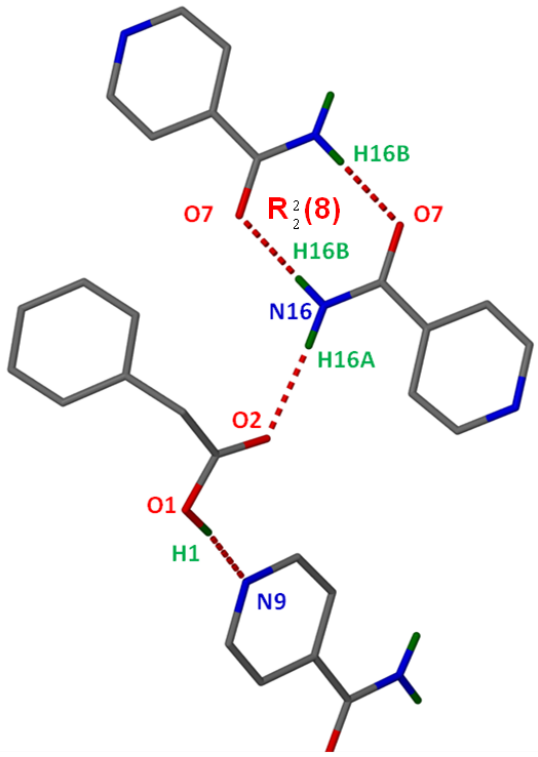

Figure 4.4.7: Hydrogen bonding in **PAA•INM**.

4.4.5 Phenyl acetic acid and nicotinamide (2PAA•2NAM)

The co-crystal was obtained by dissolving a 1: 1 ratio of both starting materials in acetone with gently heating on a hot plate. The solution was allowed to evaporate at room temperature and crystals with a molar ratio of 2:2 were obtained after a few days. Similar crystals were also obtained when using ethyl methyl ketone as a solvent. Co-crystal formation was predicted due to the ΔpK_a (ΔpK_{a1}= pK_a (base) - pK_a (acid) = 0.50[29] - 4.31[10] = - 3.81 and pK_{a2} = 3.40[29] - 4.31[10] = - 0.91) of this acid:base combination

The asymmetric unit of the **2PAA•2NAM** is illustrated in **Figure 4.5.1**.

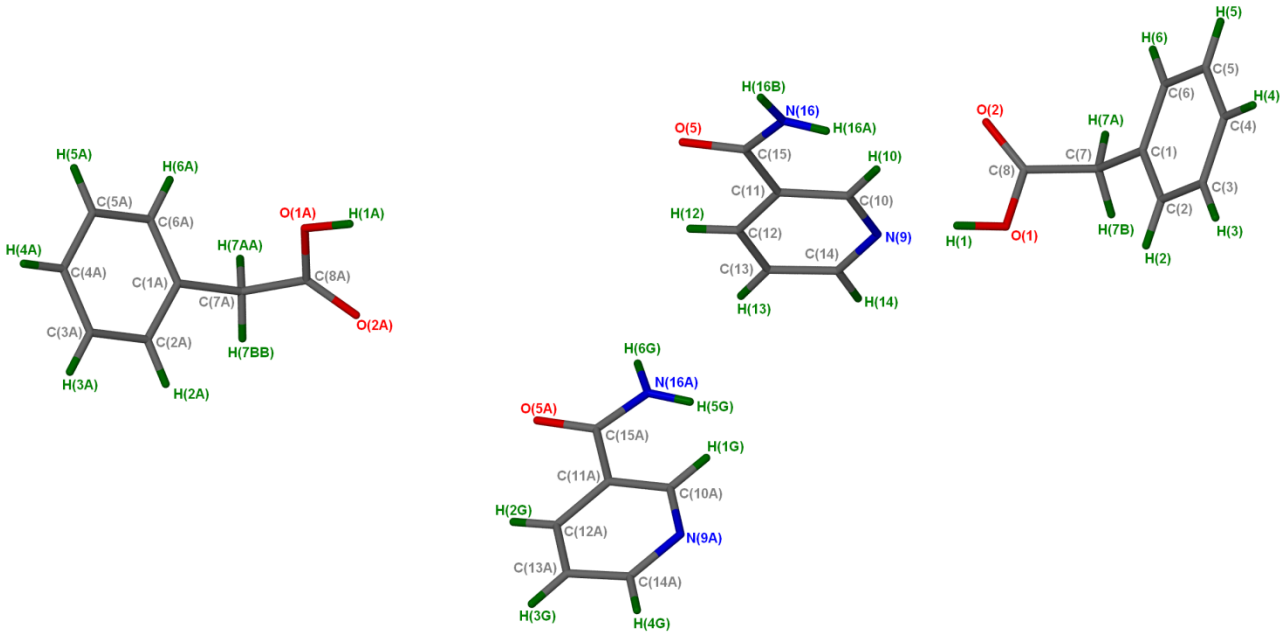

Figure 4.5.1: Asymmetric unit of **2PAA•2NAM** structure with all the hydrogen atoms shown for numbering clarity.

4.5.1 Thermal Analysis

The melting point of the **2PAA•2NAM** co-crystal was found to be lower than both PAA and NAM. This indicates that there is decrease in the thermal stability of the co-crystal.[17] **Table 4.17** lists the thermal analysis data of **2PAA•2NAM**.

Table 4.17: Thermal analysis data of **2PAA•2NAM**.

Compounds	**DSC Endo$_1$(T_{onset},K)**
Nicotinamide	401.6
Phenyl acetic acid	351.8
2PAA•2NAM	344.5

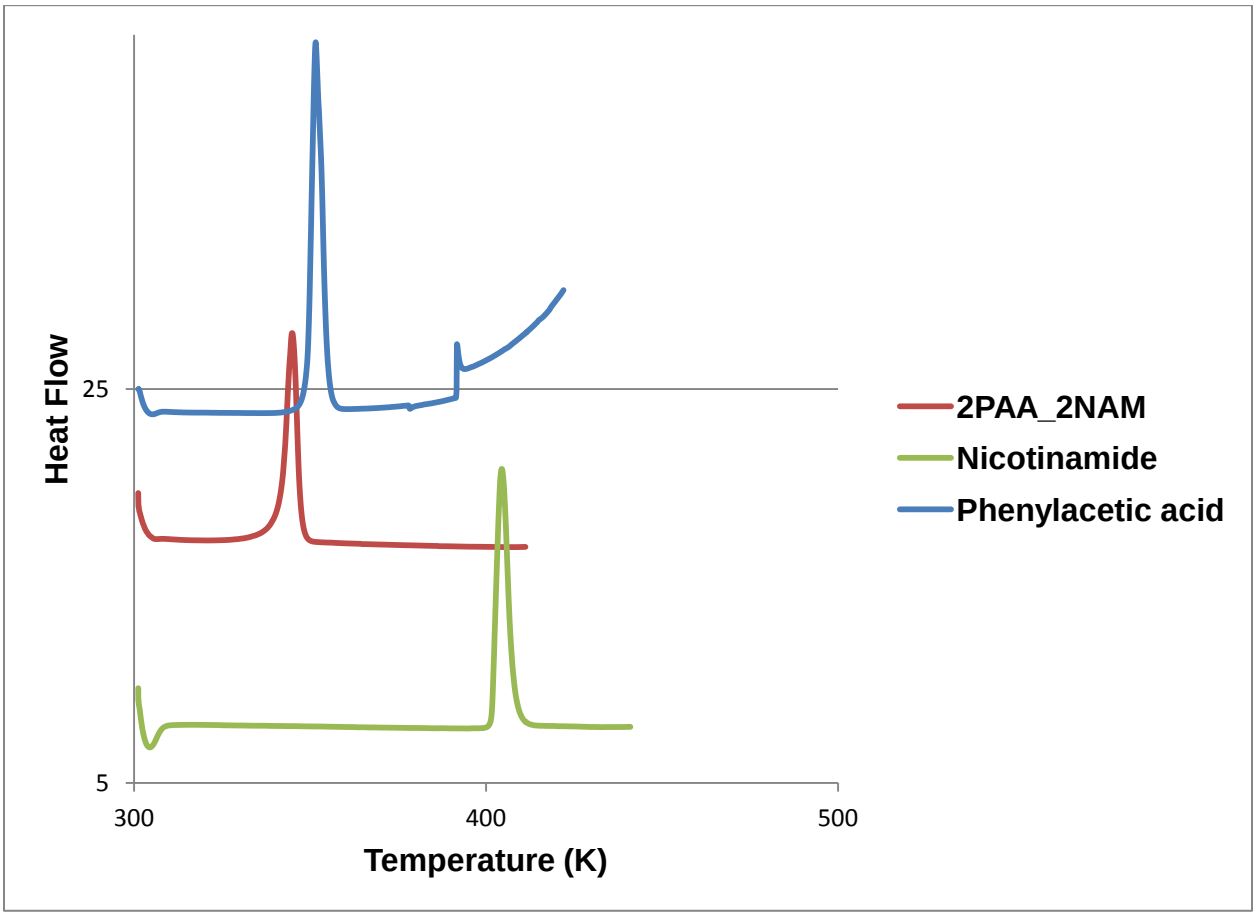

Figure 4.5.2: DSC curves of **2PAA•2NAM** (red), nicotinamide (green) and phenyl acetic acid (blue).

4.5.2 Hot Stage Microscopy

Figure 4.5.3 shows HSM photographs of **2PAA•2NAM**. At a temperature of 295 K, needle-like crystals were immersed in silicone oil and placed on the hot stage microscope. The crystals started losing transparency at 332 K and the melt commenced at 348 K.

(a) 295 K **(b) 332 K**

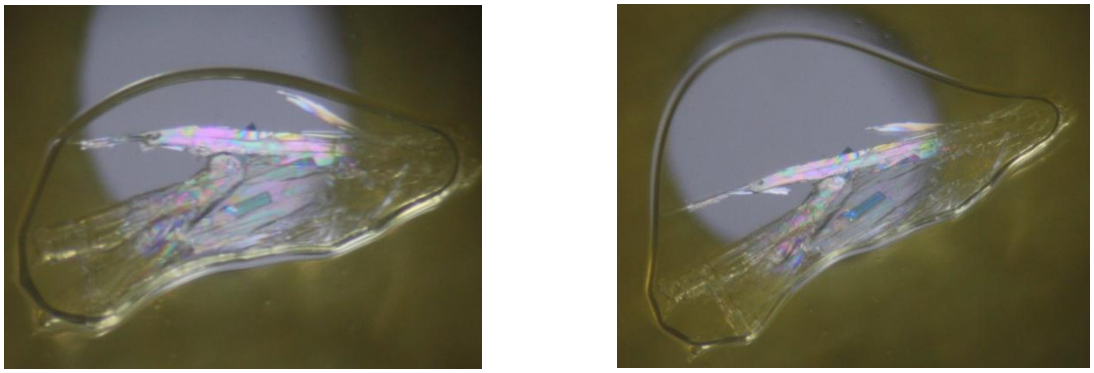

(c) 348 K **(d) 352 K**

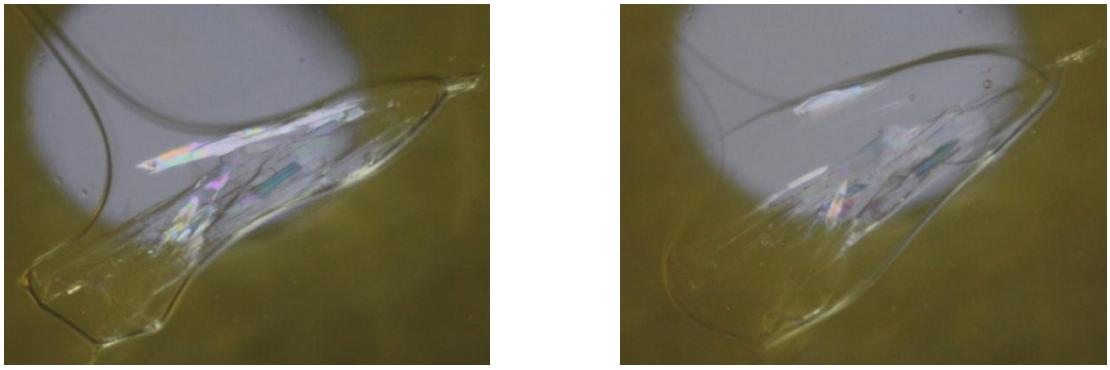

Figure 4.5.3: HSM photography of **2PAA•2NAM: (a)** crystal immersed in silicone oil, **(b)** crystal loss of transparency, **(c)** crystal starts melting and **(d)** melting of the crystal.

4.5.3 IR Spectroscopy

The formation of a co-crystal leads to a broadening in the carbonyl band region around 1650 cm^{-1}.[15] A broad band at 1711 cm^{-1} in the IR spectrum of the **2PAA•2NAM** (**Figure**

4.5.4) indicates co-crystal formation. There is perturbation of the force constants of the carbonyl group and the NH_2 group of the amide group involve in the interaction. There is also formation of new bands at 3385 and 3160 cm^{-1}.

There is a shift in the vibrational frequencies for the C-N stretch and N-H bends in the co-crystal (1408 cm^{-1}). This is an indication that the patterns of molecular motion of the supramolecular synthon are significantly different to those of the initial reactants, which implies that the force constants of the homosupramolecular synthons (i.e., NAM and PAA) are strongly changed upon formation of the heterosupramolecular synthon of the co-crystal. IR assignment of the co-crystal and the individual compounds are given in **Table 4.18**.

Table 4.18: IR positions and assignments of peaks in PAA, **2PAA•2NAM** and NAM.

PAA	**2PAA•2NAM**	NAM	Proposed assignment
3123	3160	-	OH stretch
-	3385	3366, 3163	H-bonded NH_2 stretching mode
2750, 2620	2788, 2484	3060, 2360	C-C ring modes
1699	1711, 1631	1683	C=O
-	1631	1619	Amide II band (NH_2 scissor), C-N, C=O stretching mode combination
1498, 1454, 1407	1595, 1495,1454	1593, 1574, 1485, 1426	C=C stretch
-	1408	1399	Amide III band (C-N stretch, N-H bend)
1290, 1243	1298	1230, 1202	C-O stretch

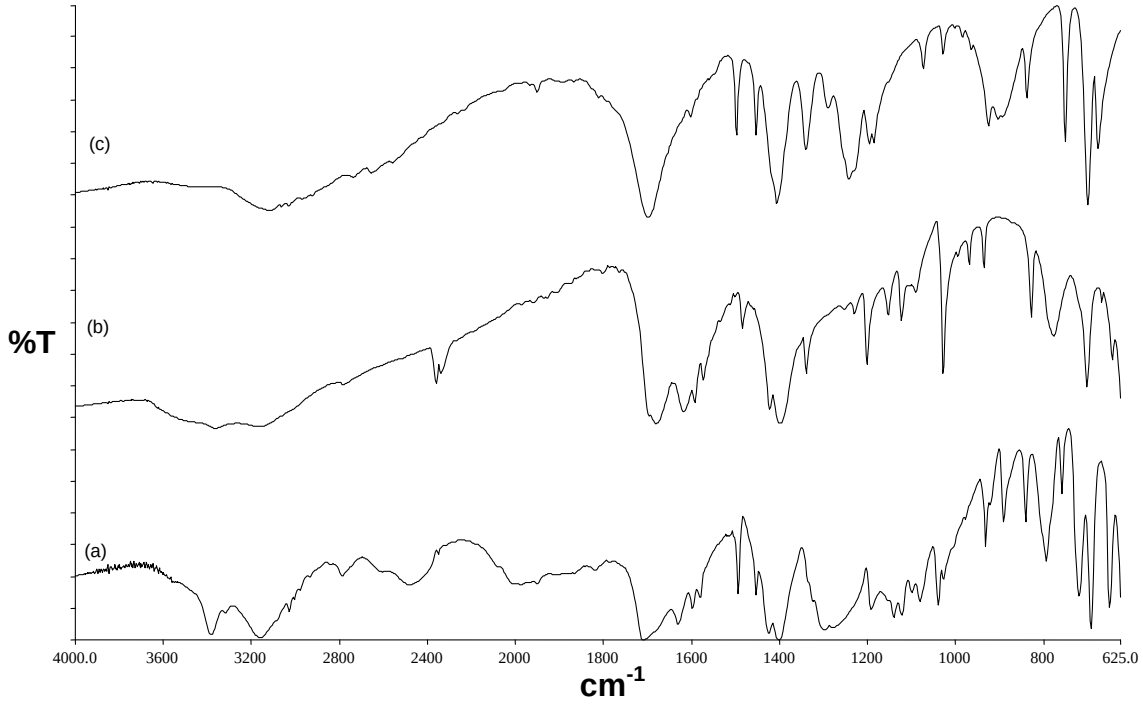

Figure 4.5.4: IR spectrum (a) **2PAA•2NAM**, (b) NAM and (c) PAA.

4.5.4 Powder X-ray Diffraction

There is overall agreement between the PXRD patterns of the ground product (30 min) and the physical mixture. The PXRD pattern of the slurry experiment also did not match that of the calculated pattern from LAZYPULVERIX.[16] Thus the **2PAA•2NAM** co-crystal could not be prepared from the grinding or the slurry experiments. PXRD patterns of all type of experiment are shown in **Figure 4.5.5**.

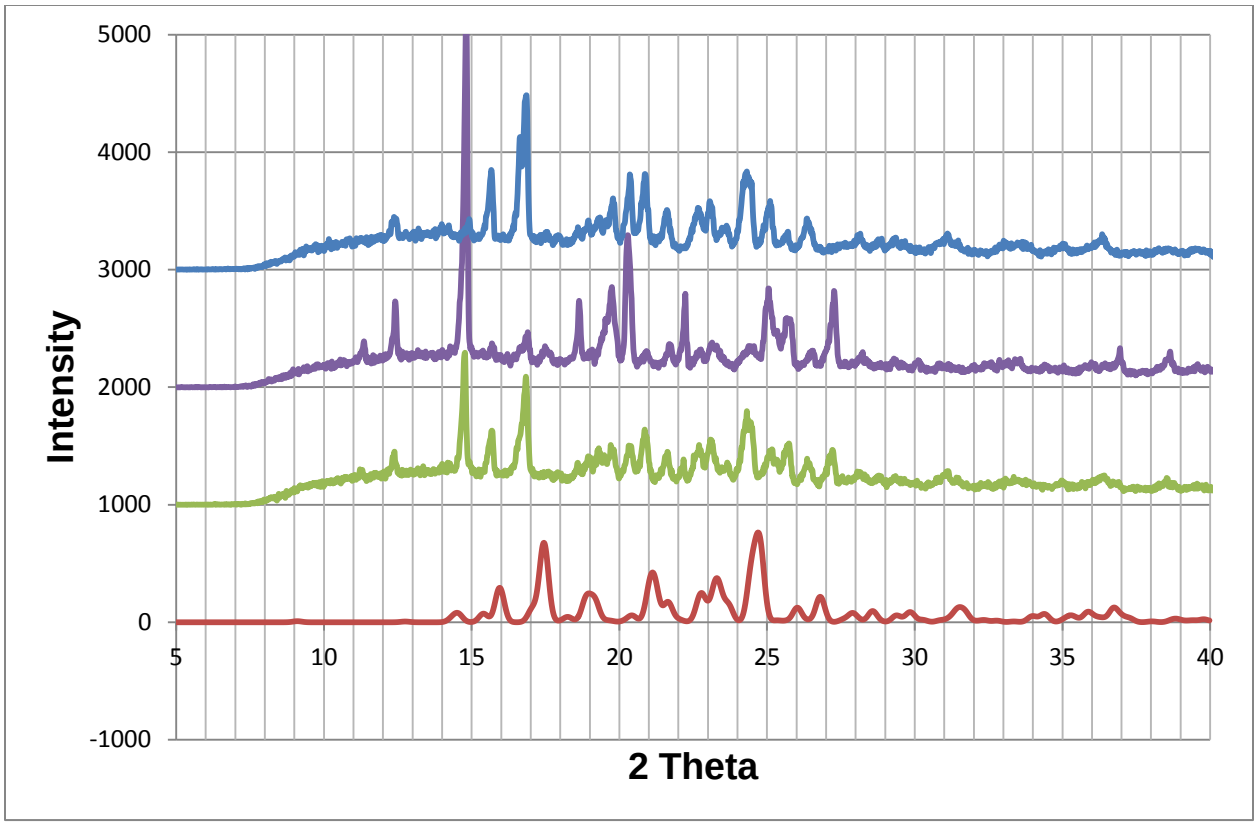

Figure 4.5.5: PXRD patterns of **2PAA•2NAM** (red), ground product at 30 min (green), physical mixture (purple) and slurry (blue).

4.5.5 Structure Determination

The crystal structure of **2PAA•2NAM** refined successfully in the monoclinic space group $P2_1/n$ to R_1= 0.0518 with wR_2= 0.1146 ([I>2sigma (I)]). All non-hydrogen atoms were found by direct methods in the difference electron density map and refined anisotropically. PAA and NAM molecules were located in general positions with a molar ratio of 2: 2. The crystal data and experimental conditions are given in **Table 4.19**.

Table 4.19: 2PAA•2NAM crystal data.

Compound	**2PAA•2NAM**
Structural Formula	$2C_8H_8O_2•2C_6H_6N_2O$
PAA:NAM ratio	2: 2
Molecular Mass (g mol^{-1})	516.55
Data collection temperature (K)	173(2)
Crystal system	Monoclinic
Space group	$P2_1/n$
a (Å)	12.389 (3)
b (Å)	5.0838 (10)
c (Å)	41.803 (8)
α (°)	90.00
β (°)	95.79 (3)
γ (°)	90.00
Volume ($Å^3$)	2619.3 (9)
Z	4
D_c, Calculated density (g cm^{-3})	1.310
Final R indices [I>2sigma(I)]	R_1= 0.0518
	wR_2 = 0.1146
R indices (all data)	R_1 = 0.0836
	wR_2 = 0.1289
Largest diff. peak and hole ($eÅ^{-3}$)	0.171; -0.200

The packing diagram of **2PAA•2NAM** along the [010] direction is shown in **Figure 4.5.6**.

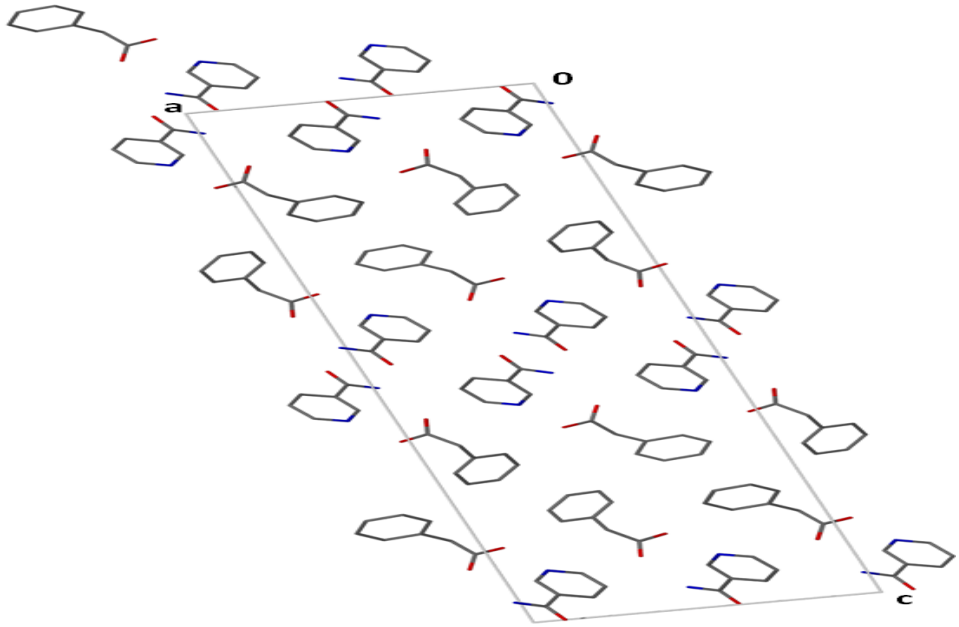

Figure 4.5.6: Packing diagram of **2PAA•2NAM** down [010] with the hydrogen atoms removed.

Stabilization of the co-crystal structural network occurs via the hydrogen bonded $R_2^2(8)$ ring motif between two NAM molecules. The same interaction occurs for the second NAM molecule in the asymmetric unit.

There is further stabilization between (PAA) O1-H1•••N9 (NAM) and (NAM) N16-H16A•••O2 (PAA). The second PAA molecule has the same hydrogen bond connection which is between (PAA) O1A-H1A•••N9A (NAM) and (NAM) N16A-H5G•••O2A (PAA) as shown in **Figure 4.5.7**. The graph sets of the **2PAA•2NAM** network can be characterized as: $D_1^1(2)$, $C_2^2(10)$, $D_3^3(9)$ and $D_3^3(15)$. Hydrogen bonding parameters of **2PAA•2NAM** are listed in **Table 4.20**.

Table 4.20: 2PAA•2NAM hydrogen bonding parameters.

COMPOUND	D-H···A	D···A (Å)	D-H (Å)	H···A (Å)	D-H···A (º)
2PAA•2NAM	O1-H1···N9	2.604 (2)	0.996 (3)	1.614 (3)	172 (3)
	N16A-H5G···O2A[a]	2.973 (2)	0.872 (2)	2.110 (2)	171 (2)
	N16-H6G···O5 [a]	2.885 (2)	0.908 (2)	1.978 (2)	177 (2)
	O1A-H1A···N9A[b]	2.606 (2)	1.020 (3)	1.588 (3)	176 (2)
	N16-H16A··· O2[c]	3.038 (2)	0.866 (2)	2.178 (2)	172 (2)
	N16-h16B···O5[d]	2.878 (2)	0.883 (2)	1.996 (3)	176 (2)

a = -x+1, -y+1, -z ; b = -x+1, -y, -z ; c = x, y-1, z ; d = -x+2, -y, -z

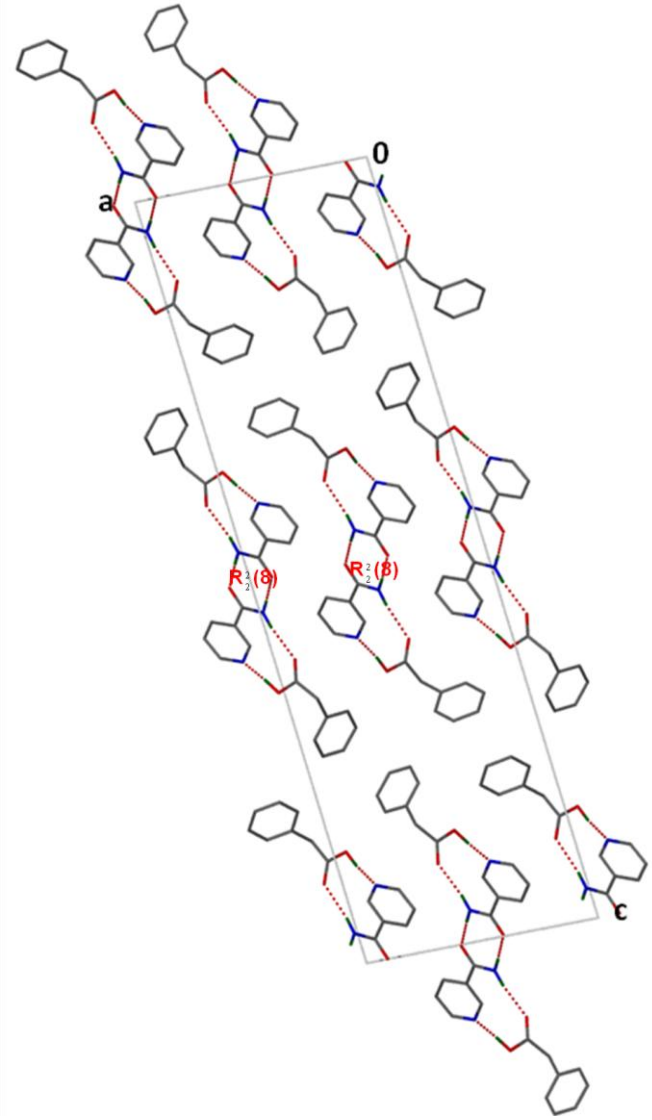

Figure 4.5.7: Hydrogen bonding in **2PAA•2NAM** down [010].

4.6 Phenyl acetic acid and quinidine $(PAA^{-})(QUID^{+})\bullet H_2O$

Quinidine, $C_{20}H_{24}N_2O_2$ is originally derived from the bark of the cinchona tree and it is a stereoisomer of quinine. Quinidine is an antimalarial agent[30] and it is used as an anti-arrythmatic agent with anti-muscarinic and α-adrenoceptor blocking proprieties[31-33] or for the treatment of neurological disorders.[34]

A 1:1 ratio of PAA and a quinidine (QUID) was dissolved in acetone by gently heating on a hot plate. The solution was allowed to evaporate at room temperature and after a few days crystals were obtained. This crystal structure had a water molecule included. The same crystal was obtained when ethyl methyl ketone, tetrahydrofuran, isopropanol, ethanol and methanol were used as solvents.

The asymmetric unit of **$(PAA^{-})(QUID^{+})\bullet H_2O$** is shown in **Figure 4.6.1**.

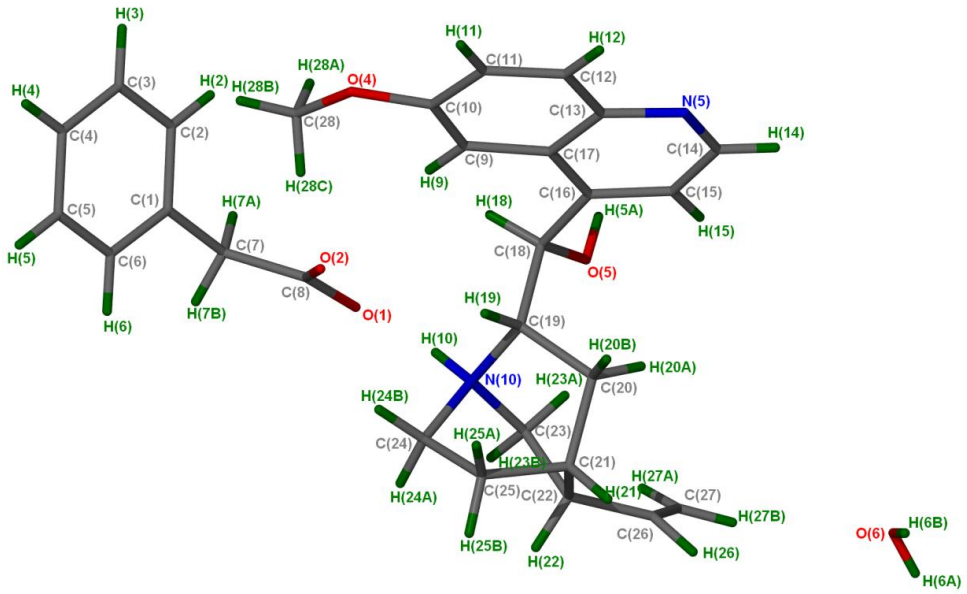

Figure 4.6.1: Asymmetric unit of **$(PAA^{-})(QUID^{+})\bullet H_2O$** structure with all the hydrogen atoms shown for numbering clarity.

4.6.1 Thermal Analysis

There is good agreement between the experimental and calculated percentage mass losses obtained for the TG results. The thermal analysis results are given in **Table 4.21**. The TG curve shows a single mass loss of 3.0 % which corresponds to the loss of the water molecule. The first DSC endotherm observed corresponds to dissolution of the salt upon release of water and the second endotherm is the decomposition of the salt. Thermal analysis results are shown in **Figure 4.6.2**.

Table 4.21: Thermal analysis data for **$(PAA^-)(QUID^+)\bullet H_2O$**.

Compounds	PAA	**$(PAA^-)(QUID^+)\bullet H_2O$**	Quinidine
DSC $Endo_1$ (T_{onset},K)	-	374.7	-
DSC $Endo_2$ (T_{onset},K)	351.8	510.0	444.9
TG calculated % mass loss	-	3.8	-
TG experimental % mass loss	-	3.0	-
PAA^-: $QUID^+$: H_2O	-	1: 1: 1	-

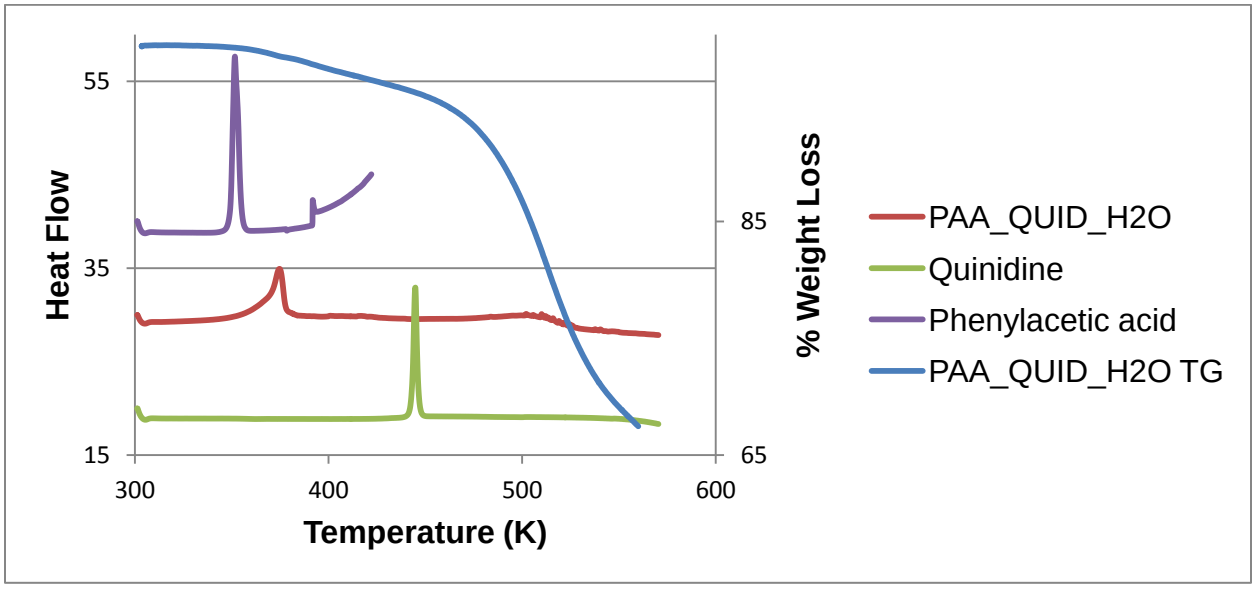

Figure 4.6.2: Thermal analysis curves of **$(PAA^-)(QUID^+)\bullet H_2O$**: DSC (red), TG (blue), QUID (green) and PAA (purple).

4.6.2 Hot Stage Microscopy

A block-like crystal immersed in silicone oil was placed on the hot stage at a temperature of 295 K. Water included in the crystal structure was released at 349 K and the crystal started melting at 376 K. The melting process was obtained at a temperature of about 380 K as shown in **Figure 4.6.3**.

(a) 295 K **(b) 349 K**

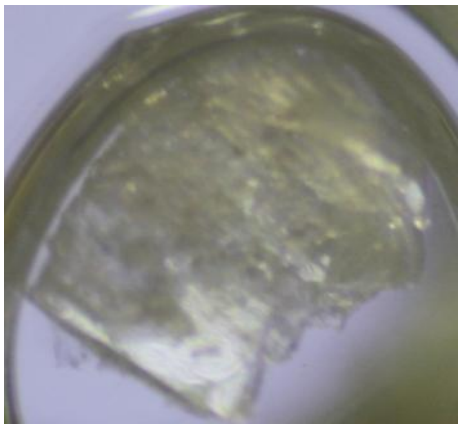

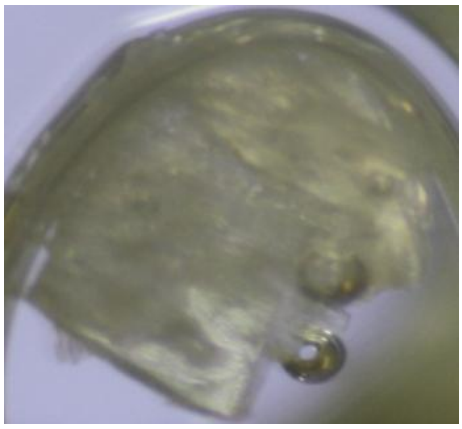

(c) 376 K **(d) 380 K**

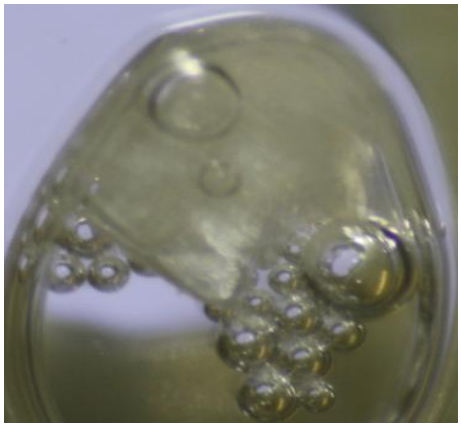

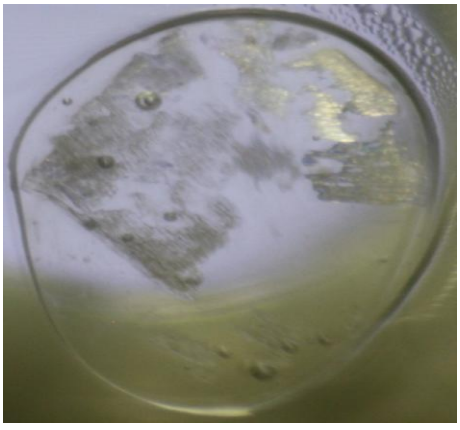

Figure 4.6.3: HSM photography of **(PAA^-)($QUID^+$)•H_2O**: **(a)** crystal immersed in silicone oil, **(b)** releasing of the water, **(c)** crystal starts melting and **(d)** melt of the crystal.

4.6.3 IR Spectroscopy

The IR spectrum of **$(PAA^-)(QUID^+)\bullet H_2O$** (**Figure 4.6.4**) shows a new broad band at 1587 cm^{-1} which indicates the formation of a salt ie. Transfer of a proton.[26] The band at 3455 cm^{-1} can be assigned to the solvated water in the structure and 3210 cm^{-1} to the N-H stretching vibration. The IR position and assignments are given in **Table 4.22**.

Table 4.22: IR positions and assignments of peaks in PAA, **$(PAA^-)(QUID^+)\bullet H_2O$** and QUID.

PAA	**$(PAA^-)(QUID^+)\bullet H_2O$**	QUID	Proposed assignment
3123	3455	3448, 3124	OH stretch
-	3210	-	N-H stretching mode
2750, 2620	2878, 2360	2932, 2868, 2710	C-C ring modes
1699	1670, 1587	-	C=O
-	1619	1620	C-N, C=O stretching mode combination
1498, 1454, 1407	1508, 1473,1448	1589, 1561, 1549, 1464	C=C stretch
-	1399	1400	C-N stretch, N-H bend
1290, 1243	1268	1282	C-O stretch

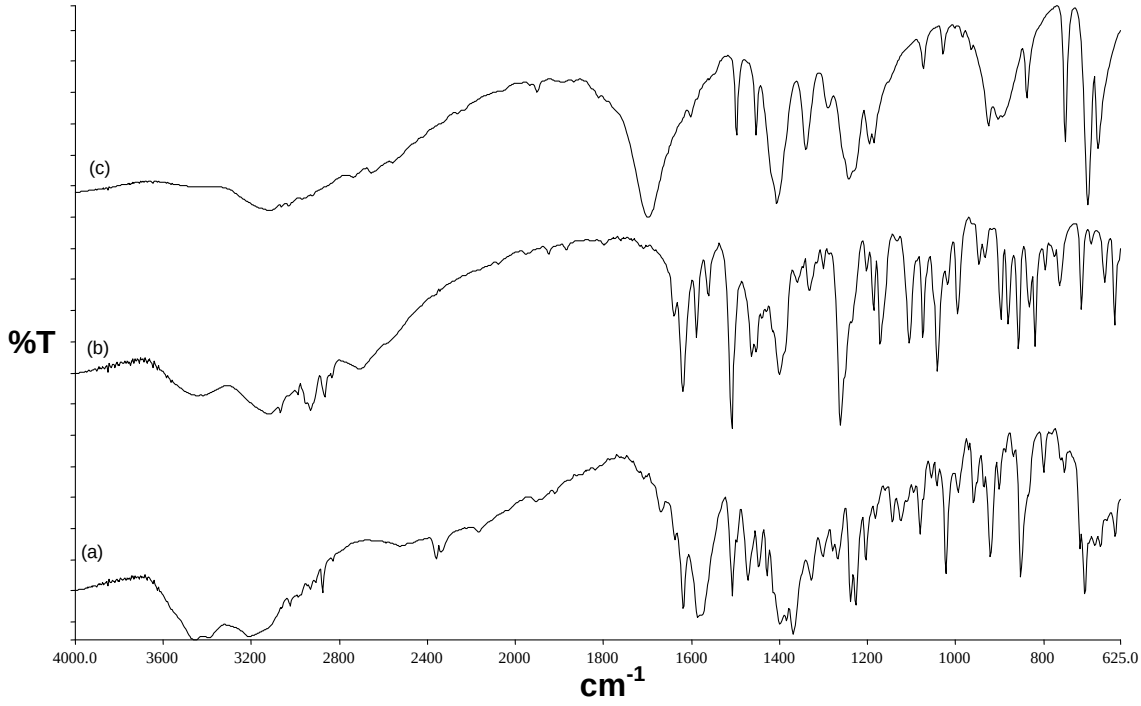

Figure 4.6.4: IR spectrums (a) **(PAA^-)($QUID^+$)•H_2O**, (b) QUID and (c) PAA.

4.6.4 Powder X-ray Diffraction

There good agreement between the slurry conversion experiment performed in isopropanol and the calculated pattern obtained from LAZYPULVERIX[16] as shown in **Figure 4.6.5**.

Grinding and solvent drop grinding experiments were not possible due to the formation of a paste obtained when PAA and QUID were ground together. The resultant product (paste) could not be analyzed using powder X-ray diffractometer.

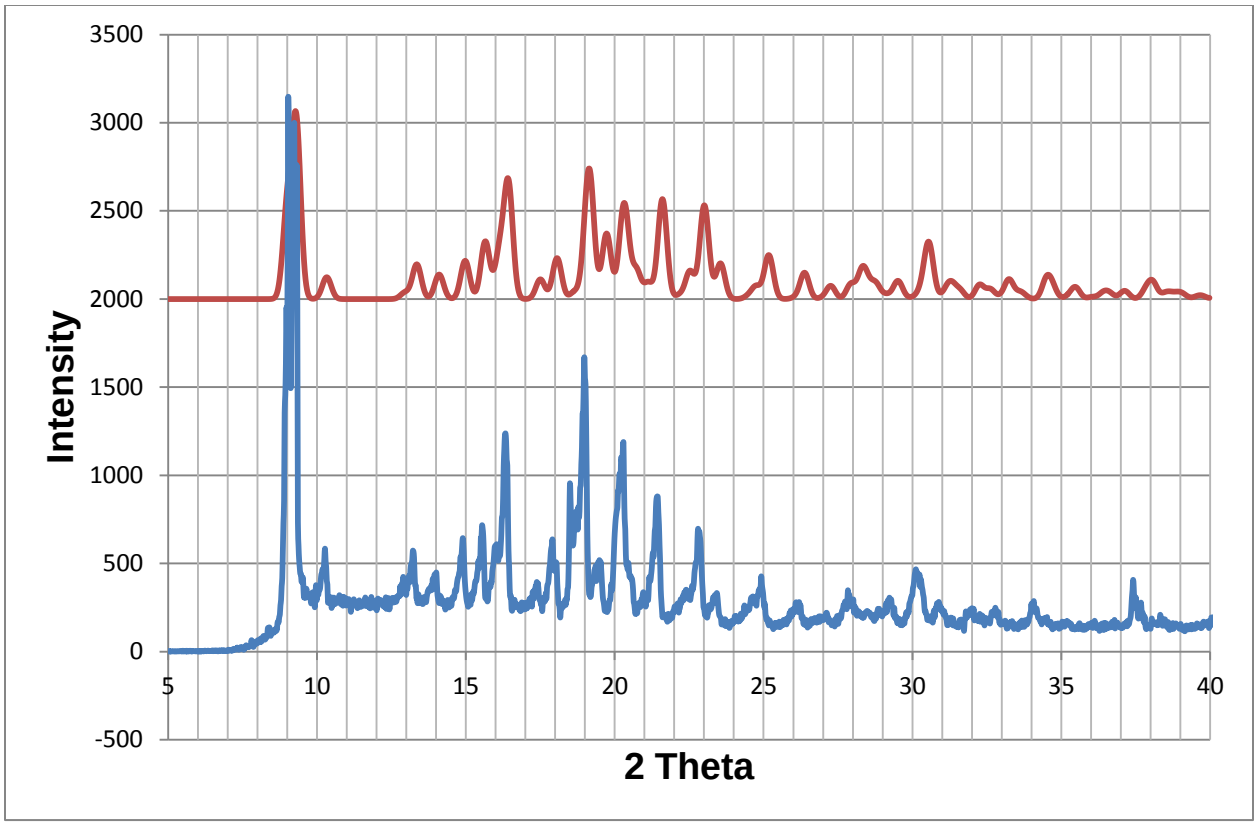

Figure 4.6.5: PXRD pattern of **$(PAA^{-})(QUID^{+})\bullet H_2O$** (red) and slurry (blue).

4.6.5 Structure Determination

$(PAA^{-})(QUID^{+})\bullet H_2O$ successfully refined to R_1= 0.0340 with wR_2= 0.0859 ([I>2sigma (I)]). All non-hydrogen atoms were located by direct methods in the difference electron density map and refined anisotropically. The nitrogen atoms of the QUID were identified by the highest peak magnitude in the rings. PAA and QUID ions were found in general positions. The crystal data is given in **Table 4.23**.

Table 4.23: $(PAA^-)(QUID^+)\bullet H_2O$ crystal data.

Compound	**$(PAA^-)(QUID^+)\bullet H_2O$**
Structural Formula	$(C_8H_7O_2^-)(C_{20}H_{25}N_2O_2^+)\bullet H_2O$
$PAA^-:QUID^+:H_2O$ ratio	1: 1: 1
Molecular Mass (g mol^{-1})	478.59
Data collection temperature (K)	173(2)
Crystal system	Monoclinic
Space group	$P2_1$
a (Å)	6.7225 (13)
b (Å)	19.648 (4)
c (Å)	9.6505 (19)
α (°)	90.00
β (°)	99.45 (3)
γ (°)	90.00
Volume ($Å^3$)	1257.4 (4)
Z	2
D_c, Calculated density (g cm^{-3})	1.264
Final R indices [I>2sigma(I)]	R_1= 0.0340
	wR_2 = 0.0859
R indices (all data)	R_1 = 0.0372
	wR_2 = 0.0885
Largest diff. peak and hole ($eÅ^{-3}$)	0.201; -0.217

$(PAA^-)(QUID^+)\bullet H_2O$ crystallized in a 1: 1: 1 ratio in the monoclinic space group $P2_1$, Z= 2. Proton transfer from PAA to QUID was observed. There is a single molecule of water trapped in the crystal system. The C-O distances of the PAA anion of the salt hydrate are such as:

- C8-O1 = 1.265 Å
- C8-O2 = 1.248 Å

These C-O distances are a confirmation of a proton transfer from the COOH group of PAA to one of the nitrogen atom (N10) in QUID to form a salt.

There are four C-H•••π interactions in the crystal structure; the first C-H•••π interaction is between the PAA aromatic ring and the hydrogen atom (H20B) in the QUID cation with a distance of 2.669 Å and a C-H•••π angle of 149º. The second C-H•••π interaction is between a quinidine ring (C9 – C17) and the hydrogen atom (H27A) attached to the carbon atom (C27) in the QUID molecule. This interaction (C27-H27A•••π) is strong and has a distance of 3.052 Å and a C-H•••π angle of 159 º. The third C-H•••π interaction is weak and it is between PAA ring (C1 – C6) and C28-H28B having a distance of 3.303 Å and a C-H•••π angle of 108 º. The last C-H•••π interaction involved QUID ring (N5 – C14) and C28-H28C with a distance of 3.176 Å and a C-H•••π angle of 112 º.

The crystal packing is illustrated in **Figure 4.6.6: (a)** showing the carboxylate group of PAA directed towards a QUID cation. The cavities (contact surface) in which the water molecules are located down [100] have a volume of 14.25 $Å^3$ and a unit cell percentage of 1.10 % using a probe radius of 1.2 Å and grid spacing of 0.70 Å as shown in **Figure 4.6.6: (b)**. A probe size of 1.4 Å supposed to be used but at that probe size there is no indication of the water voids that why a lower probe size of 1.2 Å was used.

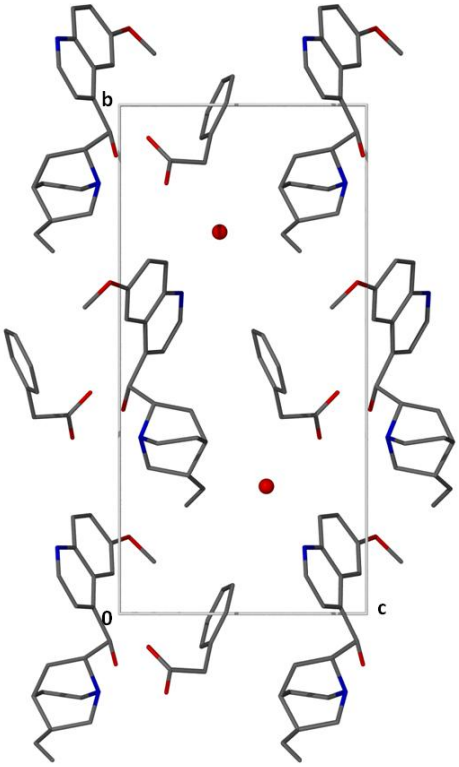

(a)

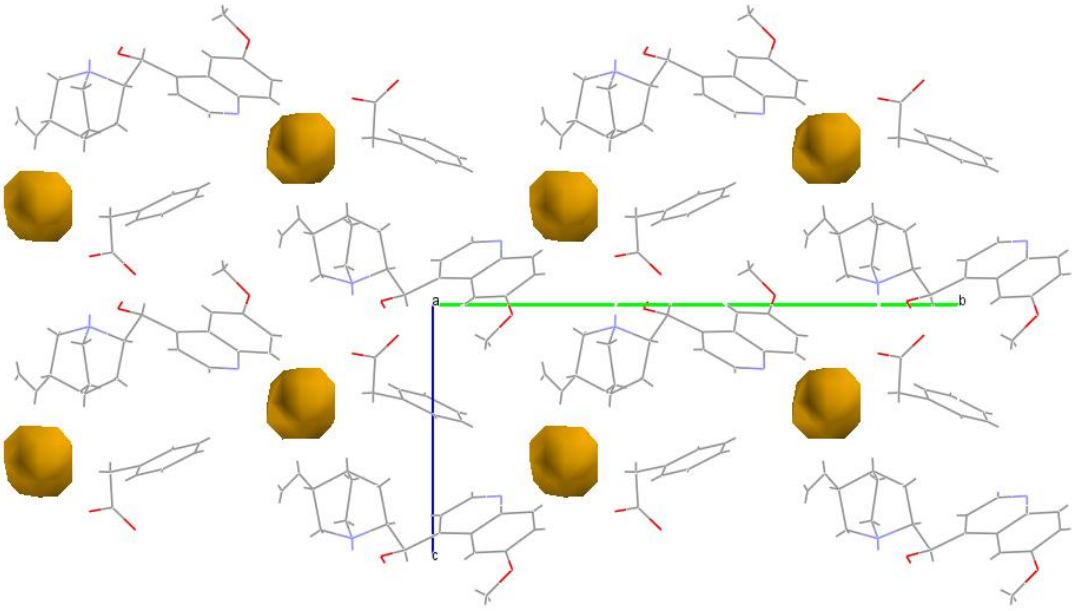

(b)

Figure 4.6.6: (a) Crystal packing of **(PAA^-)($QUID^+$)•H_2O**with hydrogen atoms removed down [100] **(b)** cavities in which water molecules are located down [100].

Hydrogen bonding in **$(PAA^-)(QUID^+)\bullet H_2O$** is shown in **Figure 4.6.7**. There are several hydrogen bonds in the structure due to the water molecule trapped in the crystal system. The protonated hydrogen atom (H10) attached to the nitrogen atom (N10) is involved in the hydrogen bonding. H10 is connected to O1 in the carboxylate group of PAA anion.

In the other hand, oxygen atom labeled O1 plays a role of a bifurcated acceptor. O1 is hydrogen bonded to the protonated hydrogen (H10) and to one of the hydrogen atom labeled H6B in the water molecule. H6A in the water molecule is connected to the nitrogen atom labeled N5 in QUID cation.

The oxygen atom labeled O2 in PAA is hydrogen bonded to the hydrogen atom (H5A) in QUID cation. Inspection of the lattice arrangement of the whole crystal structure interactions contains six graph sets: $D_1^1(2)$, $D_2^1(3)$, $D_2^2(5)$, $D_2^2(9)$, $C_2^2(9)$ and $D_2^2(10)$ that consolidate the hydrogen bonding. Hydrogen bonding parameters of the salt hydrate are listed in **Table 4.24**.

Table 4.24: $(PAA^-)(QUID^+)\bullet H_2O$ hydrogen bonding parameters.

COMPOUND	D-H···A	D···A (Å)	D-H (Å)	H···A (Å)	D-H···A (º)
$(PAA^-)(QUID^+)\bullet H_2O$	N10-H10···O1	2.682 (2)	0.912 (2)	1.776 (2)	172 (2)
	O5-H5A···O2 [a]	2.712 (2)	0.837 (2)	1.922 (2)	157 (2)
	O6-H6A···N5[b]	2.904 (2)	0.784 (4)	2.121 (4)	177 (3)
	O6-H6B···O1[c]	2.871 (2)	0.905 (3)	1.969 (3)	175 (2)

a = x+1, y, z ; b = -x+1, y-1/2, -z +1; c = x+1, y, z+1

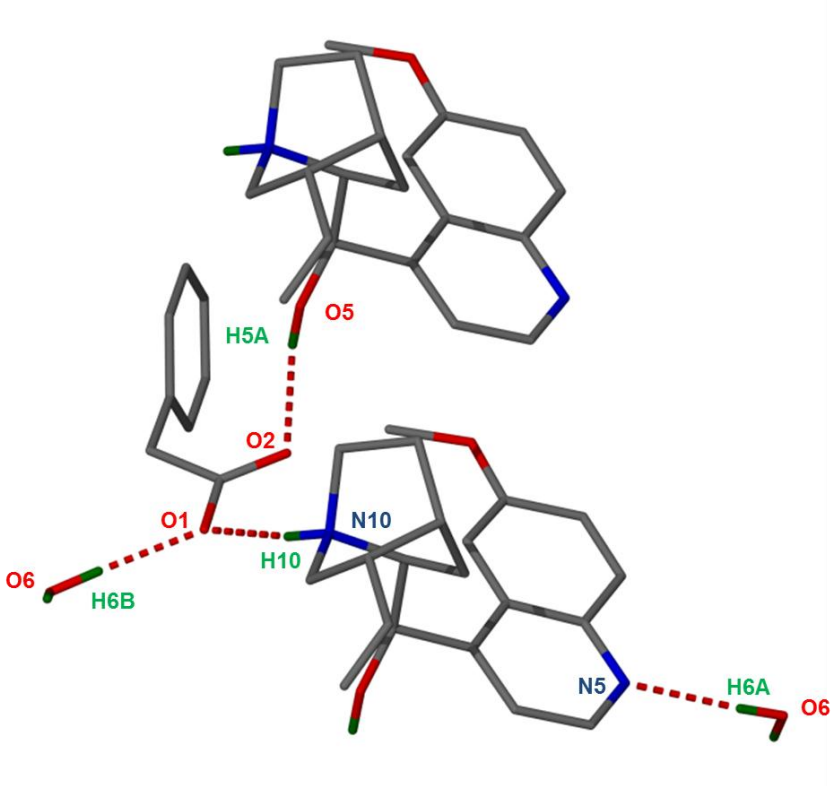

Figure 4.6.7: Hydrogen bonding in **$(PAA^{-})(QUID^{+})\bullet H_2O$**.

4.7 Phenyl acetic acid and quinine $(PAA^{-})(QUIN^{+})\bullet H_2O$

Quinine is the most commonly used anti-malarial drug. The optically active derivatives of (-)-quinine are used in asymmetric synthesis.[35] Quinine has been used as a resolving agent for acidic racemates through formation of diastereomeric salts.[36]

The salt hydrate was obtained by dissolving a 1: 1 ratio of PAA and quinine (QUIN) in acetone with slight heating on a hot plate. The solution was allowed to evaporate at ambient temperature and after two days block-like crystals were obtained. Similar crystals were also obtained when ethanol, methanol, isopropanol, tetrahydrofuran and ethyl methyl ketone were used as solvents.

The asymmetric unit of **$(PAA^-)(QUIN^+)•H_2O$** is illustrated in **Figure 4.7.1**.

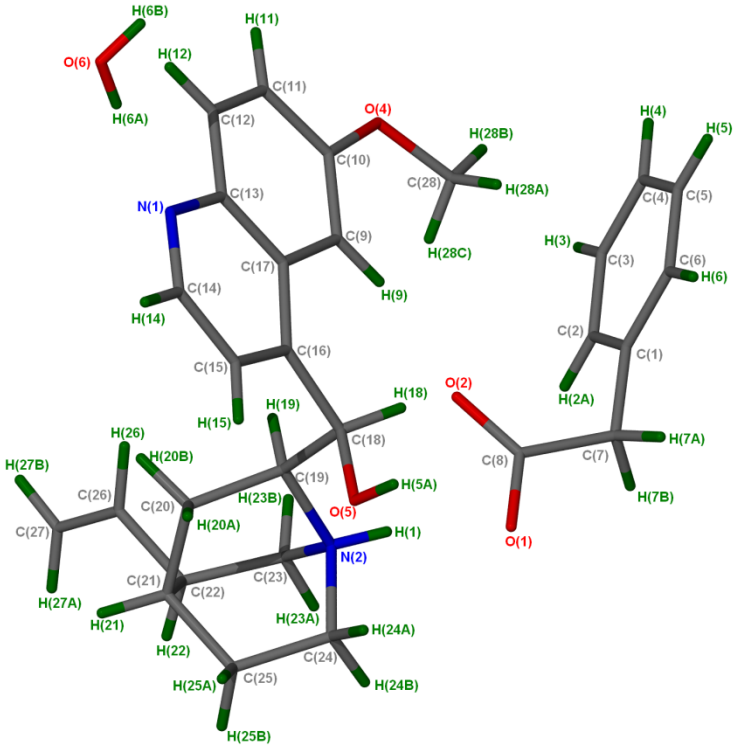

Figure 4.6.1: Asymmetric unit of **$(PAA^-)(QUIN^+)•H_2O$** with all the hydrogen atoms shown for numbering clarity.

4.7.1 Thermal Analysis

The **$(PAA^-)(QUIN^+)•H_2O$** thermal analysis data is listed in **Table 4.25**. A single mass loss of 3.0 % was observed in the TG curve and the DSC shows two endotherms at T_{on} = 357.0 K and T_{on} = 420.4 K. The first endotherm is the release of the water molecule. The second sharp endotherm is due to the melt of the salt. Thermal analysis curves of the starter materials and the salt hydrate are shown in **Figure 4.7.2**.

Table 4.25: Thermal analysis data of **$(PAA^-)(QUIN^+)•H_2O$**.

Compounds	PAA	**$(PAA^-)(QUIN^+)•H_2O$**	Quinine
DSC Endo$_1$ (T_{onset},K)	-	357.0	-
DSC Endo$_2$ (T_{onset},K)	351.8	420.4	449.8
TG calculated % mass loss	-	3.8	-
TG experimental % mass loss	-	3.0	-
PAA^-:$QUIN^+$:H_2O	-	1: 1: 1	

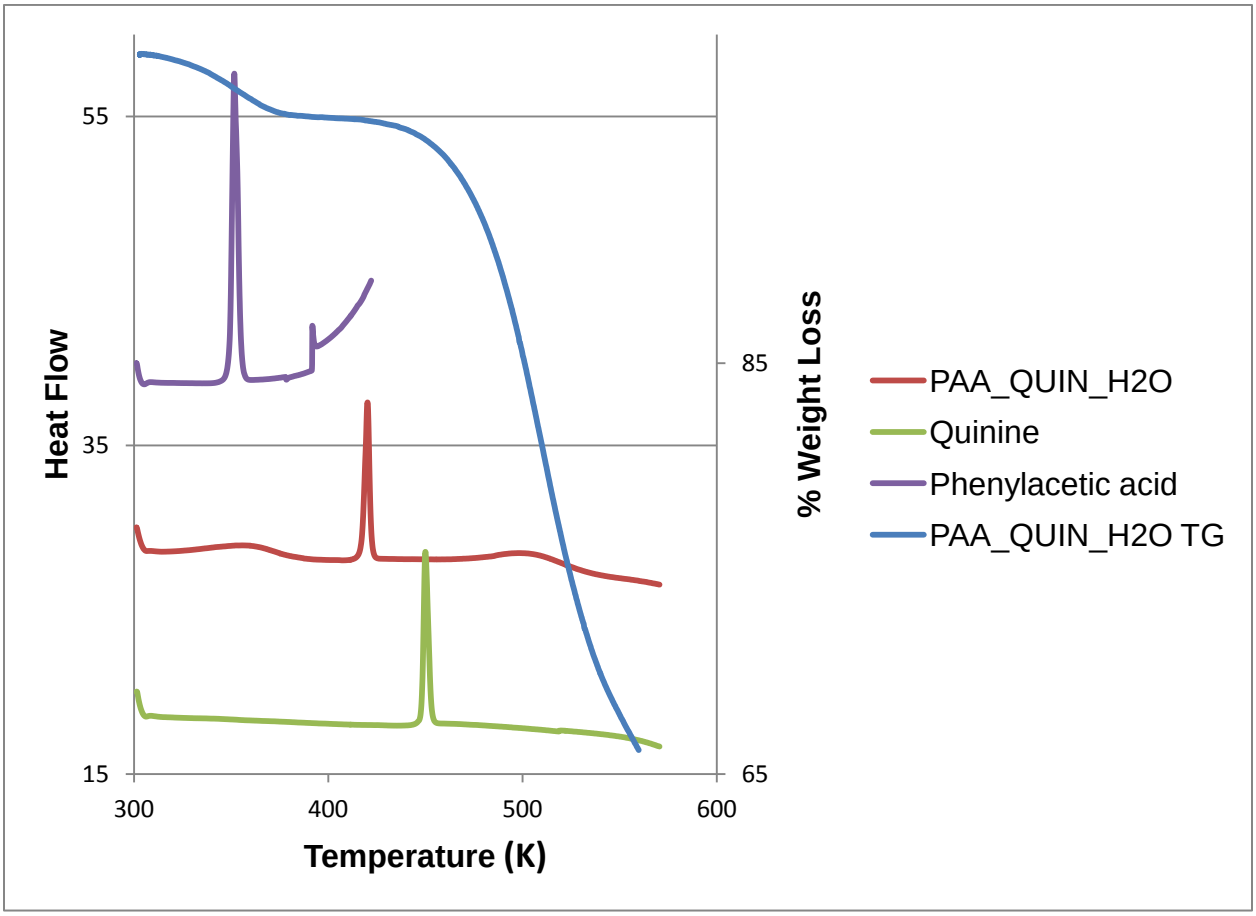

Figure 4.7.2: Thermal analysis curves of **$(PAA^-)(QUIN^+)•H_2O$** DSC (red)**,** TG (blue), quinine (green) and PAA (purple).

4.7.2 Hot Stage Microscopy

Hot stage microscopy of **$(PAA^-)(QUIN^+)\bullet H_2O$** was performed by immersing of a crystalline block in silicone oil at a temperature of 295 K. The release of water was observed at 350 K and the salt started melting at 418 K. A melt of the salt was obtained at 425 K. HSM photographs of **$(PAA^-)(QUIN^+)\bullet H_2O$** are illustrated in **Figure 4.7.3**.

(a) 295 K **(b) 350 K**

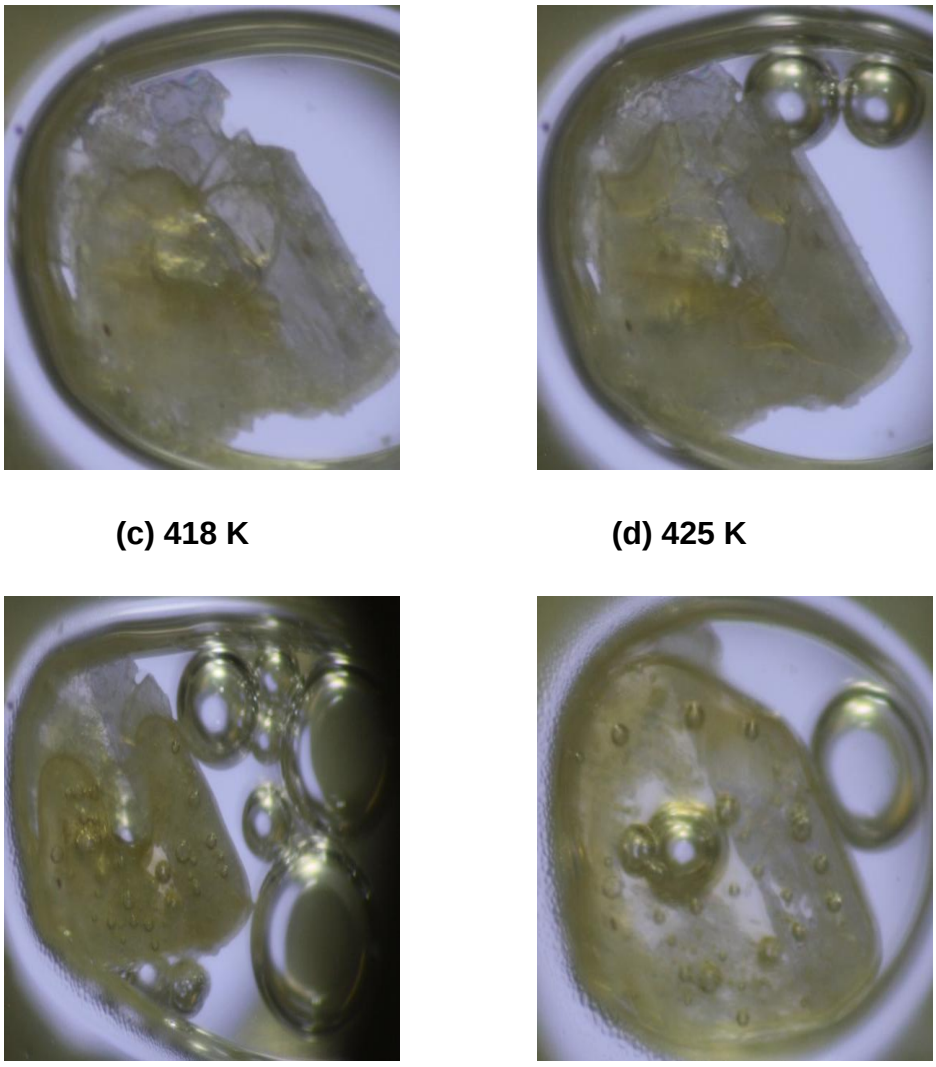

(c) 418 K **(d) 425 K**

Figure 4.7.3: HSM photography of **$(PAA^-)(QUIN^+)\bullet H_2O$**: **(a)** crystal immersed in silicone oil, **(b)** releasing of the water, **(c)** crystal starts melting and **(d)** melt of the crystal.

4.7.3 IR Spectroscopy

The **$(PAA^-)(QUIN^+)\bullet H_2O$** IR spectrum (**Figure 4.7.4**) has vibrational frequencies of both PAA and QUIN. IR results are given in **Table 4.26**. Similar to the **$(PAA^-)(QUID^+)\bullet H_2O$** structure, the **$(PAA^-)(QUIN^+)\bullet H_2O$** salt has a broad band at 1590 cm^{-1} which is in the region of the C=O stretching mode for salt formation.[26] Another broad band is observed at 3206 cm^{-1} which can be attributed to N-H stretching vibration. The band at 3455 cm^{-1} is attributed to the solvated water in the structure.

Table 4.26: IR positions and assignments of peaks in PAA, **$(PAA^-)(QUIN^+)\bullet H_2O$** and QUIN.

PAA	**$(PAA^-)(QUIN^+)\bullet H_2O$**	QUIN	Proposed assignment
3123	3455	3451, 3170	OH stretch
-	3206	-	N-H stretching mode
2750, 2620	2997, 2974, 2360	2936, 2360, 2342	C-C ring modes
1699	1663, 1590	-	C=O
-	1619	1624	C-N, C=O stretching mode combination
1498, 1454, 1407	1509, 1475,1446	1590, 1508, 1469, 1449	C=C stretch
-	1374	1400	C-N stretch, N-H bend
1290, 1243	1260	1260	C-O stretch

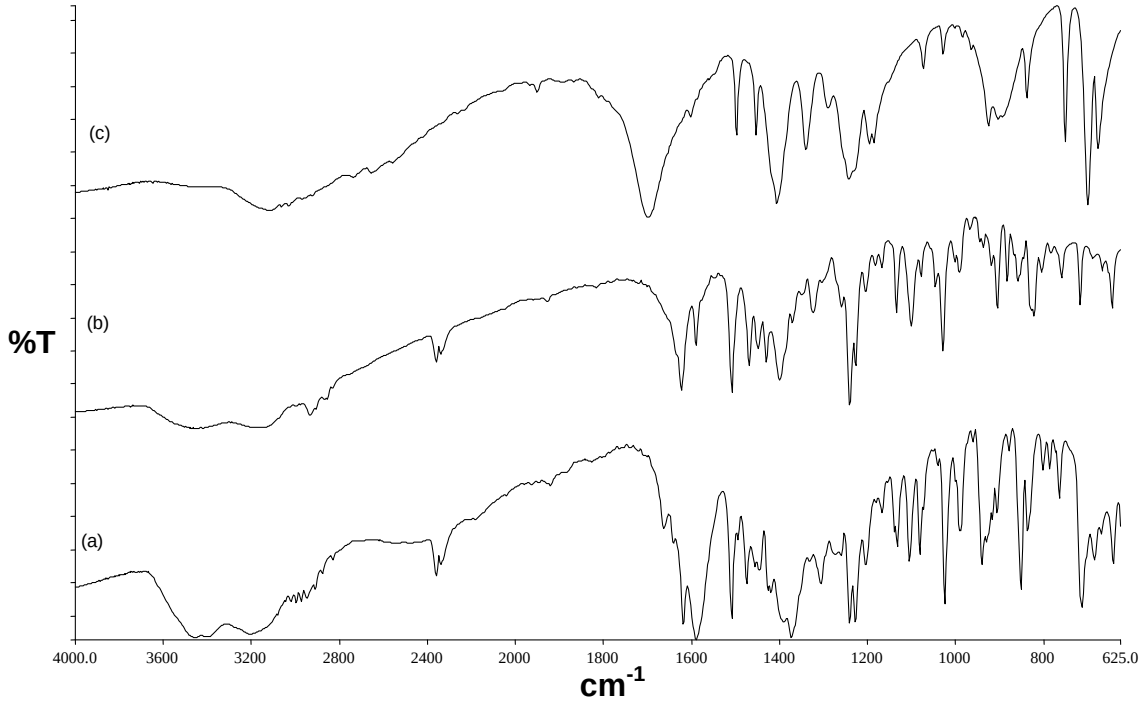

Figure 4.7.4: IR spectra (a) **$(PAA^-)(QUIN^+)\bullet H_2O$**, (b) QUIN and (c) PAA.

4.7.4 Powder X-ray Diffraction

The PXRD pattern of the slurry conversion performed in distilled water showed good agreement to that of the calculated PXRD pattern obtained from LAZYPULVERIX[16] as illustrated in **Figure 4.7.5**.

Experiments such as grinding and solvent drop grinding were not possible due to the formation of the paste when PAA and QUIN were ground together. The ground product could not be analyzed using powder X-ray diffraction.

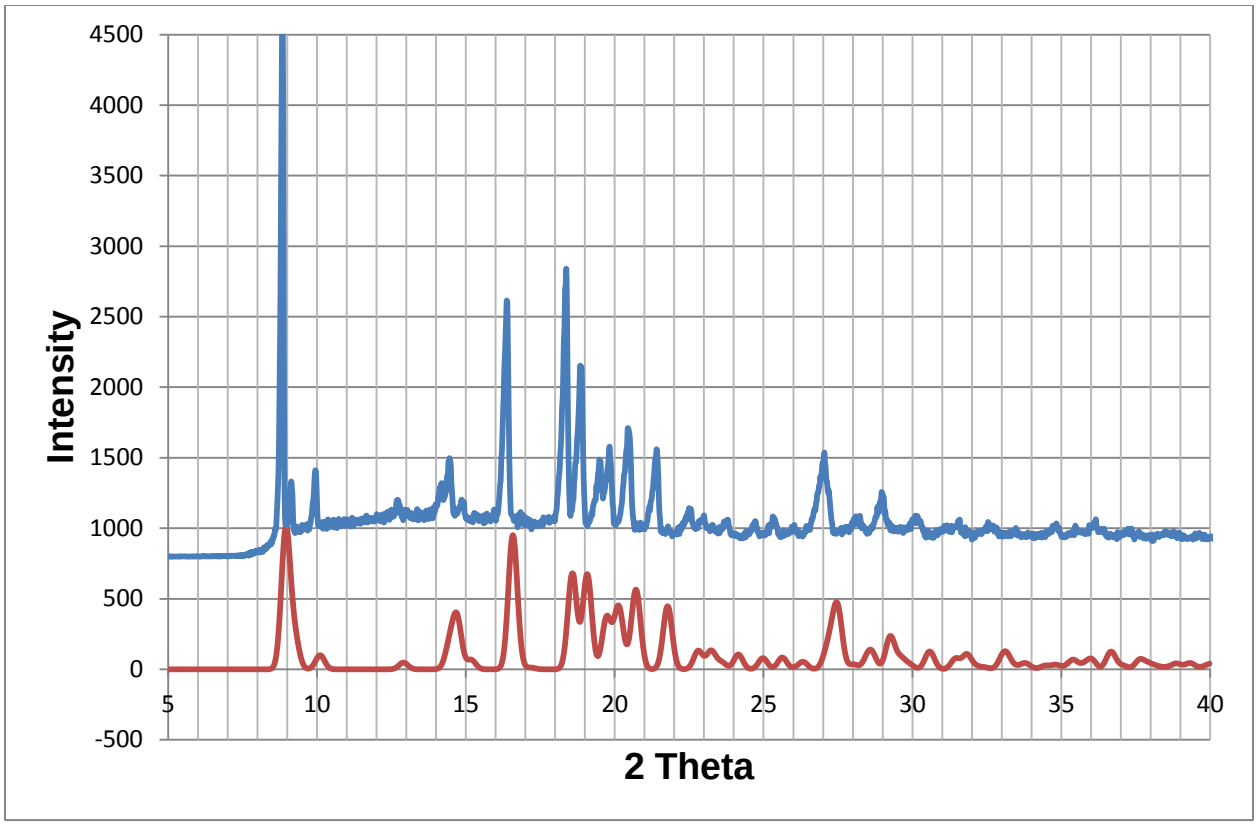

Figure 4.7.5: PXRD patterns of **$(PAA^{-})(QUIN^{+})\bullet H_2O$** (red) and slurry (blue).

4.7.5 Structure Determination

Direct methods yielded all PAA and QUIN non-hydrogen atoms which were refined anisotropically. The protonated hydrogen atom (H1) was located in the difference electron density map and has a N-H distance of 0.856 Å. The hydrogen atoms of the water molecule (H6A and H6B) were fixed in position with an O-H distance of 0.80 Å each. The structure refined successfully to R_1= 0.0395 with wR_2= 0.1024 ([I>2sigma (I)]). The crystal data is reported in **Table 4.27**.

Table 4.27: $(PAA^-)(QUIN^+)\bullet H_2O$ crystal data.

Compound	**$(PAA^-)(QUIN^+)\bullet H_2O$**
Structural Formula	$(C_8H_7O_2^-)(C_{20}H_{25}N_2O_2^+)\bullet H_2O$
PAA^-:$QUIN^+$:H_2O ratio	1: 1: 1
Molecular Mass (g mol^{-1})	478.59
Data collection temperature (K)	173(2)
Crystal system	Monoclinic
Space group	*$P2_1$*
a (Å)	6.5880 (13)
b (Å)	19.111 (4)
c (Å)	10.230 (2)
α (°)	90.00
β (°)	105.30 (3)
γ (°)	90.00
Volume ($Å^3$)	1242.3 (4)
Z	2
D_c, Calculated density (g cm^{-3})	1.279
Final R indices [I>2sigma(I)]	R_1= 0.0395
	wR_2 = 0.1024
R indices (all data)	R_1 = 0.0445
	wR_2 = 0.1064
Largest diff. peak and hole ($eÅ^{-3}$)	0.277; -0.188

$(PAA^-)(QUIN^+)\bullet H_2O$ crystallized in the monoclinic space group *$P2_1$* with Z = 2. The salt hydrate has a structural formula of $(C_8H_7O_2^-)(C_{20}H_{25}N_2O_2^+)\bullet H_2O$ and a ratio of 1: 1: 1. There is a proton transfer from the PAA to the QUIN molecule.

Four weak C-H•••π interactions were observed in the structure; the first and second C-H•••π interactions involves the PAA^- ring (C1 – C6) and C14 and C28 of the $QUIN^+$ cation: d (C14•••π (C1-C6)) = 3.095 Å, θ(C14-H14•••π(C1-C6)) = 141 º; d (C28•••π(C1-C6)) = 2.976 Å, θ(C28-H28B•••π(C1-C6)) = 112 °. The third and fourth C-H•••π

interactions have dimensions of : d(C14-H14•••π(C9 – C17)) = 3.351 Å, θ(C14-H14•••π(C9-C17) = 114 °and d(C24-H24B•••π(C9-C17)) = 3.053 Å, θ(C24-H24B•••π(C9-C17) = 118 ° respectively. The crystal packing shows that the carboxylate group of PAA face the QUIN molecule as illustrated in **Figure 4.7.6 (a)**.

The void volume (contact surface) occupied by the water molecules (**Figure 4.7.6 (b)**) was found to be 27.51 $Å^3$ with a unit cell percentage of 2.20 % and a probe radius of 1.0 Å and a grid spacing of 0.70 Å.

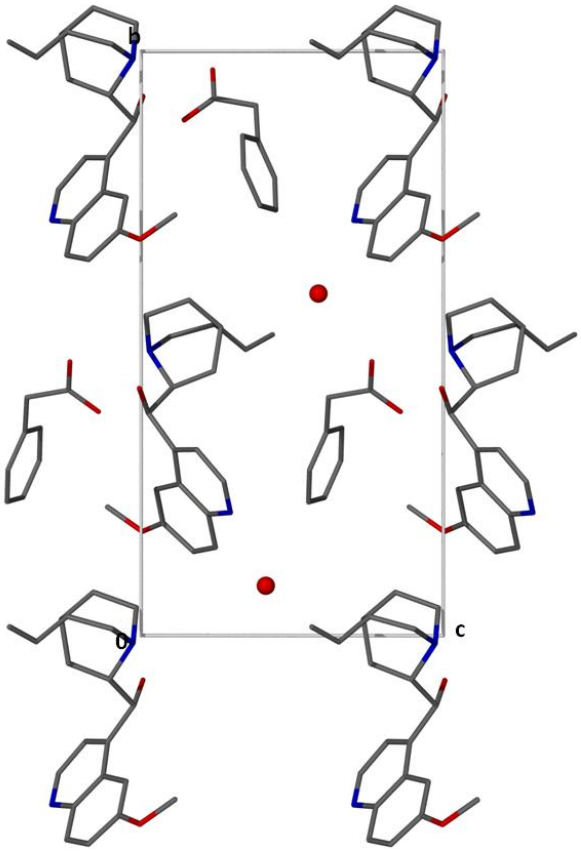

(a)

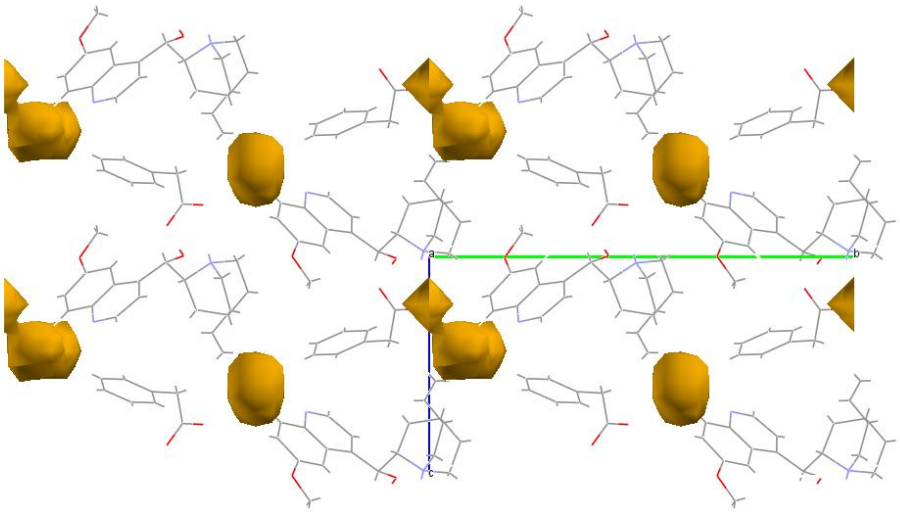

(b)

Figure 4.7.6: (a) crystal packing of **$(PAA^{-})(QUIN^{+})\bullet H_2O$** with hydrogen atoms removed down [100] and **(b)** cavities in which water molecules are located down [100].

The hydrogen bonding in **$(PAA^{-})(QUIN^{+})\bullet H_2O$** (**Figure 4.7.7**) is similar to that found in the **$(PAA^{-})(QUID^{+})\bullet H_2O$** crystal structure. The protonated hydrogen atom (H1) acts as a bifurcated donor, connecting two oxygen atoms (O1 and O2) in the PAA^{-} anion.

Both oxygen atoms labeled O1 and O2 act as bifurcated acceptors. O1 is hydrogen bonded to the protonated hydrogen (H1) and H6B in the water molecule. The oxygen atom labeled O2 is connected to H1 and H5A in the $QUIN^{+}$ cation.

In addition, the hydrogen (H6A) is hydrogen bonded to the nitrogen atom (N1) in the $QUIN^{+}$ cation. The graph sets for the **$(PAA^{-})(QUIN^{+})\bullet H_2O$** structure are the same as in **$(PAA^{-})(QUID^{+})\bullet H_2O$**. Hydrogen bond parameters of the salt hydrate are given in **Table 4.28**.

Table 4.28: $(PAA^{-})(QUIN^{+})\bullet H_2O$ hydrogen bonding parameters.

COMPOUND	D-H···A	D···A (Å)	D-H (Å)	H···A (Å)	D-H···A (º)
$(PAA^{-})(QUIN^{+})\bullet H_2O$	O5-H5A···O2[a]	2.679 (2)	0.875 (3)	1.852 (3)	157 (2)
	O6-H6A···N1	2.931 (2)	0.800 (1)	2.133 (1)	175 (3)
	O6-H6B···O1[b]	2.896 (2)	0.800 (1)	2.101 (1)	172 (3)
	N2-H1···O1	2.687 (2)	0.856 (2)	1.844 (2)	168 (2)

a = x-1, y, z ; b = -x+2, y-1/2, -z

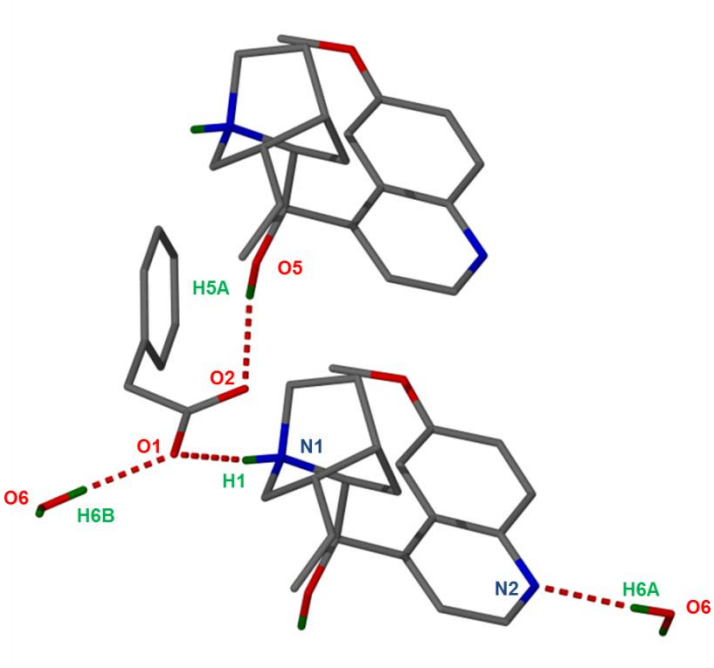

Figure 4.7.7: Hydrogen bonding in **$(PAA^{-})(QUIN^{+})\bullet H_2O$**.

4.8 Selectivity Experiments

This selectivity of PAA for a 50:50 mixture of QUIN: QUID was determined. Two ratios were set up, a 1: 1: 1 co-crystallization of PAA: QUIN: QUID and a 2: 1: 1 ratio of the same compounds. In this experiment, 50/50 (*v/v*) of hexane/acetone and 50/50 (*v/v*) hexane/ethyl methyl ketone were used as solvents.

In both experiments the PAA preferred to form a salt hydrate with QUIN instead of QUID. The crystals obtained were analyzed using DSC. Single x-ray diffraction was done on one suitable crystal and the same unit cells as **$(PAA^-)(QUIN^+)\cdot H_2O$** was obtained.

REFERENCES

1. Chaudhari. S. R & Suryaorakask. N. *J. Mol. Struct.* 2012, 1016, 163.
2. Odani. T & Matsumoto. A. *CrystEngComm.* 2002, 4, 467.
3. Arman. H. D, Kaulgud. T & Tiekink. E. R. T. *Acta. Crystallogr. Sect.E: Struct.Rep.Online*. 2010, 66, o2684.
4. Arman. H. D, Kaulgud. T & Tiekink. E. R. T. *Acta. Crystallogr. Sect.E: Struct.Rep.Online*. 2010, 66, o2629.
5. Sridhar. B & Ravikumar. K. *Acta. Crystallogr. Sect.C: Cryst. Struct. Comm.* 2007, 63, o415.
6. Dega-Szafran. Z, Jaskolski. M & Szafran. M. *J. Mol. Struct*. 2000, 555, 191.
7. Mak. T. C. W, Chen Xiaoming, Shi kailiang, Yao Jiaxing & Zheng Chaode. *J. Crystallogr. Spectrosc. Res*. 1986, 16, 639.
8. Allen. F.H. *Acta. Crystallogr*. 2002, B58, 380 - 388.
9. Brown. H. C, Baude. E. A & Nacho*d.* F. C. *Determination of Organic Structures by Physical Methods.* Academic Press, New York. 1955.
10. Dippy. J. F. J, Hughes. S. R.C & Rozanski. A. *J. Chem. Soc*. 1959, 2492 - 2498.
11. Huang. K. S, Britton. D, Etter. M. C & Byrn. S. R. *J. Mater. Chem*. 1997, 7, 713 - 720.
12. Stahl. P. H & Wermuth. C. G. *Handbook of Pharmaceutical Salts: Properties, Selection and Use. International Union of Pure and Applied Chemistry*, VHCA: Wiley-VCH: Weinheim, New York. 2002.
13. Smith. M, March. J & March. J. *March's advanced organic chemistry: reactions, mechanisms, and structure*, 5th ed.; J.Wiley: New York. 2001.
14. Bhogala. B. R, Basavoju. S & Nangia. A. *CrystEngComm*. 2005, 7, 551 - 562.
15. Brittain. H. G. *Cryst. Growth Des.* 2009, 9 (5), 2492 - 2499.
16. Yvon. K, Jeitschko. W & Parthe. E. *Appl. Crystallogr.* 1977, 10, 73 - 74.
17. Frišcˇic´. T & Jones. W. *Faraday. Discuss*. 2007, 136, 167 – 178.
18. Berry. D. J, Seaton. C. C, Clegg. W, Harrington. R. W, Coles. S. J, Horton. P. N, Hurst-House. M. B, Storey. R, Jones. W, Frišcˇic´. T & Blagden. N. *Cryst. Growth Des*. 2008, 8, 1697 – 1712.

19. Kacprzak. K & Gawroñski. J. *Synthesis*. 2001, 961 - 998.
20. Hoffmann. H. M. R & Frackenpohl. J. *Eur. J. Org. Chem*. 2004, 4293 - 4312.
21. Tian. S-K, Chen. Y, Hang. J, Tang. L & Deng. L. *Acc. Chem. Res.* 2004, 37, 621-631.
22. Marcelli. T, Van Maarseveen. J. H & Hiemstra. H. *Angew. Chem. Int. Ed.* 2006, 45, 7496 - 7504.
23. Connon. S. *J. Chem. Comm.* 2008, 2499 - 2510.
24. Cinchona Alkaloids in Synthesis and Catalysis, Ligands, immobilization and Organocatalysis; Song, C.E, Ed: Wiley-VCH: Weinheim, 2009.
25. Marcelli. T & Hiemstra. H. *Synthesis*. 2010, 1229 - 1279.
26. Adalder. T. K, Sankali. R & Dastidar. P. *Cryst. Growth Des*. 2012, 12, 2533.
27. Macrae. C. F, Eddington. P. R, McCabe. P, Pidcock. E, Shields. G. P, Taylor. R, Towler. M. & van de Streek. J. Mercury: visualization and analysis of crystal structures. *J. Appl. Crystallogr*. 2006, 39, 453 - 457.
28. Sikorski. A & Trzybiński. D. *Tetrahedron Letters.* 2013, 54, 1463 - 1466.
29. Gressel. P. D & Galleli. S. F. *J. Pharm*. Sci. 1968, 57, 335.
30. Ashida. T. HBLS-V. The Universal Crystallographic Computing System-Osaka. The Computation Center, Osaka. Univ. Japan. 1973.
31. Wahbi. A. M, Moneed. M. S, Hewala. I. I & Bahnasy. M. F. *Chem. Pharm. Bull*. 2008, 56, 787 - 79.
32. Kashino. S & Haisa. M. *Acta. Crystallogr.* 1983, C39, 310 - 312.
33. Pniewska. B & Suszko-Purzycka. A. *Acta. Crystallogr.* 1989, C45, 638 - 642.
34. Smith. R. A. *Exp. Opin. Pharmacother.* 2006, 7, 2581 - 2591.
35. Hubel. R, Polborn. K & Beck. W. *Eur. J. Inorg. Chem*. 1999, 471 - 482.
36. Gjerløv. A. B & Larsen. S. *Acta. Crystallogr. Sect.C.* 1997, C53, 1505 - 1508.

CHAPTER 5

4-HYDROXYPHENYL ACETIC ACID CO-CRYSTALS AND SALTS

A search of the Cambridge Structural Database (CSD, version 5.34, November 2012)[1] shows that 4-hydroxyphenyl acetic acid (HPAA) has formed a co-crystal with 4, 4-bipyridine.[2]

HPAA was used as the main compound in this chapter and formed a co-crystal with isonicotinamide (INM). HPAA formed salt hydrates with cinchonidine (CIND), quinidine (QUID) and quinine (QUIN) and has also formed a hybrid salt-co-crystal with acridine (ACRI).

The numbering system of HPAA is illustrated in **Figure 5.1**.

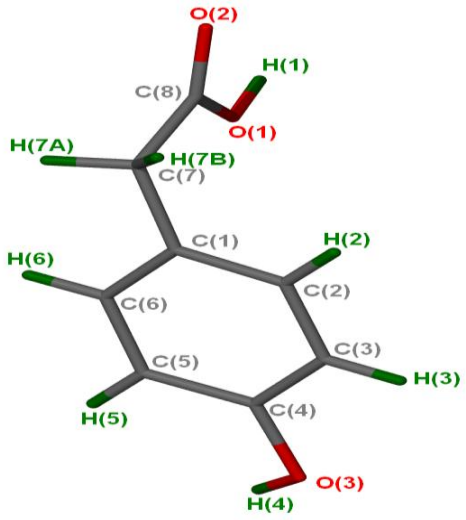

Figure 5.1: Atomic numbering of the HPAA molecule.

5.1 HPAA and Acridine ($HPAA^-$)($ACRI^+$)•HPAA•ACRI

The **($HPAA^-$)($ACRI^+$)•HPAA•ACRI** hybrid salt-co-crystal was obtained by dissolving both HPAA and acridine (ACRI) (1: 1 ratio) in diethyl ether with slight heating on a hot

plate. The solution was allowed to evaporate under ambient conditions and crystals were obtained after a few days. The resultant compound is interesting because the asymmetric unit contains one HPAA molecule, one ACRI molecule, one $HPAA^-$ anion and one $ACRI^+$ cation (**Figure 5.1.1**).

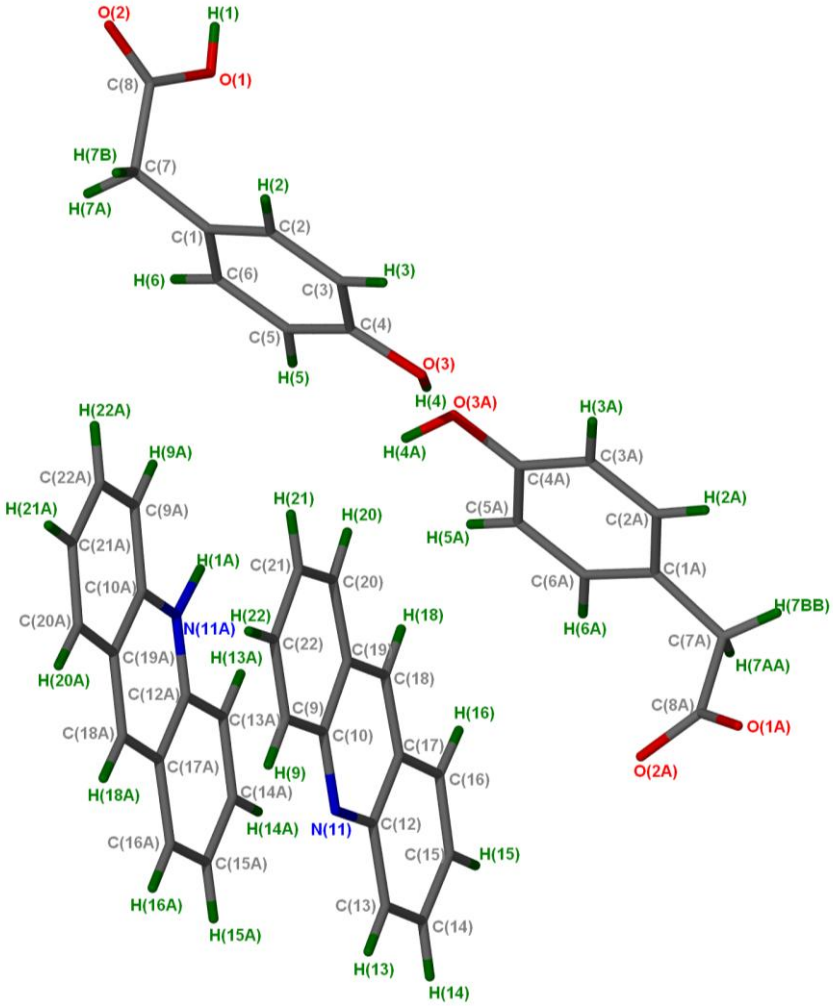

Figure 5.1.1: Atomic numbering of the asymmetric unit in **$(HPAA^-)(ACRI^+)$•HPAA•ACRI** with all the hydrogen atoms shown.

5.1.1 Thermal Analysis

The compound **(HPAA$^-$)(ACRI$^+$)•HPAA•ACRI** did not show an improvement in the thermal stability compared to the pure components. The melting point of **(HPAA$^-$)(ACRI$^+$)•HPAA•ACRI** was determined using DSC (**Figure 5.1.2**) as indicated in **Table 5.1**, which is lower than the starter materials.[3]

Table 5.1: Thermal analysis data for **(HPAA$^-$)(ACRI$^+$)•HPAA•ACRI**.

Compounds	**DSC Endo$_1$(T_{onset},K)**	**DSC Endo$_2$(T_{onset},K)**
Acridine	363.5	375.8
HPAA	-	425.1
(HPAA$^-$)(ACRI$^+$)•HPAA•ACRI	336.9	371.4

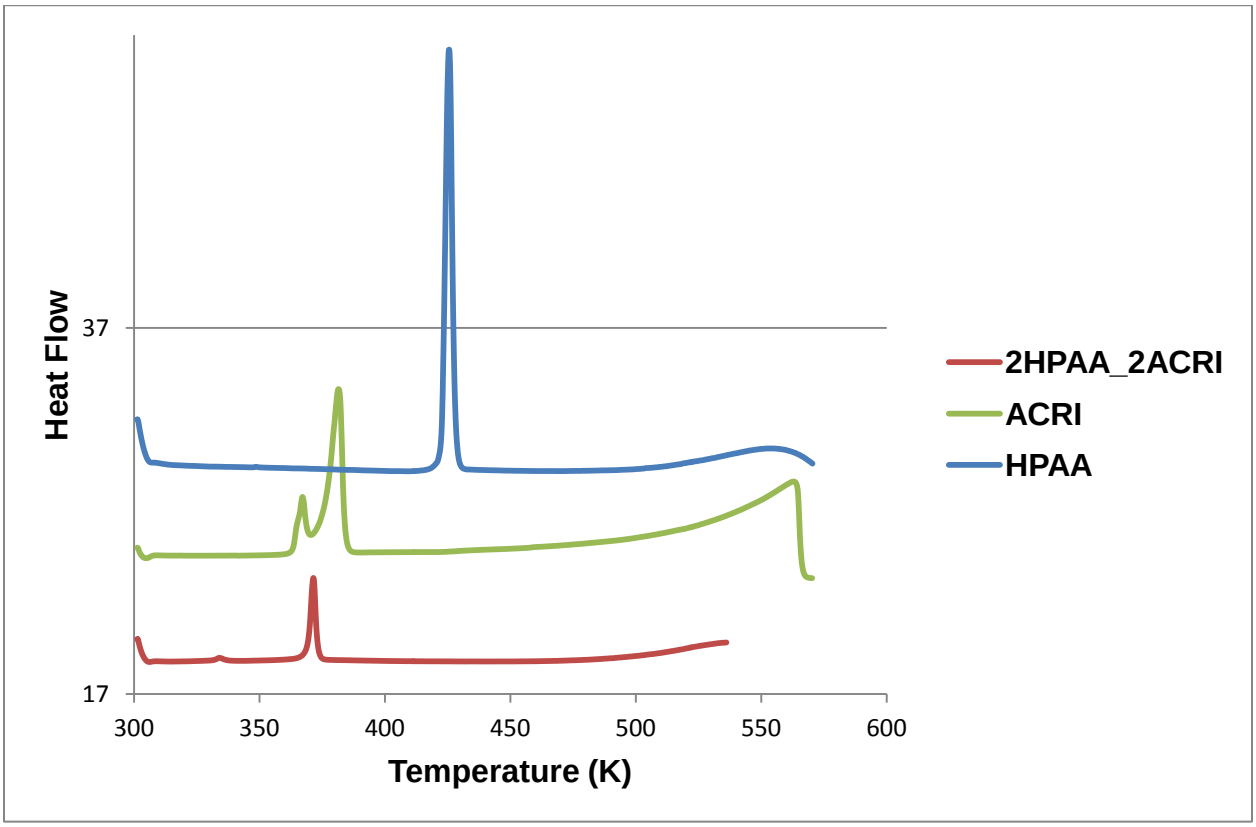

Figure 5.1.2: DSC curves of HPAA (blue), acridine (green) and **(HPAA$^-$)(ACRI$^+$)•HPAA•ACRI** (red).

5.1.2 IR Spectroscopy

The **(HPAA$^-$)(ACRI$^+$)•HPAA•ACRI** IR spectrum (**Figure 5.1.3**) contains peaks found in both starter materials. There is confirmation of co-crystal formation with the shift of the C=O frequency vibration at 1697 cm^{-1} (1711 cm^{-1} for HPAA) and an indication of salt formation with the presence of a new band at 1566 cm^{-1} in the crystal structure.[4] The broad band at 3280 cm^{-1} for the compound is assigned to the hydrogen bonding of the OH group. The IR results are shown in **Table 5.2**.

Table 5.2: IR positions and assignments for the peaks in HPAA, **(HPAA$^-$)(ACRI$^+$)•HPAA•ACRI** and ACRI.

HPAA	**(HPAA$^-$)(ACRI$^+$)•HPAA•ACRI**	ACRI	Proposed assignment
3243	3280	-	OH stretch
2707, 2616	2987	3051	Aromatic ring stretch
1965, 1905	1938	2285, 1815	Overtone or combination bands
1711, 1618, 1600	1697, 1566	-	C=O
1519, 1446, 1414	1517,1480	1617,1461, 1437	C=C stretch
1210	1246	-	C-O stretch

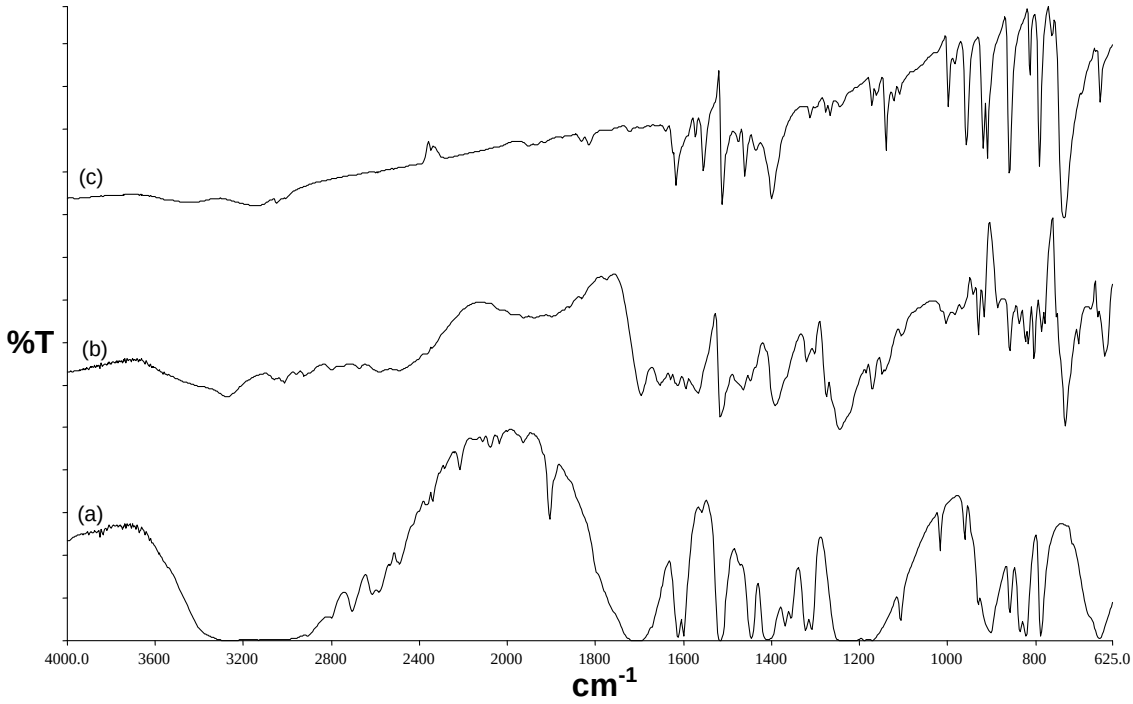

Figure 5.1.3: IR spectra (a) HPAA, (b) **(HPAA$^-$)(ACRI$^+$)•HPAA•ACRI** and (c) ACRI.

5.1.3 Powder X-ray Diffraction

There is good agreement between the ground product at 30 min and the calculated PXRD pattern obtained from LAZYPULVERIX[5] as illustrated in **Figure 5.1.4**. However, the peak at around 10.83 (2θ) in the calculated pattern has a very low height compare to the peak at approximately 10.89 (2θ) in the ground pattern.

The slurry conversion performed in diethyl ether did not entirely match the PULVERIX trace due to the fact that the first peak at around 7.65 (2θ) in the calculated pattern is missing in the slurry conversion.

The peak at approximately 10 (2θ) has high intensity in the slurry (and ground product and physical mixture) but a very low intensity in the PULVERIX. This maybe a formation of a new compound or the reaction was not completed in the slurry conversion. None of the performed experiments were similar to the physical mixture pattern.

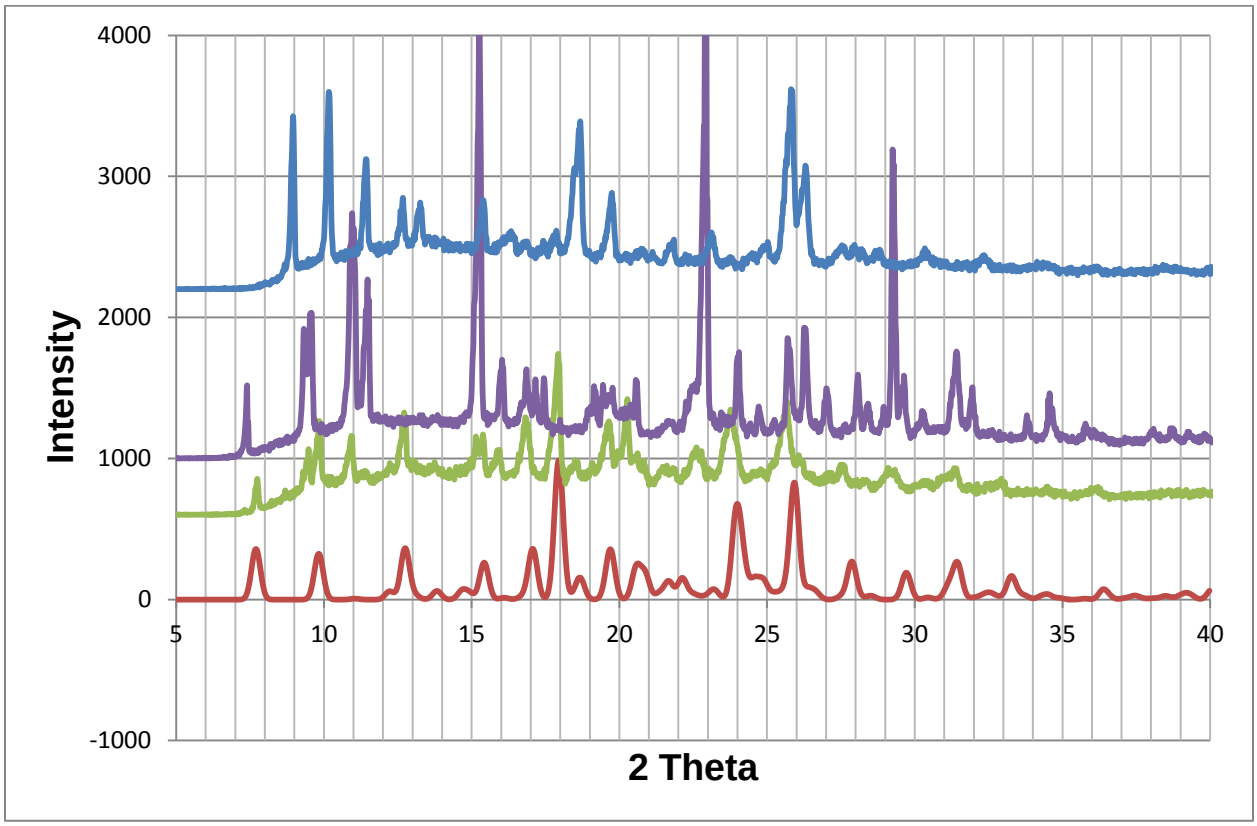

Figure 5.1.4: PXRD patterns of **(HPAA$^-$)(ACRI$^+$)•HPAA•ACRI** (red), ground product (green), physical mixture (purple) and slurry (blue).

5.1.4 Structure Determination

Direct methods yielded the positions of all non-hydrogen atoms. The hydroxyl hydrogen in HPAA and the hydrogen bonded to the nitrogen in the ACRI$^+$ cation were located in the difference electron density map. The nitrogen atoms of the acridine cation and molecule were identified by the highest peak magnitude in the aromatic rings. The crystal data of **(HPAA$^-$)(ACRI$^+$)•HPAA•ACRI** is given in **Table 5.3**.

Table 5.3: $(HPAA^-)(ACRI^+)$•HPAA•ACRI crystal data.

Compound	**$(HPAA^-)(ACRI^+)$•HPAA•ACRI**
Structural Formula	$(C_8H_7O_3^-)(C_{13}H_{10}N^+)$•$C_8H_8O_3$ •$C_{13}H_9N$
HPAA: ACRI: $HPAA^-$: $ACRI^+$ ratio	1:1:1:1
Molecular Mass (g mol^{-1})	662.74
Data collection temperature (K)	173(2)
Crystal system	Triclinic
Space group	*P 1*
a (Å)	8.0188(16)
b (Å)	9.0116 (18)
c (Å)	11.511 (2)
α (°)	87.52 (3)
β (°)	86.68 (3)
γ (°)	88.95 (3)
Volume ($Å^3$)	829.6 (3)
Z	1
D_c, Calculated density (g cm^{-3})	1.326
Final R indices [I>2sigma(I)]	R_1= 0.0405
	wR_2 = 0.0938
R indices (all data)	R_1 = 0.0630
	wR_2 = 0.1257
Largest diff. peak and hole ($eÅ^{-3}$)	0.213; -0.354

The hybrid salt-co-crystal was found to belong to the triclinic crystal system, space group *P 1* which was confirmed by the successful refinement of the structure. The asymmetric unit has two molecules of each component all in general positions. The programme PLATON/ADDSYM[6] suggested a centre of symmetry relating two ACRI molecules and two HPAA molecules. However the structure could not be solved in P-1, attempts at solving the structure in P-1 resulted in an R-factor of 0.30. The ADDSYM

program does not take into account the hydrogen atoms thus do not distinguish the co-crystal from the salt. The structure solved in P1 with good thermal parameters. The structure refined successfully to R_1 = 0.0405 with wR_2 = 0.0935 ([I>2sigma (I)]).

Closer inspection of the structure showed that a pseudo centre of symmetry relates the neutral ACR and the ACR^+ cation as well as the neutral HPAA and the $HPAA^-$ anion. The packing diagram of **$(HPAA^-)(ACRI^+)$•HPAA•ACRI** is shown in **Figure 5.1.5** with Z = 1. The structure is stabilized by face-to-face π-π stacking interactions between a neutral ACRI molecule and an ACRI cation with a minimum distance of 3.723 Å.

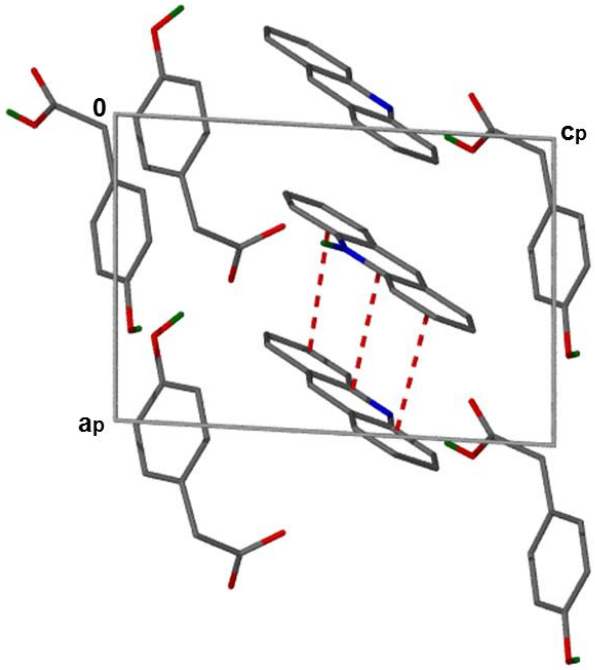

Figure 5.1.5: Packing diagram of **$(HPAA^-)(ACRI^+)$•HPAA•ACRI** along [010].

The oxygen atom labeled O1A of the $HPAA^-$ anion is a bifurcated acceptor. O1A is hydrogen bonded to the hydroxyl group of a second $HPAA^-$ anion.

The neutral HPAA is hydrogen bonded to the nitrogen atom of the neutral ACRI molecule via (HPAA) O1-H1•••N11 (ACRI) with an O•••O distance of 2.697 (4) Å and an O-H•••N angle of 163 (4) º.

In addition, the protonated nitrogen ($^{+}$N11-H1A) is bonded to O2A as shown in **Figure 5.1.6**. The graph sets of the structure are: $D_1^1(2)$, $C_1^1(9)$, $D_2^1(3)$, $D_2^2(10)$, $D_2^2(12)$, $D_3^3(12)$ and $D_3^3(14)$. The hydrogen bonding parameters are given in **Table 5.4**.

Table 5.4: (HPAA^{-})(ACRI^{+})•HPAA•ACRI hydrogen bonding parameters.

COMPOUND	D-H···A	D···A (Å)	D-H (Å)	H···A (Å)	D-H···A (º)
(HPAA^{-})(ACRI^{+})•HPAA•ACRI	O3A-H4A···O1A[a]	2.528 (4)	0.935 (6)	1.600 (6)	171 (5)
	O3-H4···O3A	2.769 (3)	0.918 (4)	1.859 (4)	171 (4)
	O1-H1···N11 [b]	2.697 (4)	0.776 (5)	1.944 (5)	163 (4)
	N11A-H1A···O2A [a]	2.603 (4)	0.861 (2)	1.745 (6)	175 (4)

a = x-1, y, z ; b = x-1, y, z-1

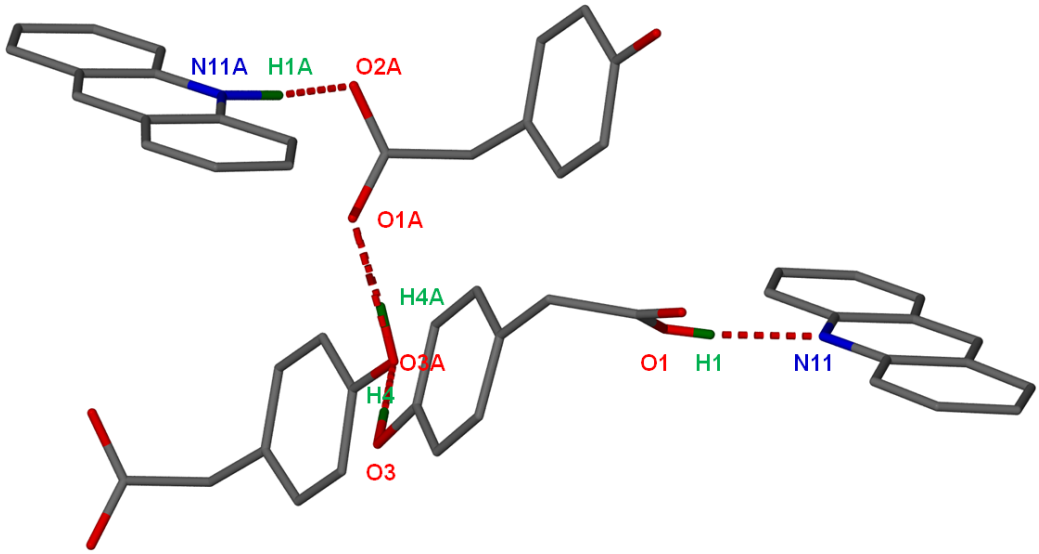

Figure 5.1.6: Hydrogen bonding in **(HPAA^{-})(ACRI^{+})•HPAA•ACRI**.

5.2 HPAA and cinchonidine (HPAA^{-})(CIND^{+})(0.5H_2O)

The hemi hydrate salt was obtained by dissolving a 1: 1 ratio of HPAA and cinchonidine (CIND) in ethyl methyl ketone with slight heating on a hot plate. The solution was

allowed to evaporate at ambient temperature and needle-like crystals were obtained. In this crystal structure a hydrogen atom is transferred from the HPAA to the CIND. Thus the asymmetric unit contains one $HPAA^-$ anion, one $CIND^+$ cation and one half of a water molecule. The asymmetric unit of **$(HPAA^-)(CIND^+)(0.5H_2O)$** is represented in **Figure 5.2.1**.

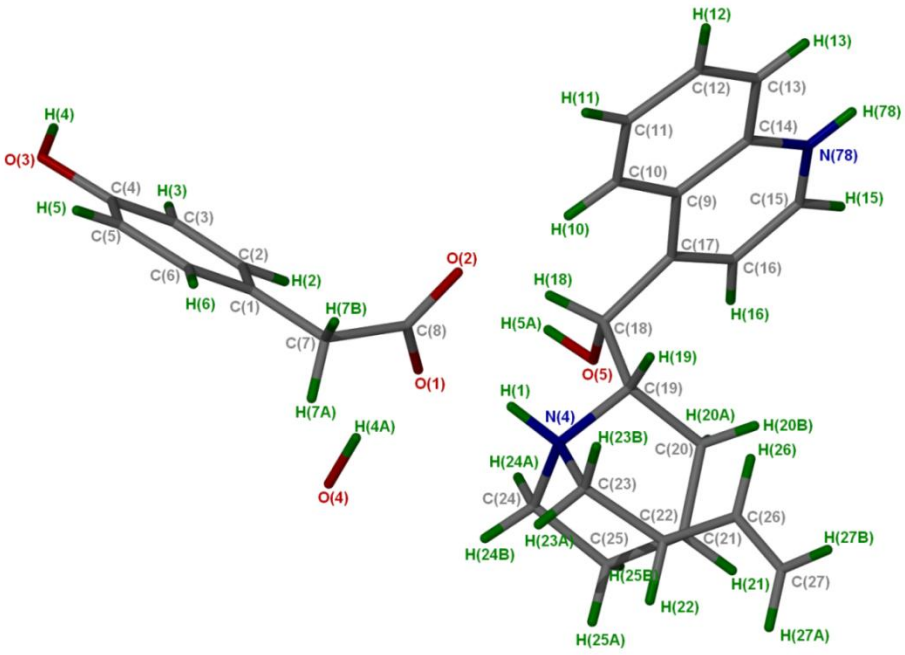

Figure 5.2.1: Asymmetric unit of **$(HPAA^-)(CIND^+)(0.5H_2O)$** structure with all the hydrogen atoms shown for numbering clarity.

5.2.1 Thermal analysis

The TG experimental percentage mass loss was in good agreement with the calculated percentage mass loss as given in **Table 5.5**. The first broad DSC endotherm is due to the loss of a water molecule and the second endotherm corresponds to the dissolution of the salt. Thermal analysis curves are shown in **Figure 5.2.2**.

Table 5.5: Thermal analysis data of **$(HPAA^-)(CIND^+)(0.5H_2O)$**.

Compound	**$(HPAA^-)(CIND^+)(0.5H_2O)$**
$HPAA^-$: $CIND^+$: H_2O	1: 1: 0.5
TG calculated % mass loss	1.5
TG experimental % mass loss	1.5
DSC $Endo_1$ (T_{onset}, K)	359.8 (broad)
DSC $Endo_2$ (T_{onset}, K)	443.0

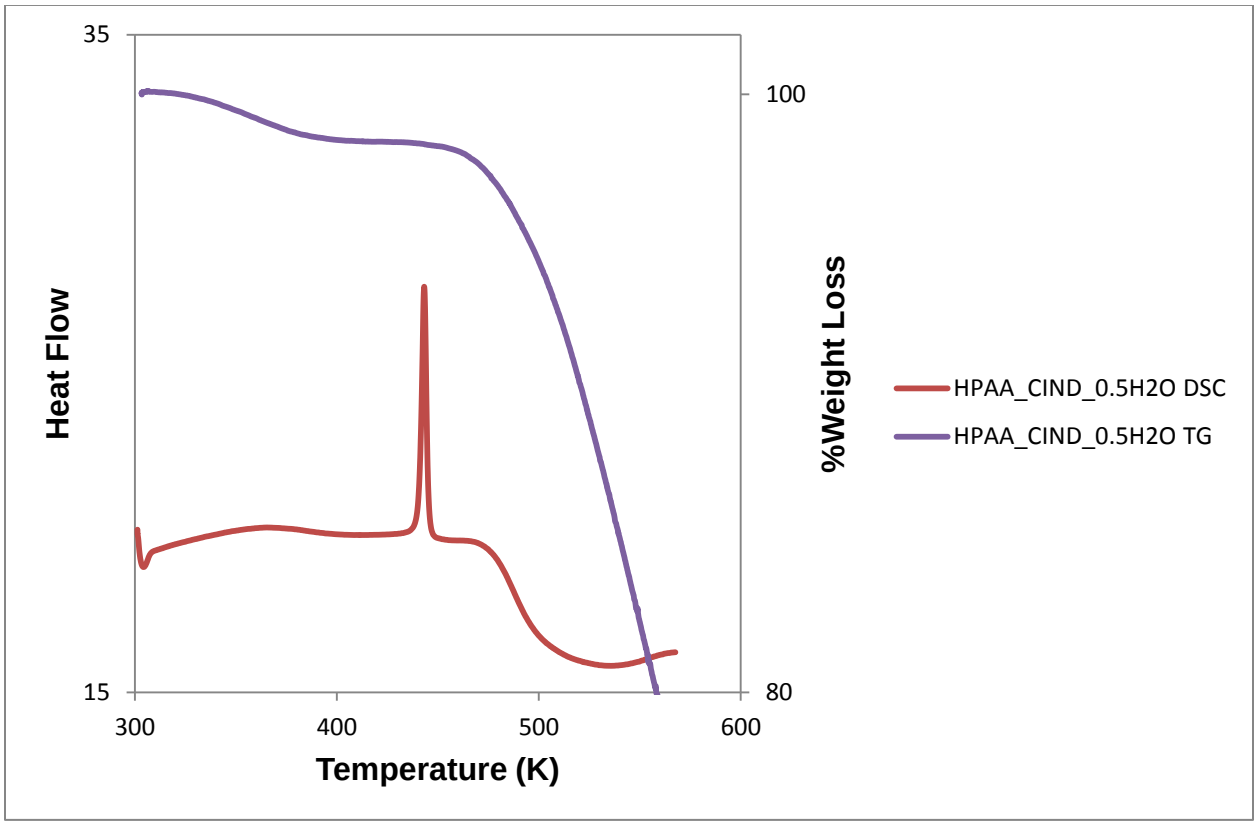

Figure 5.2.2: Thermal analysis curves of **$(HPAA^-)(CIND^+)(0.5H_2O)$** DSC (red) and TG (purple).

5.2.2 IR Spectroscopy

The IR spectra of the hemi hydrate salt and the starting materials are shown in **Figure 5.2.3**. The spectrum of **(HPAA$^-$)(CIND$^+$)(0.5H$_2$O)** is different from the pure components. The new band at 1640 cm^{-1} indicates salt formation according to Adalder *et al*.[4] The new band illustrates a proton transfer and is within the expected range of 1550 to 1650 cm^{-1}. The band at 3399 cm^{-1} is attributed to the OH group involved in hydrogen bonding.

Table 5.6: IR positions and assignments for the peaks in HPAA, **(HPAA$^-$)(CIND$^+$)(0.5H$_2$O)** and CIND.

HPAA	**(HPAA$^-$)(CIND$^+$)(0.5H$_2$O)**	CIND	Proposed assignment
3243	3399	3396	OH stretch
2707, 2616	2948	3072, 3003, 2939, 2866, 2720	C=C and C-H Stretching mode
1965, 1905	-	1941	Overtone or combination bands
1711, 1618, 1600	1667, 1640	-	C=O
1519, 1446, 1414	1537 , 1454, 1448	1636, 1618,1590, 1567, 1508	C=C stretch
1210	1237	-	C-O stretch

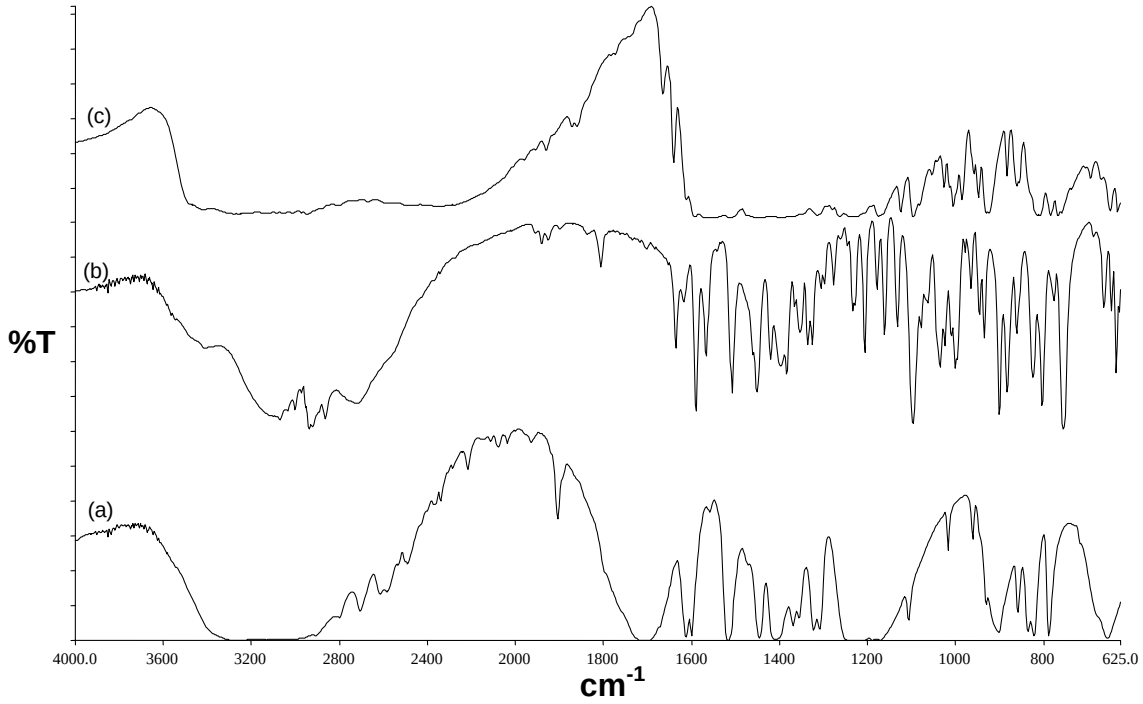

Figure 5.2.3: IR spectrums (a) HPAA, (b) CIND and (c) **(HPAA$^-$)(CIND$^+$)(0.5H_2O)**.

5.2.3 Powder X-ray Diffraction

The PXRD pattern of the ground product at 30 min matched that of the physical mixture, thus indicating no reaction.

Drops of water were added to the ground product and ground for 15 min as shown in **Figure 5.2.4**. The PXRD patterns of the liquid assisted ground product and that from the slurry conversion performed in distilled water were an excellent match with the calculated pattern obtained from LAZYPULVERIX.[5]

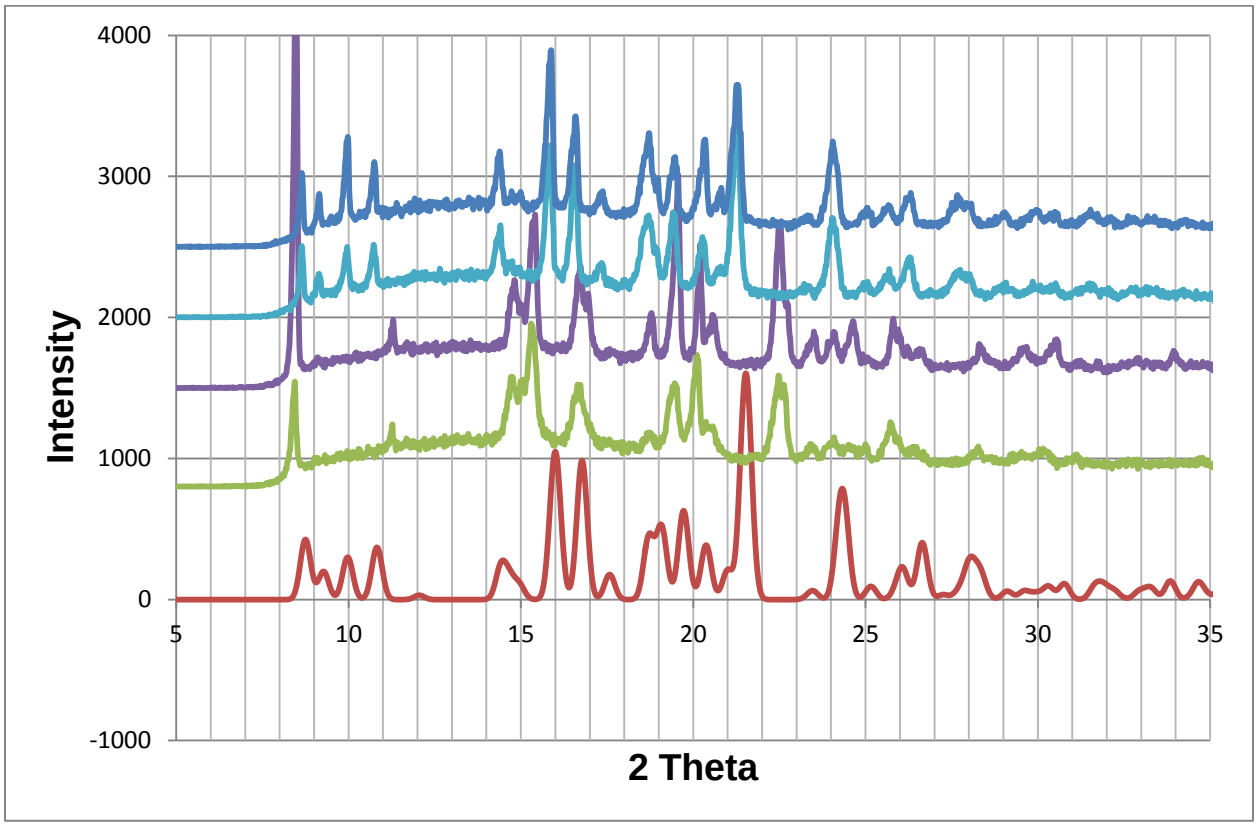

Figure 5.2.4: PXRD patterns of **(HPAA$^-$)(CIND$^+$)(0.5H$_2$O)** (red), ground product (green), physical mixture (purple), assistance liquid ground product (sky blue) and slurry (blue).

5.2.4 Structure Determination

Non-hydrogen atoms were modeled anisotropically. The hydrogen atoms of the hydroxyl ion and the hydrogen atoms attached to the nitrogen in CIND$^+$ were located in the difference electron density map, therefore their positional parameters refined freely. The water molecule sits on a two-fold axis at (0, y, 0). Only one hydrogen atom attached to the water molecule in general position is found and the oxygen atom has the occupancy 0.5 by virtue of its special position. The crystal data of **(HPAA$^-$)(CIND$^+$)(0.5H$_2$O)** is given on **Table 5.7**.

Table 5.7: Crystal data of **$(HPAA^-)(CIND^+)(0.5H_2O)$**.

Compound	**$(HPAA^-)(CIND^+)(0.5H_2O)$**
Structural Formula	$(C_8H_7O_3^-)(C_{19}H_{23}N_2O^+)\ 0.5(H_2O)$
$HPAA^-$: $CIND^+$: H_2O ratio	1: 1: 0.5
Molecular Mass (g mol^{-1})	455.54
Data collection temperature (K)	173 (2)
Crystal system	Monoclinic
Space group	*C2*
a (Å)	20.500 (4)
b (Å)	6.3585 (13)
c (Å)	19.061 (4)
α (°)	90.00
β (°)	111.60 (3)
γ (°)	90.00
Volume ($Å^3$)	2310.0 (8)
Z	4
D_c, Calculated density (g cm^{-3})	1.311
Final R indices [I>2sigma(I)]	R_1= 0.0452
	wR_2 = 0.0946
R indices (all data)	R_1 = 0.0695
	wR_2 = 0.1058
Largest diff. peak and hole ($eÅ^{-3}$)	0.188; -0.213

$(HPAA^-)(CIND^+)(0.5H_2O)$ crystallized in a monoclinic crystal system with *C2* as space group. The asymmetric unit contains one HPAA anion, one CIND cation and half water molecule. The crystal used for data collection has size dimensions of 0.05 x 0.06 x 0.52 mm with Z = 4. One of the hydrogen in the carboxylic group on the HPAA is transferred to the nitrogen atom in the CIND cation. The crystal packing of the salt hydrate along [010] direction is illustrated in **Figure 5.2.5 (a)**.

Figure 5.2.5 (b) shows the cavities in which water molecules are located down [010] with a void volume of 18.70 $Å^3$ and a unit cell volume percentage of 0.80 % using Mercury[7] software at a probe of 1.40 Å and a grid spacing of 0.70 Å.

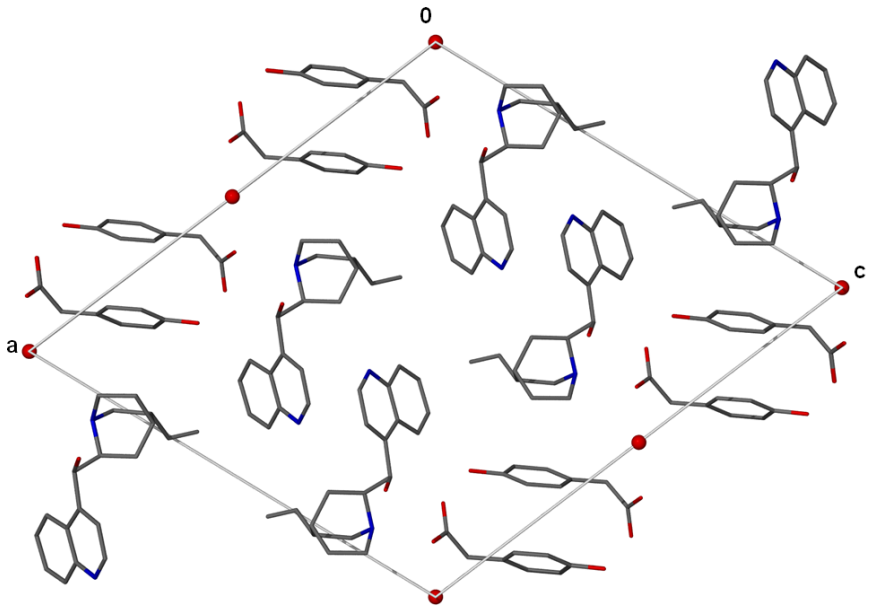

(a)

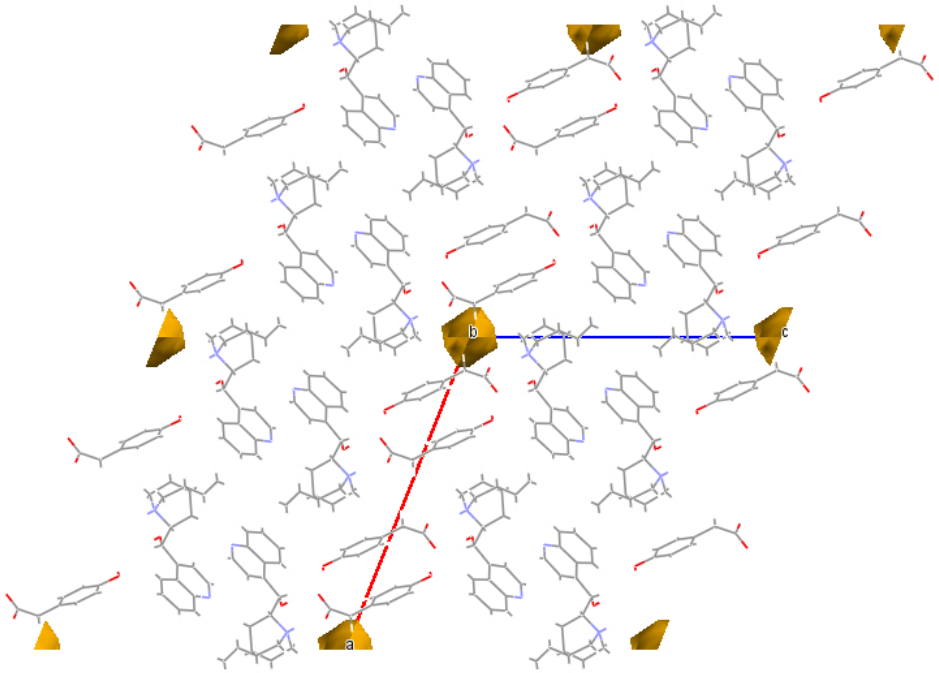

(b)

Figure 5.2.5: (a) Packing diagram of **(HPAA$^-$)(CIND$^+$)(0.5H$_2$O)** with hydrogen atoms removed view down [010] **(b)** Cavities in which water molecules are located down [010].

Both oxygen atoms on the carboxylate group play the role of a bifurcated acceptor. O1 is hydrogen bonded to H1 the protonated hydrogen on the nitrogen atom (N4) and H4A from the water molecule. O2 is connected to H4 the hydroxyl group on the HPAA anion and H5A the hydroxyl group on the CIND cation as shown in **Figure 5.2.6**.

There are two chain motifs found in the structure and characterized as $C_1^1(9)$ and $C_2^2(9)$. The crystal structure also has D motifs distinguish as $D_1^1(2)$, $D_2^1(3)$, $D_2^2(5)$, $D_3^2(12)$ and $D_3^3(14)$.

Hydrogen bonding details of **(HPAA$^-$)(CIND$^+$)(0.5H$_2$O)** are given in **Table 5.8**.

Table 5.8: hydrogen bonding parameters in **(HPAA$^-$)(CIND$^+$)(0.5H$_2$O)**.

COMPOUND	D-H···A	D···A (Å)	D-H (Å)	H···A (Å)	D-H···A (º)
(HPAA$^-$)(CIND$^+$)(0.5H$_2$O)	N4-H1···O1	2.633 (2)	0.900 (2)	1.754 (1)	164 (2)
	O5-H5A···O2[a]	2.770 (3)	0.908 (3)	1.907 (3)	158 (3)
	O3-H4···O2 [b]	2.627 (3)	0.900 (2)	1.769 (3)	158 (2)
	O4-H4AA···O1	2.794 (2)	1.043 (4)	1.760 (4)	170 (3)

a = x, y-1, z ; b = -x+3/2, y-1/2, -z + 2

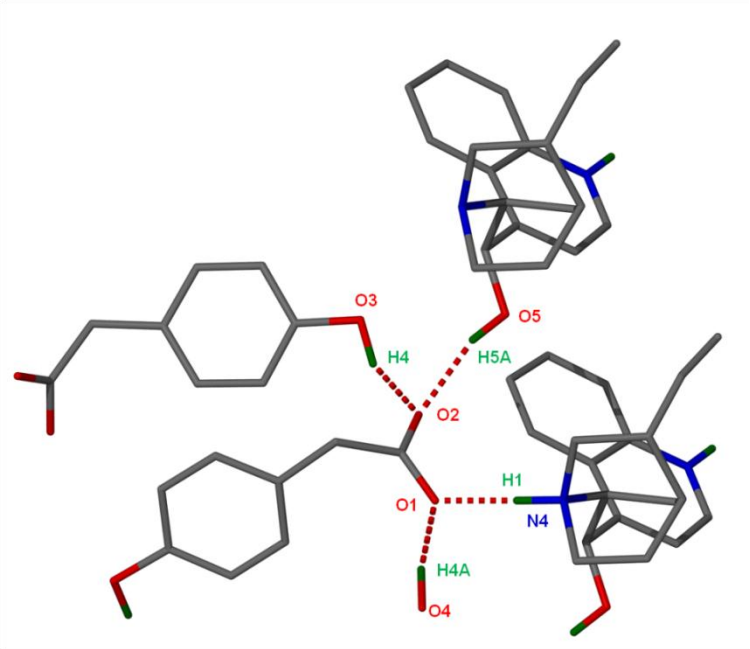

Figure 5.2.6: Hydrogen bonding in **(HPAA$^-$)(CIND$^+$)(0.5H$_2$O)**.

5.3 HPAA, cinchonidine and isopropanol (HPAA$^-$)(CIND$^+$)•IPA•H$_2$O

A 1:1 ratio of HPAA and CIND was dissolved in isopropanol by gentle heating on a hot plate. The solution was allowed to evaporate at room temperature and crystals were obtained. The asymmetric unit of **(HPAA$^-$)(CIND$^+$)•IPA•H$_2$O** is represented in **Figure 5.3.1**.

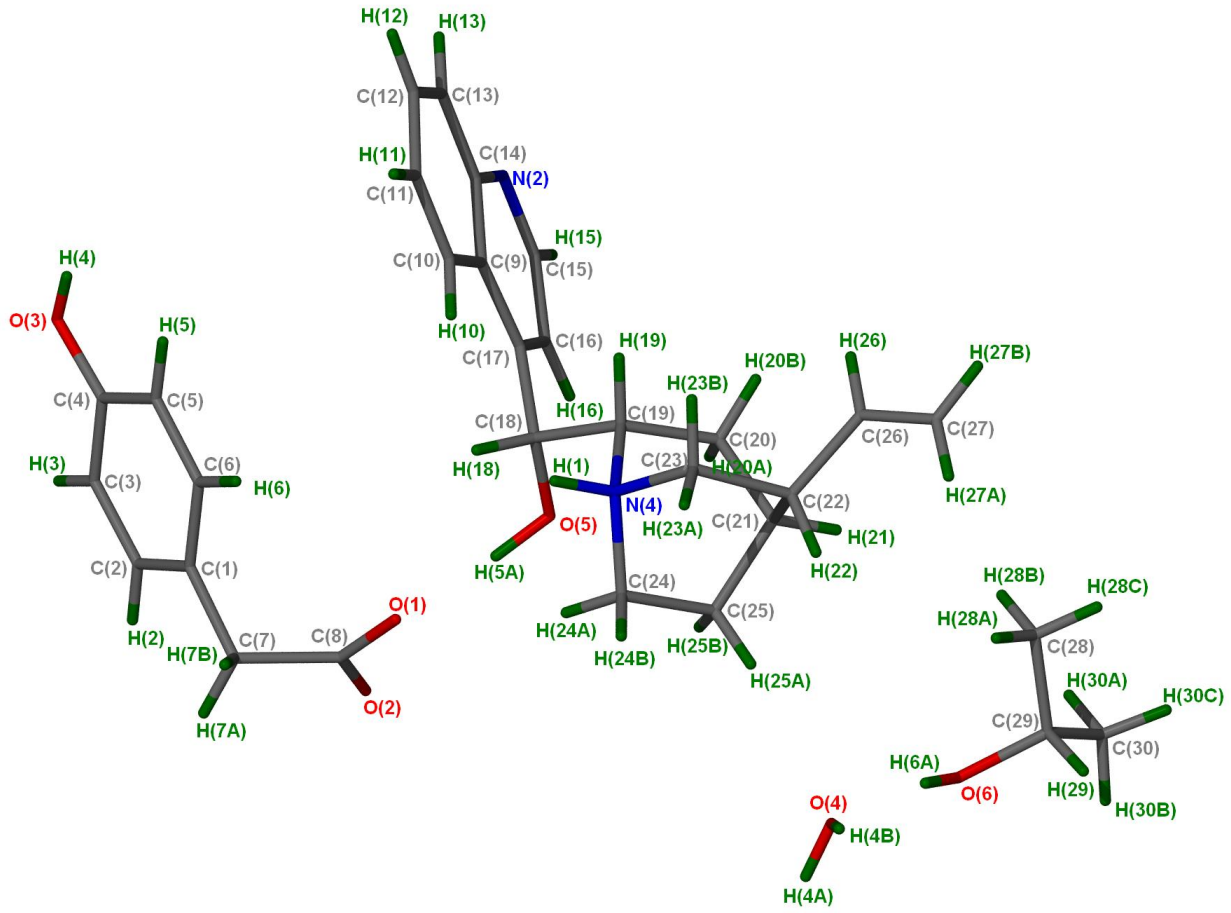

Figure 5.3.1: Asymmetric unit of **$(HPAA^{-})(CIND^{+})$•IPA•H_2O** structure with all the hydrogen atoms shown for numbering clarity.

5.3.1 Thermal Analysis

Thermal analysis results are shown in **Figure 5.3.2**. A single mass loss step of 14.7 % is observed in the TG curve which corresponds to the release of both water and isopropanol. Two sharp peaks are observed in the DSC, the first corresponding to the loss of solvent (T_{on}= 360.4 K) and the second due to the melt of the salt. The thermal analysis data is given in **Table 5.9**.

Table 5.9: Thermal analysis data of **$(HPAA^-)(CIND^+)$•IPA•H_2O**.

Compound	**$(HPAA^-)(CIND^+)$•IPA•H_2O**
$HPAA^-$: $CIND^+$: IPA: H_2O ratio	1: 1: 1: 1
TG calculated % mass loss	14.9
TG experimental % mass loss	14.7
DSC $Endo_1$ (T_{onset}, K)	360.4
DSC $Endo_2$ (T_{onset}, K)	444.9

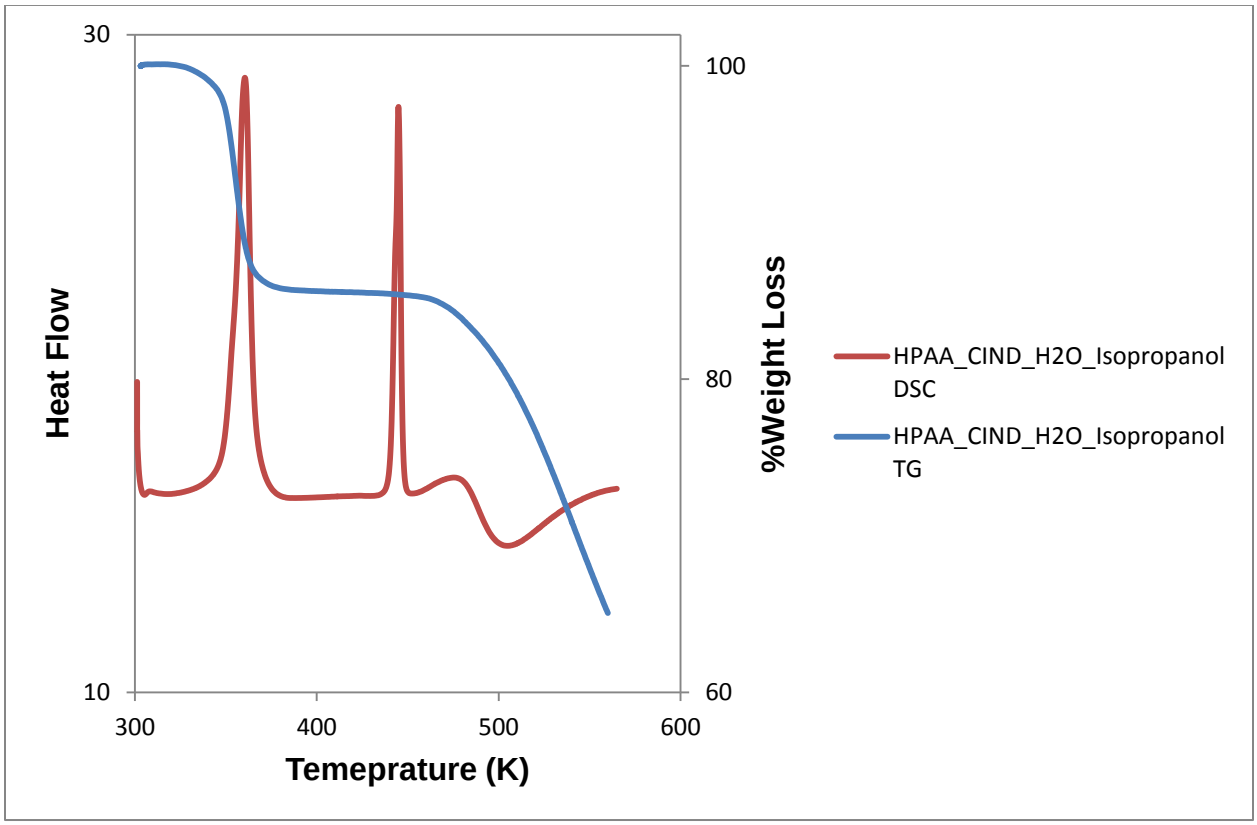

Figure 5.3.2: Thermal analysis curves of **$(HPAA^-)(CIND^+)$•IPA•H_2O** DSC (red) and TG (blue).

5.3.2 IR Spectroscopy

IR spectra are shown in **Figure 5.3.3**. The IR spectrum of the salt solvate shows a new band at 3142 cm^{-1} that can be attributed to the hydrogen bonded OH group. There are two new frequency vibrations at 1642 and 1613 cm^{-1} indicating a proton has been transferred in the crystal structure. IR results are given in **Table 5.10**.

Table 5.10: IR positions and assignments for the peaks in HPAA, **$(HPAA^{-})(CIND^{+})$•IPA•H_2O** and CIND.

HPAA	**$(HPAA^{-})(CIND^{+})$•IPA•H_2O**	CIND	Proposed assignment
3243	3142	3396	OH stretch
2707, 2616	2967, 2590	3072, 3003, 2939, 2866, 2720	C=C and C-H Stretching mode
1965, 1905	1935	1941	Overtone or combination bands
1711, 1618, 1600	1685, 1642, 1613	-	C=O
1519, 1446, 1414	1519 , 1454	1636, 1618,1590, 1567, 1508	C=C stretch
1210	1274	-	C-O stretch

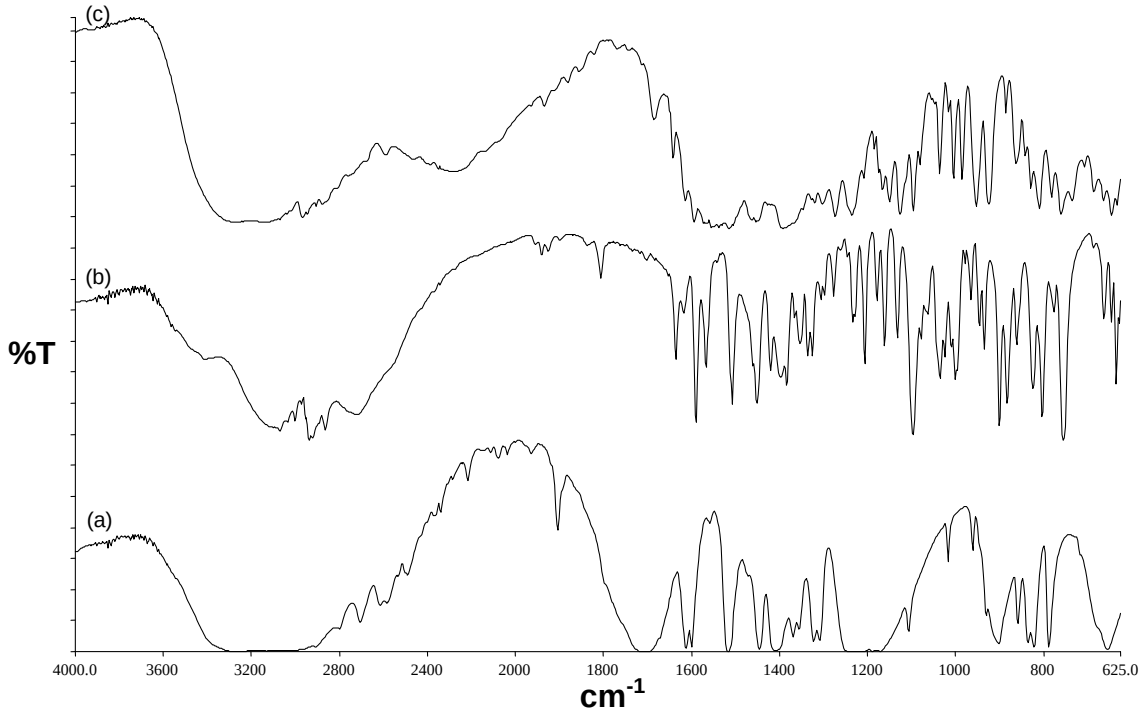

Figure 5.3.3: IR spectra (a) HPAA, (b) CIND and (c) **$(HPAA^{-})(CIND^{+})\bullet IPA\bullet H_2O$**.

5.3.3 Powder X-ray Diffraction

There is good agreement between the PXRD pattern of the ground product at 30 min and the pattern of the physical mixture. Therefore the grinding experiment was unsuccessful.

The slurry conversion pattern performed in 50/50 (*v/v*) water/isopropanol did not match the calculated pattern of the inclusion compound. The slurry pattern was similar to **$(HPAA^{-})(CIND^{+})(0.5H_2O)$** calculated PXRD pattern.

However, drops of 50/50 (*v/v*) water/isopropanol were added to the ground product and after further grinding for another 30 min the PXRD pattern was recorded. The PXRD pattern resulting from the solvent drop grinding also did not match that of the calculated pattern obtained from LAZYPULVERIX.[5]

PXRD patterns of the different experiments are shown in **Figure 5.3.4**.

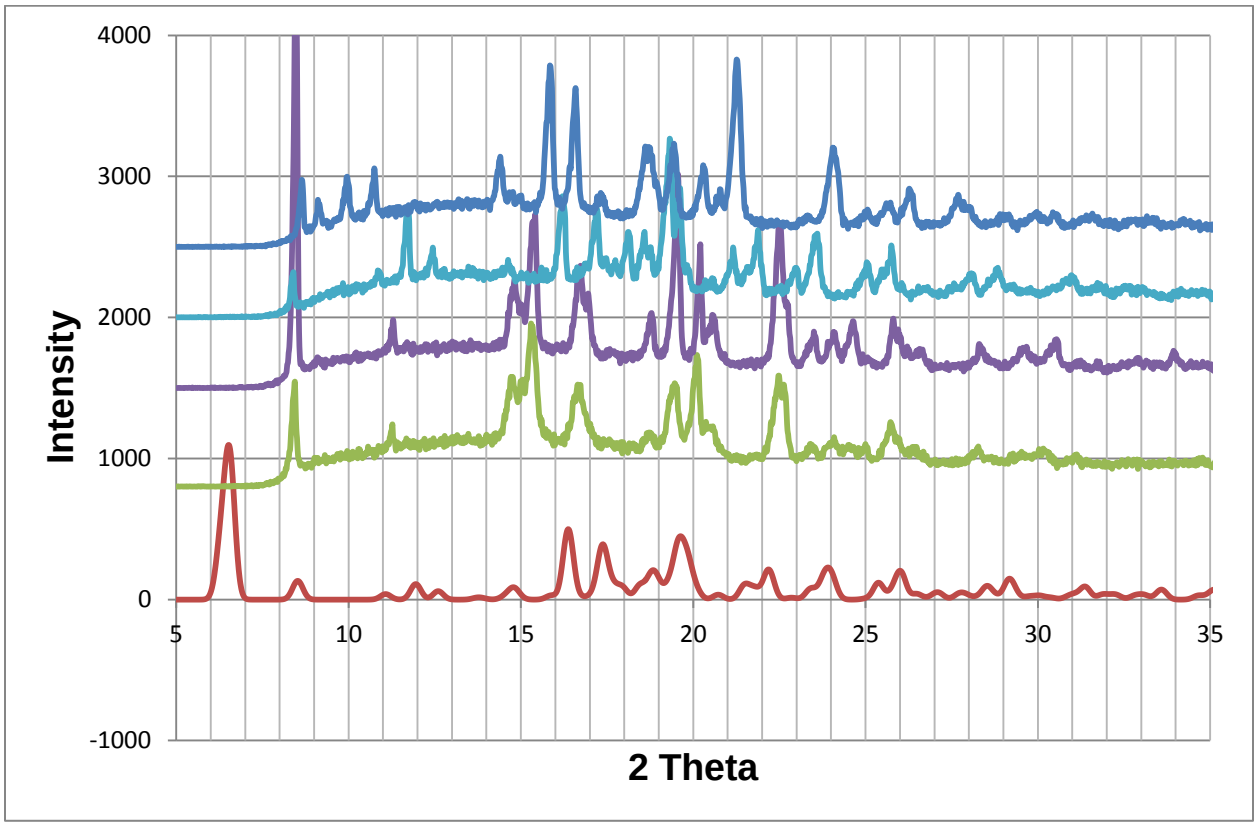

Figure 5.3.4: PXRD patterns of **$(HPAA^-)(CIND^+)$•IPA•H_2O** (red), ground product (green), physical mixture (purple), slurry (sky blue) and liquid assisted ground product (blue).

5.3.4 Structure Determination

Table 5.11 provides a summary of the crystal data results. The non-hydrogen atoms were found in the difference electron density map and the aromatic hydrogens of $HPAA^-$ and $CIND^+$ were placed with geometric constraints and refined isotropically. The $HPAA^-$ anion, $CIND^+$ cation, isopropanol and water molecules were located in general positions. The hydrogen atoms not involved in the hydrogen bond of **$(HPAA^-)(CIND^+)$•IPA•H_2O** were placed manually and refined isotropically.

Table 5.11: Crystal data of **$(HPAA^-)(CIND^+)$•IPA•H_2O**.

Compound	**$(HPAA^-)(CIND^+)$•IPA•H_2O**
Structural Formula	$(C_8H_7O_3^-)(C_{19}H_{23}N_2O^+)$•$C_3H_8O$•$H_2O$
$HPAA^-$:$CIND^+$:IPA:H_2O ratio	1: 1: 1: 1
Molecular Mass (g mol^{-1})	524.67
Data collection temperature (K)	173(2)
Crystal system	Orthorhombic
Space group	$P2_12_12_1$
a (Å)	6.6247 (13)
b (Å)	15.335 (3)
c (Å)	28.075(6)
α (°)	90.00
β (°)	90.00
γ (°)	90.00
Volume ($Å^3$)	2852.2 (10)
Z	4
D_c, Calculated density (g cm^{-3})	1.222
Final R indices [I>2sigma(I)]	R_1= 0.0418
	wR_2 = 0.0888
R indices (all data)	R_1 = 0.0612
	wR_2 = 0.0973
Largest diff. peak and hole ($eÅ^{-3}$)	0.293; -0.200

$(HPAA^-)(CIND^+)$•IPA•H_2O crystallized in an orthorhombic crystal system with a space group $P2_12_12_1$. The asymmetric unit contains one $HPAA^-$ anion, one $CIND^+$ cation, one isopropanol and one water with Z = 4. The crystal used for data collection had crystal size dimensions of 0.05 x 0.11 x 0.43 mm. There is proton transfer from the carboxylic group of the HPAA to the nitrogen atom (N4) in the CIND cation with an N-H distance of 0.970 Å. The oxygen atoms (O1 and O2) in the carboxylate group are such that: d (C8-O1) = 1.250 Å and d(C8-O2) = 1.264 Å which indicates salt formation. The packing

diagram of **$(HPAA^{-})(CIND^{+})$•IPA•H_2O** is shown in **Figure 5.3.5 (a)** running in the [100] direction.

Channels (contact surface) in which the water and isopropanol molecules are located have a void volume of 443.64 $Å^3$ and a unit cell volume percentage of 15.60 % at a probe radius of 1.40 Å and a grid spacing of 0.70 Å using Mercury[7] software as shown in **Figure 5.3.5 (b)**.

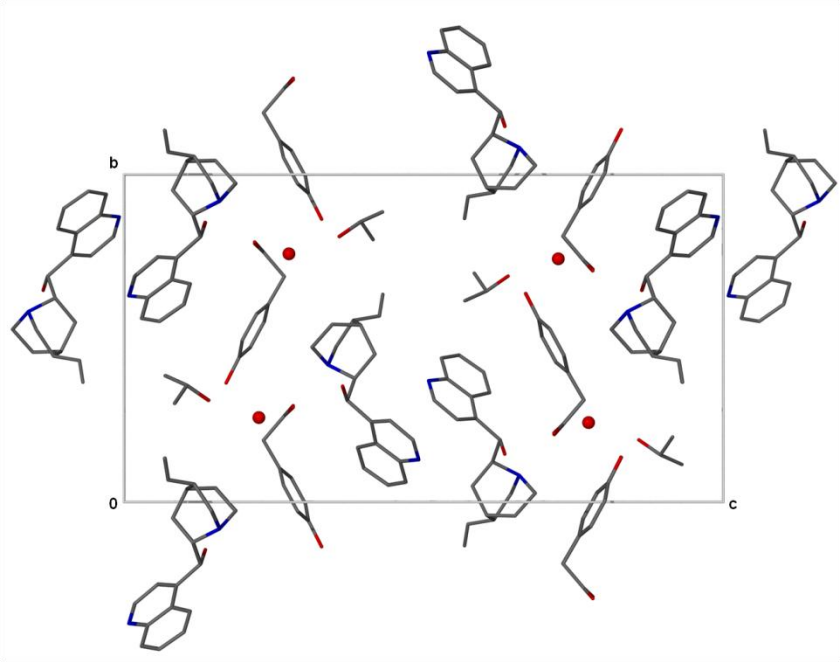

(a)

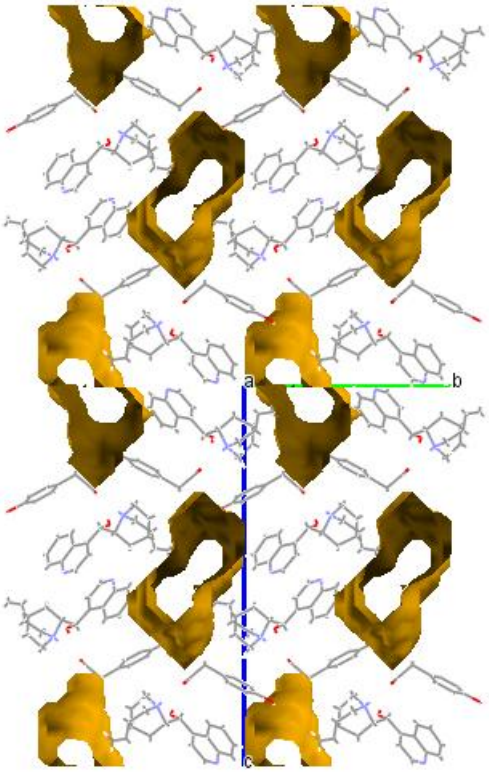

(b)

Figure 5.3.5: (a) packing diagram of **(HPAA$^-$)(CIND$^+$)•IPA•H_2O** with hydrogen atoms removed down [100] **(b)** channels in which water and isopropanol molecules are located down [100].

The connectivity diagram of **(HPAA$^-$)(CIND$^+$)•IPA•H_2O** is shown in **Figure 5.3.6** in which the hydrogen bonds: (CIND$^+$) OH•••(HPAA$^-$), (H2O) OH••• (HPAA$^-$), (IPA) OH•••(H2O), (IPA) OH•••(CIND$^+$), (HPAA$^-$) OH•••IPA) and (CIND$^+$) NH••• (HPAA$^-$) is noted. The two oxygen atoms (O1 and O2) in the carboxylate group play the role of bifurcated acceptors. Two chain motifs $C_2^2(6)$ and $C_2^2(9)$ are present. There are also D motifs involved in the graph set which can be characterized as $D_1^1(2)$, $D_2^1(3)$, $D_2^2(4)$, $D_2^2(5)$ and $D_2^2(11)$. The metrics of the hydrogen bonding are given in **Table 5.12**.

Table 5.12: Hydrogen bonding parameters in **(HPAA$^-$)(CIND$^+$)•IPA•H_2O**.

COMPOUND	D-H···A	D···A (Å)	D-H (Å)	H···A (Å)	D-H···A (º)
(HPAA$^-$)(CIND$^+$)•IPA•H_2O	N4-H1···O2 [a]	2.651 (2)	0.970 (1)	1.686 (3)	173 (2)
	O6-H6A···O4	2.717 (2)	0.809 (3)	1.928 (3)	165 (3)
	O5-H5A···O1	2.627 (2)	0.951 (2)	1.683 (2)	171 (2)
	O4-H4A···O2 [b]	2.767 (2)	0.884 (4)	1.892 (4)	170 (3)
	O4-H4B···O1 [c]	2.789 (2)	0.880 (4)	1.928 (4)	166 (3)
	O3-H4···O6 [d]	2.686 (2)	0.812 (2)	1.885 (2)	169 (2)

a = x-1, y, z ; b = -x+2, y-1/2, -z + 3/2 ; c = -x+1, y-1/2, -z+3/2 ; d = x, y+1, z

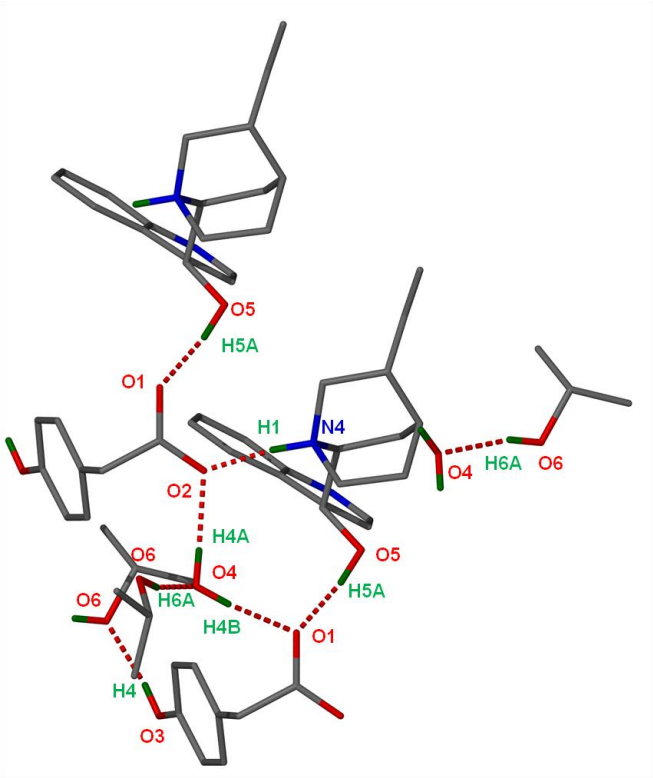

Figure 5.3.6: Intermolecular connectivity in **(HPAA$^-$)(CIND$^+$)•IPA•H_2O**.

5.4 HPAA and isonicotinamide (HPAA•2INM)

HPAA•2INM crystals were obtained by slow evaporation of a saturated solution of a 1: 1 ratio of HPAA and isonicotinamide (INM) in acetone. The crystals were obtained after a

few days. Similar crystals resulted when ethanol, methanol, isopropanol and tetrahydrofuran were used as solvents. The asymmetric unit of the co-crystal is illustrated in **Figure 5.4.1**.

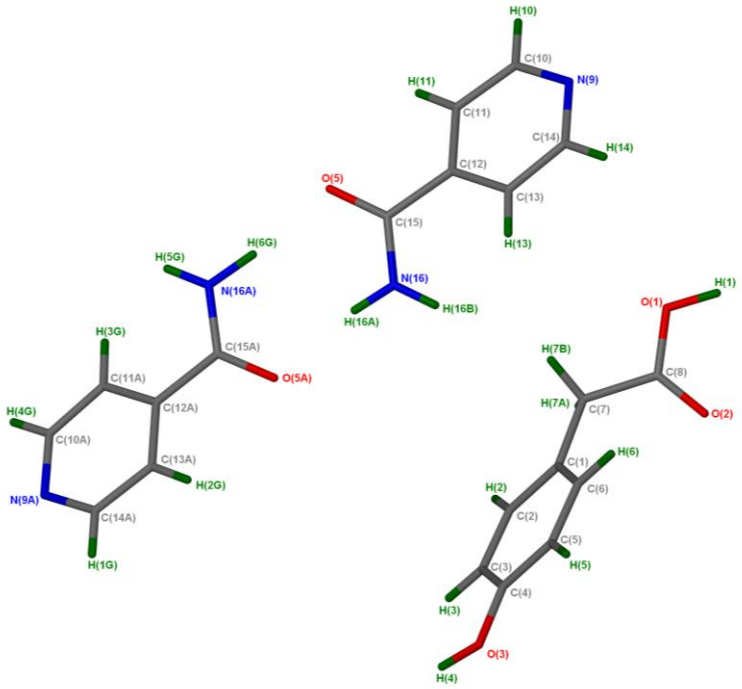

Figure 5.4.1: HPAA•2INM asymmetric unit with all the hydrogen atoms shown for numbering clarity.

5.4.1 Thermal Analysis

The DSC curve of the co-crystal, as illustrated in **Figure 5.4.2,** exhibits an endotherm which does not correspond to that of the HPAA or INM melts. This is a confirmation of a new compound formation. The endotherm has a lower onset temperature than that of the two pure components indicating a decrease in thermal stability. Thermal analysis results are given in **Table 5.13**.

Table 5.13: Thermal analysis data of **HPAA•2INM**.

Compounds	**DSC Endo$_1$(T_{onset},K)**	**DSC Endo$_2$(T_{onset},K)**
Isonicotinamide	382.1(minor)	428.4 (major)
HPAA	-	425.1
HPAA•2INM	-	403.1

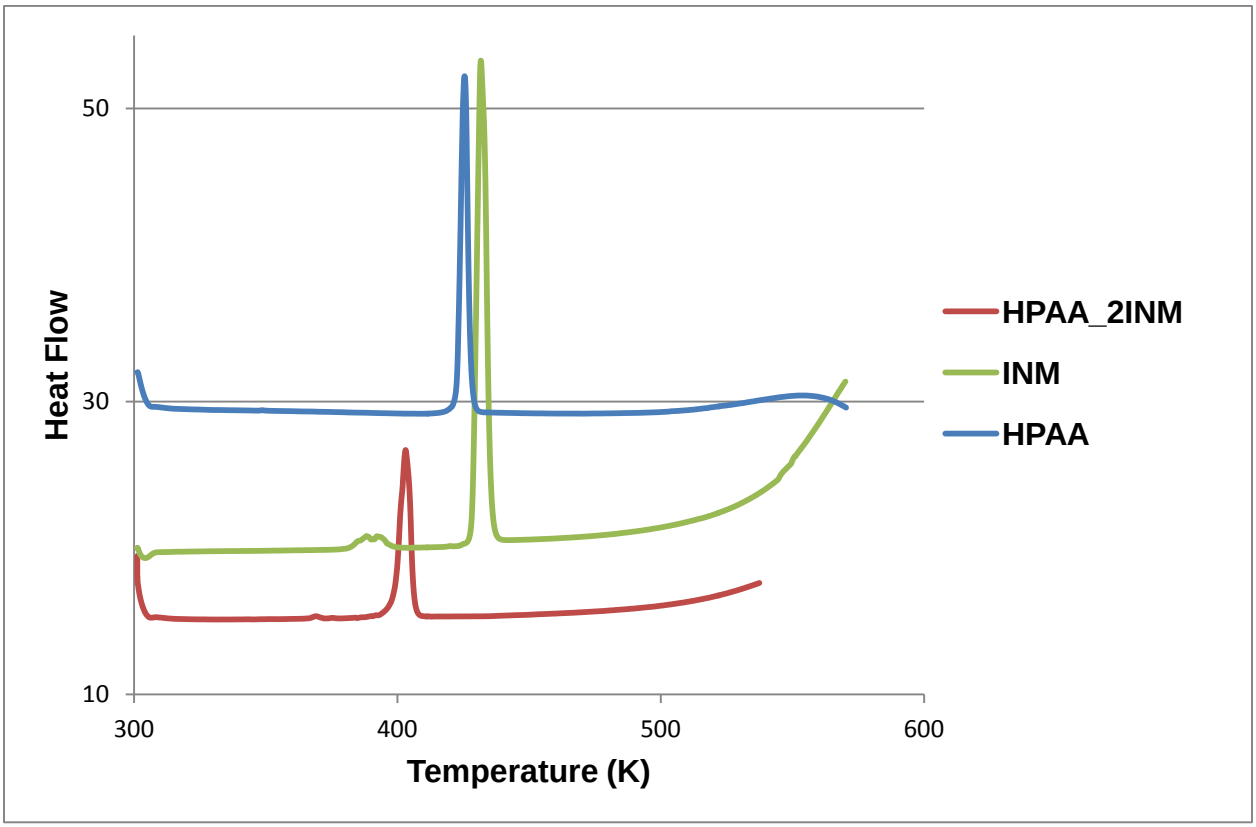

Figure 5.4.2: DSC curve of HPAA (blue), INM (green) and **HPAA•2INM** (red).

5.4.2 IR Spectroscopy

Figure 5.4.3 shows the FTIR spectra of HPAA, INM and the co-crystal prepared in acetone. The stretching of the amide group in INM is represented by absorption bands at 3370 and 3180 cm^{-1} respectively, which was assigned to the free anti-NH

(asymmetrical) and hydrogen-bonded NH (symmetrical) vibration. The absorption band at 1680 cm^{-1} was assigned to the carbonyl (C=O) stretching and the band at 1399 cm^{-1} to CN stretching.

The spectrum of the co-crystal showed changes in the peak positions of the carbonyl and amide groups, which suggested interactions between HPAA and INM. There is a shift in the carbonyl stretching bands for the co-crystal at 1673 and 1617cm^{-1}. Additionally, there is also a shift in the N–H vibration band at 3354 and 3182 cm^{-1}. The new band at 3398 cm^{-1} can be attributed to the OH group involved in hydrogen bonding. **Table 5.14** shows the IR results.

Table 5.14: IR positions and assignments of peaks in HPAA, **HPAA•2INM** and INM.

HPAA	**HPAA•2INM**	INM	Proposed assignment
3243	3398	-	OH stretch
2707, 2616	3354, 3182	3370, 3186	H-bonded NH_2 stretching mode
2707, 2616	2809	2783	C-C ring modes
1711, 1618, 1600	1673, 1617	1680	C=O
-	1604,	1624	Amide II band (NH_2 scissor), C-N, C=O stretching mode combination
1519, 1446, 1414	1553, 1518, 1470,1414	1595, 1551,	C=C stretch
	1342	1399	Amide III band (C-N stretch, N-H bend)
1210	1297, 1275, 1235	1218	C-O stretch

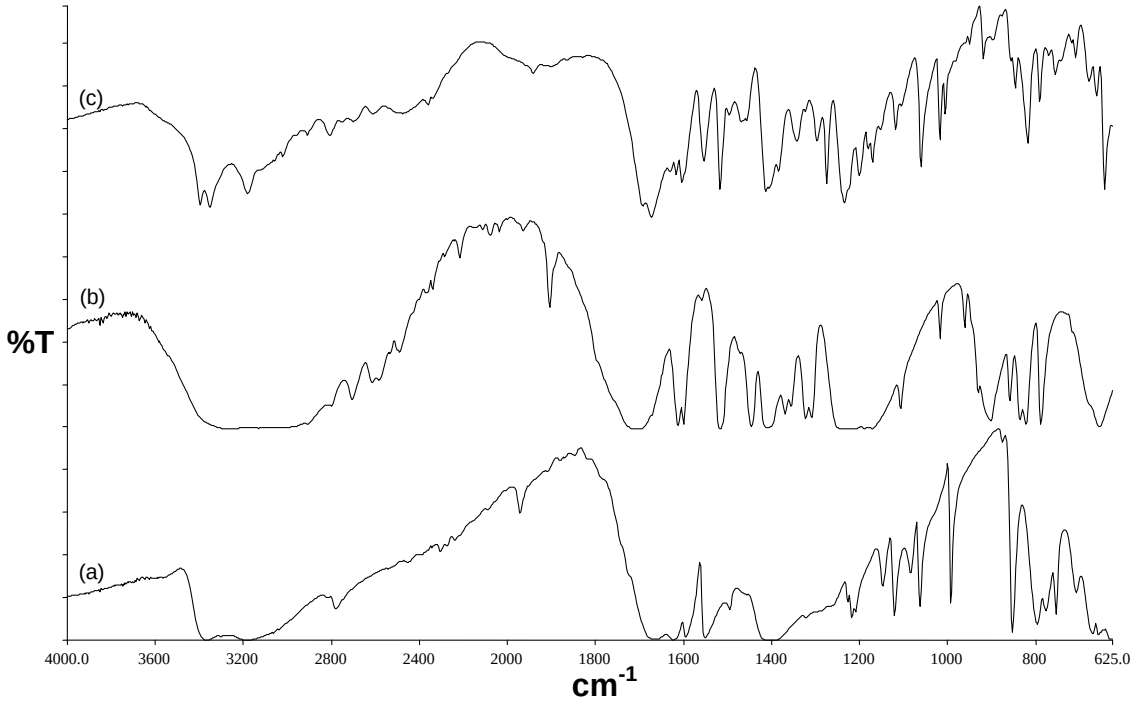

Figure 5.4.3: IR spectrum of (a) INM (b) HPAA and (c) **HPAA•2INM**.

5.4.3 Powder X-ray Diffraction

The dry grinding of a 1: 2 molar ratio of HPAA and INM produced a powdered material which showed a PXRD pattern containing peaks found both in the physical mixture and in the calculated pattern but mostly resembles the physical mixture. This indicates a partial conversion of the ground product.

The PXRD pattern of the slurry conversion performed in methanol showed good agreement to that of the calculated pattern obtained from LAZYPULVERIX[5] as shown in **Figure 5.4.4**.

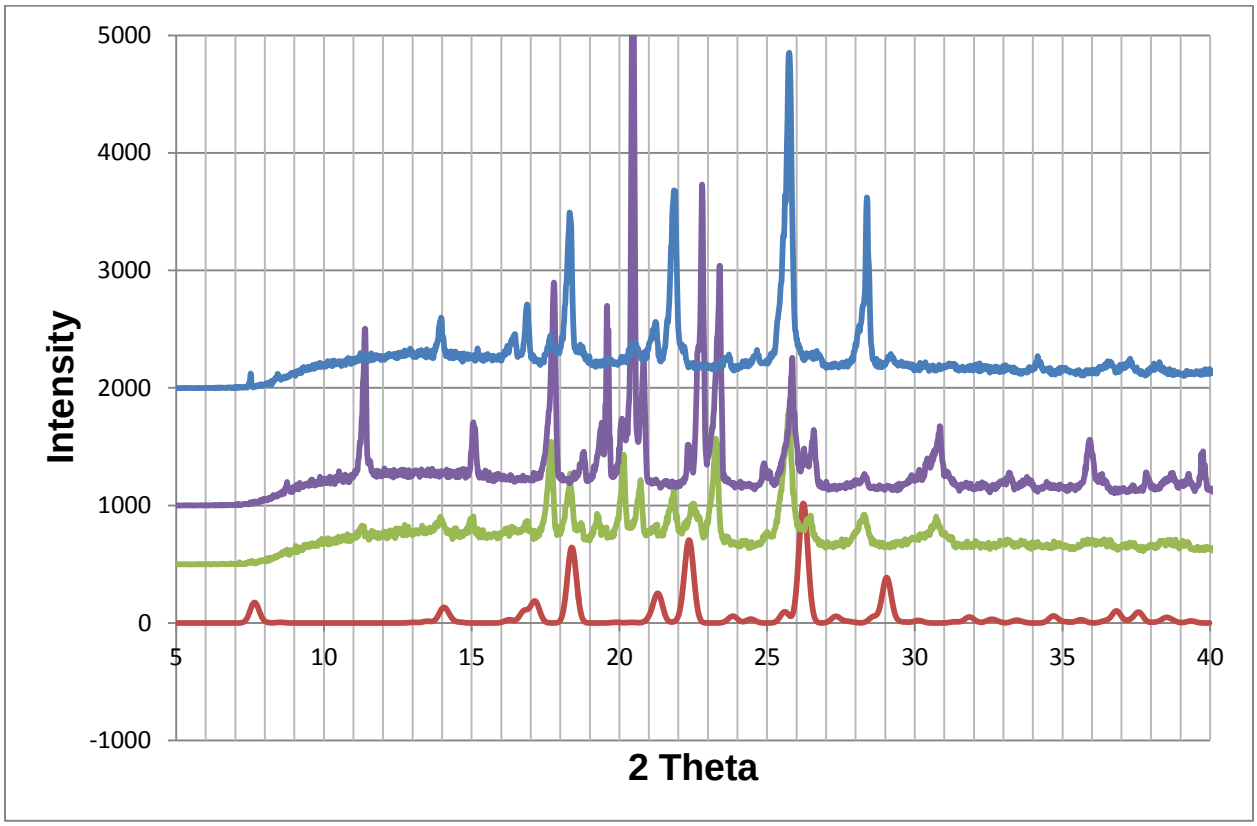

Figure 5.4.4: PXRD patterns of **HPAA•2INM** (red), ground product (green), physical mixture (purple) and slurry (blue).

5.4.4 Structure Determination

All non-hydrogen atoms were found in the difference electron density map. H atoms on C atoms were refined isotropically. H atoms on the amine and carboxylic group were located from the difference-electron density map and refined freely. HPAA and INM molecules were found in general positions. **Table 5.15** provides experimental details of the X-ray analyses.

Table 5.15: Crystallographic data for the **HPAA•2INM** co-crystal.

Compound	**HPAA•2INM**
Structural Formula	$C_8H_8O_3$•$2C_6H_6N_2O$
HPAA:INM ratio	1: 2
Molecular Mass (g mol^{-1})	396.40
Data collection temperature (K)	173(2)
Crystal system	Triclinic
Space group	*P-1*
a (Å)	6.7760 (14)
b (Å)	12.370 (3)
c (Å)	12.686 (3)
α (°)	111.82 (3)
β (°)	96.57 (3)
γ (°)	99.53 (3)
Volume ($Å^3$)	955.4 (3)
Z	2
D_c, Calculated density (g cm^{-3})	1.378
Final R indices [I>2sigma(I)]	R_1= 0.0487
	wR_2 = 0.1283
R indices (all data)	R_1 = 0.0683
	wR_2 = 0.1423
Largest diff. peak and hole ($eÅ^{-3}$)	0.554; -0.592

HPAA•2INM was solved in the triclinic space group *P-1* with one HPAA and two INM molecules in the asymmetric unit (**Figure 5.4.1**) with Z = 2. The crystal packing view down [100] is shown in **Figure 5.4.5**.

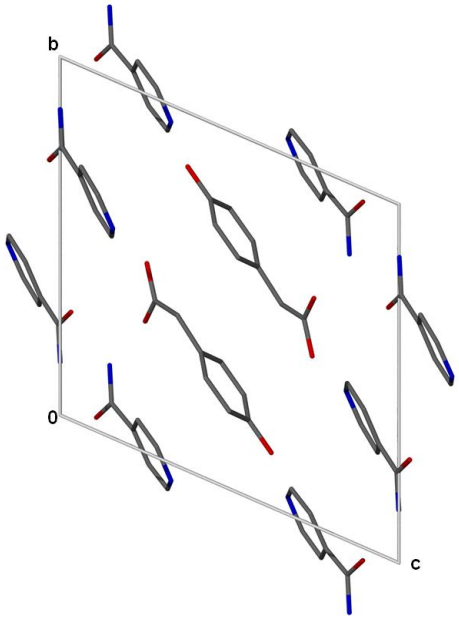

Figure 5.4.5: Crystal packing of **HPAA•2INM** with hydrogen atoms removed viewed down [100].

The crystal structure of **HPAA•2INM** displays an extensive hydrogen-bond network generated by amide-amide synthons. Each INM molecule is involved in two intermolecular N--O···H hydrogen bonds (**Figure 5.4.6**). These units are linked together through a complementary amide dimer, formed by N16A—H5G···O5 at (- x, - y+2, - z+2).

The chains are linked through a second complementary interaction formed by N16A—H6G···O5 at (x, y, z), resulting in the formation of rings with a graph set $R_2^2(8)$. The ring $R_4^4(16)$ motif is formed between four isonicotinamide molecules and the graph set $R_4^4(32)$ is between two molecules of each compound. N16A—H5G···O5 interactions between two INM molecules are also revealed with a graph set $R_4^2(8)$. The structure is further stabilized by the (HPAA) O1-H1•••N9A (INM), (INM) N16-H16B•••O2 (HPAA) and (HPAA) O3-H4•••N9 (INM) hydrogen bonding connections. The $D_1^1(2)$ motif is observed between two INM molecules. The other D motifs ($D_2^2(5)$, $D_2^2(6)$, $D_2^2(8)$, $D_2^2(9)$ and $D_2^2(12)$ in the structure are between one molecule of HPAA and two molecules of INM. The hydrogen bonding parameters are given in **Table 5.16**.

Table 5.16: HPAA•2INM hydrogen bonding parameters.

COMPOUND	D-H···A	D···A (Å)	D-H (Å)	H···A (Å)	D-H···A (º)
HPAA•2INM	N16A-H6G···O5	2.932 (2)	0.963 (1)	1.973 (1)	174 (1)
	N16-H16A···O5A	2.877 (2)	0.912 (1)	1.977 (1)	169 (1)
	N16-H16B···O2 [a]	2.881 (2)	0.871 (1)	2.017 (1)	171 (1)
	N16A-H5G···O5 [b]	2.941 (2)	0.768 (2)	2.240 (2)	152 (2)
	O3-H4···N9 [c]	2.760 (2)	0.921 (3)	1.853 (3)	168 (2)
	O1-H1···N9A [d]	2.611 (2)	0.960 (1)	1.679 (1)	163 (2)

a = -x+1, -y+1, -z +1; b = -x, y+2, -z +2 ; c = x-1, y-1, z; d = x+1, y, z-1

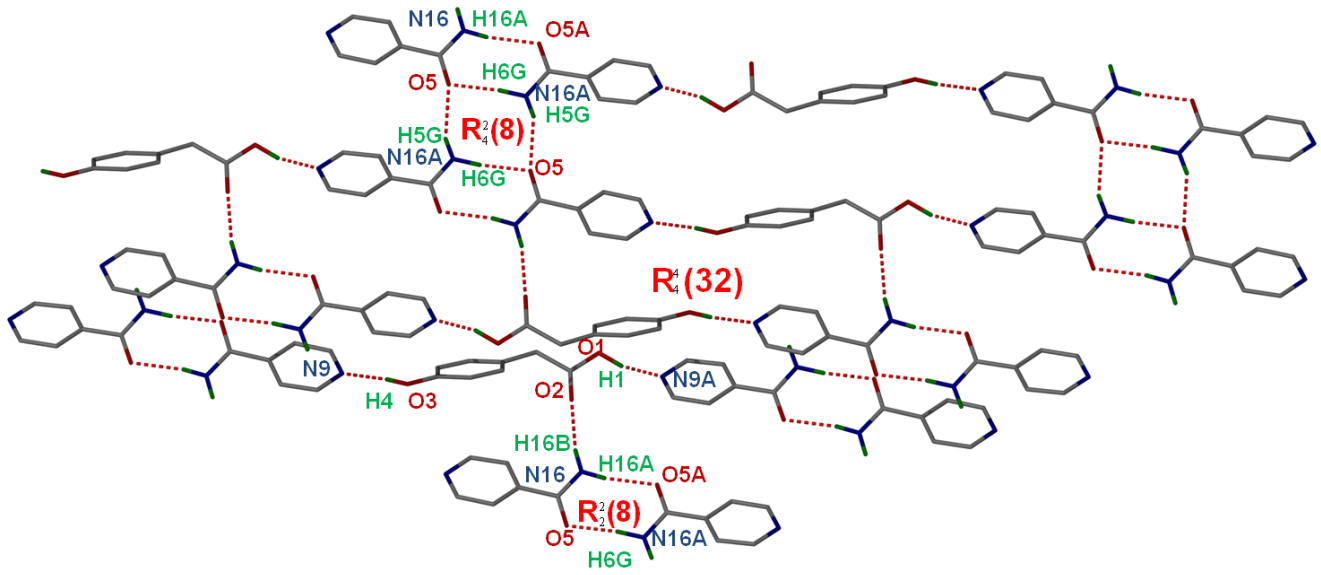

Figure 5.4.6: Hydrogen bonding in **HPAA•2INM**.

5.5 HPAA and Quinidine ($HPAA^-$)($QUID^+$)•H_2O

The salt hydrate was achieved from an equimolar mixture of HPAA and QUID in ethanol. The solution was allowed to evaporate at ambient temperature and after a few weeks crystals were obtained. Similar crystals were obtained when methanol, isopropanol and tetrahydrofuran were used as solvents.

The asymmetric unit of **(HPAA$^-$)(QUID$^+$)•H_2O** is shown in **Figure 5.5.1**.

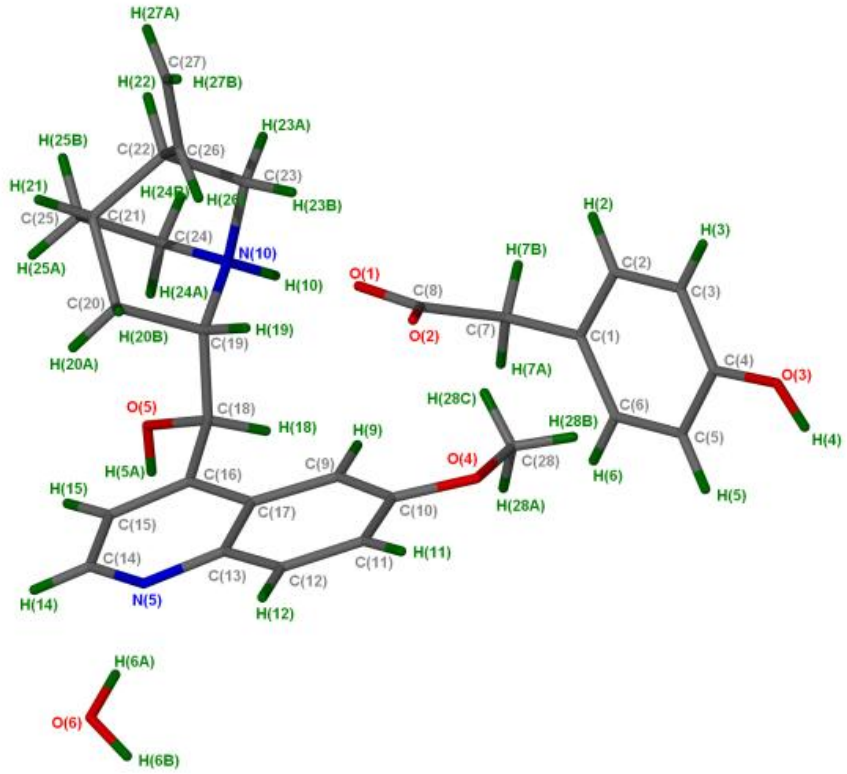

Figure 5.5.1: Asymmetric unit of **(HPAA$^-$)(QUID$^+$)•H_2O** with all the hydrogen atoms shown for numbering clarity.

5.5.1 Thermal Analysis

Thermal analysis results are given in **Table 5.17**. There is good agreement between the calculated and the experimental percentage mass loss. **(HPAA$^-$)(QUID$^+$)•H_2O** displays two mass loss steps in the TG curve (**Figure 5.5.2**) which shows a mass loss of 3.2 % up to 410.4 K with a corresponding endotherm in the DSC.

Table 5.17: Thermal analysis data of **$(HPAA^-)(QUID^+)\bullet H_2O$**.

Compound	**$(HPAA^-)(QUID^+)\bullet H_2O$**
$HPAA^-:QUID^+:H_2O$ ratio	1: 1: 1
TG calculated % mass loss	3.6
TG experimental % mass loss	3.2
DSC Endo (T_{onset}, K)	410.4

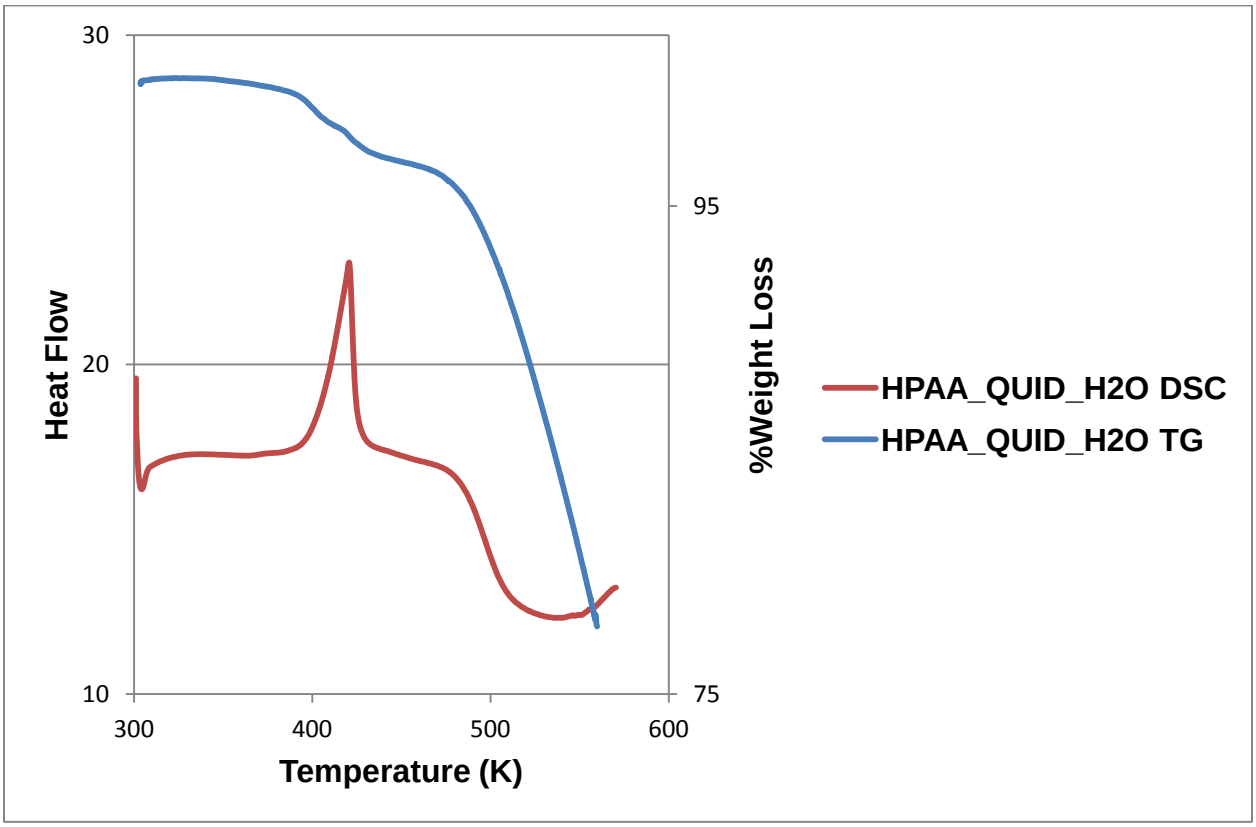

Figure 5.5.2: Thermal analysis curves of **$(HPAA^-)(QUID^+)\bullet H_2O$** DSC (red) and TG (blue).

5.5.2 IR Spectroscopy

The IR spectrum of **$(HPAA^-)(QUID^+)\bullet H_2O$** is different from the starter components as illustrated in **Figure 5.5.3**. There is a broad band at 3200 cm^{-1}, which can be attributed to the combination of OH stretching and the N-H stretch mode. The new frequency vibration at 1584 cm^{-1} confirms the formation of a salt according to Adalder *et al*[4] due to the a proton being transferred from the carboxylic group of the HPAA molecule to the nitrogen atom (N10) of the QUID. The compound **$(HPAA^-)(QUID^+)\bullet H_2O$** is extremely stable and only release water at high temperatures.

Table 5.18: IR positions and assignments of peaks in HPAA, **$(HPAA^-)(QUID^+)\bullet H_2O$** and QUID.

HPAA	**$(HPAA^-)(QUID^+)\bullet H_2O$**	QUID	Proposed assignment
3243	3200	3448, 3124	OH stretch
2707, 2616	3200	-	N-H stretching mode
2707, 2616	2977, 2905	2932, 2868, 2710	C-C ring modes
1711, 1618, 1600	1584	-	C=O
-	1619	1620	C-N, C=O stretching mode combination
1519, 1446, 1414	1513, 1476,1454	1589, 1561, 1549, 1464	C=C stretch
-	1380	1400	C-N stretch, N-H bend
1210	1267	1282	C-O stretch

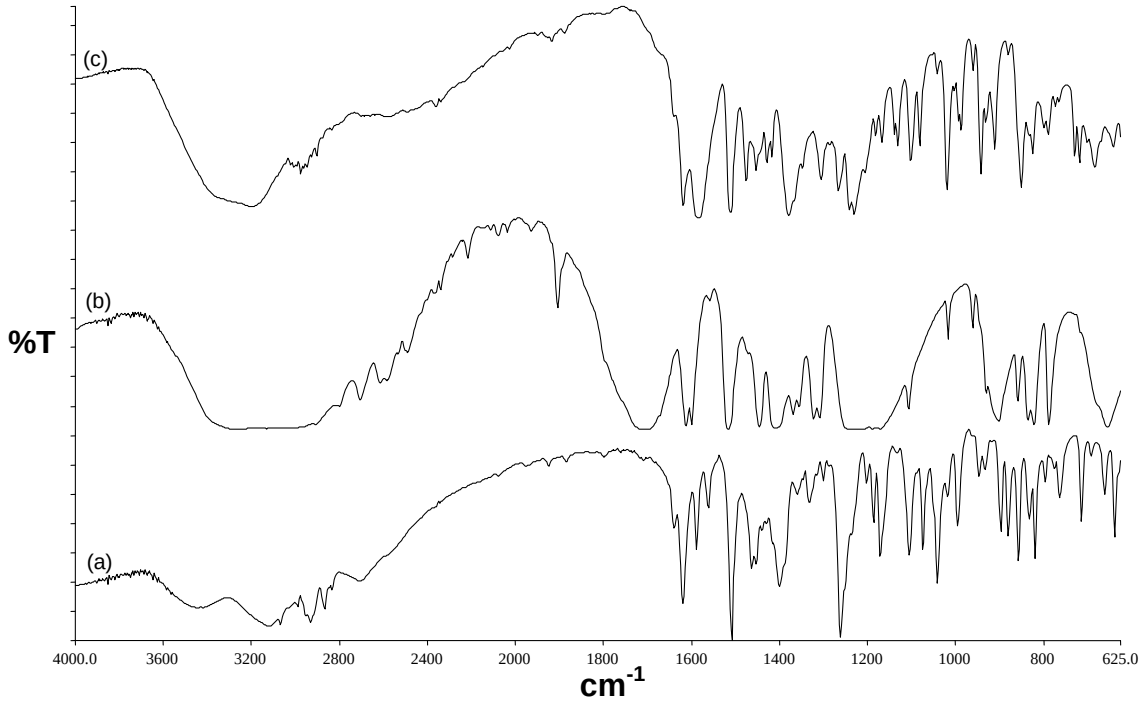

Figure 5.5.3: IR spectra (a) QUID, (b) HPAA and (c) **$(HPAA^{-})(QUID^{+})\bullet H_2O$**.

5.5.3 Powder X-ray Diffraction

The neat grinding PXRD pattern did not match either the physical mixture or the calculated pattern of the salt hydrate. This may be another form of the co-crystal or the anhydrous compound **$(HPAA^{-})(QUID^{+})$,** but crystallization of this form was unsuccessful.

The slurry conversion performed in ethanol also did not match the physical mixture and the calculated pattern obtained from LAZYPULVERIX[5] and can be a formation of a new compound.

The PXRD patterns of the different experiments performed on the **$(HPAA^{-})(QUID^{+})\bullet H_2O$** are shown in **Figure 5.5.4**.

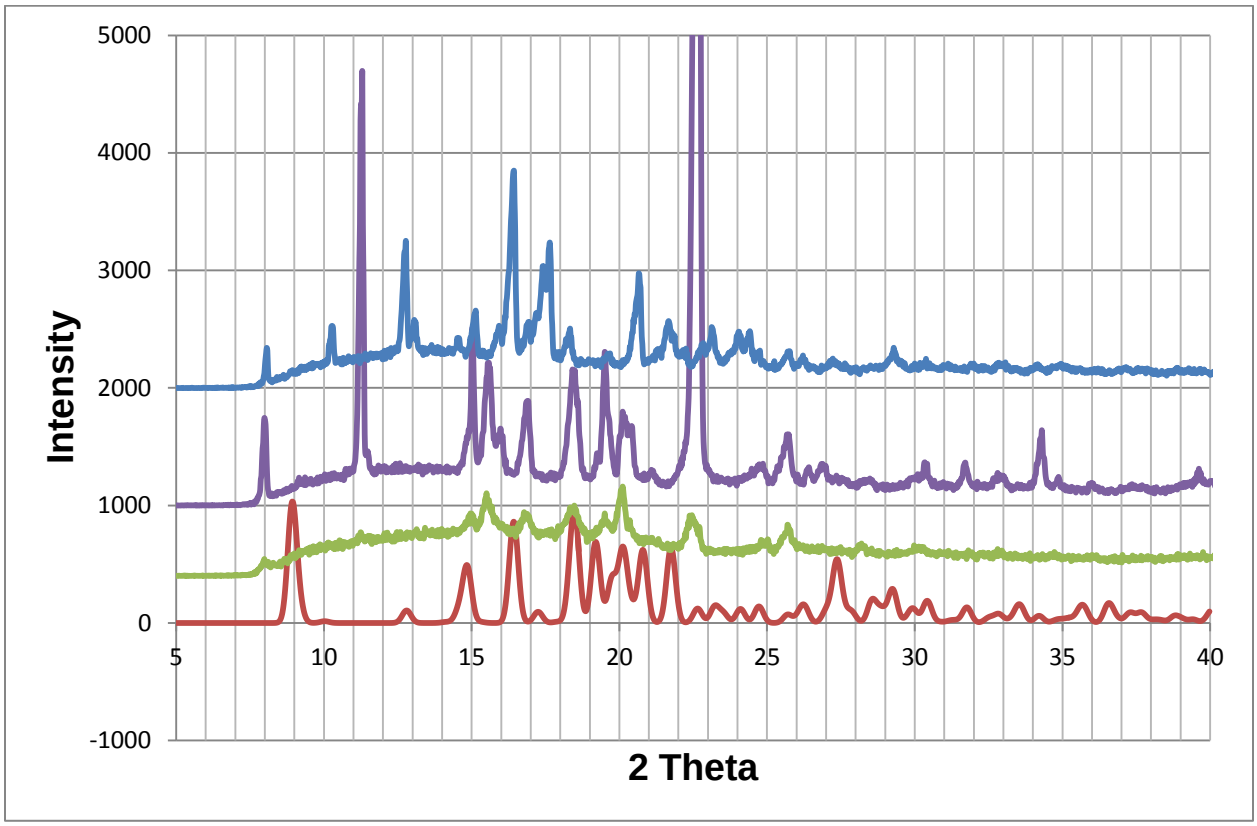

Figure 5.5.4: PXRD patterns of **(HPAA$^-$)(QUID$^+$)•H_2O** (red), ground product at 30 min (green), physical mixture (purple) and slurry (blue).

5.5.4 Structure Determination

The crystal structure of **(HPAA$^-$)(QUID$^+$)•H_2O** was solved in the monoclinic space group $P2_1$. . The hydroxyl hydrogen of the HPAA$^-$ anion and the hydrogen atom bonded to the nitrogen atom in the QUID$^+$ cation were located in the difference electron density map. The structure refined successfully to R_1= 0.0376 with wR_2= 0.0933 ([I>2sigma (I)]). The summary of the crystal data is given in **Table 5.19**.

Table 5.19: Crystal data of **$(HPAA^-)(QUID^+)\bullet H_2O$**.

Compound	**$(HPAA^-)(QUID^+)\bullet H_2O$**
Structural Formula	$(C_8H_7O_3^-)(C_{20}H_{25}N_2O_2^+)\bullet H_2O$
$HPAA^-:QUID^+:H_2O$ ratio	1: 1: 1
Molecular Mass (g mol^{-1})	494.59
Data collection temperature (K)	173(2)
Crystal system	Monoclinic
Space group	*$P2_1$*
a (Å)	6.4974 (13)
b (Å)	19.303 (4)
c (Å)	10.263 (2)
α (°)	90.00
β (°)	105.29 (3)
γ (°)	90.00
Volume ($Å^3$)	1241.6 (4)
Z	2
D_c, Calculated density (g cm^{-3})	1.323
Final R indices [I>2sigma(I)]	R_1= 0.0376
	wR_2 = 0.0933
R indices (all data)	R_1 = 0.0409
	wR_2 = 0.0955
Largest diff. peak and hole ($eÅ^{-3}$)	0.264; -0.187

The crystal used for data collection had size dimensions of 0.07 x 0.20 x 0.45 mm. The packing diagram of **$(HPAA^-)(QUID^+)\bullet H_2O$** along the [100] direction is shown in **Figure 5.5.5 (a)**. Cavities (contact surface) in which water molecules are located down [100] are illustrated in **Figure 5.5.5 (b)** with a void volume of 7.09 $Å^3$ and percentage unit cell volume of 0.60 % using a probe of 1.0 Å and a grid spacing of 0.70 Å. A probe size of 1.4 Å supposed to be used for the hydrate but at that value, a void volume of 0.00 $Å^3$ is indicated.

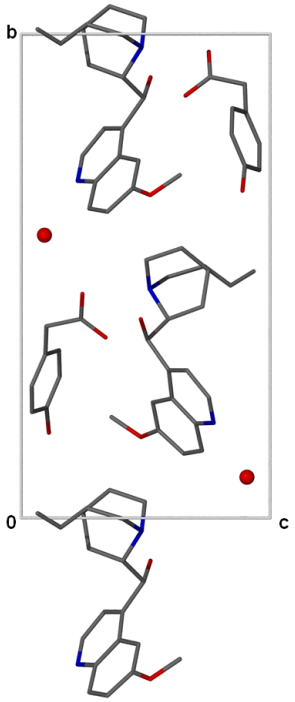

(a)

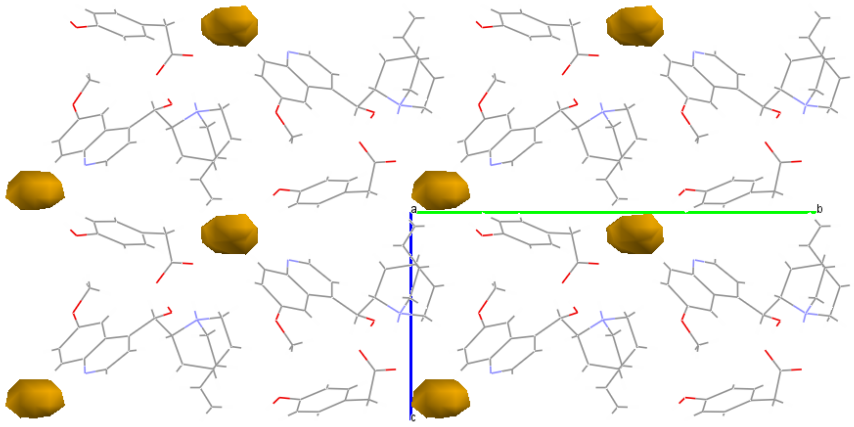

(b)

Figure 5.5.5: (a) Crystal packing diagram of **(HPAA$^-$)(QUID$^+$)•H_2O**, with hydrogen atoms removed, down [100], **(b)** cavities in which water molecules are located down [100].

All the nitrogen atoms of the $QUID^+$ cation are involved in hydrogen bonding. The protonated $^+$N10-H10 is connected to the oxygen atoms O1 of the carboxylate group (**Figure 5.5.6**).

O1 is a bifurcated acceptor; it is linked to $QUID^+$ and to a water molecule. Each water molecule is connected to the nitrogen atom (N5) of the $QUID^+$ cation, the hydroxyl group of an $HPAA^-$ anion and the carboxyl group of an $HPAA^-$ anion. There are many graph sets involved in the crystal structure which are characterized as $D_1^1(2)$, $D_2^1(3)$, $D_2^2(4)$, $D_2^2(5)$, $D_2^2(9)$, $C_2^2(9)$, $D_2^2(10)$, $D_2^2(11)$ and $C_2^2(11)$. **Table 5.20** summarizes the details of the **$(HPAA^-)(QUID^+)\bullet H_2O$** connectivity.

Table 5.20: Connectivity of the **$(HPAA^-)(QUID^+)\bullet H_2O$** salt hydrate.

COMPOUND	D-H···A	D···A (Å)	D-H (Å)	H···A (Å)	D-H···A (º)
$(HPAA^-)(QUID^+)\bullet H_2O$	N10-H10···O1	2.747 (2)	0.915 (2)	1.853 (2)	165 (2)
	O6-H6A···N5	2.826 (2)	0.922 (3)	1.919 (3)	168 (2)
	O5-H5A···O2 [a]	2.679 (2)	0.847 (2)	1.876 (2)	158 (2)
	O6-H6B···O1[b]	2.828 (2)	0.840 (3)	1.992 (3)	173 (3)
	O3-H4···O6 [c]	2.723 (2)	0.845 (3)	1.883 (3)	172 (3)

a = x-1, y, z ; b = -x+1, y-1/2, -z +1; c = x+1, y, z-1

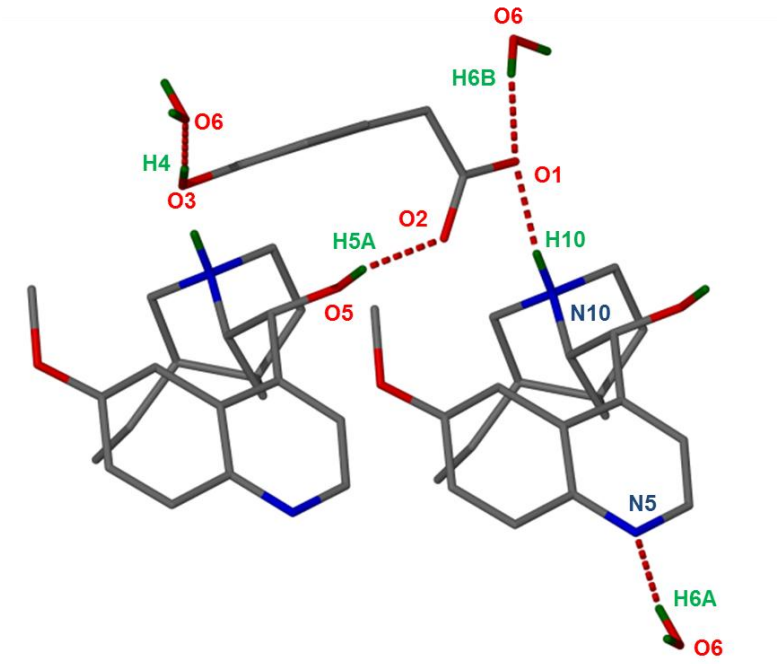

Figure 5.5.6: Connectivity in **(HPAA$^-$)(QUID$^+$)•H_2O**.

5.6 HPAA and Quinine (HPAA$^-$)(QUIN$^+$)

The salt was obtained by dissolving a 1: 1 ratio of both compounds in methanol. The solution evaporated at room temperature and after a few weeks crystals were obtained. Similar crystals were obtained when ethanol, isopropanol and tetrahydrofuran were used as solvents.

The asymmetric unit of the salt is represented in **Figure 5.6.1**.

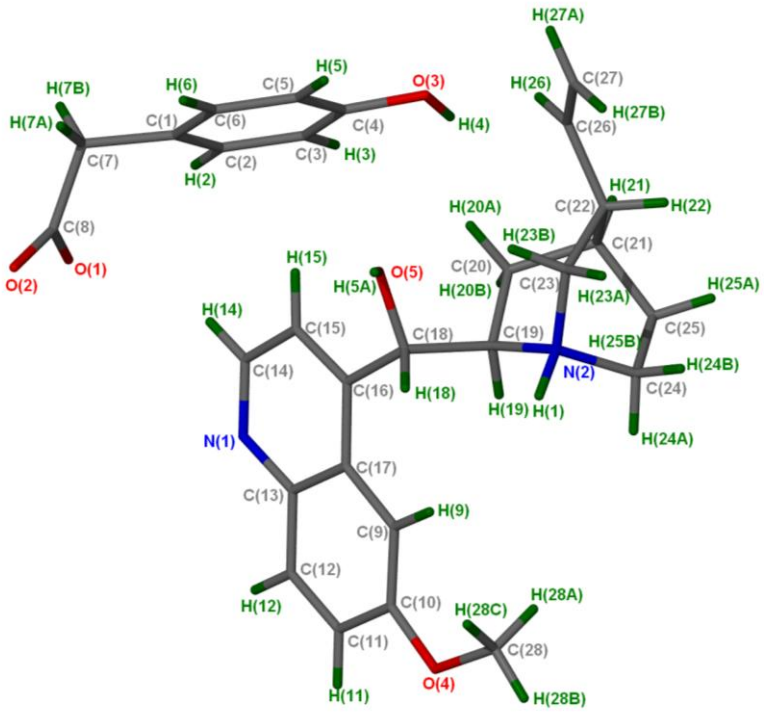

Figure 5.6.1: Asymmetric unit of **(HPAA$^-$)(QUIN$^+$)**with all the hydrogen atoms shown for numbering clarity.

5.6.1 Thermal Analysis

Table 5.21 gives the thermal analysis results of **(HPAA$^-$)(QUIN$^+$)**. There is an increase in the thermal stability of the salt, [3] because its melting point is higher than that of either pure compound as shown in **Figure 5.6.2**.

Table 5.21: Thermal analysis results of **(HPAA$^-$)(QUIN$^+$)**.

Compounds	**DSC Endo(T_{onset},K)**
QUIN	449.8
HPAA	425.1
(HPAA$^-$)(QUIN$^+$)	489.8

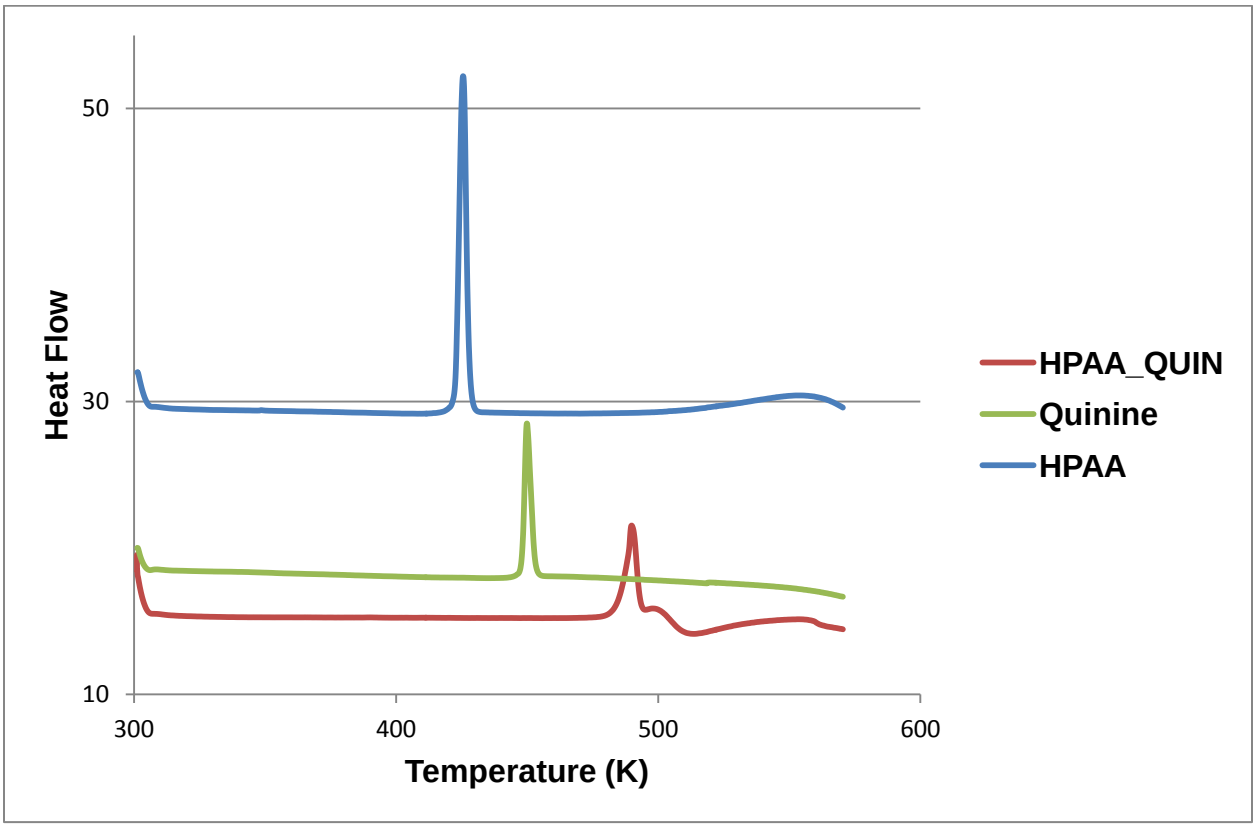

Figure 5.6.2: DSC curves of **(HPAA$^-$)(QUIN$^+$)** (red), HPAA (blue) and quinine (green).

5.6.2 IR Spectroscopy

IR spectra of the salt and the individual components are shown in **Figure 5.6.2**. For the IR spectrum of the salt there is a new broad absorption peak at 3451 cm^{-1} assigned to the OH group involved in the hydrogen bonding. A new band at 3085 cm^{-1} is observed and is attributed to the N-H stretch. The band at 1577 cm^{-1} is attributed to the COO$^-$ group and the shift indicates that a proton has been transferred.[4] The IR results are given in **Table 5.22**.

Table 5.22: IR positions and assignments of peaks in HPAA, **$(HPAA^-)(QUIN^+)$** and QUIN.

HPAA	**$(HPAA^-)(QUIN^+)$**	QUIN	Proposed assignment
3243	34551	3451, 3170	OH stretch
2707, 2616	3085	-	N-H stretching mode
2707, 2616	2950, 2360	2936, 2360, 2342	C-C ring modes
1711, 1618, 1600	1577	-	C=O
-	1619	1624	C-N, C=O stretching mode combination
1519, 1446, 1414	1511, 1469,1434	1590, 1508, 1469, 1449	C=C stretch
	1388	1400	C-N stretch, N-H bend
1210	1268	1260	C-O stretch

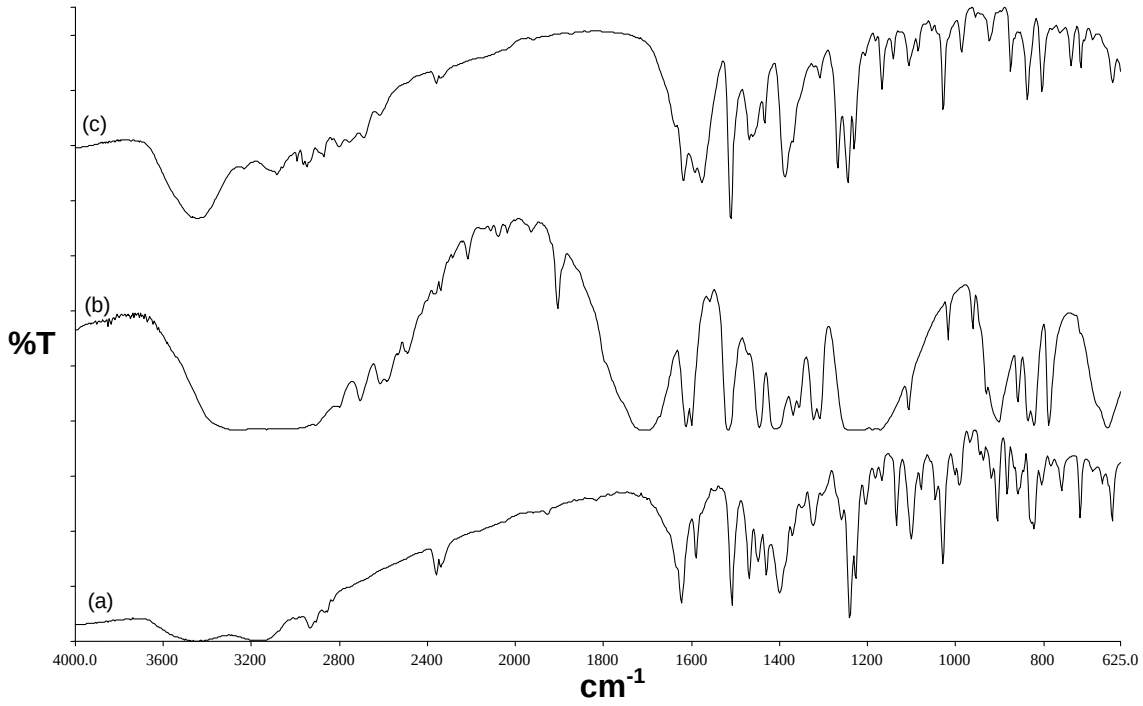

Figure 5.6.3: IR spectra (a) QUIN, (b) HPAA and (c) **$(HPAA^-)(QUIN^+)$**.

5.6.3 Powder X-ray Diffraction

The salt PXRD patterns are shown in **Figure 5.6.4**. The dry ground product did not correspond to either the physical mixture or the calculated pattern from LAZYPULVERIX.[5]

The slurry conversion experiment was performed in isopropanol and the resultant product PXRD pattern was different from the physical mixture and the calculated pattern from the salt. The exact identity of this pattern is still unknown and may be a solvate of the salt or a different form of the salt hydrate.

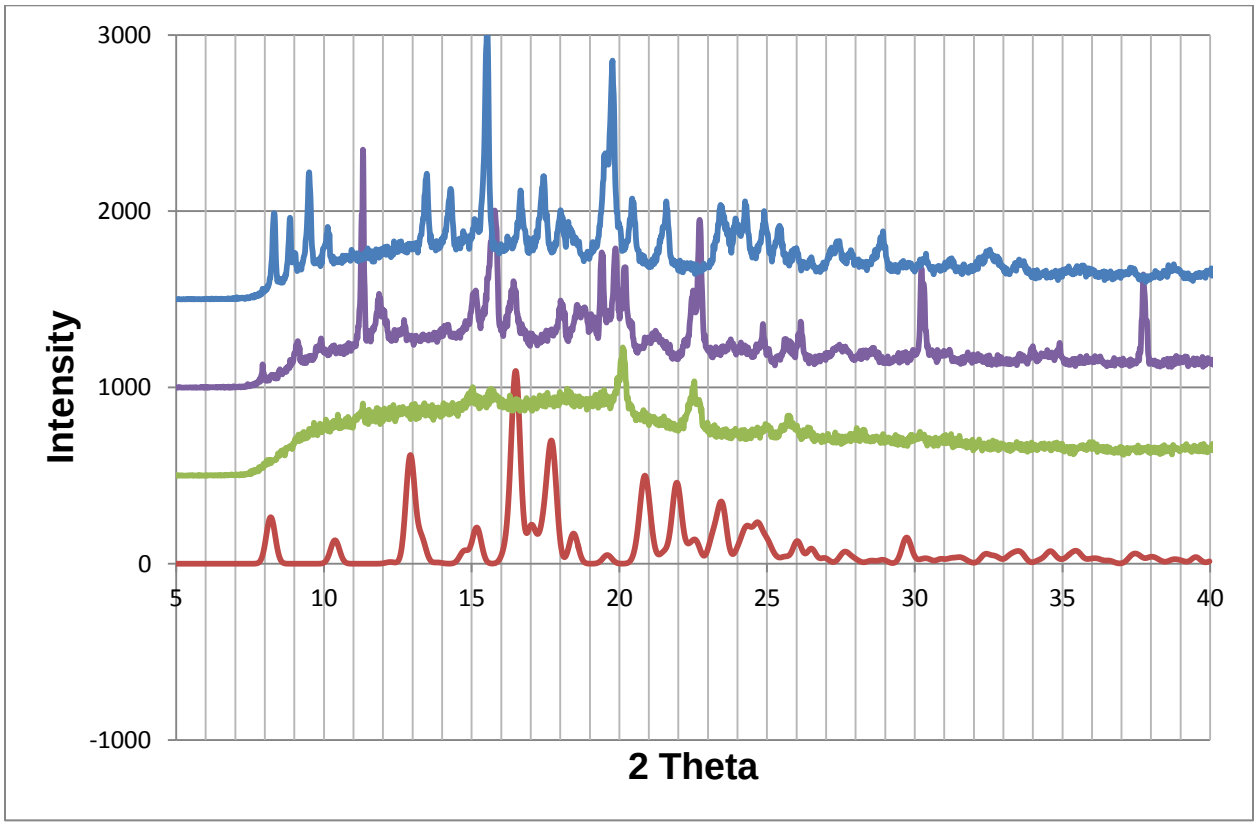

Figure 5.6.4: PXRD patterns of **(HPAA$^-$)(QUIN$^+$)** (red), ground product (green), physical mixture (purple) and slurry (blue).

5.6.5 Structure Determination

The structure was solved by direct methods and all hydrogen atoms except those from the vinyl groups were found in the subsequent difference electron density map. All non-hydrogen atoms were refined anisotropically. The final refinement converged at R_1 = 0.0404, wR_2 = 0.0887 ([I>2sigma (I)]). **Table 5.23** gives the crystal data of **$(HPAA^-)(QUIN^+)$**.

Table 5.23: Crystal data of **$(HPAA^-)(QUIN^+)$**.

Compound	**$(HPAA^-)(QUIN^+)$**
Structural Formula	$(C_8H_7O_3^-)(C_{20}H_{25}N_2O_2^+)$
$HPAA^-$:$QUIN^+$ ratio	1: 1
Molecular Mass (g mol^{-1})	476.54
Data collection temperature (K)	173(2)
Crystal system	Orthorhombic
Space group	$P2_12_12_1$
a (Å)	8.4540 (17)
b (Å)	13.900 (3)
c (Å)	21.579 (4)
α (°)	90.00
β (°)	90.00
γ (°)	90.00
Volume ($Å^3$)	2535.8 (9)
Z	4
D_c, Calculated density (g cm^{-3})	1.248
Final R indices [I>2sigma(I)]	R_1= 0.0404
	wR_2 = 0.0887
R indices (all data)	R_1 = 0.0533
	wR_2 = 0.0952
Largest diff. peak and hole (e$Å^{-3}$)	0.221; -0.151

The salt structure crystallizes in orthorhombic space group $P2_12_12_1$ with Z = 4. The asymmetric unit (**Figure 5.6.1**) consists of one ion of both compounds and the structural formula of the crystal structure is as $(C_8H_7O_3^-)(C_{20}H_{25}N_2O_2^+)$. The carboxylic group of the $HPAA^-$ acts as a proton donor with respect to the quinuclidine (N1) atom of one of the $QUIN^+$ cations. The packing diagram of the salt along [100] is illustrated in **Figure 5.6.5**.

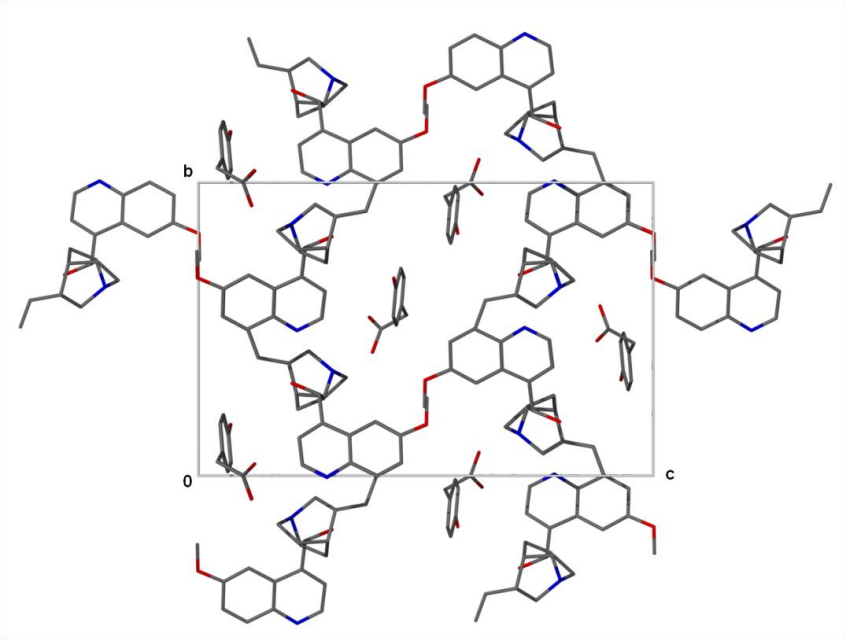

Figure 5.6.5: Crystal packing diagram of **$(HPAA^-)(QUIN^+)$** down [100].

The carboxylate group of the $HPAA^-$ anion is hydrogen bonded to the quinine cation via the nitrogen atom N2. This connection between the oxygen atom labeled O1 in carboxylate group and the protonated nitrogen gives the $^+$N1-H1. The oxygen atom O2 is hydrogen bonded to the hydroxyl group (O3-H4) of a $HPAA^-$ anion.

In addition, two $QUIN^+$ cations are linked via the O5-H5A•••N1 connection. There are two chain motifs, $C_1^1(7)$ between two $QUIN^+$ cations and $C_1^1(9)$ linking $HPAA^-$ anions. $D_3^3(14)$ and $D_3^3(16)$ motifs are between two ions of each component. The hydrogen

bonding parameters of the salt are given in **Table 5.24** and their connectivity is shown in **Figure 5.6.6**.

Table 24: Hydrogen bonding parameters of **(HPAA$^-$)(QUIN$^+$)**.

COMPOUND	D-H···A	D···A (Å)	D-H (Å)	H···A (Å)	D-H···A (º)
(HPAA$^-$)(QUIN$^+$)	N2-H1···O1[a]	2.656 (2)	1.027 (2)	1.630 (2)	176 (2)
	O5-H5A···N1 [a]	2.722 (2)	0.965 (3)	1.758 (3)	178 (2)
	O3-H4···O2 [b]	2.624 (2)	0.906 (3)	1.720 (3)	175 (3)

a = -x+2, y+1/2, -z +1/2; b = x+1, y, z

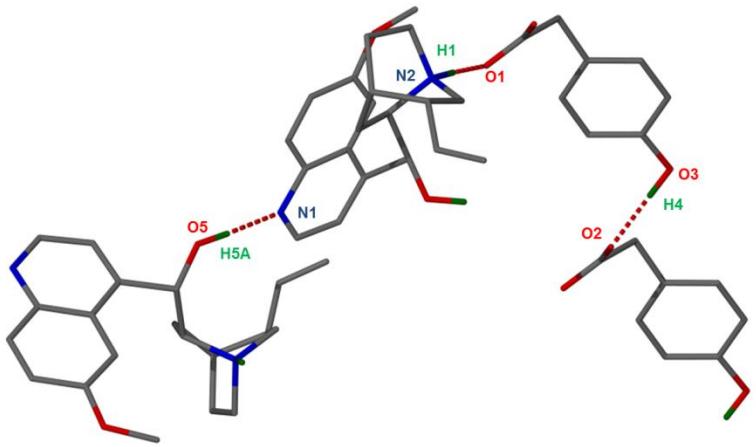

Figure 5.6.6: Hydrogen bonding in **(HPAA$^-$)(QUIN$^+$)**.

5.7 Selectivity Experiment

A selectivity experiment was performed by preparing two set of ratios. A 1: 1: 1 co-crystallization of HPAA: QUIN: QUID and a 2: 1: 1 ratio of the same compounds. In this experiment, 50/50 (*v/v*) of hexane/acetone and 50/50 (*v/v*) hexane/ethyl methyl ketone were used as solvents. Crystals were obtained after three days and were analyzed onto the DSC and a suitable crystal was chosen a single x-ray diffraction. The compound found was **(HPAA$^-$)(QUID$^+$)•H$_2$O** due to the same unit cell dimensions.

REFERENCES

1. Allen. F.H. *Acta. Crystallogr*. 2002, B58, 380 - 388.
2. Jian-Feng. L & Guo-Liang. Z. *Acta. Crystallogr. Sect. E. Struct. Rep. Online*. 2010, 66, o1455.
3. Friščić. T & Jones. W. *Faraday. Discuss*. 2007, 136, 167 – 178.
4. Adalder. T. K, Sankali. R & Dastidar. P. *Cryst. Growth Des*. 2012, 12, 2533.
5. Yvon. K, Jeitschko. W & Parthe. E. *Appl. Crystallogr.* 1977, 10, 73 - 74.
6. Spek. A. L. PLATON: A multipurpose crystallographic tool: Version 10500: e 1980 - 2003.
7. Macrae. C. F, Eddington. P. R, McCabe. P, Pidcock. E, Shields. G. P, Taylor. R, Towler. M. & van de Streek. J. Mercury: visualization and analysis of crystal structures. *J. Appl. Crystallogr*. 2006, 39, 453 - 457.

CHAPTER 6

3-CHLORO-4-HYDROXYPHENYL ACETIC ACID CO-CRYSTALS

A Cambridge Structural Database (CSD, version 5.34, November 2012)[1] search on 3-chloro-4-hydroxyphenylacetic acid (CHPAA) shows that there are no reported structures involving this molecule.

6.1 CHPAA

Crystals of CHPAA were obtained by dissolving CHPAA in ethanol by slightly heating on a hot plate. The CHPAA asymmetric unit and thermal ellipsoid plot are shown in **Figure 6.1.1 (a)** and **(b)**.

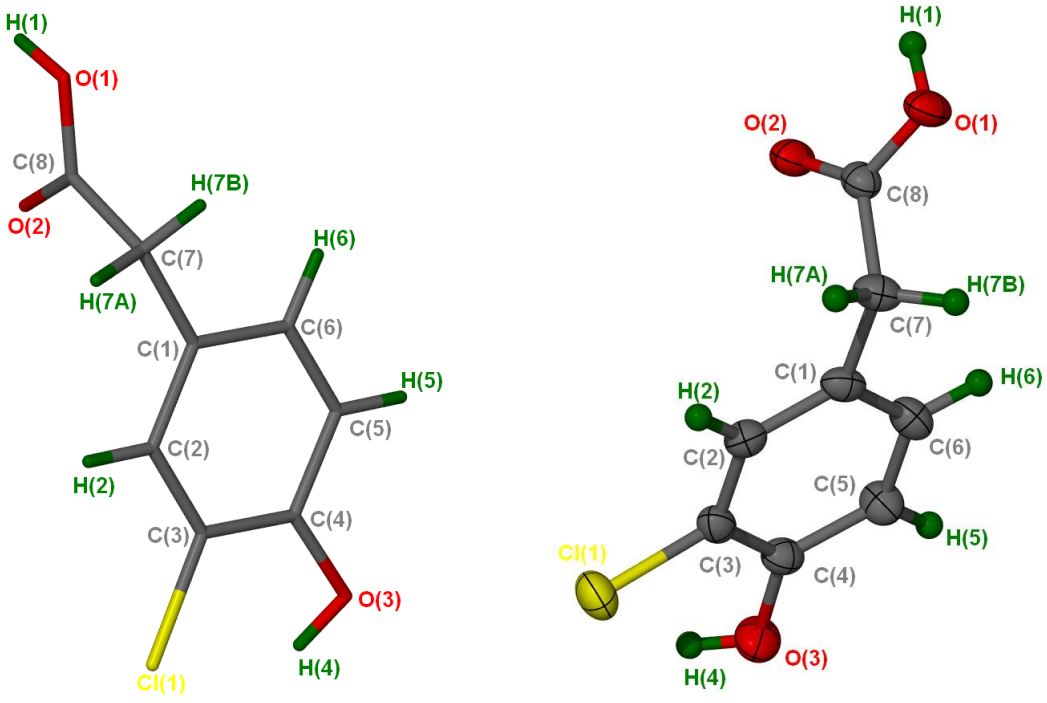

(a) **(b)**

Figure 6.1.1: (a) Asymmetric unit of **CHPAA** and **(b)** Thermal ellipsoid plot of 3-chloro-4-hydroxyphenyl acetic acid at the 50% probability level indicating the atomic numbering scheme.

6.1.1 Thermal Analysis

The pure CHPAA has a melting point of 379.3 K which is 6 K higher than the **CHPAA** crystal found in ethanol as shown in **Figure 6.1.2**. **Table 6.1** gives the thermal analysis data of **CHPAA**.

Table 6.1: Thermal analysis data of **CHPAA**.

Compounds	**DSC Endo(T_{onset},K)**
CHPAA	379.3
CHPAA pure compound	373.3

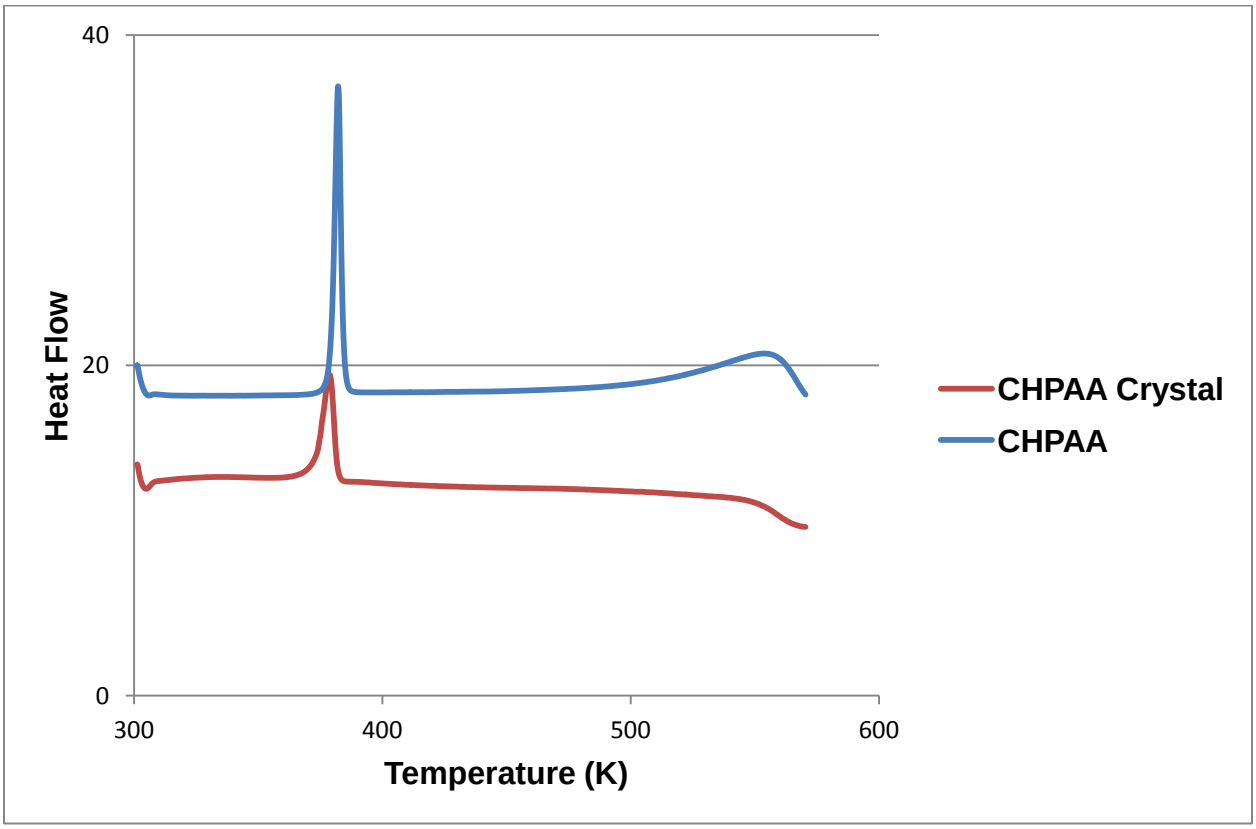

Figure 6.1.2: Thermal analysis results of **CHPAA** (red) and pure CHPAA (blue).

6.1.2 Structure Determination

The structure was solved by direct methods. Both OH hydrogens were located in the difference electron density map and refined isotropically. All other hydrogen atoms were fixed in idealized positions. All non-hydrogen atoms were refined using anisotropic thermal parameters. The refinement details of **CHPAA** are listed in **Table 6.2**.

Table 6.2: CHPAA crystal data.

Compound	**CHPAA**
Structural Formula	$C_8H_7O_3Cl$
Molecular Mass (g mol^{-1})	186.59
Data collection temperature (K)	173(2)
Crystal system	Triclinic
Space group	*P-1*
a (Å)	7.5147(15)
b (Å)	7.6302 (15)
c (Å)	7.8110 (16)
α (°)	94.87 (3)
β (°)	95.76 (3)
γ (°)	113.12 (3)
Volume ($Å^3$)	406.04 (14)
Z	2
D_c, Calculated density (g cm^{-3})	1.526
Final R indices [I>2sigma(I)]	R_1= 0.0370
	wR_2 = 0.0819
R indices (all data)	R_1 = 0.0527
	wR_2 = 0.0912
Largest diff. peak and hole ($eÅ^{-3}$)	0.249; -0.216

The CHPAA structure was solved in the triclinic space group *P-1*. The asymmetric unit contains one CHPAA molecule as illustrated in **Figure 6.1.1 (a)**. The packing diagram for the CHPAA structure along [001] is shown in **Figure 6.1.3**.

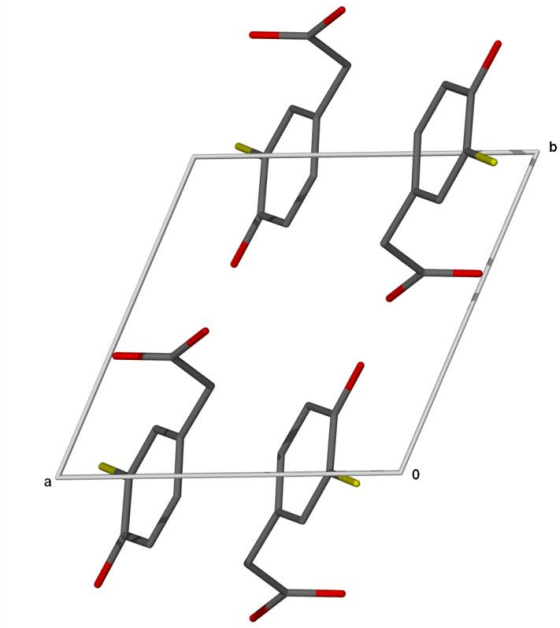

Figure 6.1.3: Crystal packing diagram of **CHPAA** along [001] with the hydrogen atoms removed.

The hydrogen bonding details are given in **Table 6.3**. The molecule has intermolecular O3-H4•••Cl1 contacts.[2-4] The hydroxyl group on CHPAA compound is connected to the oxygen atom labeled O2 of another CHPAA molecule. O2 plays the role of a bifurcated acceptor due to the fact it is hydrogen bonded to two hydrogen atoms H1 and H4. The carboxylic acid moiety of CHPAA forms a ring dimer through a homosynthon with a graph set $R_2^2(8)$. A bigger ring with a graph set $R_2^2(18)$ is obtained via the hydroxyl and the carboxylic acid group (**Figure 6.1.4**). Chain motifs involved in the crystal structure are characterized as $C_2^1(11)$, $C_2^2(13)$ and $C_4^3(24)$.

Table 6.3: CHPAA hydrogen bonding parameters.

COMPOUND	D-H···A	D···A (Å)	D-H (Å)	H···A (Å)	D-H···A (º)
CHPAA	O1-H1···O2[a]	2.669 (2)	0.875 (3)	1.797 (3)	174 (2)
	O3-H4···O2 [b]	2.847 (2)	0.841 (3)	2.146 (3)	141 (2)

a = -x, -y+1, -z + 2; b = -x, -y+2, -z+1

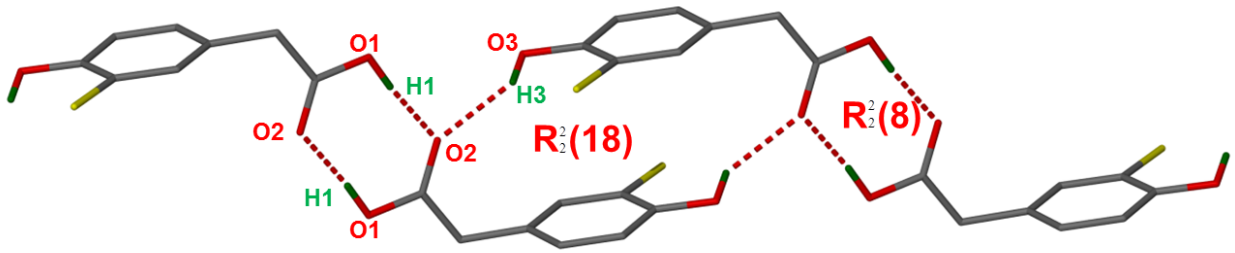

Figure 6.1.4: Connectivity in **CHPAA**.

6.2 CHPAA and acridine (CHPAA•ACRI)

The acid: base (1: 1) combination was dissolved in diethyl ether by heating the mixture on a hot plate. The solution was allowed to evaporate at room temperature and crystals were obtained after a few days.

The asymmetric unit of the co-crystal is illustrated in **Figure 6.2.1**.

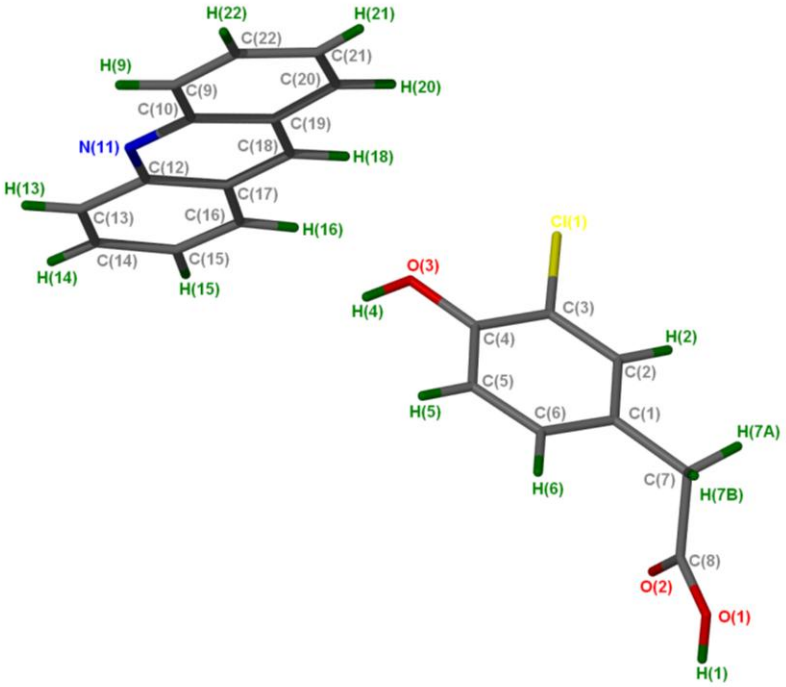

Figure 6.2.1: Asymmetric unit of **CHPAA•ACRI** with all the hydrogen atoms shown for numbering clarity.

6.2.1 Thermal Analysis

The melting point of the **CHPAA•ACRI** co-crystal is higher than both pure components as given in **Table 6.4**; therefore, there is an increase of the thermal stability of the co-crystal. [5] The DSC curves of the acid: base combination is shown in **Figure 6.2.2**.

Table 6.4: Thermal analysis data of **CHPAA•ACRI**.

Compounds	**DSC Endo$_1$(T_{onset},K)**	**DSC Endo$_2$(T_{onset},K)**
Acridine	363.5	375.8
CHPAA	-	379.3
CHPAA•ACRI	-	402.3

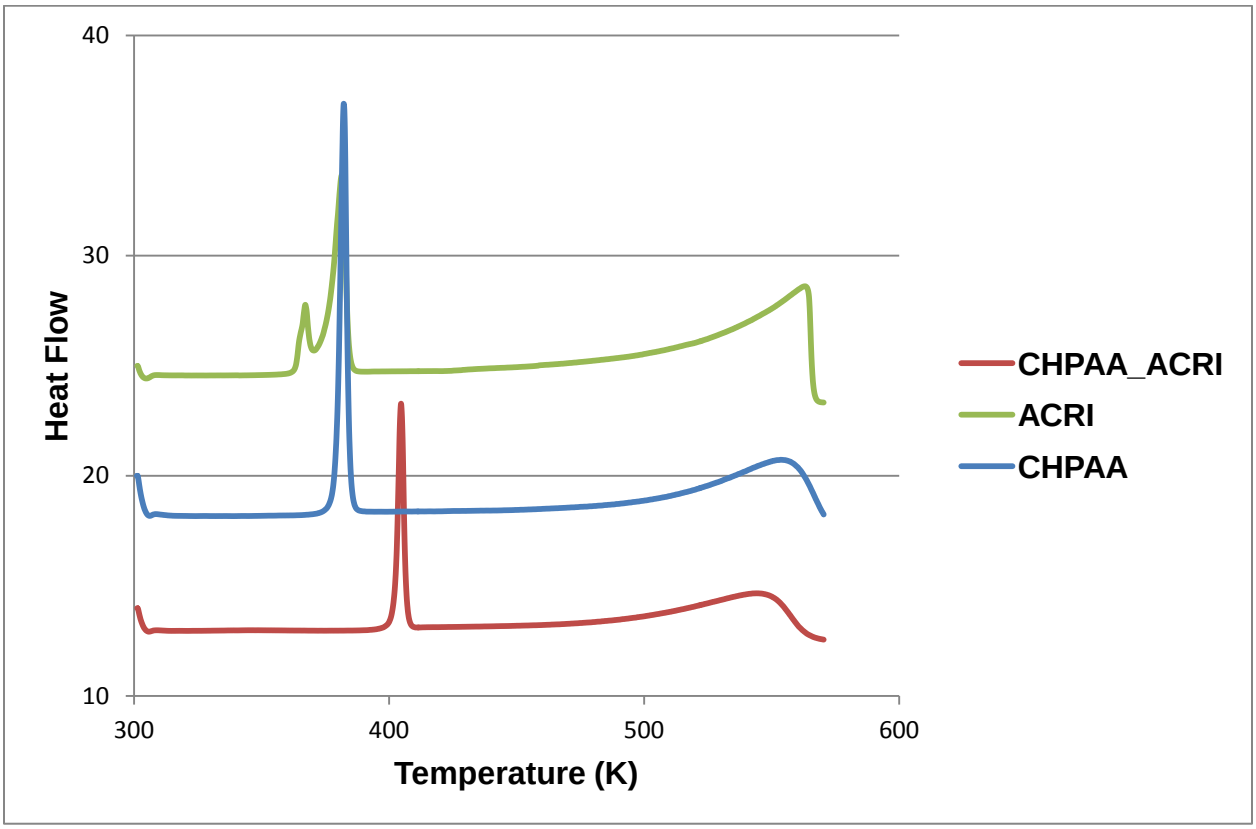

Figure 6.2.2: DSC curves of **CHPAA•ACRI** (red), CHPAA (blue) and acridine (green).

6.2.2 IR Spectroscopy

The **CHPAA•ACRI** IR spectrum as illustrated in **Figure 6.2.3.** There is confirmation of the formation of a new compound due to the new band at 3110 cm^{-1} indicating hydrogen bonded OH stretch mode. The peak at 1708 and 1613 cm^{-1} in the co-crystal spectrum can be attributed to the C=O stretch. IR results are listed in **Table 6.5**.

Table 6.5: IR positions and assignments for the peaks in CHPAA, **CHPAA•ACRI** and ACRI.

CHPAA	**CHPAA•ACRI**	ACRI	Proposed assignment
3449, 3103	3110	-	OH stretch
2923, 2749	2919	3051	Aromatic ring stretch
1873	1870	2285, 1815	Overtone or combination bands
1703, 1614	1708, 1613	-	C=O
1577, 1500, 1423	1563, 1518, 1464, 1423	1617,1461, 1437	C=C stretch
1295, 1257	1293, 1247	-	C-O stretch

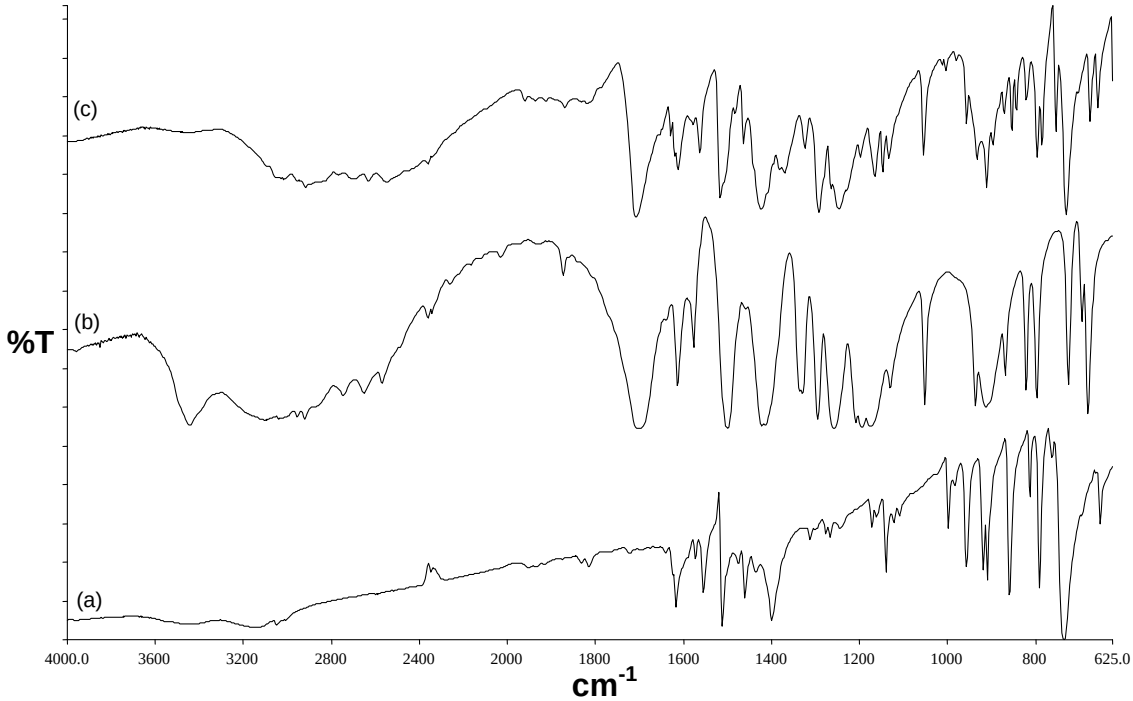

Figure 6.2.3: IR spectrum of (a) Acridine, (b) CHPAA and (c) **CHPAA•ACRI**.

6.2.3 Powder X-ray Diffraction

The neat grinding experiment was unsuccessful; its PXRD pattern (**Figure 6.2.4**) did not match the pattern of the co-crystal. The slurry conversion product pattern performed in diethyl ether did not match both the physical mixture and the calculated pattern obtained from LAZYPULVERIX.[6] The PXRD pattern contained some peaks found in the physical mixture.

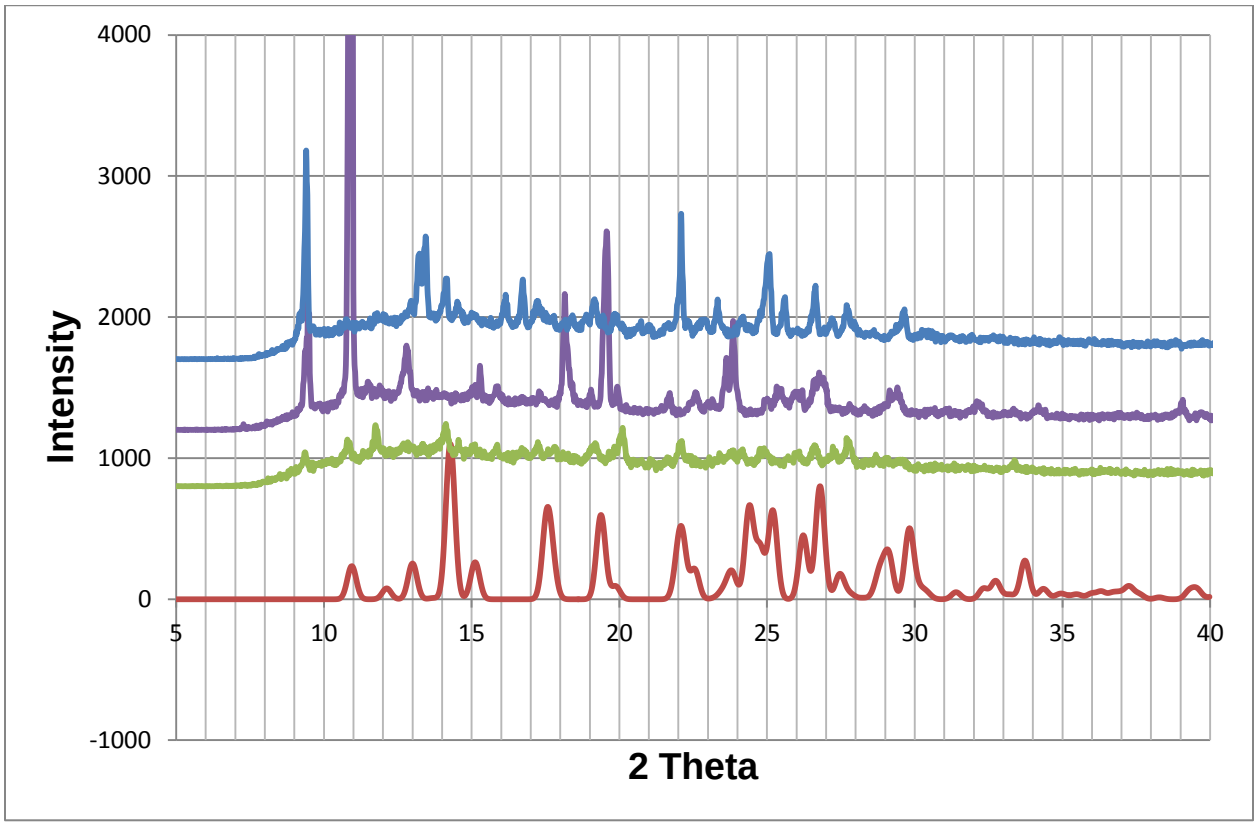

Figure 6.2.4: PXRD patterns of **CHPAA•ACRI** (red), ground product (green), physical mixture (purple) and slurry (blue).

6.2.4 Structure Determination

The crystal that was used for the data collection had approximate dimensions of 0.07 x 0.20 x 0.39 mm. The structure was solved using direct methods and all the hydrogen

atoms were found in the difference electron density map. The crystal data of the structure is given in **Table 6.6**.

Table 6.6: CHPAA•ACRI crystal data.

Compound	**CHPAA•ACRI**
Structural Formula	$C_8H_7O_3Cl•C_{13}H_9N$
CHPAA:ACRI ratio	1: 1
Molecular Mass (g mol^{-1})	365.81
Data collection temperature (K)	173(2)
Crystal system	Triclinic
Space group	*P-1*
a (Å)	7.3891(5)
b (Å)	8.5830 (6)
c (Å)	14.256 (9)
α (°)	72.730 (2)
β (°)	87.9130 (10)
γ (°)	81.0200 (10)
Volume ($Å^3$)	852.71 (10)
Z	2
D_c, Calculated density (g cm^{-3})	1.425
Final R indices [I>2sigma(I)]	R_1= 0.0377
	wR_2 = 0.0922
R indices (all data)	R_1 = 0.0509
	wR_2 = 0.0994
Largest diff. peak and hole ($eÅ^{-3}$)	0.282; -0.243

The assignment of *P-1* as space group results from successful solution of the structure with Z = 2. There are face-to-face π-π stacking interactions between acridine aromatic rings with a minimum distance of 3.742 Å. The pyridine ring is planar with a C10-N11-C12 bond angle of 118. 6 º is 1.6 ° larger than those pyridine compounds (~ 117 º).

This can be caused by the stronger interaction between (H4) and (N11) atoms in hydrogen bond. The packing diagram of the co-crystal along [010] is shown in **Figure 6.2.5**.

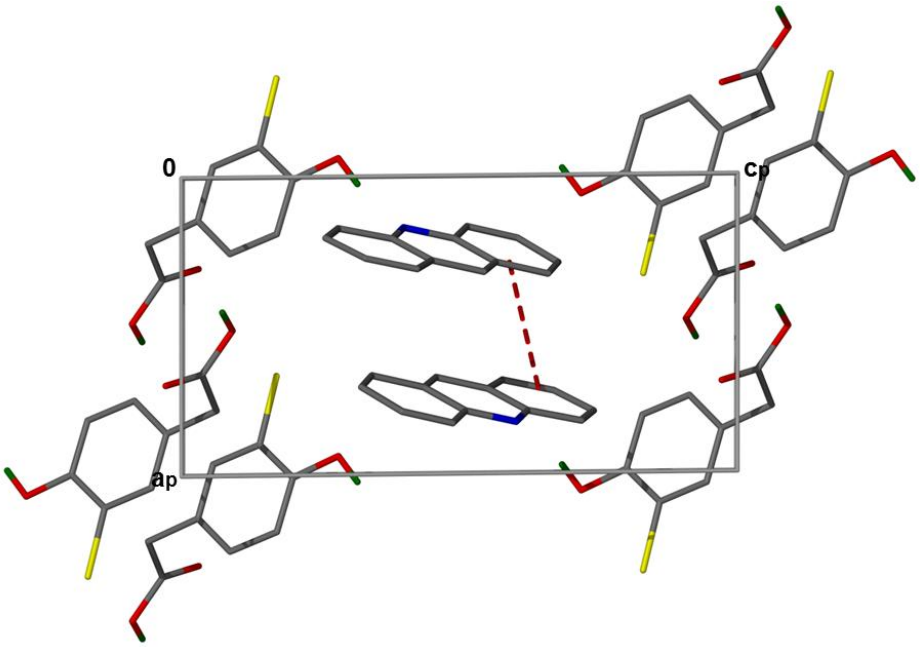

Figure 6.2.5: Crystal Packing diagram of **CHPAA•ACRI** with the hydrogen atoms removed down [010].

CHPAA molecules are linked by means of O-H•••O hydrogen bonds with O•••O distance of 2.669 (2) Á. This forms a ring dimer of the carboxylic group in CHPAA with a graph set of $R_2^2(8)$ as shown in **Figure 6.2.6**. O-H•••N hydrogen bond between the hydroxyl group of CHPAA and the nitrogen atom on an aromatic six-membered ring in the acridine is observed with two graph sets $D_1^1(2)$ and $D_3^3(21)$. **Table 6.7** gives hydrogen bonding parameters of **CHPAA•ACRI**.

Table 6.7: CHPAA•ACRI hydrogen bonding parameters.

COMPOUND	D-H···A	D···A (Å)	D-H (Å)	H···A (Å)	D-H···A (º)
CHPAA•ACRI	O3-H4···N11[a]	2.718 (2)	0.901 (2)	1.824 (2)	171 (2)
	O1-H1···O2 [b]	2.669 (2)	0.847 (2)	1.825 (2)	174 (2)

a = -x, -y+2, -z + 1; b = -x-1, -y, -z+2

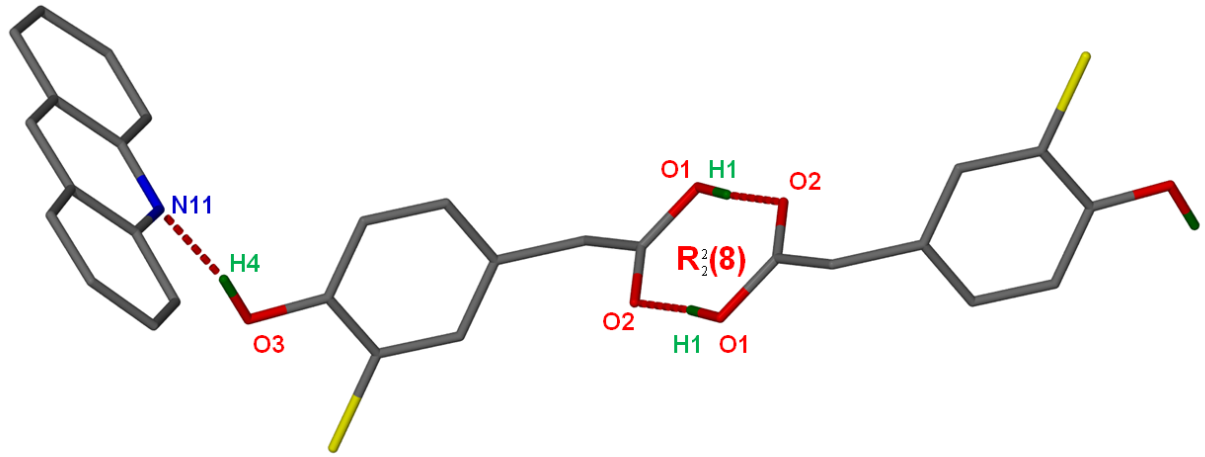

Figure 6.2.6: Hydrogen bonding in **CHPAA•ACRI**.

REFERENCES

1. Allen. F.H. *Acta. Crystallogr*. 2002, B58, 380 - 388.
2. Otwinowski. Z & Minor. W, Inc: Carter. W. Jr., Sweet RM (eds). Methods in enzymology macromolecular crystallography, part A, vol 276. Academic Press, New York. 1997, 307.
3. Taylor. R & Kennard. O. *J. Am. Chem. Soc*. 1982, 104, 5063 – 5070.
4. Lommerse. J. P. M, Stone. A. J, Taylor. R & Allen. F. H. *J. Am. Chem. Soc*. 1996, 118, 3108 – 3116.
5. Chang. C-H, Yang. D. S. C, Yoo. C. S, Wang. B-C, Pletcher. J, Sax. M & Terrence. C. F. *Acta. Crystallogr. B38*. 1982, 2065 – 2067.
6. Yvon. K, Jeitschko. W & Parthe. E. *Appl. Crystallogr.* 1977, 10, 73 - 74.

CHAPTER 7

HYDROXYCINNAMIC ACID CO-CRYSTALS AND SALT HYDRATES

Caffeic acid (CFA), *p*-coumaric acid (*p*CA) and *trans*-ferulic acid (*t*FER) are the nutraceutical compounds studied in this chapter.

A search of the Cambridge Structural Database[1] (CSD, version 5.34, November 2012) revealed only one co-crystal structure of caffeic acid (CFA) with nicotinamide.[2]

However, *p*-coumaric acid (*p*CA) has formed a co-crystal with caffeine[3], two co-crystals with theophylline[3] and a co-crystal hydrate with caffeine [3] according to the CSD.

Trans-ferulic acid (*t*FER) on another hand formed co-crystals with 3, 5-dinitrobenzoic acid and isonicotinamide,[4] 2, 3, 5, 6-tetramethylpyrazine,[5] a hemihydrate with baclofen,[6] and a monohydrate with isonicotinamide and nicotinamide.[2]

7.1 Caffeic acid with Isonicotinamide

The co-crystal was obtained by dissolving a 1: 1 ratio of caffeic acid and isonicotinamide in acetone by slightly heating the solution on a hot plate. Block-like crystals were obtained the same day having a 1: 3 ratio (**CFA•3INM**). The asymmetric unit of the **CFA•3INM** is illustrated in **Figure 7.1.1**.

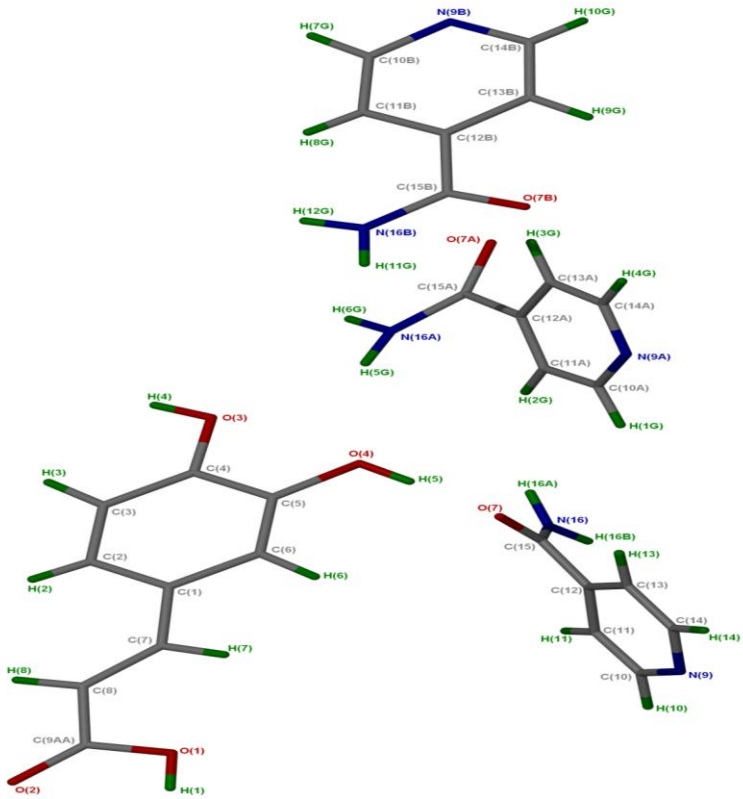

Figure 7.1.1: Asymmetric unit of **CFA•3INM** with all the hydrogen atoms shown.

7.1.1 Thermal Analysis

The thermal analysis data is listed in **Table 7.1** and the resultant DSC curves are shown in **Figure 7.1.2**. The melting point of the **CFA•3INM** co-crystal is lower than both starter materials; therefore there is a decrease in thermal stability of the co-crystal.

Table 7.1: Thermal analysis data of **CFA•3INM**.

Compounds	**DSC Endo$_1$(T_{onset},K)**	**DSC Endo$_2$(T_{onset},K)**
Isonicotinamide	382.1	428.4
CFA	-	490.2
CFA•3INM	-	420.3

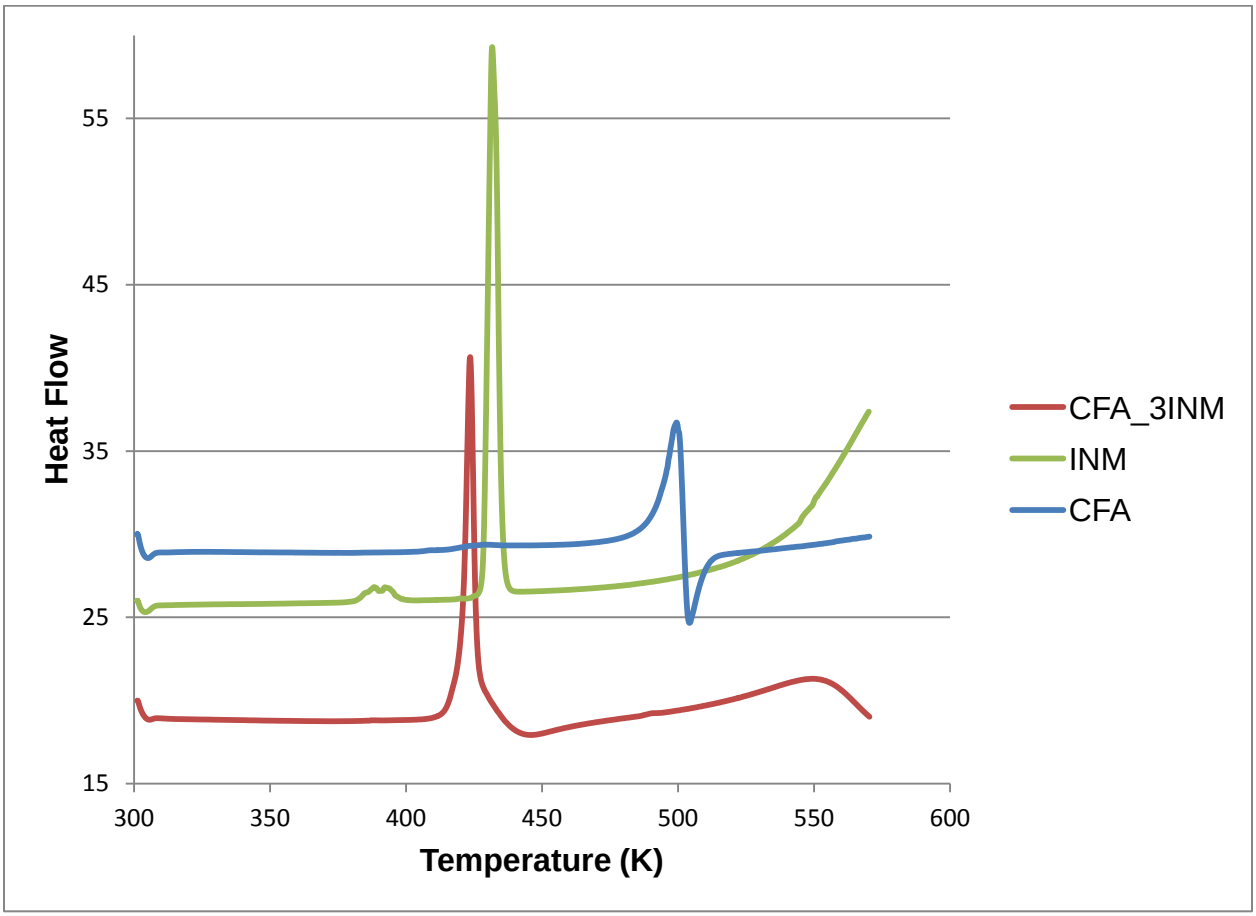

Figure 7.1.2: DSC curves of **CFA•3INM** (red), isonicotinamide (green) and caffeic acid (blue).

7.1.2 Structure Determination

Single crystal X-ray diffraction measurements of the 1:3 co-crystal of caffeic acid and isonicotinamide were refined using SHELXL-97.[7] Direct methods were used for primary atom site locations and secondary atom site locations were found from the difference electron density map. The crystal data is given in **Table 7.2**.

Table 7.2: Crystal data of the 1:3 co-crystal of caffeic acid and isonicotinamide (**CFA•3INM**).

Compound	**CFA•3INM**
Structural Formula	$C_9H_8O_4$•$3C_6H_6N_2O$
CFA:INM ratio	1: 3
Molecular Mass (g mol^{-1})	546.54
Data collection temperature (K)	173(2)
Crystal system	Triclinic
Space group	*P-1*
a (Å)	8.8282 (18)
b (Å)	9.6946 (19)
c (Å)	15.702 (3)
α (°)	78.60 (3)
β (°)	74.27 (3)
γ (°)	74.27 (3)
Volume ($Å^3$)	1233.9 (4)
Z	2
D_c, Calculated density (g cm^{-3})	1.471
Final R indices [I>2sigma(I)]	R_1= 0.0481
	wR_2 = 0.1400
R indices (all data)	R_1 = 0.0609
	wR_2 = 0.1708
Largest diff. peak and hole ($eÅ^{-3}$)	0.415; -0.403

The 1: 3 molar ratio co-crystal crystallized in the triclinic system, space group *P-1* with four molecules in the asymmetric unit. The packing diagrams are represented in **Figure 7.1.3 (a)** and **(b)**.

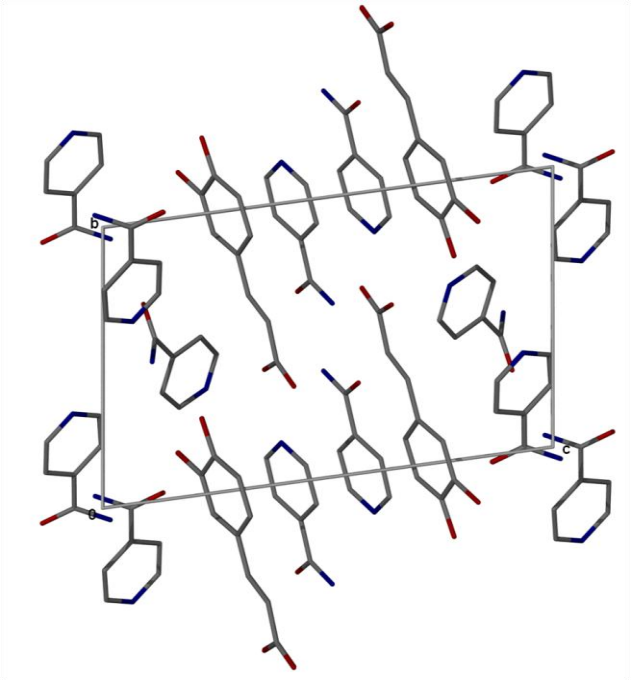

(a)

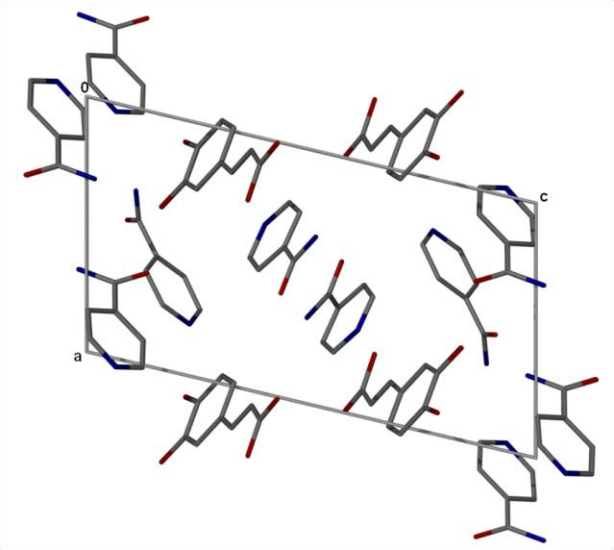

(b)

Figure 7.1.3: Packing diagram of **CFA•3INM (a)** down [100] and **(b)** down [010].

Two INM molecules form a hydrogen bonded ring, $N_1 = R_2^2(8)$. The phenolic OH groups of caffeic acid form weak hydrogen bonds, [N16A-H5G•••O3 = 3.349 (2) Å, N16A-H5G-

O3 = 145 (0) ° and N16A-H5G•••O4 = 3.162 (2) Å, N16A-H5G-O4 = 154 (0) °] with the nitrogen atom of the second INM molecule. The carboxylic acid OH group forms strong hydrogen bonds with the nitrogen atom of the second INM molecule, [O1-H1•••N9B = 2.498 (2) Å and O1-H1-N9B = 175 (3) °]. The carboxylic acid carbonyl group forms moderate hydrogen bonds, [N16B-H12G•••O2 = 2.880 (2) Å and N16B-H12G-O2 = 171 (2) °] with the nitrogen atom of the third INM molecule.

The connectivity of N16B-H11G•••O7B in the crystal structure repeats itself and forms a ring. There is a strong hydrogen bonding formation between one of the phenolic OH groups of the caffeic acid, [O4-H5•••O7 = 2.385 (2) Å and O4-H5-O7 = 176 (3) °] and the carbonyl group of the first INM molecule. The other phenolic OH group of the CFA is strongly hydrogen bonded to the nitrogen atom in the second INM molecule, [O3-H4•••N9A = 2.455 (2) Å and O3-H4-N9A = 159 (2) °]. The hydrogen bonding in the crystal structure can be described using several graph sets. These sets[8] are complex because of the three INM molecules in the asymmetric unit and are listed as:

- $N_1 = D_1^1(2)$.
- $N_1 = R_2^2(8)$.
- $N_2 = D_2^2(6)$, $D_2^2(8)$, $D_2^2(9)$, $D_2^2(11)$, $D_2^2(12)$, $D_2^2(13)$, $D_3^3(9)$ and $D_3^3(15)$.
- $N_2 = R_4^4(22)$.

The hydrogen bonding details of the co-crystal are listed in **Table 7.3** and the connectivity of **CFA•3INM** down [100] and down [010] is illustrated in **Figure 7.1.4 (a)** and **(b)** respectively.

Table 7.3: Hydrogen bonding parameters in **CFA•3INM**.

COMPOUND	D-H···A	D···A (Å)	D-H (Å)	H···A (Å)	D-H···A (º)
CFA•3INM	N16A-H5G···O4	3.162 (2)	0.886 (1)	2.342 (1)	154 (1)
	N16A-H5G···O3	3.349 (2)	0.886 (1)	2.585 (1)	145 (1)
	N16B-H11G···O7B[a]	2.782 (2)	0.835 (3)	1.952 (3)	172 (3)
	N16A-H6G···N9[b]	2.793 (3)	0.874 (3)	1.931 (3)	169 (2)
	N16B-H12G···O2[c]	2.880 (2)	0.879 (3)	2.008 (3)	171 (2)
	O3-H4···N9A[d]	2.455 (2)	0.872 (3)	1.622 (3)	159 (2)
	O1-H1···N9B[e]	2.498 (2)	0.820 (3)	1.680 (3)	175 (3)
	O4-H5···O7	2.385 (2)	0.842 (3)	1.545 (3)	176 (3)
	N16-H16A···O7A[f]	2.557 (2)	0.837 (3)	1.781 (3)	153 (3)

a = -x+1, -y+1, -z +1; b = x-1, y+1, z; c = -x, -y, -z+1; d = x-1, y, z; e=x, y-2, z; =-x+1, -y+1, -z

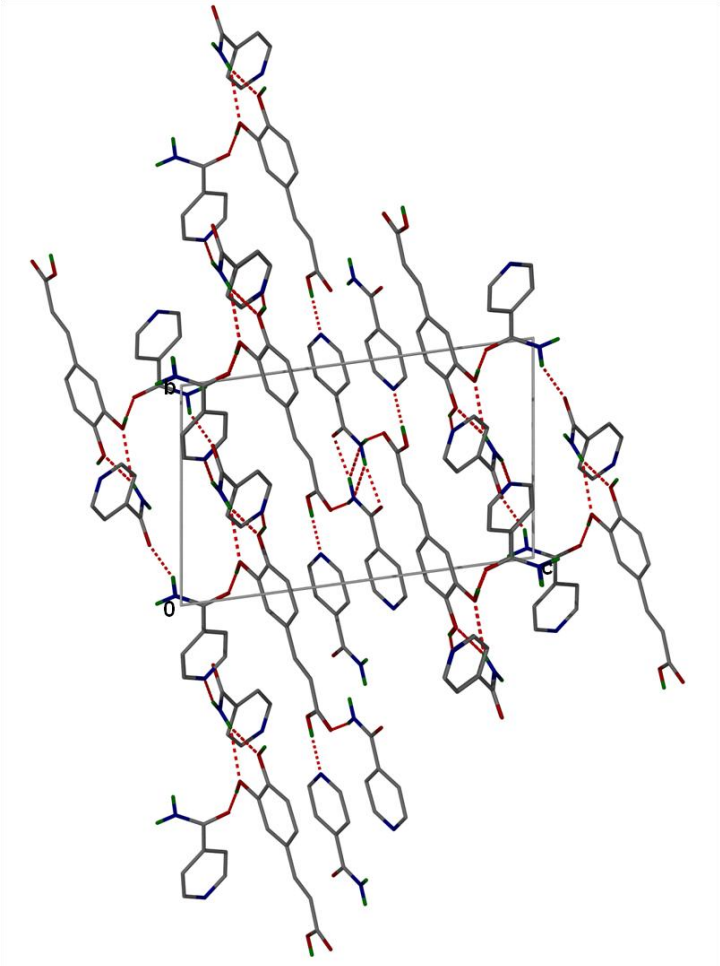

(a)

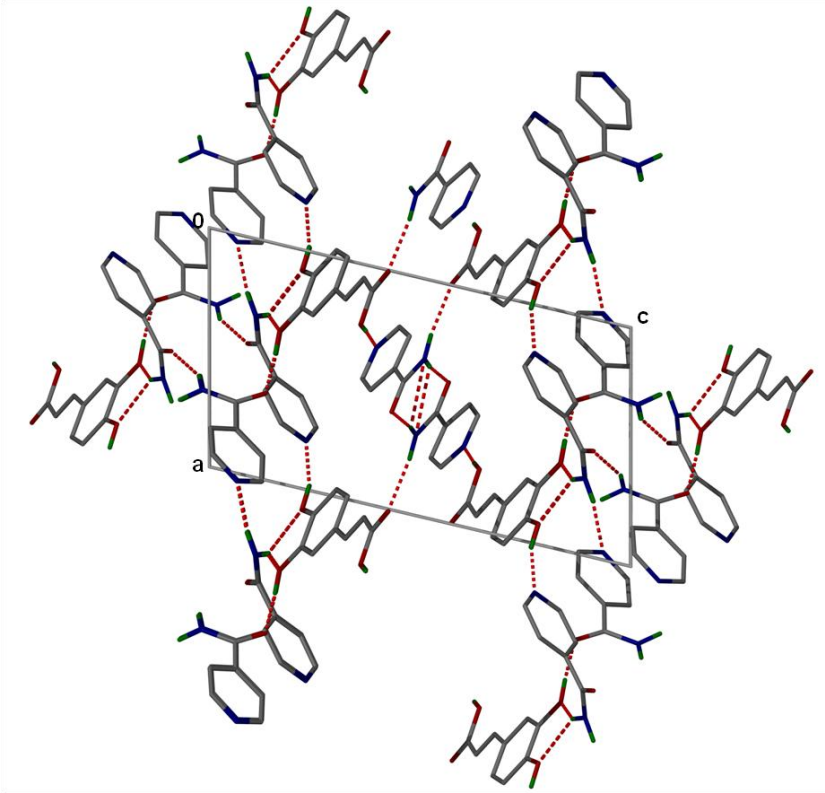

(b)

Figure 7.1.4: Connectivity in **CFA•3INM (a)** down [100] and **(b)** down [010]**.**

7.2 *p*-Coumaric acid and nicotinamide (*p*CA•NAM)

A 1: 1 molar ratio of both components was dissolved in acetone by heating the mixture on a hot plate. The solution was allowed to evaporate and crystals were obtained after four days. Similar crystals were obtained upon dissolution of the same molar ratio in ethyl methyl ketone. The asymmetric unit of ***p*CA•NAM** is shown in **Figure 7.2.1**. This structuture has already been reported by McClurg *et al*.[9]

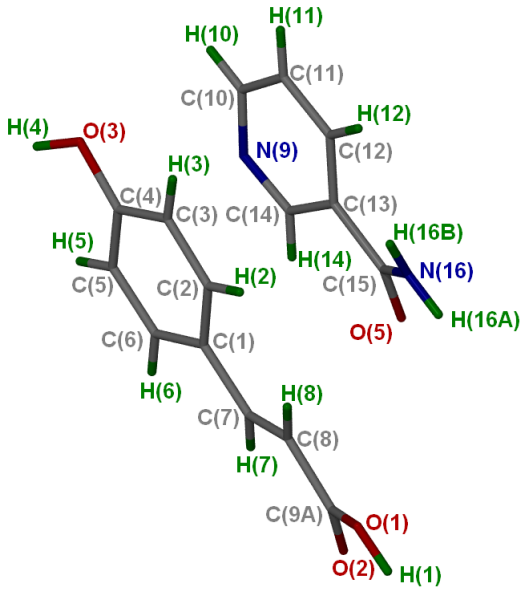

Figure 7.2.1: ***p*CA•NAM** asymmetric unit with all the hydrogen atoms shown for numbering clarity.

7.2.1 Thermal Analysis

The ***p*CA•NAM** co-crystal has a higher melting point than nicotinamide and lower than *p*-coumaric acid. The melting points of the co-crystal, nicotinamide and *p*-coumaric acid are listed in **Table 7.4**. The DSC curves of the individual components and the obtained co-crystal are shown in **Figure 7.2.2**.

Table 7.4: Thermal analysis data of ***p*CA•NAM**.

Compounds	**DSC Endo$_1$(T_{onset},K)**
Nicotinamide	401.6
p-coumaric acid	493.2
***p*CA•NAM**	432.7

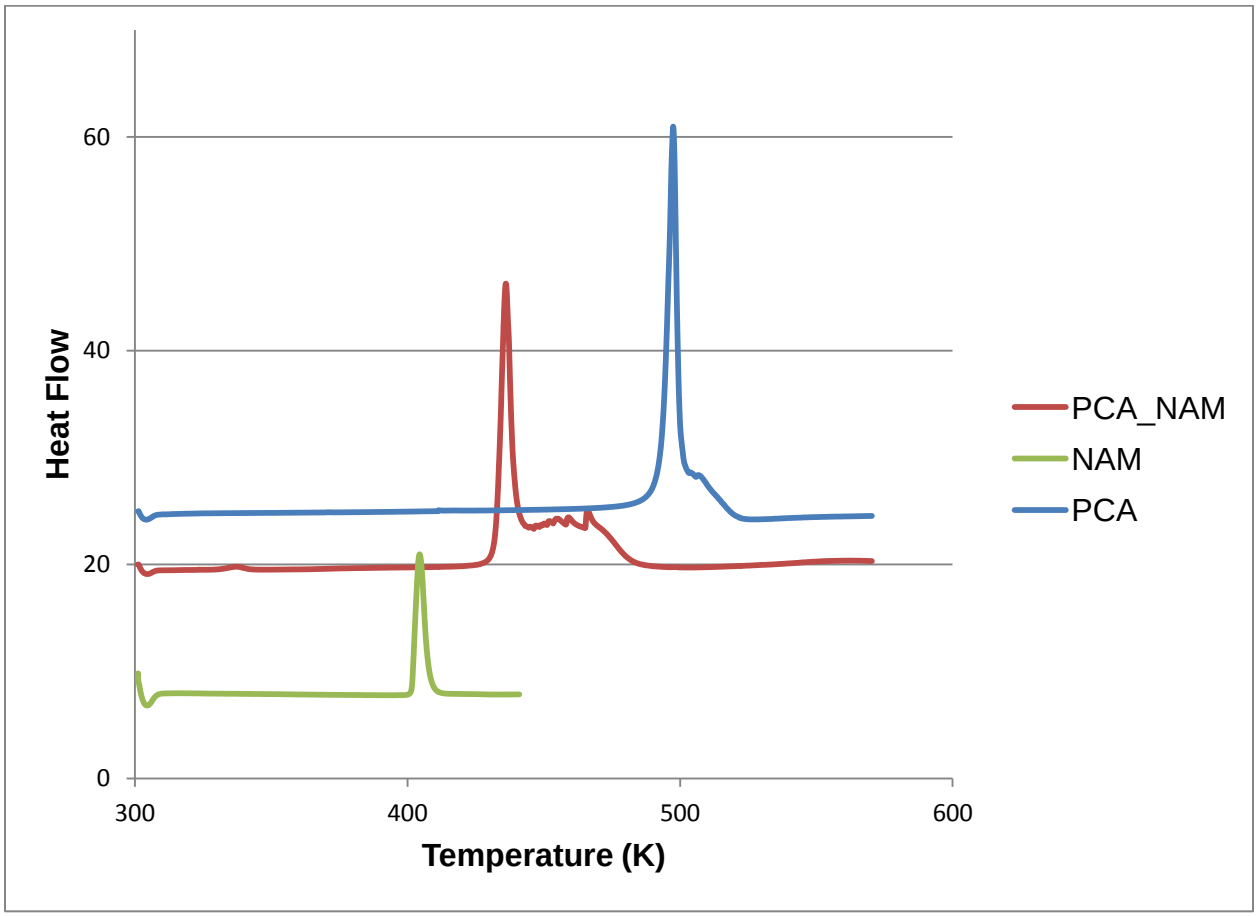

Figure 7.2.2: DSC curves of ***p*CA•NAM** (red), nicotinamide (green) and *p*-coumaric acid (blue).

7.2.2 Structure Determination

The structure was solved by direct methods without incident. Unless otherwise noted, coordinates of all –OH and –NH hydrogens were refined. All other hydrogens were riding in idealized positions. Unless otherwise noted, all non-hydrogen atoms were refined using anisotropic thermal parameters. Refinement details for the co-crystal are listed in **Table 7.5**.

Table 7.5: Crystal data of ***p*CA•NAM**.

Compound	***p*CA•NAM**
Structural Formula	$C_9H_8O_3$•$C_6H_6N_2O$
*p*CA: NAM ratio	1: 1
Molecular Mass (g mol^{-1})	286.29
Data collection temperature (K)	296 (2)
Crystal system	Monoclinic
Space group	$P2_1/c$
a (Å)	15.6003 (17)
b (Å)	6.3227 (7)
c (Å)	14.2456 (15)
α (°)	90.00
β (°)	106.309 (3)
γ (°)	90.00
Volume ($Å^3$)	1348.6 (3)
Z	4
D_c, Calculated density (g cm^{-3})	1.410
Final R indices [I>2sigma(I)]	R_1= 0.0392
	wR_2 = 0.0942
R indices (all data)	R_1 = 0.0525
	wR_2 = 0.1024
Largest diff. peak and hole ($eÅ^{-3}$)	0.268; -0.223

Unit cell parameter of ***p*CA•NAM** were previously reported.[9]

The co-crystal crystallized in a 1: 1 molar ratio, monoclinic space group $P2_1/c$ with Z = 4. The asymmetric unit contains one molecule of each component (**Figure 7.2.1**). The packing diagram of ***p*CA•NAM** running along [010] is shown in **Figure 7.2.3**.

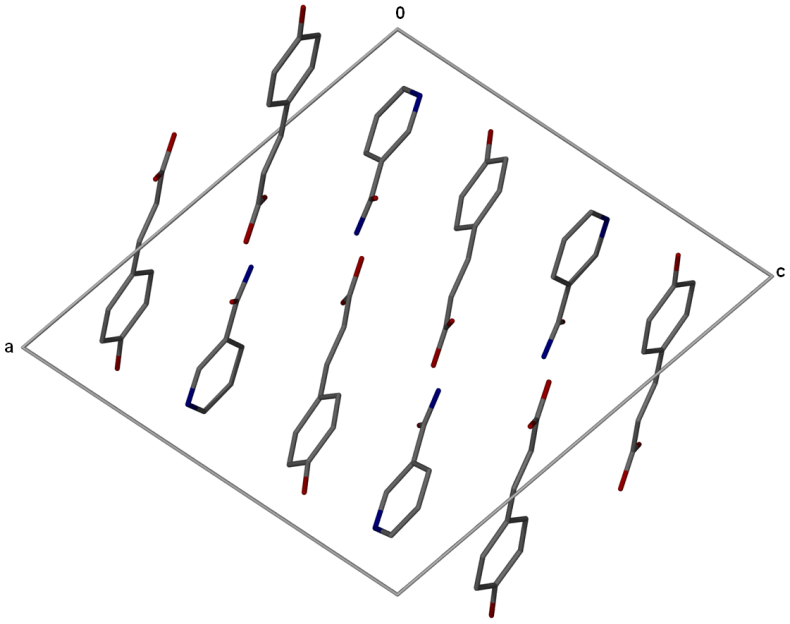

Figure 7.2.3: Crystal packing diagram of ***p*CA•NAM** down [010].

In the crystal structure, the hydrogen bond diagram is generated as shown in **Figure 7.2.4** forming two chains $C_2^2(6)$ and $C_2^2(16)$. The $C_2^2(6)$ motif is through O_1-H_1•••O_5 and along the carbonyl, nitrogen and the hydrogen atom attached to it in the nicotinamide molecule.

The second chain $C_2^2(16)$ is along the OH•••N and NH•••O hydrogen bonds respectively. The phenol moiety of *p*-coumaric acid forms an O–H•••N (O3–N9, 2.704 (2) Å) hydrogen bond with the nitrogen atom of nicotinamide, while the hydroxyl moiety forms an O–H•••O (O1–O5, 2.544 (1) Å) hydrogen bond with the carbonyl group of the nicotinamide molecule and the carboxylic acid group forms an N–H•••O (N16–O2, 2.910 (2) Å) hydrogen bond with the nitrogen atom of the nicotinamide.

This connectivity between the carboxylic acid, hydroxyl moieties of *p*-coumaric acid , the carbonyl group and the nitrogen atom including one of the hydrogen atom attached to it in the nicotinamide molecule form a ring motif $R_2^2(8)$.

The planar assembly similar to the hydrogen bonding network observed in a reported cocrystal of nicotinamide and 4-hydroxybenzoic acid[10] gives rise to alternating wave-like, one-dimensional strands (**Figure 7.2.5**). **Table 7.6** summarises the hydrogen bonding parameters in ***p*CA•NAM**.

Table 7.6: Hydrogen bonding parameters in ***p*CA•NAM**.

COMPOUND	D-H···A	D···A (Å)	D-H (Å)	H···A (Å)	D-H···A (º)
***p*CA•NAM**	N16-H16A···O2[a]	2.910 (2)	0.917 (2)	2.006 (2)	168 (2)
	N16-H16B···O1 [b]	2.957 (2)	0.878 (2)	2.104 (2)	164 (2)
	O3-H4···N9 [c]	2.704 (2)	0.913 (2)	1.824 (2)	161 (2)
	O1-H1···O5 [a]	2.544 (1)	0.938 (2)	1.623 (2)	166 (2)

a = -x+1, -y+1, -z + 1; b = -x+1, -y+2, -z+1; c = -x, y+1/2, -z+1/2

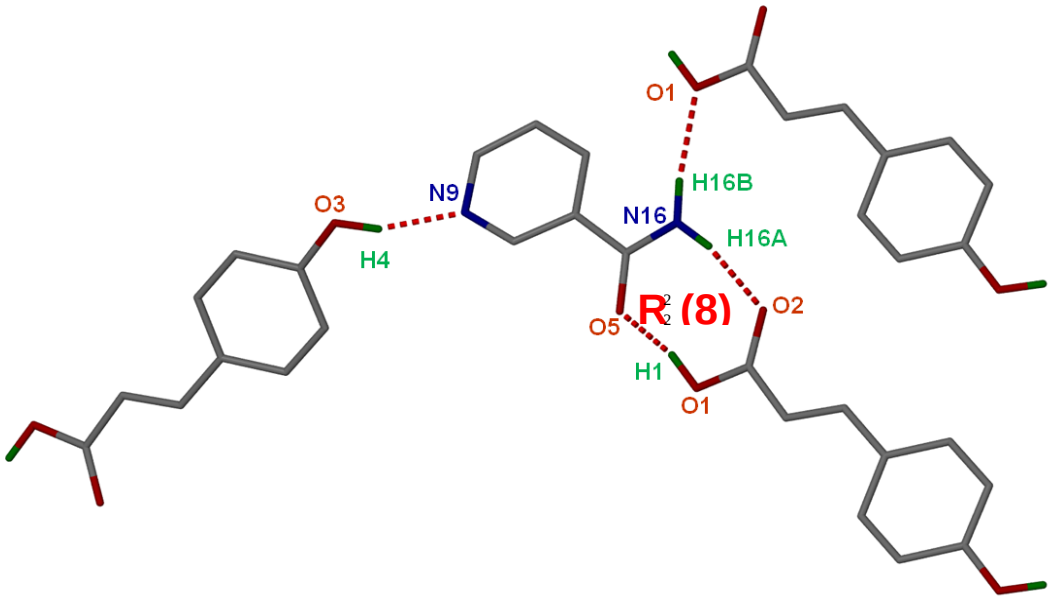

Figure 7.2.4: Hydrogen bonding in ***p*CA•NAM**.

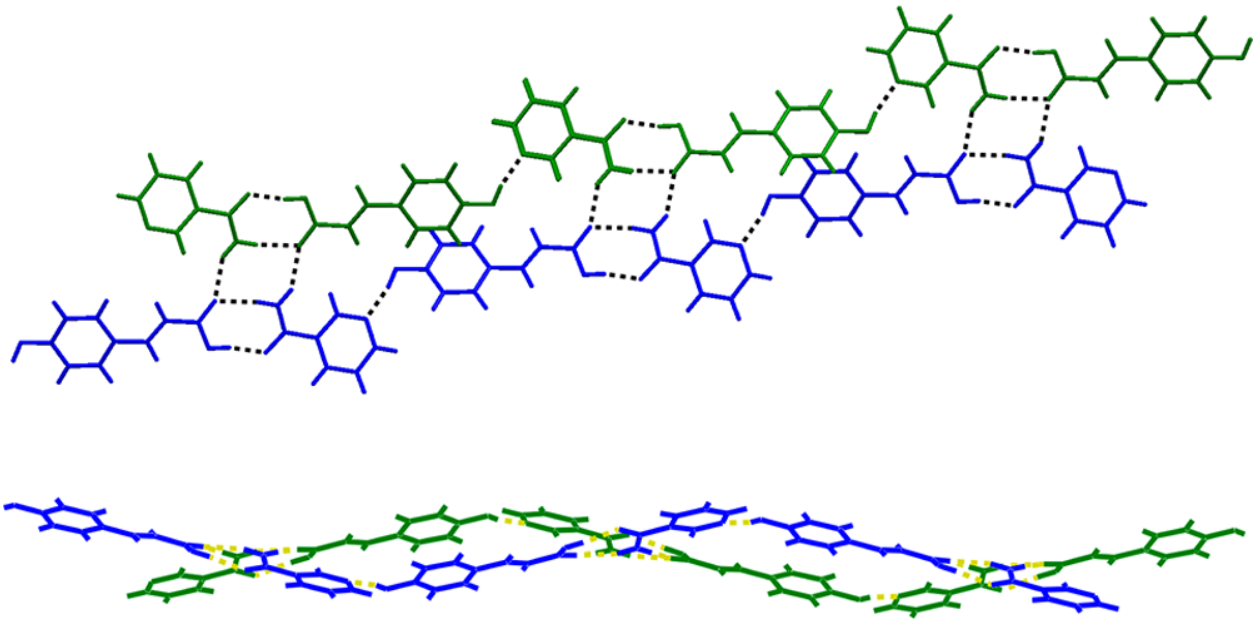

Figure 7.2.5: *p*CA•NAM two one-dimensional strands (blue and green) cross-linked by a series of N−H···O hydrogen bonds (dashed-lines).

7.3 *p*-Coumaric acid and Quinine (*p*CA$^-$)(QUIN$^+$)•*p*CA•MeOH•H_2O

The hybrid salt-co-crystal solvate was obtained by dissolving a 1: 1 molar ratio of *p*-coumaric acid and quinine in a 50/50 (*v/v*) solution of methanol/water by heating the mixture on to a hot plate. The solution was allowed to evaporate at room temperature and after one week crystals were obtained. For the quinine and p-coumaric acid system the calculated ΔpKa ≈ 4, thus salt formation was expected.

The asymmetric unit of the compound is illustrated in **Figure 7.3.1** and contains one p-coumarate anion, one quininium cation, one neutral p-coumaric acid molecule, methanol and water. This structure has been published by Jacobs *et al*.[11]

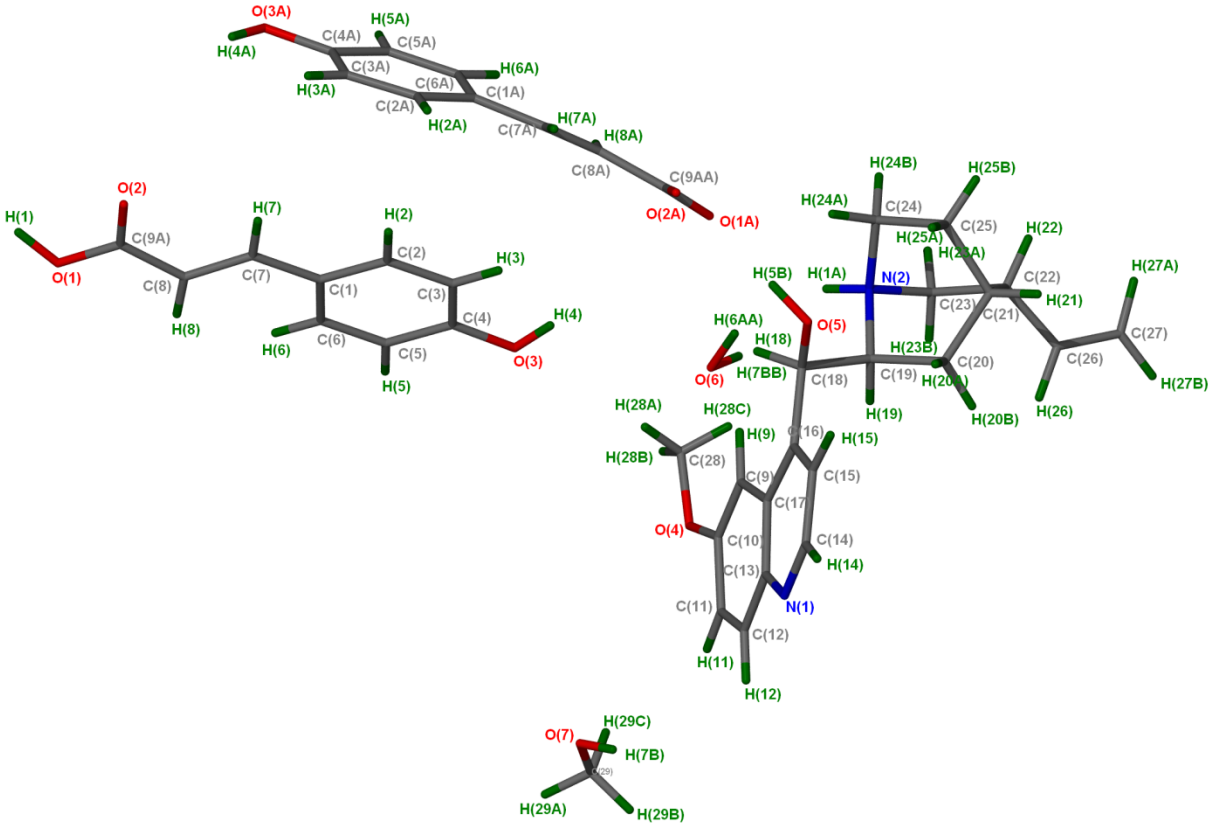

Figure 7.3.1: Asymmetric unit of **(*p*CA$^-$)(QUIN$^+$)•*p*CA•MeOH•H$_2$O** with all the hydrogen atoms for numbering clarity.

7.3.1 Thermal Analysis

The first endotherm in the DSC curve and the first mass loss in the TG curve that occurs at 373.4 K are assigned to the loss of both water and methanol molecules (methanol mass loss of 4.40 % and 2.60 % for water). The second mass loss and endotherm in the DSC and TG curves respectively can be correlated to the melt. The overall experimental mass loss obtained (both methanol and water) is close to the theoretical value as listed in **Table 7.7**. Thermal analysis curves are shown in **Figure 7.3.2**.

Table 7.7: Thermal analysis data of **(*p*CA$^-$)(QUIN$^+$)•*p*CA•MeOH•H$_2$O**.

Compounds	*p*CA	**(*p*CA$^-$)(QUIN$^+$)•*p*CA•MeOH•H$_2$O**	QUIN
DSC Endo$_1$(T$_{onset}$,K)	-	373.4	-
DSC Endo$_2$(T$_{onset}$,K)	493.2	420.6	449.8
TG calculated % mass loss	-	7.1	-
TG experimental % mass loss	-	7.0	-
***p*CA$^-$: QUIN$^+$: *p*CA: MeOH: H$_2$O**		1: 1: 1: 1: 1	

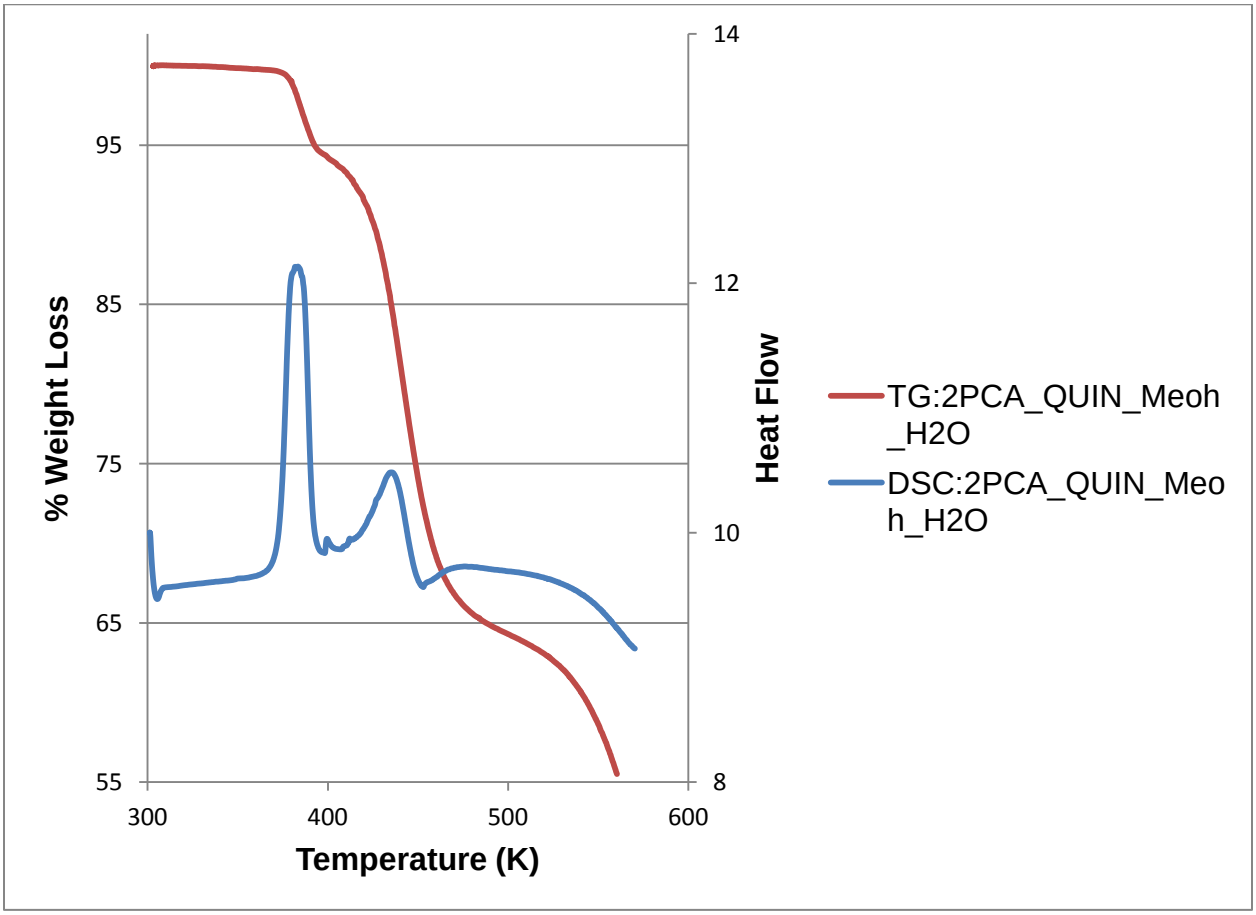

Figure 7.3.2: Thermal analysis curves of **(*p*CA$^-$)(QUIN$^+$)•*p*CA•MeOH•H$_2$O** (red) TG and (blue) DSC.

7.3.2 Hot Stage Microscopy

Figure 7.3.3 shows the HSM photographs of the hybrid salt-co-crystal and revealed its thermal stability. At 373 K **(Figure 7.3.3 c)** the rod-shaped crystals are still intact and the first visible indication of desolvation is at 426 K **(Figure 7.3.3 d)** which continues until 433 K **(Figure 7.3.3 f)**. The crystal melt at 435 K **(Figure 7.3.3 g)**.

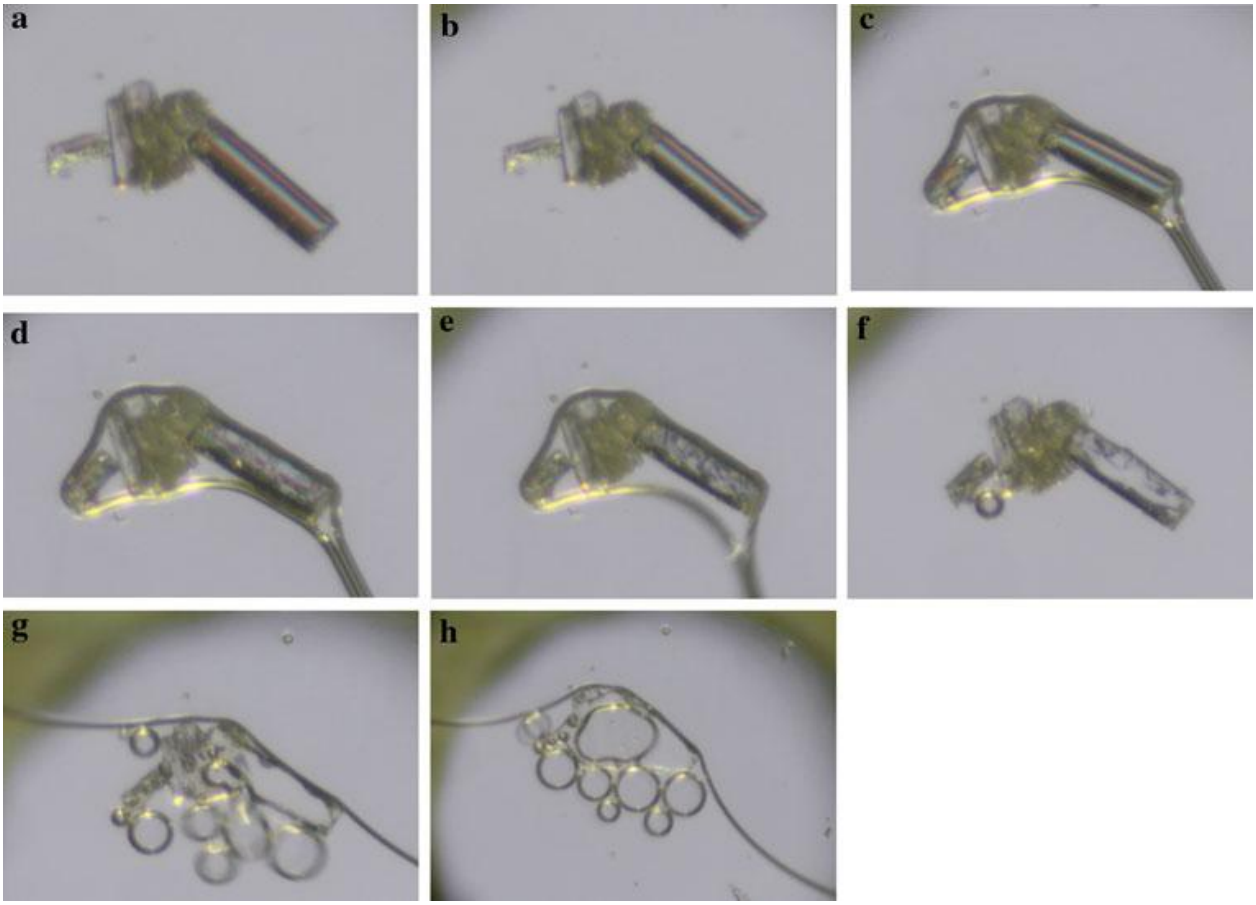

Figure 7.3.3: HSM photographs of **(*p*CA$^-$)(QUIN$^+$)•*p*CA•MeOH•H_2O**: **a** 298 K, **b** 347 K, **c** 373 K, **d** 426 K, **e** 429 K, **f** 433 K, **g** 435 K and **h** 438 K.

7.3.3 Powder X-ray Diffraction

A 2: 1 molar ratio of *p*-coumaric acid and quinine was ground for 30 min. The ground product PXRD pattern contains some of the peaks found in the physical mixture.

The PXRD pattern of the slurry conversion performed in 50/50 (*v/v*) methanol/water did not match that of the physical mixture, the calculated pattern[12] or the grinding experiment. Attempts at preparing single crystals of the powder obtained from the slurry experiment were unsuccessful and thus its identity is unknown. **Figure 7.3.4** shows the individual PXRD patterns.

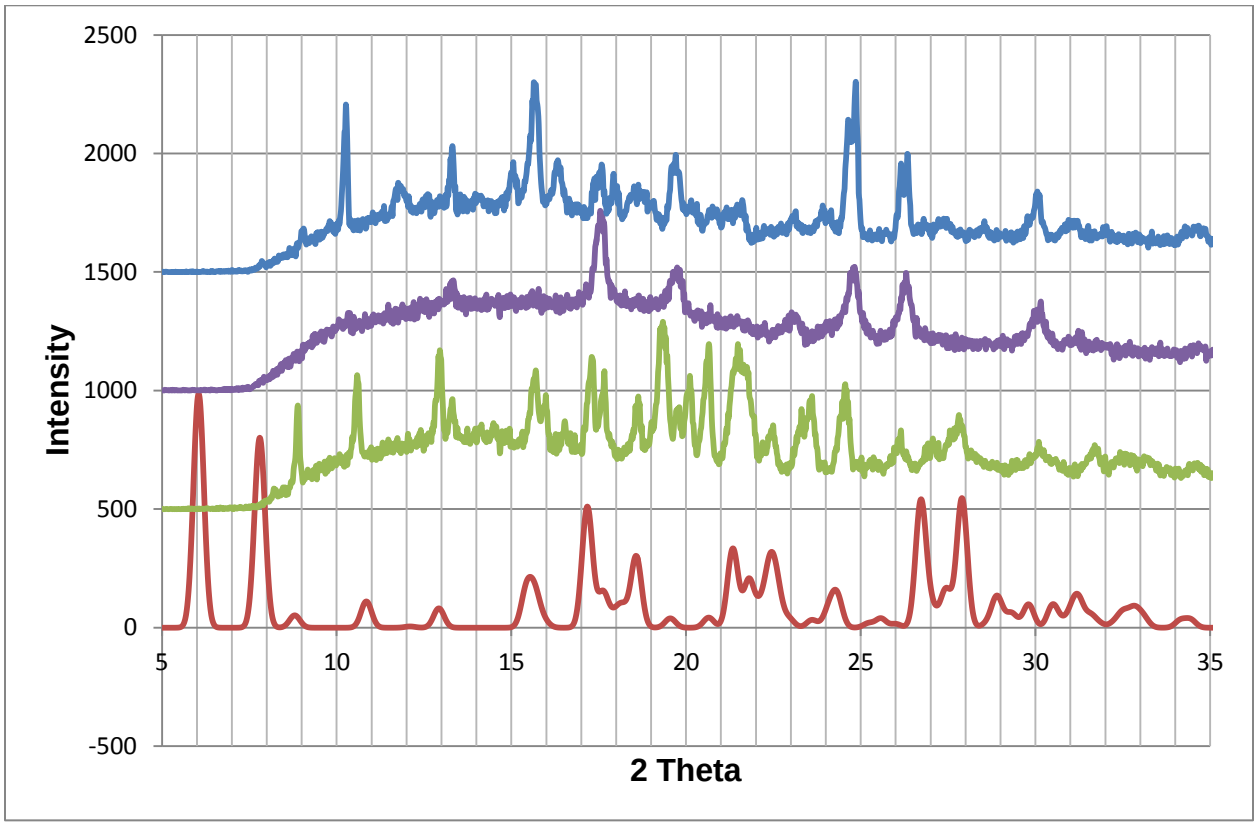

Figure 7.3.4: PXRD pattern of **(*p*CA$^-$)(QUIN$^+$)•*p*CA•MeOH•H_2O** (red), slurry (green), ground product (purple) and physical mixture (blue).

7.3.4 Non-isothermal Kinetics

Non-isothermal kinetics was used to study the desolvation of **(*p*CA$^-$)(QUIN$^+$)•*p*CA•MeOH•H_2O** using the Ozawa,[13] Flynn and Wall[14] model free method. TG mass loss curves at heating rates of 1, 2 and 6 K/min were analysed. The TG experiments at selected scan rates gave a series of –log β *vs* 1/T (K^{-1}) curves, where β is the heating rate as shown in **Figure 7.3.5**. The series gave an activation energy range of 210–272 kJ mol^{-1}, calculated from the slopes of the linear graphs. The high activation energy is due to the extensive hydrogen bonding linking methanol molecules to both p-CA and p-CA^-.[11]

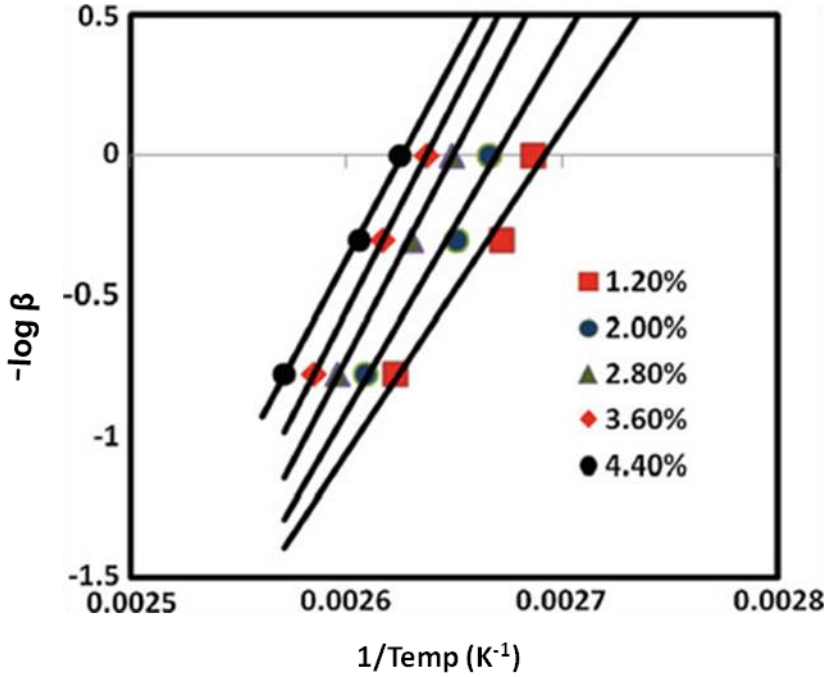

Figure 7.3.5: Plots of -log β versus 1/T.

7.3.5 Structure Determination

A suitable single crystal was chosen for X-ray structure analysis which resulted in successful determination of the structure. The C–O distances of the carboxylate moiety have nearly equal bond lengths (C9AA–O1A = 1.263 Å and C9AA–O2A = 1.268 Å). The

structure was successfully refined to R_1 = 0.0454 with wR_2 = 0.1002 (final R indices). Crystal data is given in **Table 7.8**.

Table 7.8: Crystal data of **(*p*CA$^-$)(QUIN$^+$)•*p*CA•MeOH•H_2O**.

Compound	**(*p*CA$^-$)(QUIN$^+$)•*p*CA•MeOH•H_2O**
Structural Formula	$(C_9H_7O_3^-)(C_{20}H_{25}N_2O_2^+)•C_9H_8O_3•CH_4O•H_2O$
*p*CA$^-$:QUIN$^+$: *p*CA :MeOH:H_2O ratio	1: 1: 1: 1: 1
Molecular Mass (g mol^{-1})	702.80
Data collection temperature (K)	173 (2)
Crystal system	Monoclinic
Space group	$P2_1$
a (Å)	6.4061 (4)
b (Å)	26.232 (2)
c (Å)	10.9639 (8)
α (°)	90.00
β (°)	103.707 (2)
γ (°)	90.00
Volume (Å^3)	1790.0 (2)
Z	2
D_c, Calculated density (g cm^{-3})	1.304
Final R indices [I>2sigma(I)]	R_1= 0.0454
	wR_2 = 0.1002
R indices (all data)	R_1 = 0.0595
	wR_2 = 0.1074
Largest diff. peak and hole (eÅ^{-3})	0.172; -0.186

The compound crystallized in the monoclinic space group $P2_1$ with Z = 2. The asymmetric unit contains one quininium cation ($QUIN^+$), one p-coumarate anion ($p\text{-}CA^-$), one molecule of p-CA, one water molecule and one methanol molecule.

The crystal packing diagram is illustrated in **Figure 7.3.6 (a)**. The calculated void volume contact surface at a probe radius of 1.4 Å and a grid spacing of 0.7 Å was found to be 46.81 $Å^3$ with a unit cell volume percentage of 2.6 % using Mercury[15] software as shown in **Figure 7.3.6 (b)**.

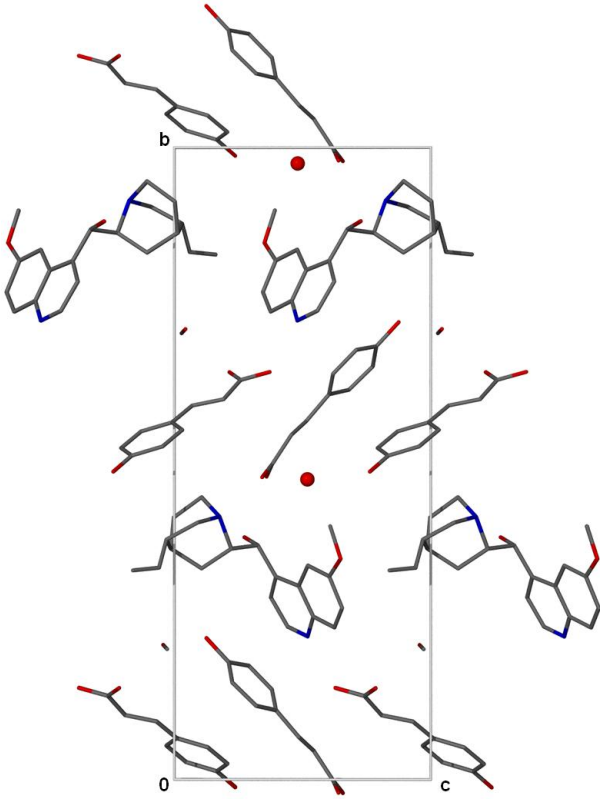

(a)

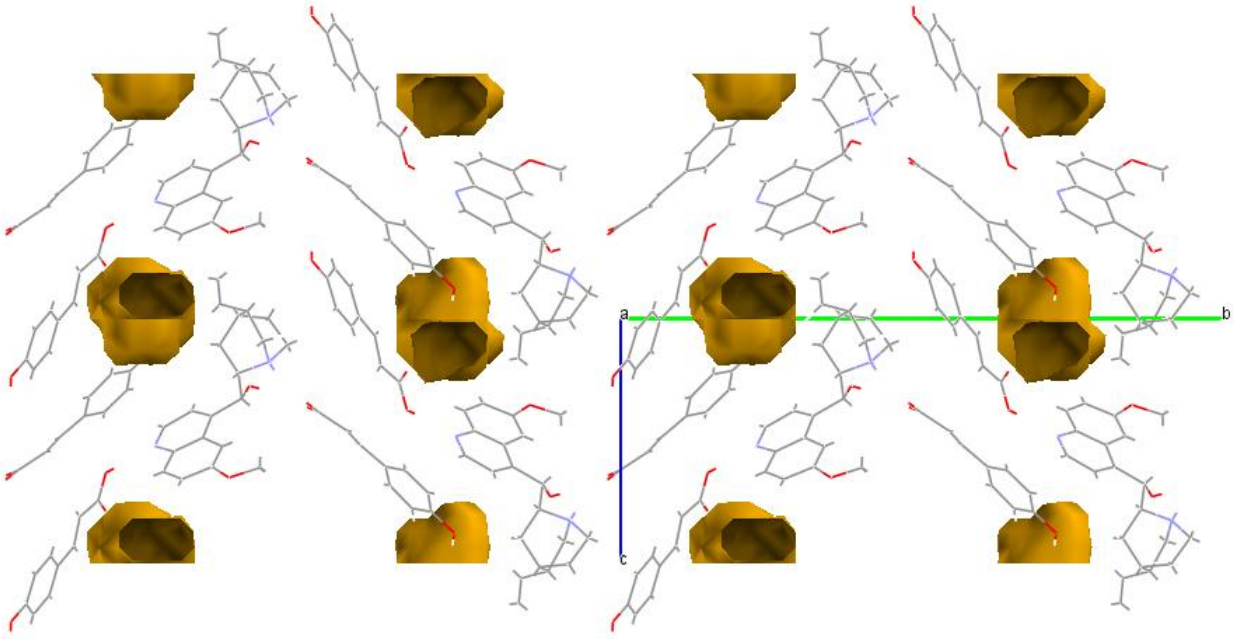

(b)

Figure 7.3.6: (a) Packing diagram of **(*p*CA$^-$)(QUIN$^+$)•*p*CA•MeOH•H_2O** down [100] and **(b)** Cavities in which methanol and water molecules are located running down [100].

One p-CA$^-$ anion and one neutral p-CA molecule are linked via methanol and water bridges to form a ring-like hydrogen bonded network which can be described in graph set notation[8] as $R_4^4(24)$.

The hybrid salt-co-crystal solvate also has a connection between two p-CA$^-$ anions, one QUIN$^+$ cation and a water molecule to form a smaller hydrogen bonded ring of the type $R_4^2(11)$ as shown in **Figure 7.3.7**.[14]

The tertiary amine is protonated forming a charge assisted hydrogen bond (N$^+$•••OH$^-$) to the p-CA$^-$ anion and the quinoline nitrogen forms a hydrogen bond (N•••OH) to the neutral p-CA molecule. The hydrogen bonding parameters are listed in **Table 7.9** and the hydrogen bond diagram is illustrated in **Figure 7.3.8**.

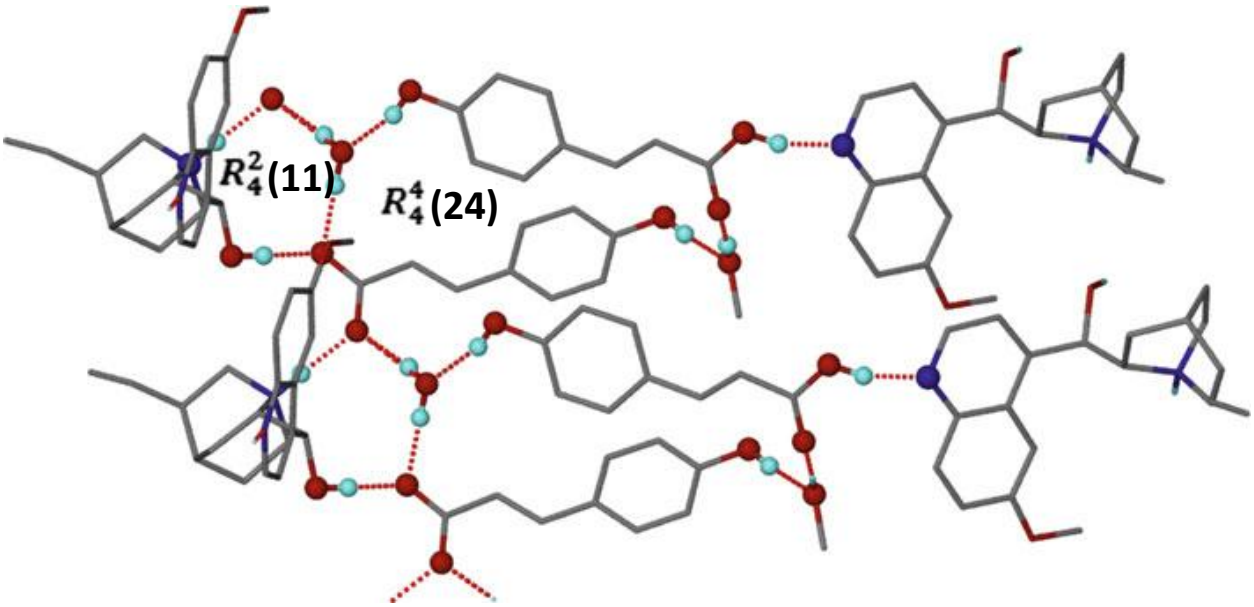

Figure 7.3.7: Hydrogen bonded rings in the hybrid salt-cocrystal solvate with dashed lines indicating the $R_4^2(11)$ and the $R_4^4(24)$ ring motifs.

Table 7.9: Hydrogen bonding parameters in **(*p*CA$^-$)(QUIN$^+$)•*p*CA•MeOH•H_2O**.

COMPOUND	D-H···A	D···A (Å)	D-H (Å)	H···A (Å)	D-H···A (º)
(*p*CA$^-$)(QUIN$^+$)•*p*CA•MeOH•H_2O	O5-H5A···O1A	2.645 (2)	0.916 (3)	1.731 (3)	176 (3)
	O3-H4···O6 [a]	2.682 (3)	0.896 (3)	1.808 (3)	164 (2)
	O1-H1···N1 [b]	2.630 (2)	0.948 (4)	1.702 (4)	165 (3)
	O3A-H4A···O7 [b]	2.662 (3)	0.872 (3)	1.793 (3)	174 (3)
	N2-H1A···O2A [c]	2.707 (2)	0.891 (2)	1.830 (2)	168 (2)
	O6-H6BB···O2A[d]	2.734 (2)	0.816 (3)	1.927 (3)	170 (3)
	O6-H6AA···O1A [c]	2.776 (2)	1.012 (4)	1.781 (4)	167 (4)
	O7-H7B···O2 [e]	2.712 (3)	0.758 (4)	1.956 (4)	175 (4)

a = x+1, y, z ; b = -x+2, y+1/2, -z+2; c = x-1, y, z ; d = x-2, y, z ; e = -x+2, y-1/2, -z+2

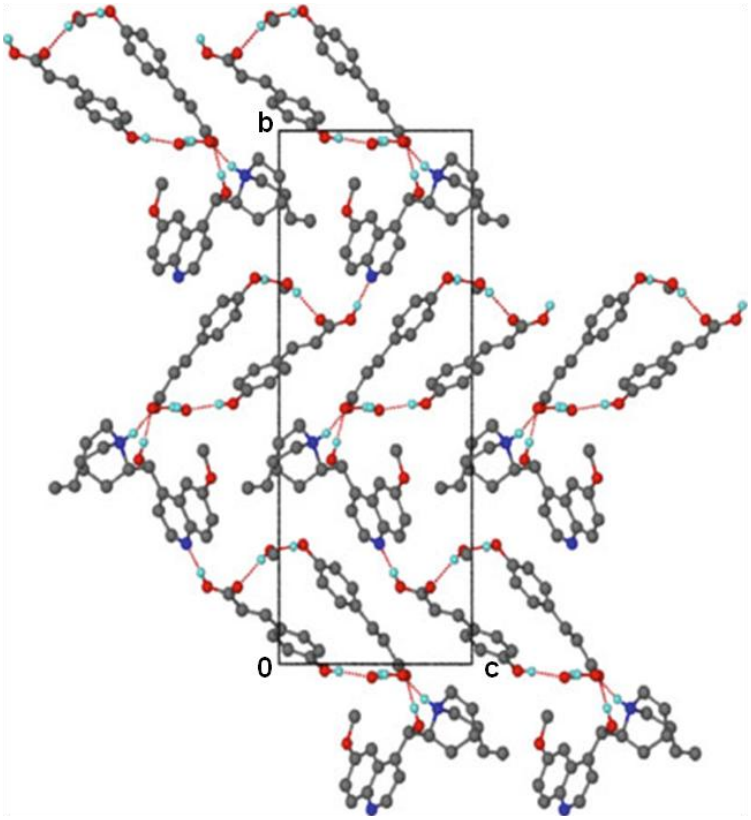

Figure 7.3.8: Packing diagram of **(*p*CA$^-$)(QUIN$^+$)•*p*CA•MeOH•H_2O** along [100] indicating the hydrogen bonded ribbons running along [010].

7.4 *t*-Ferulic acid and isonicotinamide (*tFER*•2INM)

A 1: 1 molar ratio of *trans*-ferulic acid and isonicotinamide was dissolved in ethanol and the solution was slightly heated on a hot plate. The solution was allowed to evaporate at room temperature and crystals were obtained the same day with a ratio of 1:2 (one *trans*-ferulic acid molecule and two isonicotinamide molecules). The asymmetric unit of ***tFER*•2INM** is illustrated in **Figure 7.4.1**.

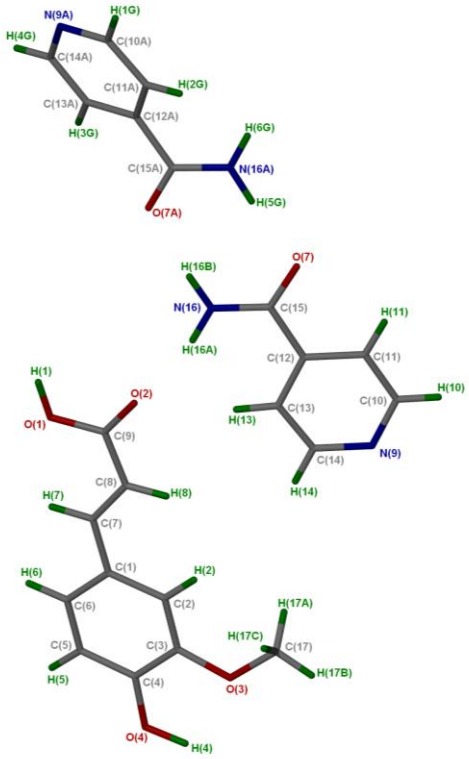

Figure 7.4.1: Asymmetric unit of ***tFER*•2INM.**

7.4.1 Thermal Analysis

The ***tFER*•2INM** co-crystal has a melting point that is lower than both *trans*-ferulic acid and isonicotinamide as listed in **Table 7.10**. The DSC curves of the individual components are shown in **Figure 7.4.2**.

Table 7.10: Thermal analysis data of ***tFER*•2INM**.

Compounds	**DSC Endo$_1$(T_{onset},K)**	**DSC Endo$_2$(T_{onset},K)**
Isonicotinamide	382.1	428.4
*t*FER	-	444.7
***tFER*•2INM**	-	422.4

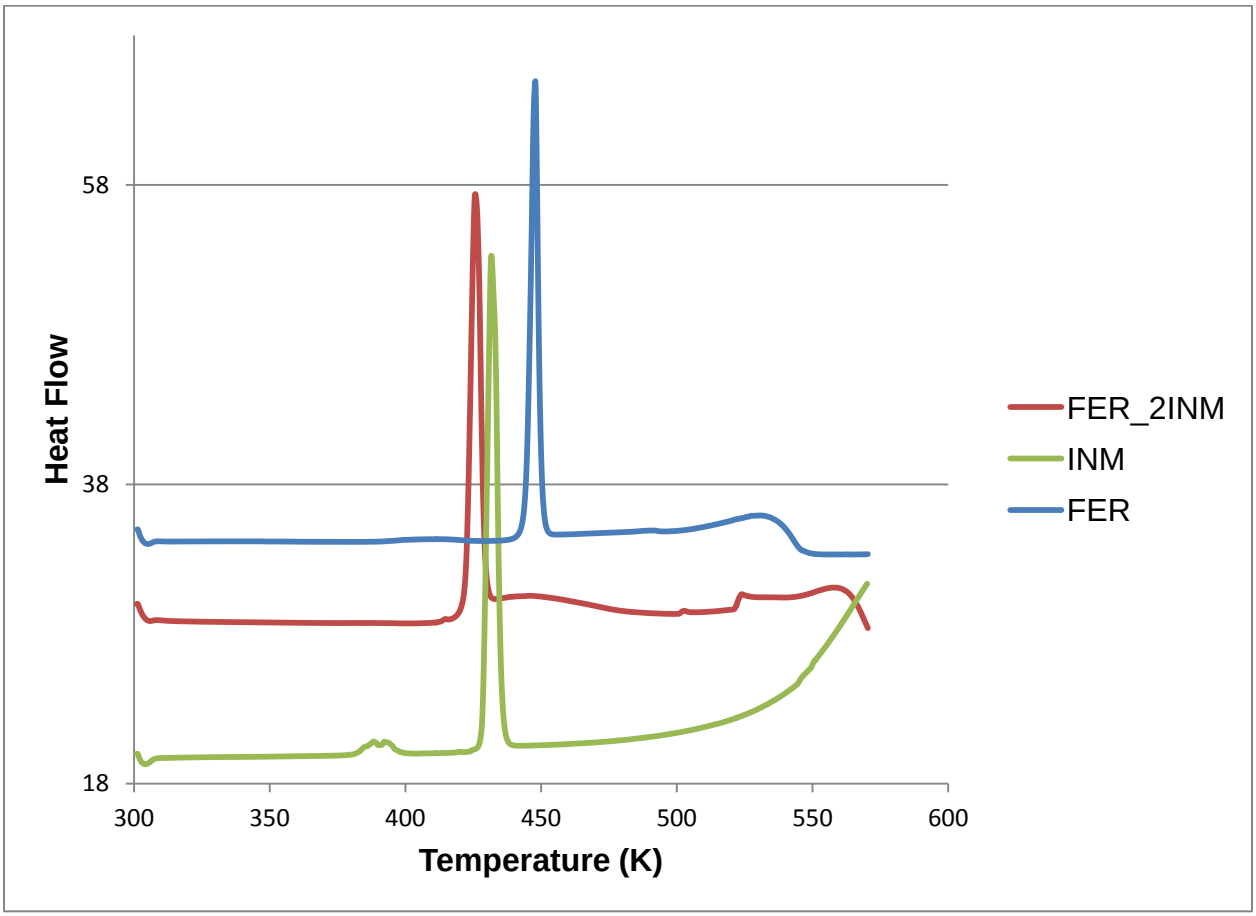

Figure 7.4.2: DSC curves of ***tFER*•2INM** (red), INM (green) and FER (blue).

7.4.2 Structure Determination

The structure was solved using direct methods and the refinement was completed by full-matrix least squares with SHELXL-97.[7] All non-hydrogen atoms were found in the difference electron density map and refined anisotropically. All of the hydrogens except the hydroxyl hydrogens and the hydrogen attached to the nitrogen were placed with geometric constraints and allowed to refine isotropically. The crystal data is given in **Table 7.11**.

Table 7.11: Crystal data of ***tFER*•2INM**.

Compound	***tFER*•2INM**
Structural Formula	$C_{10}H_{10}O_4$•$2C_6H_6N_2O$
*t*FER: INM ratio	1: 2
Molecular Mass (g mol^{-1})	438.44
Data collection temperature (K)	173 (2)
Crystal system	Triclinic
Space group	*P-1*
a (Å)	8.8446 (5)
b (Å)	9.4888 (6)
c (Å)	13.3992 (8)
α (°)	98.3530 (10)
β (°)	96.8250 (10)
γ (°)	106.7480 (10)
Volume ($Å^3$)	1049.96 (11)
Z	2
D_c, Calculated density (g cm^{-3})	1.387
Final R indices [I>2sigma(I)]	R_1= 0.0414
	wR_2 = 0.0957
R indices (all data)	R_1 = 0.0618
	wR_2 = 0.1088
Largest diff. peak and hole ($eÅ^{-3}$)	0.170; -0.229

Trans-Ferulic acid and isonicotinamide crystallised in a 1: 2 ratio in the triclinic space group *P-1* with Z = 2. The asymmetric unit comprises one *trans*-ferulic acid molecule and two isonicotinamide molecules. The packing diagram of the co-crystal down [100] is represented in **Figure 7.4.3** where layers of both *trans*-ferulic and isonicotinamide are running along [01$\bar{1}$]. .

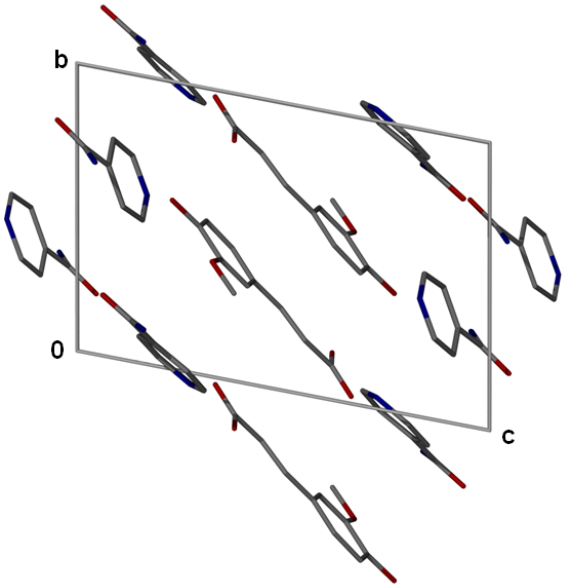

Figure 7.4.3: Packing diagram of ***tFER*•2INM** down [100].

Only the hydroxyl and carboxylic acid moieties of the *trans*-ferulic acid are involved in hydrogen bonding. The COOH hydroxyl moiety in *trans*-ferulic acid is connected to the nitrogen atom (N9) of one isonicotinamide and the carbonyl group to the hydrogen atom (H16A) of another isonicotinamide molecule.

The phenol moiety of the *trans*-ferulic acid is hydrogen bonded to the nitrogen atom (N9A) of the third isonicotinamide molecule. An $R_2^2(8)$ ring motif is formed between the two isonicotinamide molecules in the asymmetric unit.

The other hydrogen bonds present in the crystal structure can be described using the graph sets : $D_1^1(2)$, $D_2^2(5)$, $D_2^2(6)$, $D_2^2(8)$, $D_2^2(9)$, $C_2^2(11)$, $D_2^2(12)$ and D_2^2 (13). Hydrogen bonding parameters are listed in **Table 7.12** and **Figure 7.4.4 (a)** and **(b)** shows the hydrogen bonding involved in the co-crystal.

Table 7.12: Hydrogen bonding parameters in ***tFER*•2INM**.

COMPOUND	D-H···A	D···A (Å)	D-H (Å)	H···A (Å)	D-H···A (º)
***tFER*•2INM**	N16-H16A···O2	2.999 (2)	0.899 (2)	2.111 (2)	169 (2)
	N16-H16B···O7A	2.850 (2)	0.956 (2)	1.901 (2)	171 (2)
	N16A-H5G···O7	2.954 (2)	0.963 (2)	1.994 (2)	174 (2)
	O4-H4···N9A [a]	2.683 (2)	1.003 (2)	1.767 (2)	150 (2)
	N16A-H6G···O4 [b]	3.143 (2)	0.914 (2)	2.355 (2)	144 (2)
	O1-H1···N9 [c]	2.631 (2)	0.988 (2)	1.659 (3)	167 (2)

a = x+1, y-1, z + 1; b = x, y+1, z-1; c = x-1, y, z

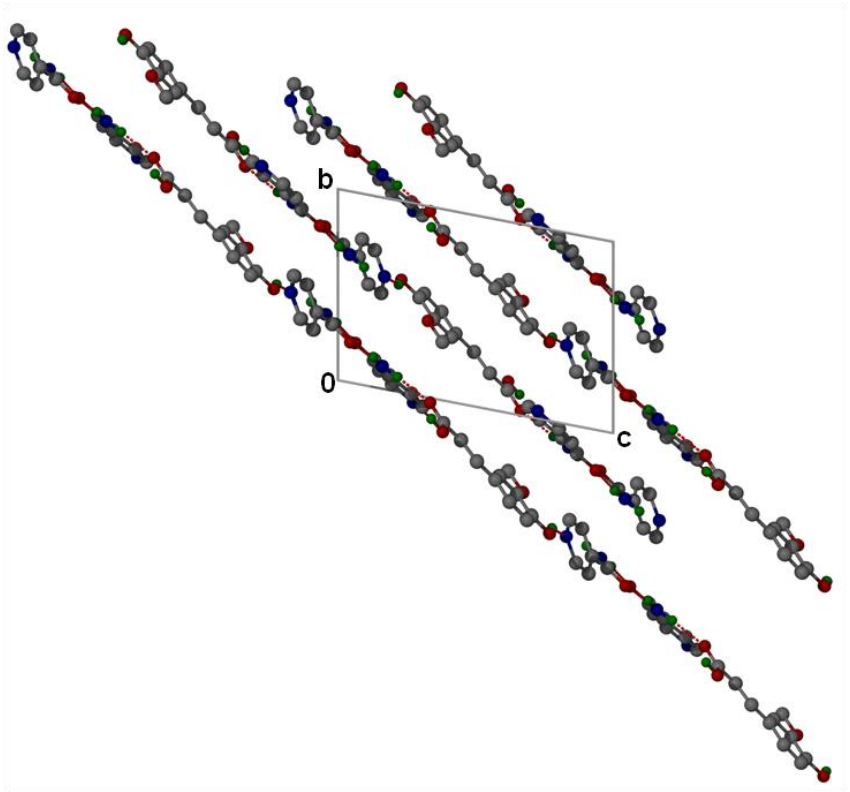

(a)

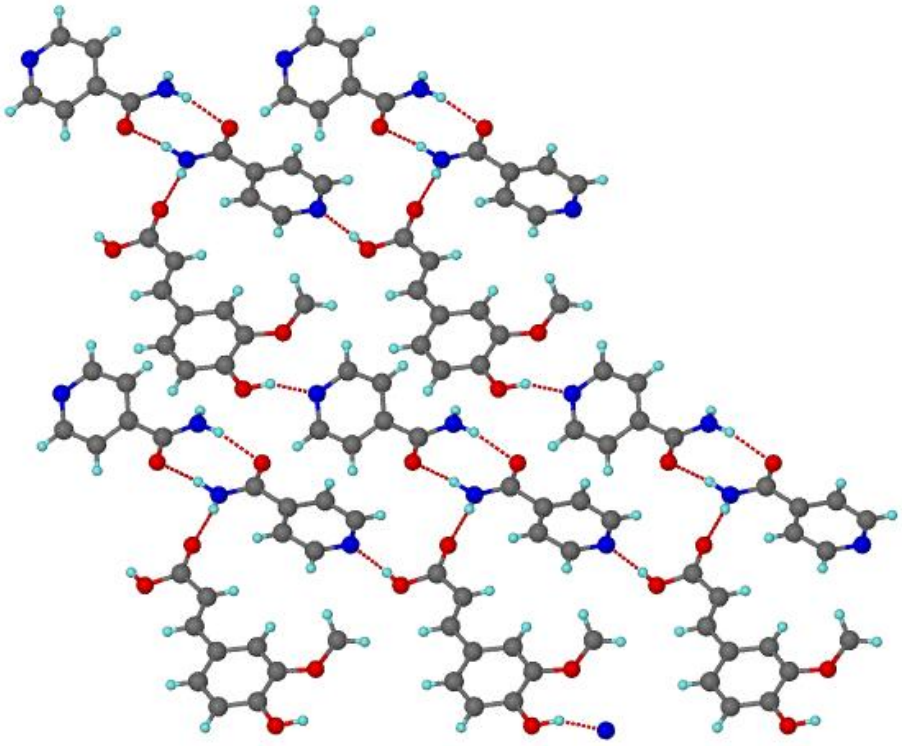

(b)

Figure 7.4.4: (a) Packing diagram of ***tFER*•2INM** along [100] with the hydrogen atoms involved in the H-bonding shown and **(b)** Hydrogen bonding in ***tFER*•2INM**.

REFERENCES

1. Clarke. H. D, Arora. K. K, Bass. H, Kavuru. P, Tien Teng Ong, Pujari. T, Wojtas. L & Zaworotko. M. J. *Cryst. Growth Des*. 2010, 10, 2152.
2. Allen. F.H. *Acta. Crystallogr*. 2002, B58, 380 - 388.
3. Schultheiss. N, Roe. M & Boerrigter. S. X. M. *CrystEngComm*. 2011, 13, 611.
4. Aakeröy. C. B, Beatty. A. M & Helfrich. B. A. *Angew. Chem. Int. Ed.* 2001, 40, 3240.
5. Zaiyou. T, Erjia. Z, Lin. L, Zhuohui. L & Ruisi. Y. *Acta. Crystallogr. Sect.E: Struct. Rep. Online.* 2011, 67, o424.
6. Kavuru. P, Aboarayes. D, Arora. K. K, Clarke. H. D, Kennedy. A, Marshall. L, Tien Teng Ong, Perman. J, Puraji. T, Wojtas. L & Zaworotko. M. J. *Cryst. Growth Des*. 2010, 10, 3568.
7. Sheldrick GM. SHELX-97, program for crystal structure refinement; University of Göttingen, Germany. 1997.
8. Etter. M. C, MacDonald. J. C & Bernstein. J. *Acta. Crystallogr.* 1990, B46, 256-262.
9. McClurg. R. B & Smit. J. P. *Pharm. Technol. Eur*. 2013, 37, 56 − 61.
10. Arenas-García. J. I, Herrera-Ruiz. D, Mondragón-Vàsquez. K, Morales-Rojas. H & Höpfl. H. *Cryst. Growth Des*. 2010, 10, 3732 – 3742.
11. Jacobs. A & Amombo Noa. F. M. *J. Chem. Crystallogr.* 2014, 44 (2), 57 - 62.
12. Yvon. K, Jeitschko. W & Parthe. E. *Appl. Crystallogr.* 1977, 10, 73-74.
13. Ozawa. T. *Bull. Chem. Soc Jpn.* 1965, 38, 1881 – 1886.
14. Flynn. J. H & Wall. L. A. *J. Polym. Sci*. 1966, 4, 323 – 328.
15. Macrae. C. F, Eddington. P. R, McCabe. P, Pidcock. E, Shields. G. P, Taylor. R, Towler. M. & van de Streek. J. Mercury: visualization and analysis of crystal structures. *J. Appl. Crystallogr*. 2006, 39, 453-457.

CHAPTER 8

RACEMIC COMPOUNDS

In this chapter, racemic 2-phenylbutyric acid (PBA) and racemic 2-phenylpropionic acid (PPA) were the two chiral compounds investigated.

A search of the Cambridge Structural Database (CSD, version 5.34, November 2012)[1] showed that (*RS*)-2-phenylbutyric acid and its enantiomers all formed co-crystals with isonicotinamide.[2]

According to the Cambridge Structural Database (CSD, version 5.34, November 2012), [1] (*RS*)-2-phenylpropionic acid formed a co-crystal with isonicotinamide,[2] (*R*)-2-phenylpropionic acid formed a co-crystal with acridine[3] and isonicotinamide.[2]

The chiral resolution of racemic 2-phenylbutyric acid and racemic 2-phenylpropionic acid has also been reported using (1R,2S)-2-amino-1,2-diphenylethanol.[4]

8.1 2-Phenylbutyric acid with cinchonidine (*S*-PBA$^-$)(CIND$^+$)•H_2O

The salt was obtained by dissolving a 1: 1 ratio of (*RS)*-2-phenylbutyric acid (PBA) and cinchonidine (CIND) in ethanol by slightly heating the solution on a hot plate. Needle-like crystals were obtained after one week with a 1: 1: 1 ratio (**PBA$^-$: CIND$^+$: H_2O**). 2-phenylbutyric acid crystallized in the (*S)* configuration and water was included in the structure (**(*S*-PBA$^-$)(CIND$^+$)•H_2O**). Thus CIND successfully resolved the racemic 2-phenylbutyric acid. The asymmetric unit of the **(*S*-PBA$^-$)(CIND$^+$)•H_2O** is illustrated in **Figure 8.1.1**.

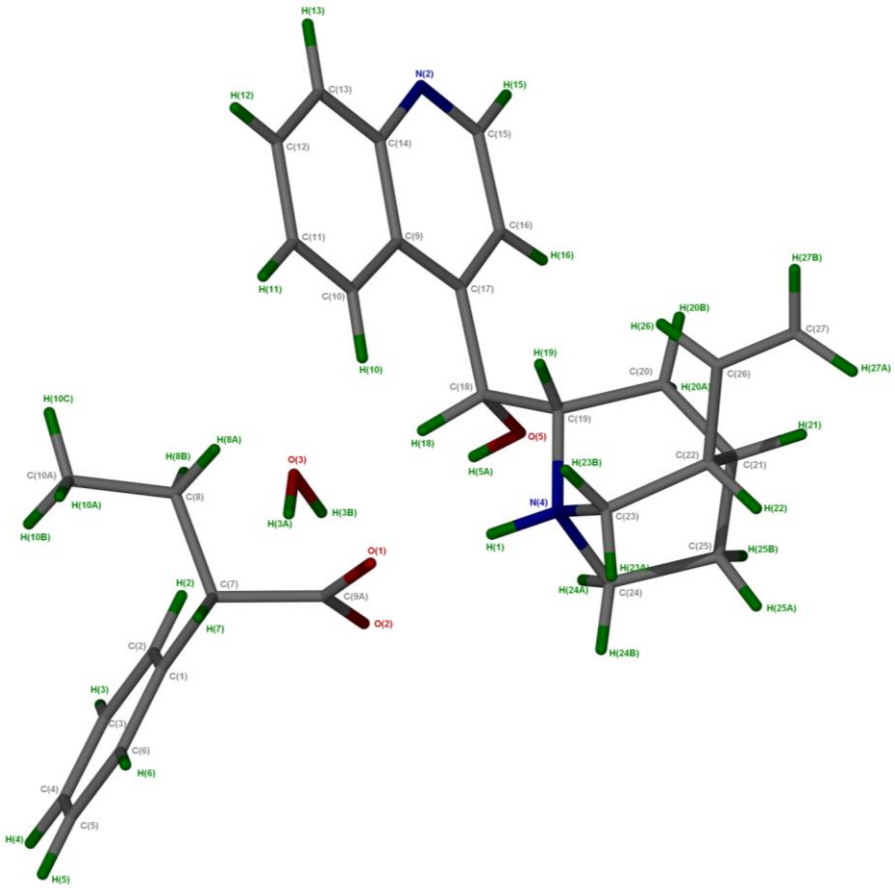

Figure 8.1.1: Asymmetric unit of **(*S*-PBA$^-$)(CIND$^+$)•H_2O** with all the hydrogen atoms shown for clarity.

8.1.1 Thermal Analysis

Thermal analysis results are shown in **Figure 8.1.2**. A single mass loss step of 3.2 % (calc 3.8 %) was observed in the TG curve which corresponds to the release of water. Three peaks were observed in the DSC, the first peak corresponding to the loss of surface water (T_{on}= 306.1 K), this is due to the fact that the crystals were not properly dried for the TG analysis. The second peak is due to the loss of the included water and the simultaneous melt (T_{on}= 362.2 K) of the salt. The third peak is due decomposition. (T_{on}= 485.2 K). The thermal analysis data is given in **Table 8.1**.

Table 8.1: Thermal analysis data of **(*S*-PBA$^-$)(CIND$^+$)•H_2O**.

Compound	**(*S*-PBA$^-$)(CIND$^+$)•H_2O**
PBA$^-$: CIND$^+$: H_2O ratio	1: 1: 1
TG calculated % mass loss	3.8
TG experimental % mass loss	3.2
DSC Endo$_1$ (T_{onset}, K)	306.1
DSC Endo$_2$ (T_{onset}, K)	362.2
DSC Endo$_3$ (T_{onset}, K)	485.2

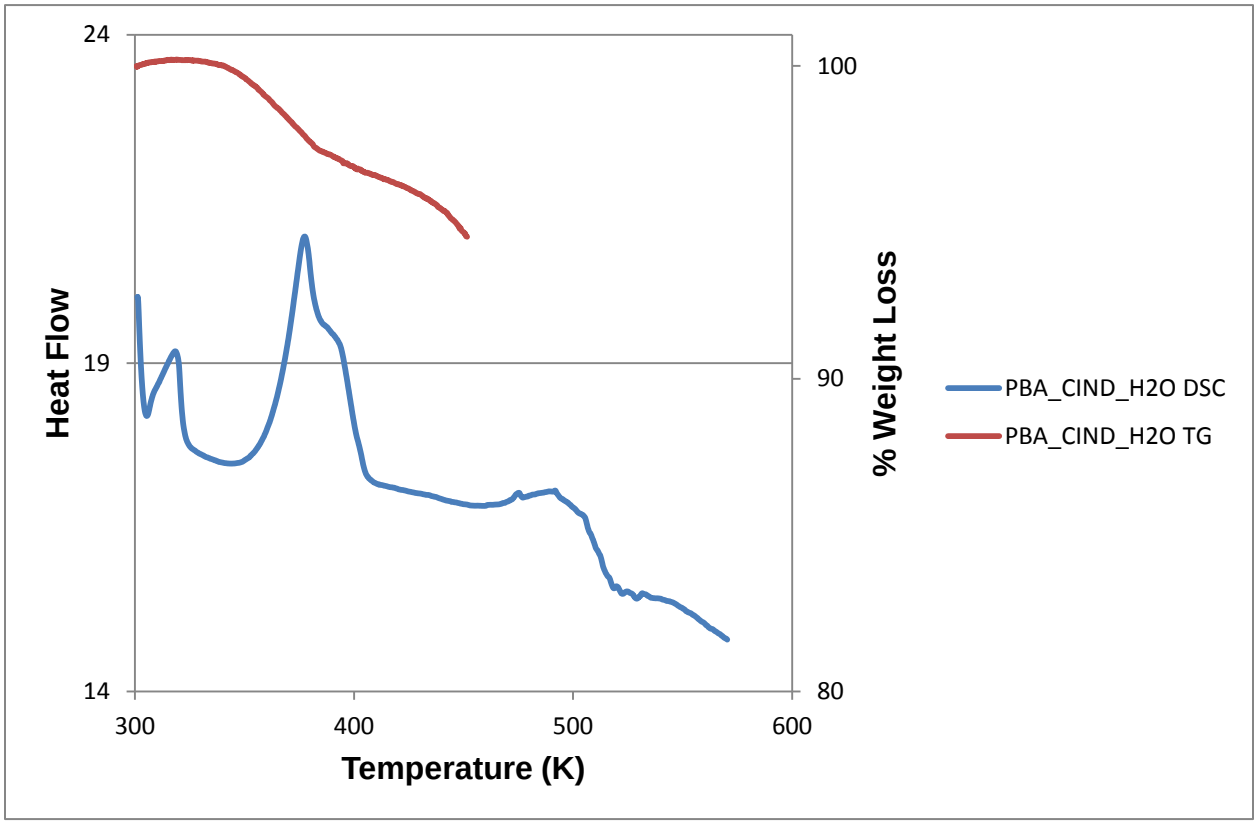

Figure 8.1.2: Thermal analysis curves of **(*S*-PBA$^-$)(CIND$^+$)•H_2O** DSC (blue) and TG (red).

8.1.2 Structure Determination

All non-hydrogen atoms were refined with anisotropic displacement parameters. The OH and NH hydrogen atoms were located in the difference electron density map. Crystallographic data for **(*S*-PBA$^-$)(CIND$^+$)•H_2O** is given on **Table 8.2**.

Table 8.2: Crystal data of **(*S*-PBA$^-$)(CIND$^+$)•H_2O**.

Compound	**(*S*-PBA$^-$)(CIND$^+$)•H_2O**
Structural Formula	$(C_{10}H_{11}O_2^-)(C_{19}H_{23}N_2O^+)\bullet H_2O$
PBA$^-$: CIND$^+$: H_2O ratio	1: 1: 1
Molecular Mass (g mol^{-1})	476.60
Data collection temperature (K)	173(2)
Crystal system	Orthorhombic
Space group	$P2_12_12_1$
a (Å)	6.6163 (10)
b (Å)	15.457 (2)
c (Å)	24.868 (4)
α (°)	90.00
β (°)	90.00
γ (°)	90.00
Volume (Å^3)	2543.3 (7)
Z	4
D_c, Calculated density (g cm^{-3})	1.245
Final R indices [I>2sigma(I)]	R_1= 0.0524
	wR_2 = 0.0960
R indices (all data)	R_1 = 0.0957
	wR_2 = 0.1115
Largest diff. peak and hole (eÅ^{-3})	0.157; -0.198

(*S*-PBA$^-$)(CIND$^+$)•H_2O crystallized in the orthorhombic space group $P2_12_12_1$ with Z = 4. The crystal used for data collection has approximate dimensions of 0.06 mm x 0.08 mm

x 0.52 mm. There is proton transfer of the hydrogen atom in the carboxylic group on the PBA to the aliphatic tertiary nitrogen (N4) atom in the $CIND^+$ cation. The packing diagram of **(*S*-PBA$^-$)(CIND$^+$)•H_2O** with all the hydrogen atoms removed is shown along [100] in **Figure 8.1.3** , the water molecules lie in isolated sites.

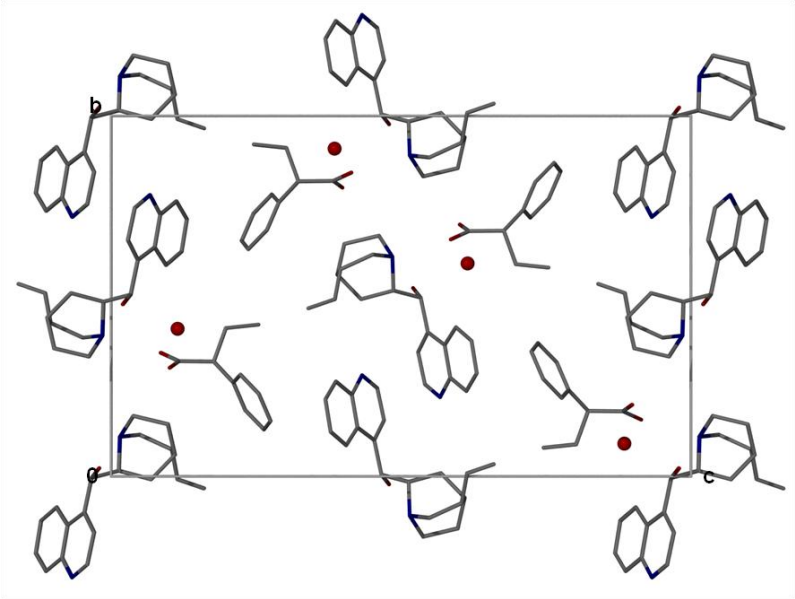

Figure 8.1.3: Crystal packing of **(*S*-PBA$^-$)(CIND$^+$)•H_2O** with all the hydrogen atoms removed down [100].

The hydrogen bonding in **(*S*-PBA$^-$)(CIND$^+$)•H_2O** is illustrated in **Figure 8.1.4** and consists of O-H•••O and N-H•••O interactions. The oxygen atom labelled O1 in PBA^- plays the role of bifurcated acceptor, O1 is connected to H1 attached to N4 in $CIND^+$ and H3B attached to the water molecule. The graph sets[6] of the structure can be characterized as: $D_1^1(2)$, $D_2^1(3)$, $D_2^2(4)$, $D_2^2(5)$, $C_2^2(6)$ and $D_2^2(8)$. Hydrogen bonding details are listed in **Table 8.3**.

Table 8.3: Hydrogen bonding parameters in **(*S*-PBA$^-$)(CIND$^+$)•H_2O**.

COMPOUND	D-H···A	D···A (Å)	D-H (Å)	H···A (Å)	D-H···A (º)
(*S*-PBA$^-$)(CIND$^+$)•H_2O	N4-H1···O1	2.699 (3)	0.964 (2)	1.738 (3)	174 (2)
	O3-H3A···O2[a]	2.731 (3)	0.900 (3)	1.841 (4)	170 (3)
	O3-H3B···O1	2.707 (3)	0.890 (3)	1.837 (4)	165 (3)
	O5-H5A···O3[b]	2.693 (3)	0.810 (3)	1.887 (3)	174 (3)

a = x+1, y, z ; b = x-1, y, z

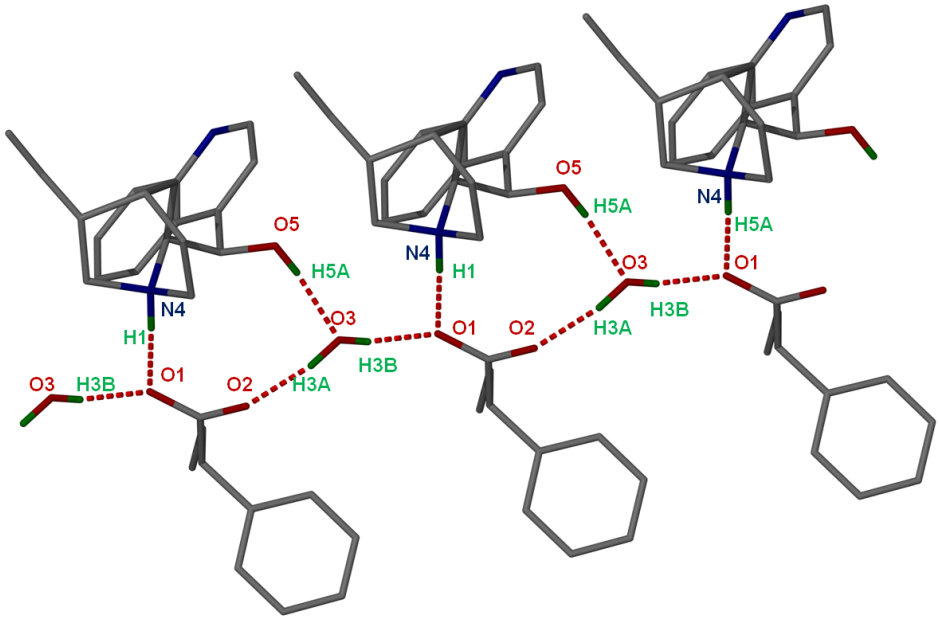

Figure 8.1.4: Hydrogen bonding in **(*S*-PBA$^-$)(CIND$^+$)•H_2O**.

8.2 2-Phenylpropionic acid with quinine (*R*-2PPA$^-$)(2QUIN$^+$)

The 2: 2 salt ratio (*R*-PPA$^-$: QUIN$^+$) was obtained by dissolving a 1: 1 molar ratio of (*RS)*-2-PPA and quinine (QUIN) in acetonitrile on a hot plate. Crystals in the form of blocks were obtained after one week. The absolute configuration of quinine is known and the chirality of the 2-phenylpropionic acid was found relative to the quinine. The asymmetric unit of **(*R*-2PPA$^-$)(2QUIN$^+$)** is shown in **Figure 8.2.1**.

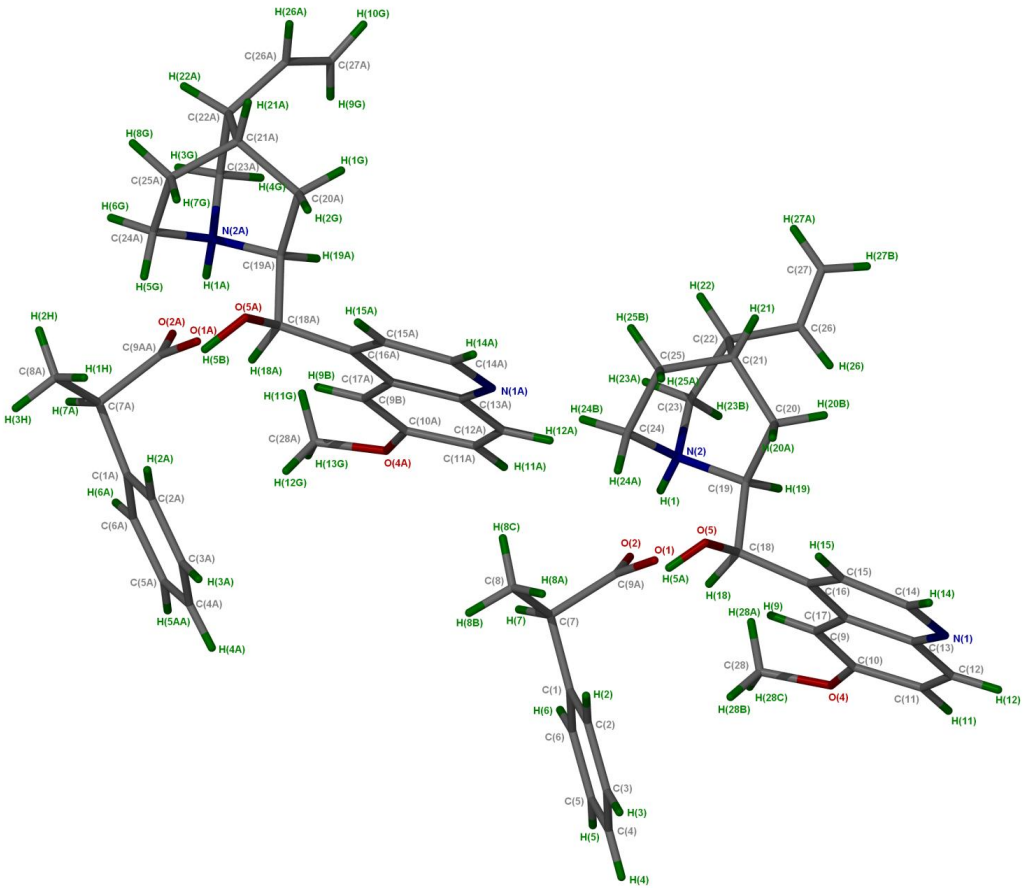

Figure 8.2.1: The asymmetric unit of **(*R*-2PPA^{-})(2QUIN^{+})** with all the hydrogen atoms shown for numbering clarity.

8.2.1 Thermal Analysis

Thermal analysis data of **(*R*-2PPA^{-})(2QUIN^{+})** are listed in **Table 8.4**. The sharp peak at 443.6 K is the melt of the salt. Decomposition of **(*R*-2PPA^{-})(2QUIN^{+})** is obtained at 464.9 K. **Figure 8.2.2** shows DSC curves of **(*R*-2PPA^{-})(2QUIN^{+})** and quinine.

Table 8.4: Thermal analysis data of **(*R*-2PPA$^-$)(2QUIN$^+$)**.

Compounds	**DSC Endo$_1$(T_{onset},K)**	**DSC Endo$_2$(T_{onset},K)**
Quinine	-	449.8
2-PPA	-	-
(*R*-2PPA$^-$)(2QUIN$^+$)	443.6	464.9

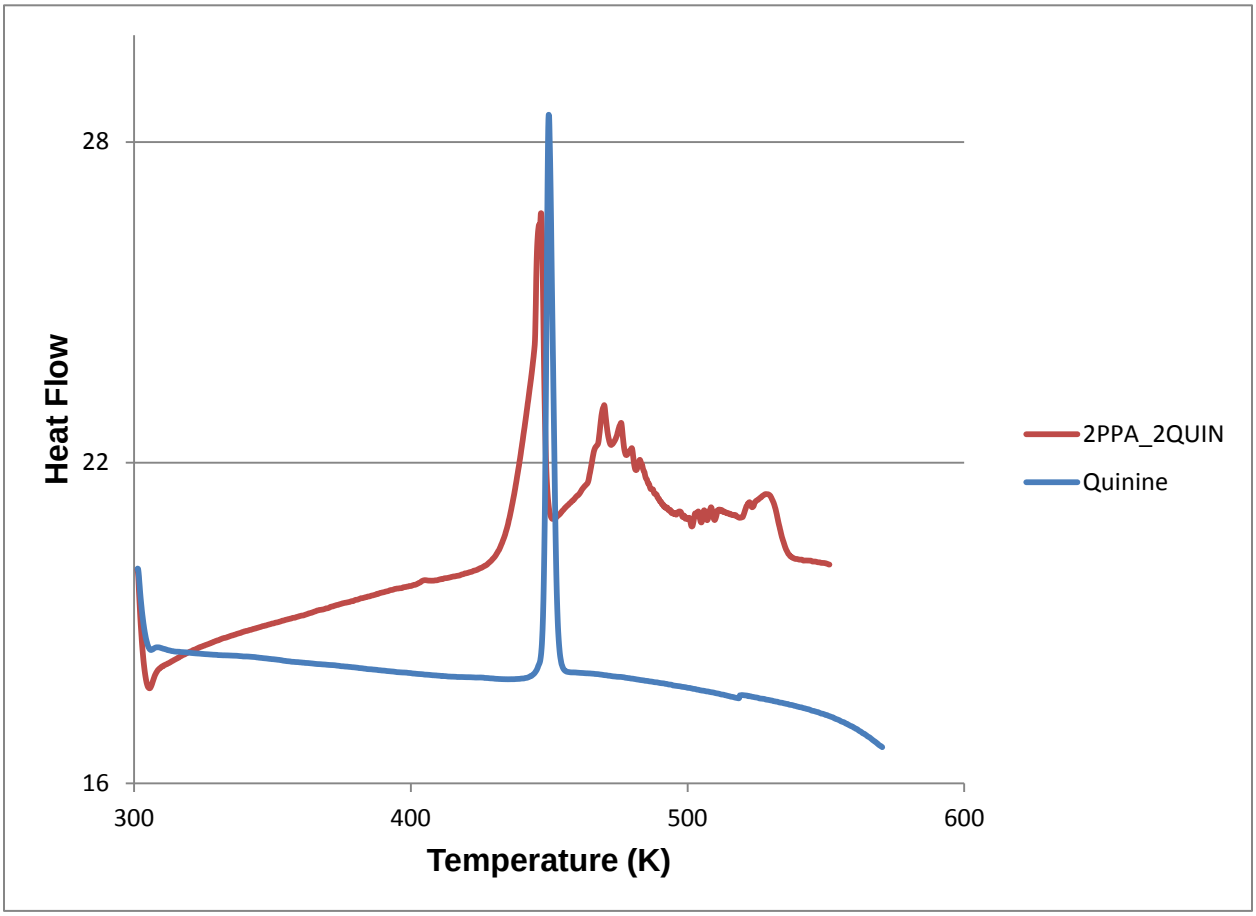

Figure 8.2.2: DSC curves of **(*R*-2PPA$^-$)(2QUIN$^+$)** (red) and quinine (blue).

8.2.2 Hot Stage Microscopy

The hot stage microscopy experiment (**Figure 8.2.3**) was performed by immersing a crystalline block in silicone oil at a temperature of 295 K. The crystal started melting at approximately 439 K and the melt was completed at 450 K.

(a) 295 K **(b) 439 K**

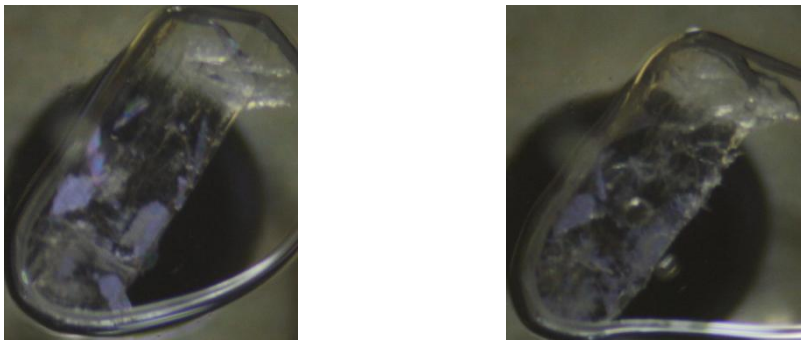

(c) 446 K **(d) 450 K**

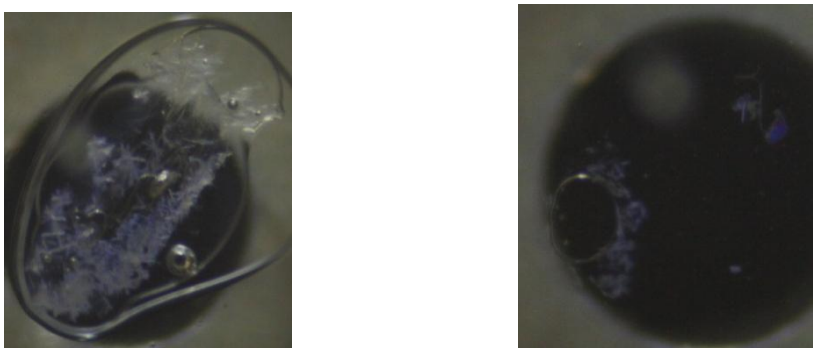

Figure 8.2.3: HSM photography of **(*R*-2PPA^{-})(2QUIN^{+})**: **(a)** crystal immersed in silicone oil, **(b)** crystal starts melting, **(c)** melt of the crystal and **(d)** complete melt of the crystal.

8.2.4 Structure Determination

All non-hydrogen atoms were refined anisotropically. The OH and NH hydrogen atoms were located in the difference electron density map. **Table 8.4** indicates the crystal data of **(*R*-2PPA^{-})(2QUIN^{+})**.

Table 8.5: Crystal data of **(*R*-2PPA$^-$)(2QUIN$^+$)**.

Compound	**(*R*-2PPA$^-$)(2QUIN$^+$)**
Structural Formula	$(2C_9H_9O_2^-)(2C_{19}H_{25}N_2O^+)$
PPA$^-$: QUIN$^+$: ratio	2: 2
Molecular Mass (g mol^{-1})	949.16
Data collection temperature (K)	173(2)
Crystal system	Monoclinic
Space group	*P2$_1$*
a (Å)	6.5192 (5)
b (Å)	19.2336 (17)
c (Å)	19.9300 (18)
α (°)	90.00
β (°)	91.639 (2)
γ (°)	90.00
Volume (Å^3)	2498.0 (4)
Z	2
D_c, Calculated density (g cm^{-3})	1.262
Final R indices [I>2sigma(I)]	R_1= 0.0513
	wR_2 = 0.1213
R indices (all data)	R_1 = 0.0759
	wR_2 = 0.1362
Largest diff. peak and hole (eÅ^{-3})	0.351; -0.247

(*R*-2PPA$^-$)(2QUIN$^+$) was solved in the monoclinic space group *P2$_1$* with Z = 2. The asymmetric unit contains two ions of each component. The crystal used for the single crystal X-ray experiment had size dimensions of 014 mm x 0.31 mm x 0.46 mm. Both PPA$^-$ anions had transferred a proton to both QUIN$^+$ cations in the structure. The **(*R*-2PPA$^-$)(2QUIN$^+$)** crystal packing along [100] is shown in **Figure 8.2.4**.

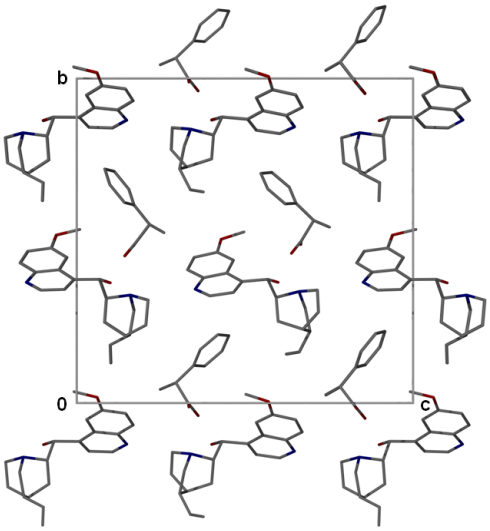

Figure 8.2.4: (*R*-2PPA$^-$)(2QUIN$^+$) packing diagram down [100] with all the hydrogen atoms removed.

The hydrogen bonding in **(*R*-2PPA$^-$)(2QUIN$^+$)** is shown in **Figure 8.2.5.** Each PPA$^-$ anion is hydrogen bonded to two QUIN$^+$ cations. The carboxylate group interacts with both the hydroxyl and the tertiary amine of two different QUIN$^+$ cations . The graph sets[6] found in the structure can be described as: $D_1^1(2)$ and $C_2^2(9)$. The hydrogen bonding parameters of the salt are listed in **Table 8.6**.

Table 8.6: Hydrogen bonding parameters in **(*R*-2PPA$^-$)(2QUIN$^+$)**.

COMPOUND	D-H···A	D···A (Å)	D-H (Å)	H···A (Å)	D-H···A (º)
(*R*-2PPA$^-$)(2QUIN$^+$)	N2-H1···O1	2.594 (2)	0.849 (3)	1.778 (3)	161 (2)
	N2-H1A···O1	2.589 (3)	0.900 (3)	1.690 (3)	177 (3)
	O5-H5A···O2[a]	2.642 (2)	0.847 (3)	1.796 (3)	176 (3)
	O5-H3B···O2A[a]	2.649 (2)	0.996 (3)	1.656 (3)	175 (3)

a = x-1, y, z

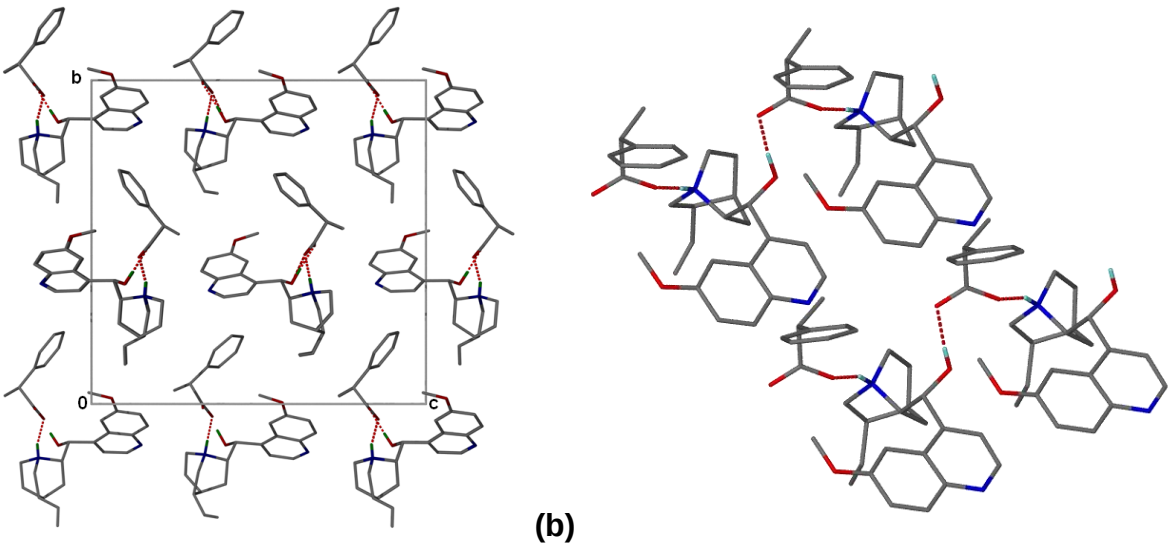

Figure 8.2.5: Hydrogen bonding in **(*R*-2PPA$^-$)(2QUIN$^+$) (a)** along [100] and **(b)** view illustrating that each PPA$^-$ anion is hydrogen bonded to two QUIN$^+$ cations.

8.3 2-phenylpropionic acid with quinine (*R,S*-PPA$^-$)(QUIN$^+$)•H_2O

A 1: 1 molar ratio of (*RS*)-2-phenylpropionic acid and quinine was dissolved in ethyl methyl ketone by heating the mixture on a hot plate. The solution was allowed to evaporate and crystals were obtained after one week. The configuration of the PPA in the structure was found to be 70% (*R)* and 30% (S) with water included in the crystal structure (**(*R,S*-PPA$^-$)(QUIN$^+$)•H_2O**). The asymmetric unit of **(*R,S*-PPA$^-$)(QUIN$^+$)•H_2O** is represented in **Figure 8.3.1**.

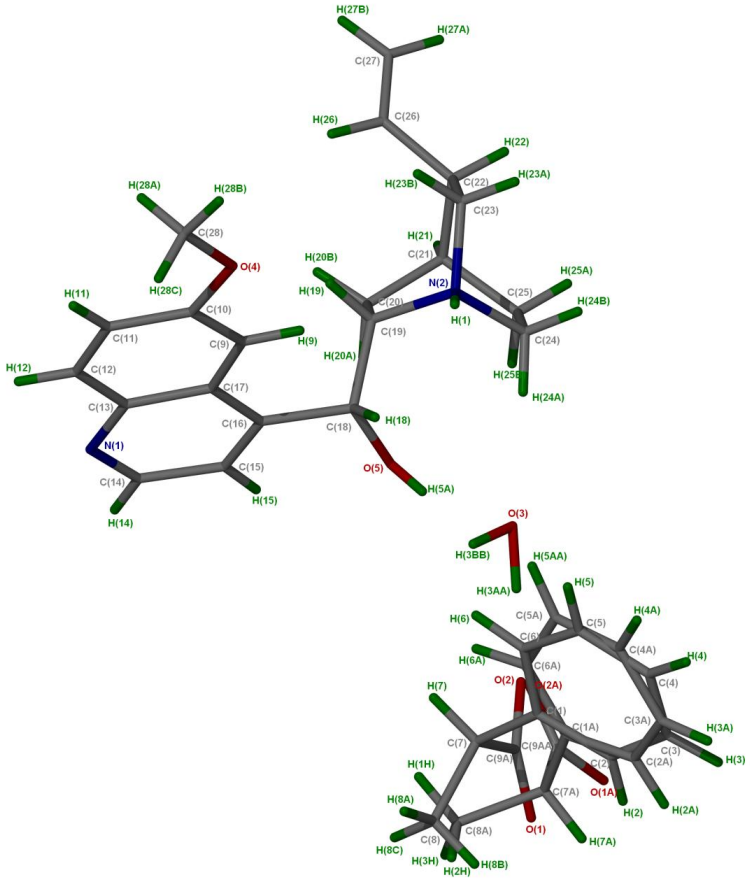

Figure 8.3.1: Asymmetric unit of **(*R,S*-PPA$^-$)(QUIN$^+$)•H_2O** with all the hydrogen atoms shown for numbering clarity.

8.3.1 Thermal Analysis

Thermal analysis curves are shown in **Figure 8.3.2** and the thermal analysis data is given in **Table 8.7**. The TG experiment indicates the loss of water at approximately 327 K; the mass loss is rapid corresponding to an experimental value of 3.8%. The DSC curve of **(*R,S*-PPA$^-$)(QUIN$^+$)•H_2O** shows three peaks, where the first peak indicates the loss of water, the second and third peaks correspond to the melt of the salt.

Table 8.7: Thermal analysis data of **(*R*,*S*-PPA$^-$)(QUIN$^+$)•H$_2$O**.

Compound	**(*R*,*S*-PPA$^-$)(QUIN$^+$)•H$_2$O**
PPA$^-$: QUIN$^+$: H$_2$O ratio	1: 1: 1
TG calculated % mass loss	3.7
TG experimental % mass loss	3.8
DSC Endo$_1$ (T_{onset}, K)	344.0
DSC Endo$_2$ (T_{onset}, K)	404.3
DSC Endo$_3$ (T_{onset}, K)	427.2

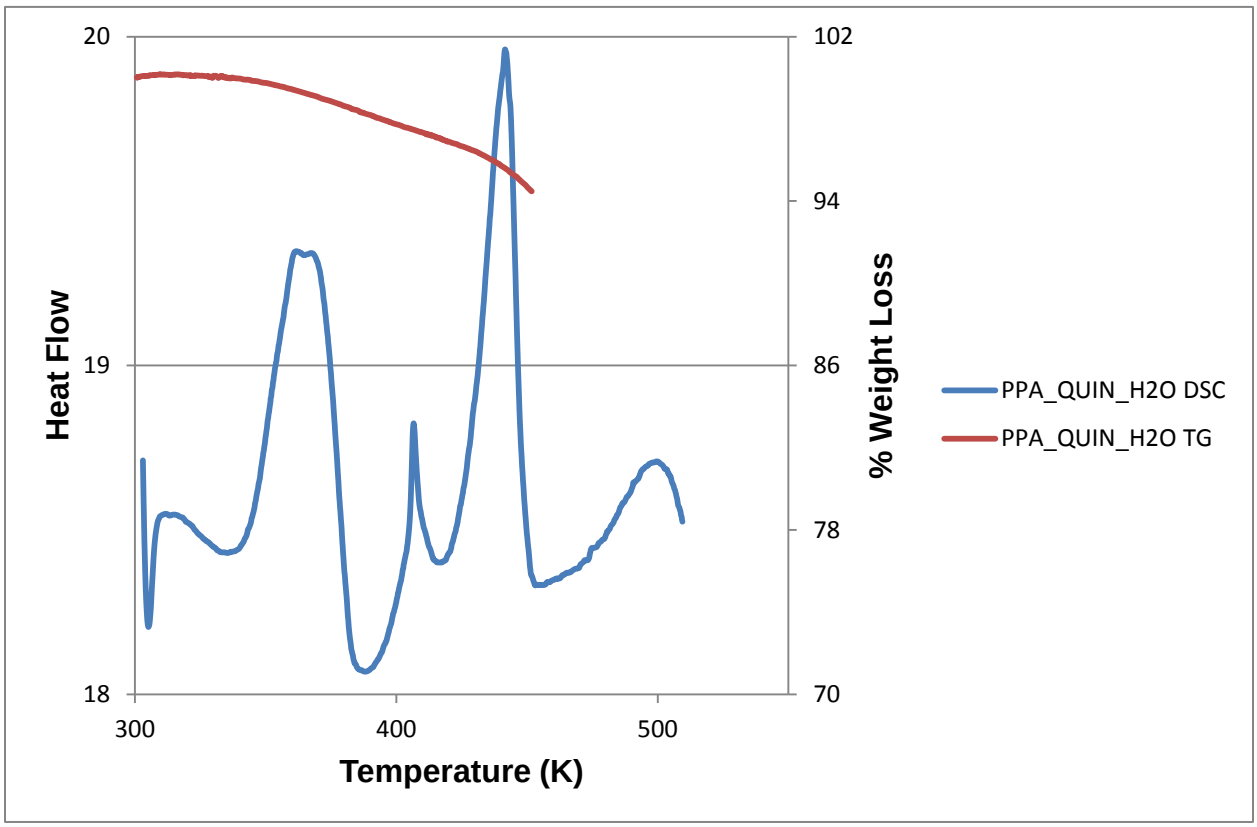

Figure 8.3.2: Thermal analysis curves of **(*R*,*S*-PPA$^-$)(QUIN$^+$)•H$_2$O** DSC (blue) and TG (red).

8.3.2 Structure Determination

The structure was solved via direct methods and the OH and NH hydrogen atoms were located in the difference electron density map. All non-hydrogen atoms were refined anisotropically. The crystal data is given in **Table 8.8**.

Table 8.8: Crystal data of **(*R,S*-PPA$^-$)(QUIN$^+$)•H_2O**.

Compound	**(*R,S*-PPA$^-$)(QUIN$^+$)•H_2O**
Structural Formula	$(C_9H_9O_2^-)(C_{19}H_{25}N_2O^+)\bullet H_2O$
PPA$^-$: QUIN$^+$: H_2O ratio	1: 1: 1
Molecular Mass (g mol^{-1})	492.60
Data collection temperature (K)	173(2)
Crystal system	Monoclinic
Space group	*C2*
a (Å)	28.087 (6)
b (Å)	6.7429 (13)
c (Å)	15.476 (3)
α (°)	90.00
β (°)	118.09 (3)
γ (°)	90.00
Volume (Å^3)	2585.7 (12)
Z	4
D_c, Calculated density (g cm^{-3})	1.265
Final R indices [I>2sigma(I)]	R_1= 0.0467
	wR_2 = 0.0983
R indices (all data)	R_1 = 0.0637
	wR_2 = 0.1077
Largest diff. peak and hole (eÅ^{-3})	0.538; -0.227

The salt hydrate crystallized in the monoclinic space group *C2* with Z = 4. The asymmetric unit contains one PPA^- anion, one $QUIN^+$ cation and one molecule of water. The structural formula of **(*R,S*-PPA^-)($QUIN^+$)•H_2O** was found to be $(C_9H_9O_2^-)(C_{19}H_{25}N_2O^+)•H_2O$ with a molecular mass of 492.60 $g.mol^{-1}$. The structure refined successfully to R_1 = 0.0467 with wR_2 = 0.0983 [I>2sigma (I)].

The PPA^- anion is disordered with the site occupancy factors for the final refinement: 0.70 (*R*)-2-PPA^- and 0.30 (*S*)-2-PPA^- respectively. The crystal packing along [010] with all the hydrogen atoms removed is illustrated in **Figure 8.3.3**. The water molecules occupy isolated sites.

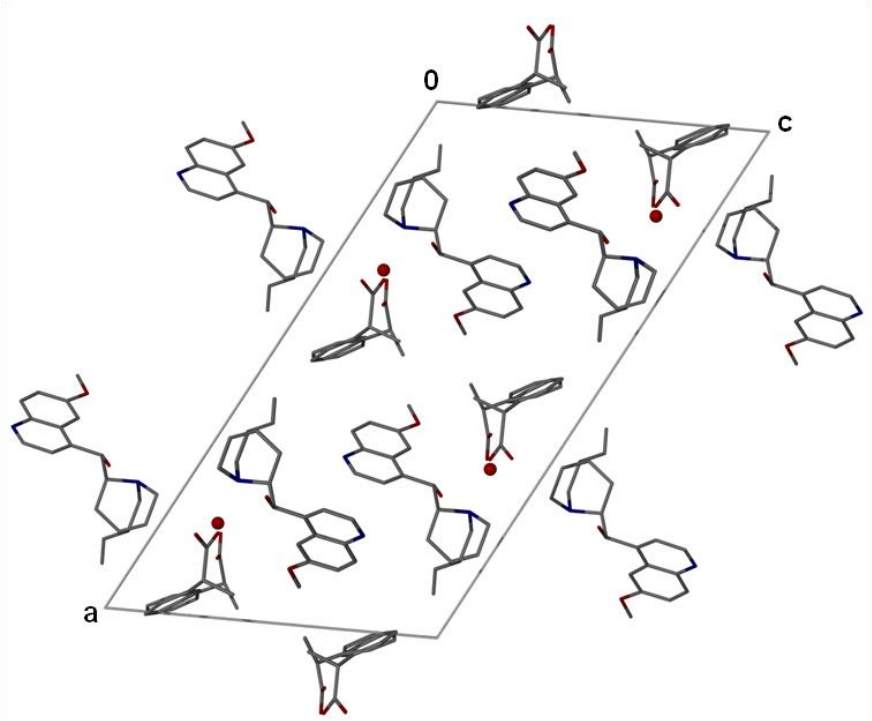

Figure 8.3.3: Crystal packing of **(*R,S*-PPA^-)($QUIN^+$)•H_2O** with all the hydrogen atoms removed down [010].

Hydrogen bonding in **(*R,S*-PPA^-)($QUIN^+$)•H_2O** has three atoms playing the role of bifurcated donor. The hydrogen atom labelled H1 connected to the nitrogen atom (N2) in $QUIN^+$ cation is a bifurcated donor. H1 is hydrogen bonded to O2 and O2A of the

PPA^- anion. The hydrogen atom labelled H3AA attached to the water molecule acts as a bifurcated donor due to the fact that it is connected to O2 and O2A found in the PPA^- anion. H3BB also acts as a bifurcated donor because it has a connection with O1 and O1A (PPA^- anion). The hydroxyl group in the $QUIN^+$ cation is hydrogen bonded to the oxygen (O3) of the water molecule (**Figure 8.3.4**). Etter[6] notation of the structure **(*R,S*-PPA^-)($QUIN^+$)•H_2O** can be characterized by: $D_1^1(2)$, $D_2^1(3)$, $D_2^2(4)$, $R_1^2(4)$, $D_2^2(5)$ and $D_2^2(8)$. The hydrogen bonding parameters of **(*R,S*-PPA^-)($QUIN^+$)•H_2O** are given in **Table 8.9**.

Table 8.9: Hydrogen bonding parameters in **(*R,S*-PPA^-)($QUIN^+$)•H_2O**.

COMPOUND	D-H···A	D···A (Å)	D-H (Å)	H···A (Å)	D-H···A (º)
(*R,S*-PPA^-)($QUIN^+$)•H_2O	N2-H1···O2_a[a]	2.710 (1)	0.919 (3)	1.795 (3)	173 (2)
	N2-H1···O2A_b[a]	2.710 (2)	0.919 (3)	1.799 (4)	171 (2)
	O5-H5A···O3	2.649 (2)	0.796 (3)	1.878 (3)	163 (3)
	O3-H3AA···O2_a	2.693 (2)	0.801 (1)	1.940 (3)	156 (5)
	O3-H3AA···O2A_b	2.745 (3)	0.801 (1)	1.994 (4)	156 (5)
	O3-H3BB···O1_a[a]	2.717 (1)	0.802 (1)	2.346 (3)	109 (2)
	O3-H3BB···O1A_b[a]	2.523 (1)	0.802 (1)	2.607 (3)	75 (2)

a = x, y+1, z

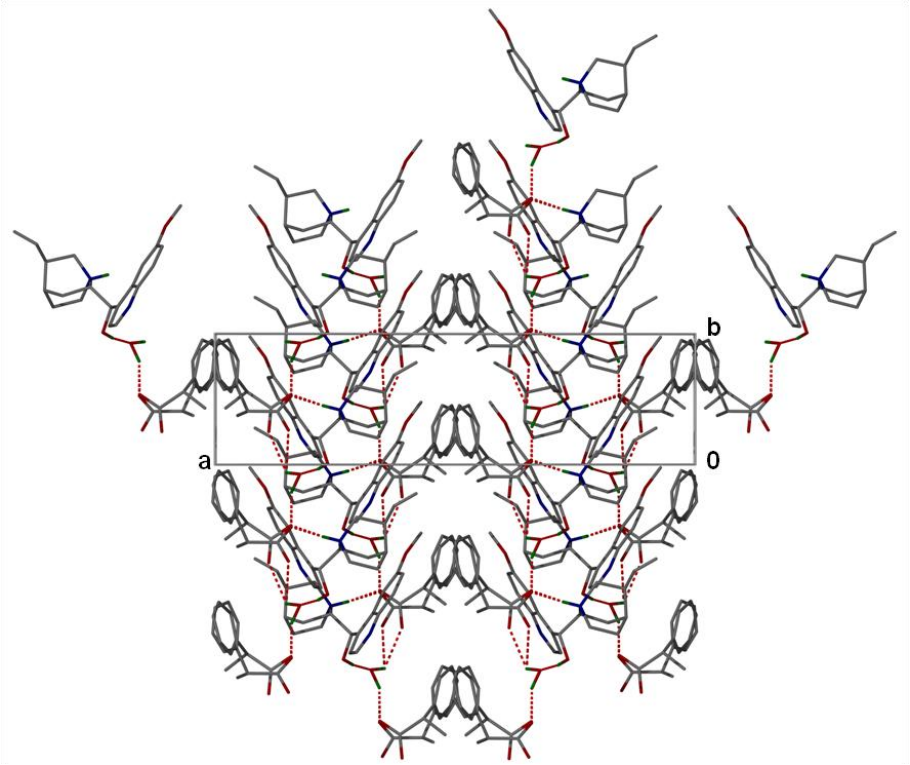

Figure 8.3.4: Hydrogen bonding in **(*R*,*S*-PPA^{-})(QUIN^{+})•H_2O**.

REFERENCES

1. Allen. F.H. *Acta. Crystalllogr*. 2002, B58, 380 - 388.
2. Lemmerer. A, Bathori.N. B & Bourne. S. A. *Acta. Crystallogr.* 2008, B64, 780.
3. Koshima. H, Nakagawa. T & Matsuura. T. *Tetrahedron. Lett*. 1997, 38, 6063.
4. Kinbara, Kobayashi & Saigo. *J. Chem. Soc. Perkin Trans*. 1998, 2.
5. Macrae. C. F, Eddington. P. R, McCabe. P, Pidcock. E, Shields. G. P, Taylor. R, Towler. M. & van de Streek. J. Mercury: visualization and analysis of crystal structures. *J. Appl. Crystallogr*. 2006, 39, 453-457.
6. Etter. M. C, MacDonald. J. C & Bernstein. J. *Acta. Crystallogr.* 1990, B46, 256-262.

CHAPTER 9

STRUCTURE COMPARISON

This chapter illustrates a variety of supramolecular networks found in the studied structures. It had been found that by changing phenolic acids (VA, PAA, HPAA, CHPAA, CFA, *p*CA and *t*FER) while using the same co-crystal former, there is an effect on the type of crystal structures obtained.

Compounds such as VA, PAA and CHPAA formed co-crystals with acridine (ACRI) in a 1: 1 ratio. A hybrid salt-co-crystal was formed between HPAA and ACRI containing a $HPAA^-$: $ACRI^-$: HPAA: ACRI ratio of 1: 1: 1: 1 (**$(HPAA^-)(ACRI^+)$•HPAA•ACRI**). Diethyl ether was used as a solvent for these new compounds. **PAA•ACRI** and **CHPAA•ACRI** were solved in the triclinic space group *P-1* but **$(HPAA^-)(ACRI^+)$•HPAA•ACRI** crystallized in the space group *P 1*.

VA•ACRI was solved in the monoclinic space group $P2_1/c$ with layers of VA molecules parallel to the ac plane, sandwiched between layers of acridine molecules. π-π interactions are found between adjacent ACRI rings (3.656 Å).

However, for **PAA•ACRI**, the π-π stacking interactions are different from that of **VA•ACRI**. These interactions in **PAA•ACRI** involve adjacent acridine rings (3.736 Å) and PAA molecules (3.835 Å). For **PAA•ACRI** also presented with a C-H•••π interaction between PAA and ACRI molecules with a C•••π (centroid) distance of 3.210 Å and an angle of 154 °.

$(HPAA^-)(ACRI^+)$•HPAA•ACRI and **CHPAA•ACRI** show similar packing with π-π stacking interactions in both structures between acridine rings with a shortest distance of 3.723 Å (**$(HPAA^-)(ACRI^+)$•HPAA•ACRI**) and 3.742 Å (**CHPAA•ACRI**).

Caffeine (CAF) formed a co-crystal with VA and PAA when used as a co-crystal former. The two co-crystals of caffeine differ in ratio. A 1: 2 molar ratio results between VA and CAF (**VA•2CAF**) with a 2:1 between PAA and CAF (**2PAA•CAF**).

VA•2CAF crystallized in the triclinic space group *P*-1 with π-π stacking interactions between the five membered and six membered rings of adjacent CAF molecules (3.420 Å).

2PAA•CAF was solved in the monoclinic space group $P2_1/c$. No π-π interactions were found in this crystal structure.

Isonicotinamide (INM) formed co-crystals with PAA, HPAA, CFA and *t*FER, but a co-crystal hydrate with VA. All of the new compounds with INM crystallised in the triclinic space group *P-1*, except for the co-crystal found between PAA and INM (monoclinic space group *C2/c*). A different ratio was found for each INM co-crystal/co-crystal hydrate.

Water molecules were involved in the co-crystal formed between VA and INM resulting in a 2: 2: 2 ratios (**2VA•2INM•2H_2O**). The water molecules present in the structure play a bridging role and makes the hydrogen bonding in **2VA•2INM•2H_2O** very complex. The structure is stabilised via face to face π-π stacking interactions between VA and INM rings (3.668 Å) and also involved weaker C-H•••π interactions between VA molecules (distance of 2.645 Å and an angle of 148 °). **2VA•2INM•2H_2O** shows VA and INM molecules in layers parallel to [$\bar{3}$33]. The ring motifs found in the structure are $R_2^2(8)$, $R_4^2(8)$, $R_4^4(16)$ and $R_4^4(20)$.

PAA and INM crystallized in a 1:1 molar ratio (**PAA•INM**). The structure also exhibited very weak C-H•••π interactions between the PAA aromatic ring and H7B in a neighbouring PAA molecule (distance of 3.269 Å and an angle of 110 °). The structure only displayed one ring motif $R_2^2(8)$.

On the other hand, there is a 1: 2 ratio between HPAA and INM (**HPAA•2INM**). The crystal structure does not involve any π-π stacking interactions or C-H•••π interactions. **HPAA•2INM** displayed ring motifs such as $R_2^2(8)$, $R_4^2(8)$, $R_4^4(16)$ and $R_4^4(32)$.

In addition, CFA and INM crystallized in a 1: 3 ratio (**CFA•3INM**). This ratio may be due to the various functional groups (-COOH and two -OH) in CFA capable of forming hydrogen bonds. The structure has two ring motifs $R_2^2(8)$ and $R_4^4(22)$.

The same ratio obtained in **HPAA•2INM**, was found between *tFER* and INM (***tFER*•2INM**). The structure displayed a hydrogen bonded ring motif which can be described as $R_2^2(8)$.

Nicotinamide (NAM) formed co-crystals with VA, PAA and *p*CA. The co-crystal obtained between VA and NAM has a 1: 1 ratio (**VA•NAM**) which was similar to the co-crystal between *p*CA and NAM (***p*CA•NAM**). **VA•NAM** was solved in the triclinic space group *P-1* with VA and NAM molecules involved in π-π stacking interactions (4.470 Å). The hydrogen bonding in **VA•NAM** resulted in two ring motifs $R_2^2(8)$ and $R_4^4(16)$.

The co-crystal obtained between PAA and NAM has a 2: 2 ratio. **2PAA•2NAM** crystallized in the monoclinic space group $P2_1/n$. Both **2PAA•2NAM** and ***p*CA•NAM** displayed ring motifs $R_2^2(8)$.

Cinchonidine (CIND) formed salt hydrates with PAA and HPAA. When using a different solvent with HPAA, CIND formed a salt solvate.

$(PAA^-)(CIND^+)•H_2O$ and **$(HPAA^-)(CIND^+)•0.5H_2O$** were solved in the monoclinic space group *C2*. **$(PAA^-)(CIND^+)•H_2O$** displayed two chains motifs $C_2^2(6)$ and $C_2^2(9)$. For both structures (**$(PAA^-)(CIND^+)•H_2O$** and **$(HPAA^-)(CIND^+)• 0.5H_2O$** the water molecules are located in cavities and link two anions.

For **$(HPAA^-)(CIND^+)•0.5H_2O$** and **$(PAA^-)(CIND^+)•H_2O$** and **$(HPAA^-)(CIND^+)•IPA•H_2O$**, a proton is transferred from the acid to the tertiary amine of the CIND. **$(HPAA^-)(CIND^+)•IPA•H_2O$** in the contrary, crystallized in an orthorhombic space group $P2_12_12_1$. Both the isopropanol and the water molecules are included in the crystal structure and are located in channels. The lattice arrangement of **$(HPAA^-)(CIND^+)•IPA•H_2O$** reveals two chain motifs differentiated as $C_2^2(6)$ and $C_2^2(9)$.

Quinidine (QUID) formed 1: 1: 1 ratio salt hydrates with PAA and HPAA. Both **(PAA$^-$)(QUID$^+$)•H_2O** and **(HPAA$^-$)(QUID$^+$)•H_2O** crystallized in the monoclinic space group *P2$_1$*. There are π-π stacking interactions between the PAA$^-$ anion and the QUID$^+$ cation (4.601 Å) stabilizing **(PAA$^-$)(QUID$^+$)•H_2O** and various C-H•••π interactions as illustrated in chapter 4. Both quinidine salts show similar packing with the water molecules located in cavities. There is one chain $C_2^2(9)$ motif in **(PAA$^-$)(QUID$^+$)•H_2O** instead of two chains motifs $C_2^2(9)$ and $C_2^2(11)$ found in **(HPAA$^-$)(QUID$^+$)•H_2O**.

Quinine (QUIN) formed a salt hydrate with PAA, a salt with HPAA and a hybrid salt-co-crystal solvate with *p*CA. The salt hydrate and the hybrid salt-co-crystal solvate were solved in the monoclinic space group *P2$_1$*. Hydrogen bonding and chain motifs in **(PAA$^-$)(QUIN$^+$)•H_2O** are similar to that in **(PAA$^-$)(QUID$^+$)•H_2O**. The water molecules in **(PAA$^-$)(QUIN$^+$)•H_2O** are located in cavities.

(HPAA$^-$)(QUIN$^+$) crystallized in the orthorhombic space group *P2$_1$ 2$_1$2$_1$*. Chain motifs in this structure can be characterized as: $C_1^1(7)$ and $C_1^1(9)$.

For **(*p*CA$^-$)(QUIN$^+$)•*p*CA•MeOH•H_2O** with the methanol and water molecules are located in cavities. Methanol and water molecules play bridging roles by connecting one p-CA$^-$ anion and one neutral p-CA molecule.[1] This hydrogen bonded network forms a bigger ring which can be described in graph set notation[2] as $R_4^4(24)$. A smaller ring between two p-CA$^-$ anions, one QUIN$^+$ cation and a water molecule can be characterized as $R_4^2(11)$.

REFERENCES

1. Jacobs. A & Amombo Noa. F. M. *J.Chem.Crystallogr.* 2014, 44 (2), 57 - 62.
2. Etter. M. C, MacDonald. J. C & Bernstein. J. *Acta. Crystallogr.* 1990, B46, 256 - 262.

CHAPTER 10

CONCLUSION

The field of crystal engineering has grown over the last ninety years, and the design of novel materials and functionality are currently being explored.[1]

In this research, selected phenolic acids were chosen for the formation of salts/co-crystals depending on the ΔpK_a with various organic amines/amides.

Successful resolution of racemic compounds (2-PPA and 2-PBA) was attained. Quinine resolved racemic 2-PPA by capturing the *R* isomer (**(*R*-2PPA$^-$)(2QUIN$^+$)**) and cinchonidine (CIND) on the other hand was able to resolve (*RS*)-2-PBA (capturing the *S* isomer(**(*S*-PBA$^-$)(CIND$^+$)•H$_2$O**)). By changing the solvent in the salt preparation of (*RS*)-2-PPA with QUIN, there was a change in the chirality of the obtained compound (capturing 70% of the (*R*) isomer and 30% of the (*S*) isomer (**(*R,S*-PPA$^-$)(QUIN$^+$)•H$_2$O**)).

Elucidation and refinement of the obtained structures were done using single crystal X-ray diffractometry as illustrated in **Table 10.1**. Analytical techniques such as PXRD, thermal methods (TG, DSC and HSM) and IR spectroscopy were used to characterize the new compounds.

A non-isothermal kinetics experiment was done to obtain the activation energy range (210 – 272 kJmol^{-1}) for the loss of methanol in **(*p*CA$^-$)(QUIN$^+$)•*p*CA•MeOH•H$_2$O**.

Mixtures of QUID and QUIN were used in selectivity experiments with HPAA and PAA respectively. Two ratios were selected for this experiment (QUIN: QUID: PAA/HPAA and QUIN: QUID: 2PAA/2HPAA). This kind of experiment was already reported with methylparaben where preferential co-crystallisation with QUID was observed.[2]

Solvents used for the crystallization experiments appeared to play a role in the interaction of amine/amide and the phenolic acids. This was observed with the two structures of HPAA and CIND. Completely different structures of HPAA and CIND were obtained from two solvents, **(HPAA$^-$)(CIND$^+$)•0.5H$_2$O** from ethyl methyl ketone (EMK) and **(HPAA$^-$)(CIND$^+$)•IPA•H$_2$O** from isopropanol.

A comparison of the structures involving the same amide/amine has been discussed in chapter 9.

An interesting situation was observed concerning the assignment of the space group for **(HPAA$^-$)(ACRI$^+$)•HPAA•ACRI**. The programme PLATON/ADDSYM[3] suggested a centre of symmetry relating two ACRI and two HPAA molecules. There was a centre of symmetry relating the ACRI molecules (disregarding the hydrogens) but not for HPAA due to the conformation of the two molecules in the asymmetric unit and the difference in torsion angles. Initial attempts to solve the structure in *P-1* resulted in a high R-factor of 0.30. However, the **(HPAA$^-$)(ACRI$^+$)•HPAA•ACRI** structure was solved in *P 1* and resulted in a good refinement with R_1 = 0.0405 and wR_2 = 0.0935 ([I>2 sigma (I)]).

Both PAA and HPAA contain the -COOH functional group but HPAA has an additional OH group capable of forming hydrogen bonds. The salt formed between PAA and QUIN had water included in the structure, **(PAA$^-$)(QUIN$^+$)•H$_2$O**. The salt formed between HPAA and QUIN did not include any water. This result can be explained by the –OH group in HPAA which is involved in the hydrogen bonding in **(HPAA$^-$)(QUIN$^+$)**. The water molecule included in the structure (**PAA$^-$)(QUIN$^+$)•H$_2$O** compensates for the absence of the –OH group in the PAA molecule.

In the selectivity experiment involving mixtures of QUIN/QUID with PAA , the PAA chose QUIN instead of QUID in the two experiment settings (1: 1: 1 and 1: 1: 2 ratios (QUIN: QUID: PAA)). HPAA in contrast chose QUID instead of QUIN. Further investigations are needed to determine possible reasons for the selectivity.

The co-crystal between VA and theophylline (THPH) has a 2: 1 ratio (VA: THPH) with the methoxy group of the second VA being disordered. The site occupancy factors for the methoxy group in the final refinement were 0.812 and 0.188 respectively.

A PXRD experiment involving **2VA•THPH** showed that the ground product patterns (20 and 30 min) and the slurry pattern were similar and resulted in the hydrate **2VA•THPH•2H$_2$O**. Attempts at obtaining crystals of **2VA•THPH•2H$_2$O** for structure solution were not successful.

Compounds formed with VA and the selected co-crystal formers mostly contained ring motifs in their structures, eg. **VA•THBR•2H$_2$O** has $R_2^2(8)$ and $R_4^4(8)$ as ring motifs and **2VA•THPH** with $R_2^2(9)$ and $R_3^3(9)$. The hydrogen bonding in **VA•2CAF** does not contain a ring motif. Ring motifs were also found in the new compounds where isonicotinamide and nicotinamide were used as co-crystal formers (**2VA•2INM•2H$_2$O**, **VA•NAM**, **PAA•INM**, **2PAA•2NAM**, **HPAA•2INM**, **CFA•3INM**, ***p*CA•NAM** and ***tFER*•2INM**).

When using Mercury[4] software for the location of the solvent in the structure, it was found out that water molecules were located in cavities for most of the new compounds except for the **(HPAA$^-$)(CIND$^+$)•IPA•H$_2$O** structure (isopropanol and water molecules were located in channels).

Changing the solvent as illustrated in chapter 3, 4, 6 and 7 did not have an effect on the crystalline products obtained. However in chapter 5, a solvent change in the preparation of HPAA and CIND salts resulted in two different crystal structures. **(HPAA$^-$)(CIND$^+$)•0.5 H$_2$O** was formed upon dissolution of HPAA and CIND in ethyl methyl ketone whereas (**HPAA$^-$)(CIND$^+$)•IPA•H$_2$O** was prepared in isopropanol.

The same observation was made in chapter 8 with the enantiomeric resolution of PPA. A salt, (**(*R*-2PPA$^-$)(2QUIN$^+$)**) was obtained when both components racemic PPA and QUIN were dissolved in acetonitrile and a salt hydrate (**(*R*,*S*-PPA$^-$)(QUIN$^+$)•H$_2$O**)) crystallised in ethyl methyl ketone. **Table 10.2** lists the solvents used in the study.

Various methods for the preparation of the compounds were attempted including neat grinding of the starting components, slurry conversion; solvent drop grinding and liquid assisted grinding. The PXRD patterns obtained were compared to the calculated PXRD patterns obtained from LAZYPULVERIX.[5]

However, the grinding experiment of PAA with the alkaloid compounds (CIND, QUID and QUIN) was not possible due to the formation of a paste-like product when PAA was ground with any of the alkaloids.

Table 10.1: Summary of selected characteristics of the structures investigated.

Complex	Bases	Complex ratio	Space group
VA•ACRI	Acridine	1: 1	*$P2_1/n$*
VA•2CAF	Caffeine	1: 2	*P-1*
2VA•2INM•2H_2O	Isonicotinamide	2: 2: 2	*P-1*
VA•NAM	Nicotinamide	1: 1	*P-1*
VA•THBR•2H_2O	Theobromine	1: 1: 2	*P-1*
2VA•THPH	Theophylline	2: 1	*$P2_1/c$*
2VA•2U	Urea	2: 2	*P-1*
PAA•ACRI	Acridine	1: 1	*P-1*
2PAA•CAF	Caffeine	2: 1	*$P2_1/c$*
(PAA^-)($CIND^+$)•H_2O	Cinchonidine	1: 1: 1	*C2*
PAA•INM	Isonicotinamide	1: 1	*C2/c*
2PAA•2NAM	Nicotinamide	2: 2	*$P2_1/n$*
(PAA^-)($QUID^+$)•H_2O	Quinidine	1: 1: 1	*$P2_1$*
(PAA^-)($QUIN^+$)•H_2O	Quinine	1: 1: 1	*$P2_1$*
($HPAA^-$)($ACRI^+$)•HPAA•ACRI	Acridine	1: 1: 1: 1	*P1*
($HPAA^-$)($CIND^+$)•0.5H_2O	Cinchonidine	1: 1: 1	*C2*
($HPAA^-$)($CIND^+$)•IPA•H_2O	Cinchonidine	1: 1: 1: 1	*$P2_12_12_1$*
HPAA•2INM	Isonicotinamide	1: 2	*P-1*
($HPAA^-$)($QUID^+$)•H_2O	Quinidine	1: 1: 1	*$P2_1$*
($HPAA^-$)($QUIN^+$)	Quinine	1: 1: 1	*$P2_12_12_1$*
CHPAA	CHPAA	-	*P-1*
CHPAA•ACRI	Acridine	1: 1	*P-1*
CFA•3INM	Isonicotinamide	1: 3	*P-1*
***p*CA•NAM**	Nicotinamide	1: 1	*$P2_1/c$*
(*p*CA^-)($QUIN^+$)•*p*CA•MeOH•H_2O	Quinine	1: 1: 1: 1: 1	*$P2_1$*
***tFER*•2INM**	Isonicotinamide	1; 2	*P-1*
(*R,S*-PPA^-)($QUIN^+$)•H_2O	Quinine	!: 1: 1	*C2*
(*R*-2PPA^-)(2$QUIN^+$)	Quinine	2: 2	*$P2_1$*
(*S*-PBA^-)($CIND^+$)•H_2O	Cinchonidine	1: 1: 1	*$P2_12_12_1$*

Table 10.2: Solvents used in the study.

Solvent names	Molecular formula	Mol wt ($g.mol^{-1}$)	Bp (°C)
Acetonitrile	C_2H_3N	41.05	81 - 82
Acetone	C_3H_6O	58.08	56
Chloroform	$CHCl_3$	119.38	61.20
Diethyl ether	$C_4H_{10}O$	74.12	34.60
Ethanol	C_2H_6O	46.07	78.37
Ethyl methyl ketone	C_4H_8O	72.11	79.64
Isopropanol	C_3H_8O	60.10	82.5
Methanol	CH_4O	32.04	65.00
Tetrahydrofuran	C_4H_8O	72.11	66.00
Water	H_2O	18.02	100.00

REFERENCES

1. Tiekink. E. R. T & Vittal. J. J. *Frontiers in Crystal Engineering*. John Wiley & Sons, Ltd, Chichester, UK. 2006.
2. Khan. M, Enkelmann. V & Brunklaus. G. *J.Am.Chem. Soc.* 2010, 132, 5254 – 5263.
3. Spek. A. L. PLATON: A multipurpose crystallographic tool: Version 10500: e 1980 - 2003.
4. Macrae. C. F, Eddington. P. R, McCabe. P, Pidcock. E, Shields. G. P, Taylor. R, Towler. M. & van de Streek. J. Mercury: visualization and analysis of crystal structures. *J. Appl. Crystallogr*. 2006, 39, 453-457.
5. Yvon. K, Jeitschko. W & Parthe. E. *Appl. Crystallogr.* 1977, 10, 73 - 74.